PRECLINICAL PHARMACOKINETIC EVALUATION OF NOVEL ANTIMALARIAL AND ANTITUBERCULOSIS DRUG LEADS

Natasha Strydom

Department of Chemistry

University of Cape Town

Thesis presented for the degree of Doctor of Philosophy

April 2018

Research supervised by Professor Kelly Chibale and Dr Lubbe Wiesner

DECLARATION

I, Natasha Strydom, declare that:

i) this thesis is my own unaided work, both in conception and execution, and that apart from the normal guidance of my supervisors, I have received no assistance apart from that acknowledged;

ii) neither the substance nor any part of the thesis has been submitted in the past, or is being, or is to be submitted for a degree in the University of Cape Town or any other University.

I grant the University of Cape Town free licence to reproduce the thesis in whole or in part for the purpose of research.

The thesis is presented for examination for the degree of Doctor of Philosophy.

Signed:_____

Date:_____

Natasha Strydom

ABSTRACT

Preclinical pharmacokinetic evaluation of novel antimalarial and anti-tuberculosis drug leads

Natasha Strydom

Preclinical pharmacokinetics relies on efficient and accurate screening to select clinical candidates from early leads. Poor pharmacokinetic interpretation can disadvantage drug discovery by promoting inadequate compounds and expelling potential drug candidates.

Objectives of this project included pharmacokinetic evaluation of antimalarial and anti-tuberculosis lead compounds with techniques aimed at improving preclinical pharmacokinetic outcomes.

This included mechanistic pharmacokinetic approaches such as non-linear mixed effects (NLME) modelling in comparison with traditional non-compartmental analysis. Where appropriate, pharmacokinetic methods were expanded to include organ distribution and capsule dosing in mice to bridge techniques from discovery to early development.

Three benzoxazole amodiaquine analogues possessing equipotent *in vitro* antiplasmodial activity and showed diverse *in vivo* efficacy in a malaria mouse model. Evaluation of their respective pharmacokinetics in mice showed their *in vivo* exposures could translate to *in vivo* efficacy. Retrospective PK/PD simulations point to a time above IC_{50} drive in efficacy.

Pharmacokinetic evaluation of an aminopyridine antimalarial compound in its cyclodextrin inclusion complex revealed a pH dependent increase in solubility that reduced variance, likely due to favoured intestinal absorption.

Investigation of two novel fusidic acid C-3 ester prodrugs aimed at repositioning fusidic acid for tuberculosis, showed high concentrations of the rodent specific 3-epifusidic acid metabolite that greatly reduced exposure of fusidic acid in mice. Further organ distribution studies showed a prodrug strategy is still viable for repositioning fusidic acid for tuberculosis, but that rodent models are inappropriate for further evaluation.

NLME modelling successfully provided unique mechanistic and mathematical insight of pharmacokinetic profiles of new leads. The level of interpretation on pharmacology parameters improved and aided in understanding why drug leads are likely to fail or succeed, assisting future compound optimisation.

ACKNOWLEDGEMENTS

I would like to express my gratitude to:

Prof Kelly Chibale and Dr Lubbe Wiesner for their excellent supervision, insight and motivation.

Prof Pete Smith and Pier Luca D'Alessandro for their kind mentorship, guidance and encouragement.

The postgraduate students of the chemistry and pharmacology research groups for their help, knowledge and friendship.

The Department of Chemistry and Division of Pharmacology staff, namely Elaine Rutherford-Jones, Saroja Naicker, Jennifer Norman, Shameema Witbooi, Zulfa Salie and Deidre Brooks.

The pharmacologists that assisted and trained me, namely Dr Liezl Gibhard, Dr Dale Taylor, Laurent Hoffman, Dr Sandra Castel, Prof Hans Hundt and Anton Joubert.

The chemists, Dr Dennis Ongarora, Dr Gurminder Kaur and Laurelle Joseph for their compounds and formulations, and willingness to follow up on additional synthesis.

Dr Sergio Wittlin and colleagues at the Swiss Tropical and Public Health Institute for conducting the *in vivo* antimalarial efficacy studies.

Dr Anne Leanerts and colleagues at Colorado State University for the *in vivo* anti-tuberculosis efficacy results.

Nina Lawrence and Lloyd Tanner for the *in vitro* ADME testing.

Dr Mathew Njoroge for the metabolite identification results and tremendous insights, with special thanks to Dr Christel Brunschwig for further assistance.

Dr Paolo Denti and his team for their help in modelling and wealth of knowledge surrounding pharmacokinetics.

The National Research Foundation, Medicines for Malaria Venture and National Institute of Health for personal and research funds, which made this project possible.

My incredible family and friends for their love and support.

CONTENTS

LIST OF TABLES

LIST OF FIGURES

1 INTRODUCTION

1.1 Project introduction

Drug discovery has taken immense strides to improve the pharmacokinetics of drug leads through compound optimisation. Attrition rates of compounds due to poor pharmacokinetics decreased from 40% in 1991 to 10% in 2010.[1,2] However, the translational gap from drug discovery to clinical trials still remains devastating with thousands of compounds lost to the "Valley of Death," causing a stagnation in approval rate, while research and development expenditure continues to increase,[3–5] Figure 1-1. The aim of this thesis was to evaluate the pharmacokinetics of novel antimalarial and anti-tuberculosis drug leads with an emphasis on improving pharmacokinetic techniques. These techniques included non-linear mixed effects modelling and the practicality of its implementation to improve pharmacokinetic outcomes and bridge the gaps in screening cascades.

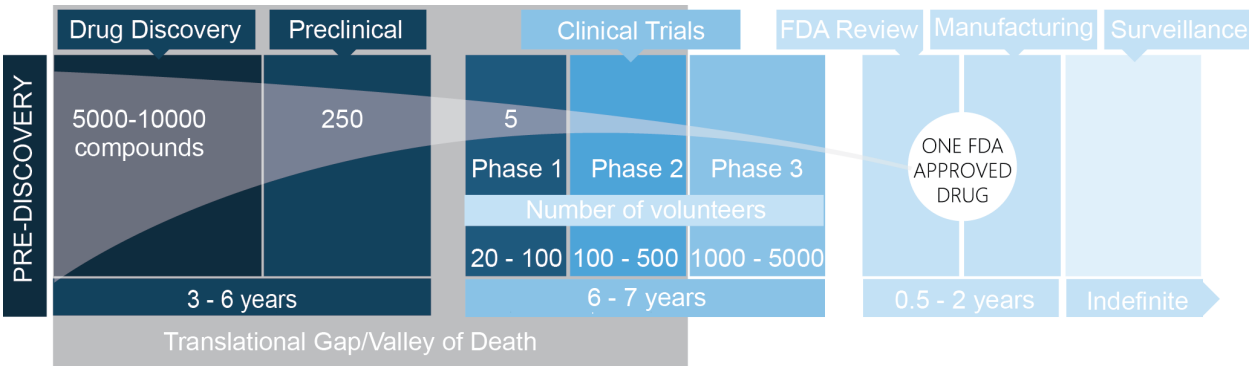

Figure 1-1: Translational gap in drug discovery[6]

Schema of the drug discovery and development showing the attrition of compounds from drug discovery to approval, requiring 5000 – 10000 compounds to have one successful candidate requiring up to 15 years of development.

1.2 Drug discovery and preclinical pharmacology

AstraZeneca reviewed their drug attrition rates from 2010 to 2015 and found efficacy and safety to be major factors, Figure 1-2.[3] Importantly the compounds lost due to preclinical pharmacokinetics/pharmacodynamics (PK/PD) was 3%, while Phase 1 trials showed an increased loss of 15%. This highlights an important issue in preclinical pharmacokinetics regarding animal translation to human response.[7] The drugs that do make it to market also often need additional dosing changes, suggesting that our current pharmacokinetic and pharmacodynamics practices show large inefficiencies.[8]

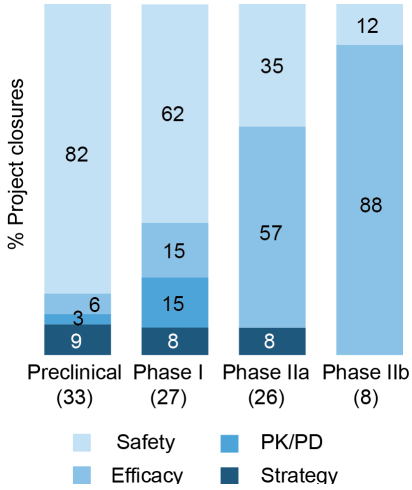

Figure 1-2: AstraZeneca project closures.[3]

Summary of project failures from AstraZeneca, classified by shortcomings in Safety, Efficacy, PK/PD and strategy, and stratified according to their respective phase of development dropout.

The lack of animal translation and the stagnation of drug approval prompted the Food and Drug Administration (FDA) of the United Sates to introduce the Critical Path Initiative in 2004. A key objective stated in Article 30 of the FDA Critical Path Opportunities (2006)[9] is:

> ***30. Improving Extrapolation from Animal Data to Human Experience.***
>
> *We urgently need new methods to bridge from animal data to predicted human experience, for both product efficacy and for product safety ..... Establishing reliable correlations between animal pharmacokinetic/pharmacodynamic data and human outcomes would dramatically improve the safety of human testing and treatment and the ability of sponsors to invest in only those candidate products most likely to be effective in humans. Conversely, re-examination of existing data could identify features of preclinical studies that were not predictive of human response.*

This objective is of great importance to preclinical pharmacokinetics that requires confident decision making in compounds to progress.[10,11] Inadequate interpretation and prediction leads to a two-fold failure where inadequate compounds are advanced, and promising leads are lost due to an insufficient screening cascade. Model-based simulations to improve success rates and to improve the efficiency and probability of obtaining informative results from preclinical experiments could aid in this objective.[12–16] The project aimed to assess the murine

pharmacokinetics of antimalarial and antituberculosis compounds of interest and compare them to their relevant murine efficacy. These studies were used as the basis to assess the use of the population pharmacokinetic tool; non-linear mixed effects modelling (NLME) in our screening cascade and evaluate the practicality of its implementation.

1.3 Comparison of pharmacokinetic methods and their limitation

1.3.1 Non-compartmental analysis

Non-compartmental analysis (NCA) has become the most popular tool for pharmacokinetic parameter calculation at the preclinical stage.[17] It is an efficient technique to calculate important decision-making properties of new lead compounds, including, maximum concentration (C_{max}), time to maximum concentration (T_{max}) and area under the curve (AUC) suggestive of drug exposure.[11,17–20]

In a practical setting, NCA's dependency on calculating pharmacokinetics from AUC is both its greatest advantage and limitation.[21] Pharmacokinetic parameters, and summary parameters including volumes and clearance calculated by NCA are all derived from the initial calculation of AUC (see section 2.4.4, page 38 for complete example of NCA calculations) and therefore are assumption free and objectively applied with ease, which is in contrast to compartmental modelling.[18,19,21,22] However, if the directly observed concentration-time profile used for empirical NCA calculations is incomplete, the resulting AUC can be mistaken and the derived parameters imprecise and inaccurate.[17,19]

The parameter determining AUC calculation of NCA is not the only numeric limitation that exists for the method. From a mathematical view, the methodology of NCA is built on linear first-order models, which often is not the function that would best describe a particular drug's ADME processes.[23] Also from a statistics perspective, pharmacokinetics is a multivariate phenomenon, and NCA cannot account for longitudinal pharmacokinetic datasets that inevitably suffer from unbalanced designs, time-varying covariates, missing data and other statistical considerations.[24]

NCA exists as an abstraction of drug processes and its original development was meant to be supplemental to compartmental modelling.[22] Despite this secondary nature, the NCA method has proved itself to be efficient, unbiased, and when the drug-concentration profile of a compound is well observed, is an excellent method to determine pharmacokinetic parameters.[17–19,25]

1.3.2 Compartmental methods

Where NCA predicts drug exposure by AUC of the observed concentration-time profile of a drug, compartmental methods use regression to describe the concentration-time profile and extrapolate exposure.[19] The use of compartmental models preceded non-compartmental modelling with work established in the early 20th century,[26,27] and popularised in the 70s and 80s, leading to compartmental modelling being deemed the "standard" of pharmacokinetic analysis.[22,28] Many of the equations used for NCA are derived from the descriptions and principles of pharmacokinetics provided by compartmental models.[22,29,30] The hypothesis behind compartmental modelling was implemented to account for the non-linear nature of drug elimination by regression.[25–27] To best capture the non-linear shape of the plasma-concentration-time curve, hypothetical "compartments" were implemented to account for the absorption, distribution and elimination of drug.[22,29,31–33] This hypothesis is of course an oversimplification of complex physiology, and the untrue assumption that the body is made up of few homogenous compartments with equivalent kinetic properties should always be kept in mind.[25]

There are excessive doubts surrounding compartmental analysis due to the discourse on how to determine the most appropriate model for a dataset. In fact, if considering the mathematical regression related to describing a pharmacokinetic curve, several models of comparable complexity can fit the same data, with no way of deeming which one is correct.[34] Even more concerning, is that certain parameters considered crucial to pharmacokinetics can be entirely left out of some models without consequence to the final conclusion,[35] questioning the validity of the method.

This consequently subjective nature of compartmental models thus inevitably faces the limitation of great bias. Additionally, compartmental modelling is considered difficult to implement and require supplementary skills and experience to become proficient in the field.

1.3.3 Non-linear mixed effects modelling

Building on compartmental models and using additional statistical methods adopted from econometrics, Lewis Sheiner is credited with developing, applying and popularising NLME modelling for estimating population pharmacokinetics.[36–42] Sheiner first introduced the method in 1972[39] and successfully applied it to digoxin pharmacokinetics where the computer model of Sheiner more accurately predicted patient response than physicians predicted.[25,28,43] Together with Arthur Beal, Sheiner released the computational NONMEM (contraction of non-linear mixed effect modelling) platform in 1980, written in the scientific program language FORTRAN.[40] Beal

and Sheiner continued to refine the platform and provide continued instruction to establish the utility and standardisation of NLME modelling to pharmacology.[36–38,42,44]

The efforts of Beal and Sheiner were readily welcomed into the discipline of pharmacometrics which aimed at developing mathematical models that could translate the relationship between dose to exposure (pharmacokinetics), and resulting exposure to response (pharmacodynamics),[28,45,46] Figure 1-3.

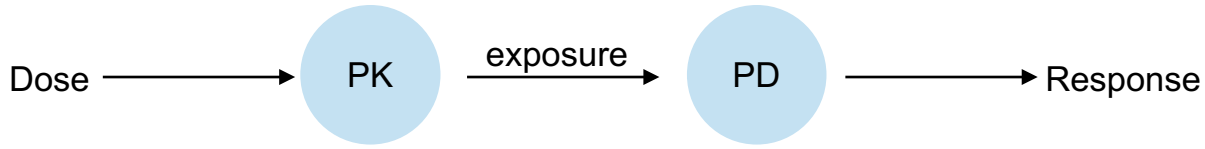

Figure 1-3: Translation of pharmacokinetic (PK) dose to pharmacodynamic (PD) response

The addition of mix effects to compartmental models provided a robust method to examine population pharmacokinetics, their relation to drug response and finally more standardised methods to affirm the most appropriate model.[42] The application of NLME modelling has been greatly beneficial to drug development, with 250 applications to the FDA between 2000 and 2010 using pharmacometric approaches.[47]

The success of NLME modelling rests on the mathematical description of both the mechanism behind the pharmacokinetic profile (structural model) and the variability in the experimental data (stochastic/variability model) with the option of adding covariates to search for trends in pharmacokinetic estimates and subject demographics,[31,48,49] Figure 1-4.

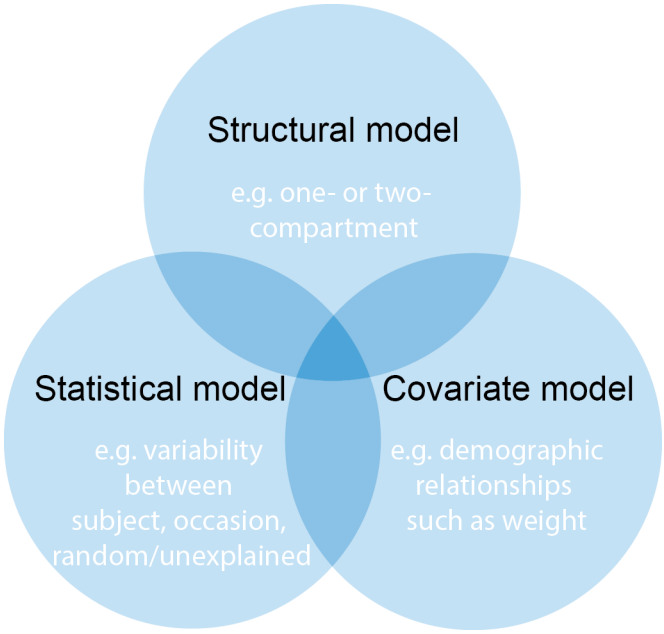

Figure 1-4: Elements of a non-linear mixed effects model

A non-linear mixed effects approach uses three models to describe population pharmacokinetics and/or pharmacodynamics. The structural model describes observed data by regression with mechanistic principles. The covariate model includes individual characteristics allowing for relationships between a patient clinical outcomes and demographics. The statistical model accounts for the distribution of observations.

The structural model describes the pharmacokinetic profiles using the same regression analysis established by compartmental modelling methods. The statistical model allows the parameters of this model to change according to a mixed-effects approach, where some of the variability is fixed/accountable, and the remaining variability described as random/unexplained.[31,36,37,39,46] The analysis then proceeds to estimate the pharmacokinetic parameter values that best describe the data, the size of the random variability between individuals, and the measurement of uncertainty.[31,39] A NLME approach is especially advantageous when there are limited data points available in each individual profile[13,31,42] Pooling data across individuals can together provide a more complete profile and allows the model to complete lacking information in absorption, distribution, and elimination phase data.[13,31,50]

Even though NLME is mathematically a much more successful tool for analysing pharmacokinetics, an important consideration of its application is to restrain from complexity. As described for compartmental models, models are based on the assumptions of researchers and are vulnerable to bias.[16,31,49,51] George Box[52] eloquently described the trouble of excessive modelling attempts:

> *Since all models are wrong, the scientist cannot obtain a "correct" one by excessive elaboration. On the contrary, following William of Occam he should seek an economical description of natural phenomena. Just as the ability to devise simple but evocative models is the signature of the great scientist, so overelaboration and overparameterization is often the mark of mediocrity.*

This was an important consideration for the pharmacokinetic evaluation, and included as an objective to assess the correct level of complexity that can be practically applied to preclinical research.

Important advantages and disadvantages of NLME that was considered for this project are summarised in Table 1-1.

Table 1-1: Advantages and disadvantages of non-linear mixed effects modelling

Advantages	Disadvantages
Fewer data per individual required	Complex mathematics
Simulation capabilities	Time consuming implementation
Hypothesis testing	Requires higher level of training
Facilitates mechanistic interpretation	Results sensitive to poor assumptions
Easier to integrate different sources of information	Excessive elaboration to fit objectives is possible
	Software can be costly

To address some of the predicted disadvantages, Monolix® software, which is an open source NLME modelling program, aimed at population pharmacokinetics was used in this project. It has a user-friendly graphical interface and built in models to promote NLME modelling as an accessible tool. [53–55] For compartmental pharmacokinetic analysis, three fundamental structural models based on one-, two- and three-compartment models able to describe both oral and intravenous administration were built with the assistance of Dr Paolo Denti, Division of Clinical

Pharmacology, University of Cape Town (South Africa). For an example of how these models were applied, refer to section 2.4.5, page 39 describing the model building process with an amodiaquine analogue as example. The models used for each compound evaluated and their respective application are discussed further within each study chapter and supplementary information is provided in Chapter 7: Experimental, page 197.

1.4 Aim, objectives and thesis outline

This thesis aimed to evaluate the pharmacokinetics of antimalarial and antituberculosis drug leads and compare their exposures to their *in vivo* efficacy. The studies were used to critically assess traditional methods with refined techniques to improve discovery outcomes that can feedback into compound optimisation and bridge the translational gap of potential leads that should be progressed to development.

Key objectives included:

1. Developing bioanalytical methods using LC/MS/MS quantification to evaluate the pharmacokinetics of antimalarial and antituberculosis drug leads in mice.

2. The use of modelling techniques to gain better insight into preclinical drug discovery outcomes as compared to an empirical non-compartmental analysis approach.

3. Expanding and refining pharmacokinetic methods used as better screening tools including capsule dosing, organ distribution studies for mechanistic-based pharmacokinetics, and simulating model results to evaluate PK/PD relationships and mouse to human translation.

The objectives were approached as follows:

The pharmacokinetic evaluation of three benzoxazole antimalarial drug leads with additional emphasis on PK/PD relationships using modelling and simulation to predict PK/PD drivers, presented in Chapter 2.

In Chapter 3 is discussed a bioequivalence study aimed at evaluating the improved *in vivo* efficacy of a cyclodextrin formulation of an aminopyridine analogue using capsule dosing.

In Chapter 4 is presented the pharmacokinetic evaluation of fusidic acid and novel fusidic C-3 ester prodrugs aimed at repositioning fusidic acid for tuberculosis. The evaluation included metabolite pharmacokinetics of the compounds and discrepancy in translation of mouse to human pharmacokinetics.

In Chapter 5, investigation of the organ distribution of fusidic acid C-3 prodrugs aimed at improving tissue distribution is discussed.

The highlights, limitations and future suggestions of these studies are discussed in Chapter 6: Conclusion.

Experimental reports on the final mouse experiments, LC/MS/MS quantification settings and statistics, and modelling outputs are described in Chapter 7: Experimental.

2 ANTIMALARIAL BENZOXAZOLE AMODIAQUINE ANALOGUES

2.1 Introduction

Amodiaquine is a 4-aminoquinoline antimalarial and an anti-inflammatory drug related to chloroquine and acts similarly by targeting the host haemoglobin degradation pathway through inhibition of hemozoin formation, which is an essential detoxification process of the plasmodium parasite.[56,57] Amodiaquine exhibits greater accumulation and activity in *Plasmodium falciparum* than chloroquine and has a reduced cross-resistance pattern than other quinolines, likely due to poor affinity for the resistant mechanism that prevents accumulation of quinolines in the plasmodium parasite.[58,59] It is rapidly metabolised by CYP2C8 to desethylamodiaquine (DEAQ).[60] The DEAQ metabolite is approximately 3.5 times less active *in vitro* than amodiaquine[61] but has a much longer half-life of up to 200 hours compared to the 5 – 12 hour half-life for amodiaquine.[56,62] The major challenge facing amodiaquine remains its unpredictable hepatotoxicity, myelotoxicity and agranulocytosis, attributed to the formation of reactive metabolites; quinone imine and aldehyde quinone imine *via* the CYP1A1/1B1 pathway, Figure 2-1.[63] Pharmacokinetic parameters between patients vary as greatly as 20 fold[56,64] leading to erratic half-lives and plasma concentrations, and irregular drug and metabolite exposures that can lead to suboptimal dosing that elicits resistance in some patients, while causing toxicity in others. This variance is not surprising as the CYP enzymes responsible for reactive metabolite formation have known diverse distribution patterns in different populations.[63,65] However, due to prevailing chloroquine resistance, amodiaquine still holds value in combination therapies with other antimalarials such as the short acting artesunate, that partners well with the slow elimination of DEAQ, to eradicate residual parasites.[66–68]

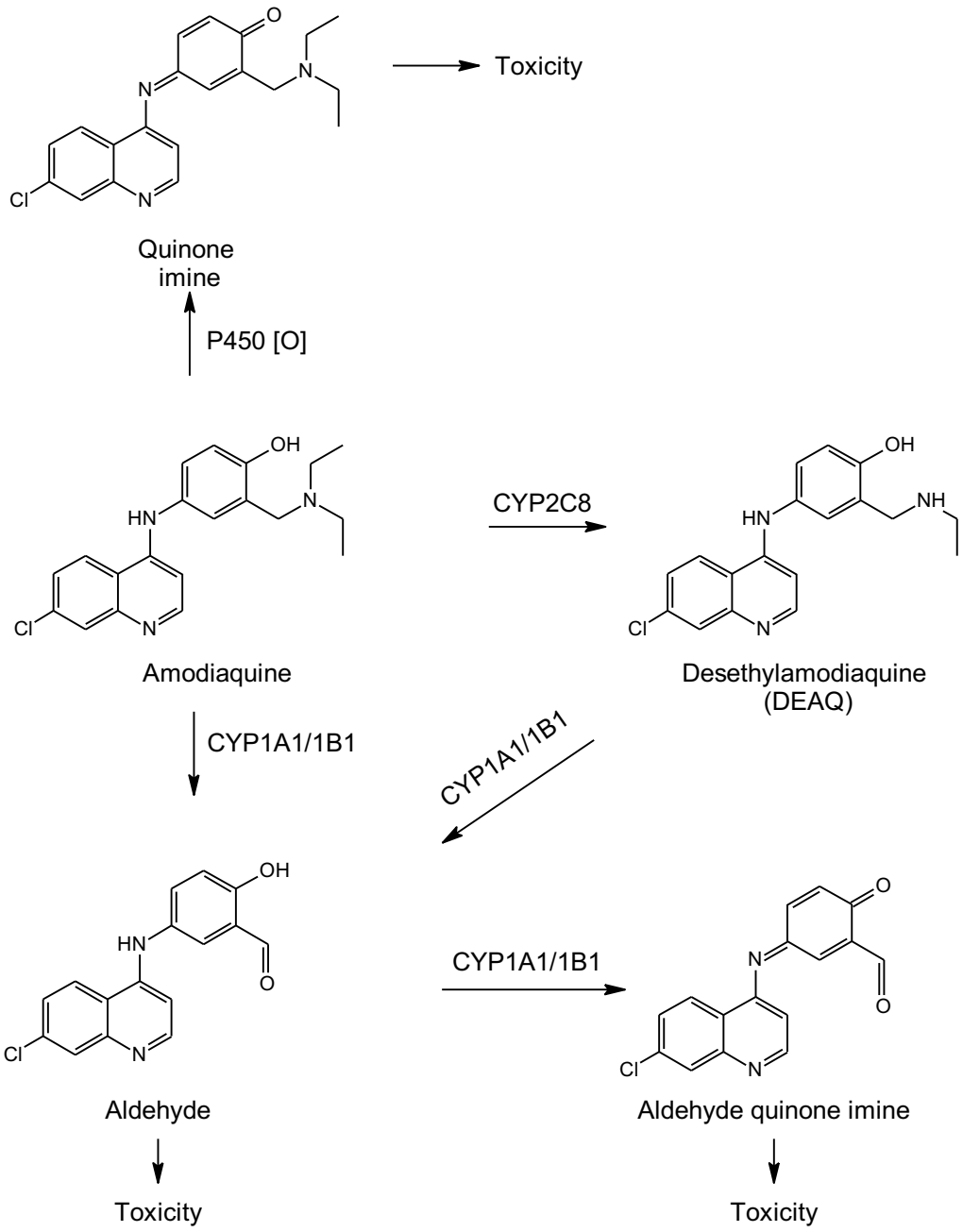

Figure 2-1: Metabolic pathway of amodiaquine[63]

Bioactivation of amodiaquine to less potent, but more pharmacokinetically attractive desethylamodiaquine (DEAQ) metabolite. Toxic metabolite formation of amodiaquine quinone imine likely *via* oxidation by cytochrome P450 (P450 [O]), amodiaquine aldehyde and aldehyde quinone imine by cytochrome P1A1 or cytochrome P1B1.

Attempts to address amodiaquine toxicity have led to preparation of several analogues with the most promising being isoquine, a regioisomer in which the formation of the toxic metabolites is not possible, Figure 2-2.

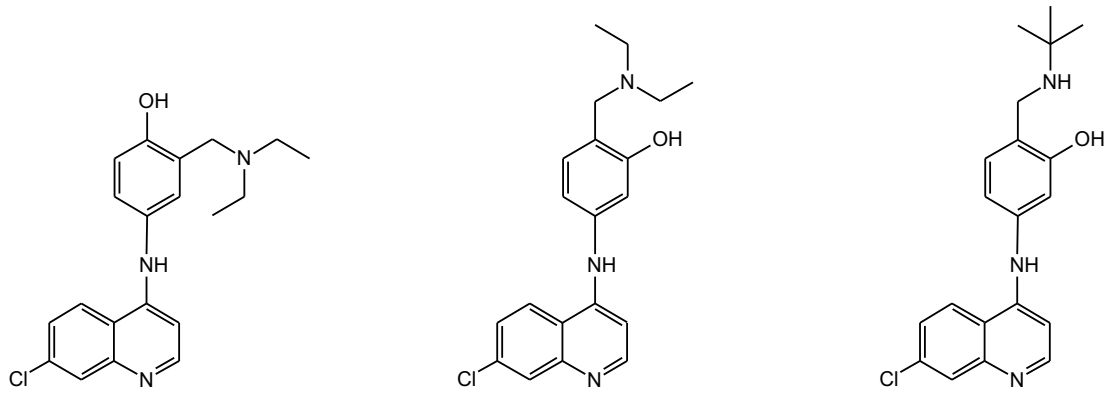

Amodiaquine	Isoquine	Tert-butyl isoquine
P. berghei ED_{50} = 2.1 mg/kg	*P. berghei* ED_{50} = 3.7 mg/kg	*P. berghei* ED_{50} = 2.8 mg/kg
hERG IC_{50} = 2.4 µM	hERG IC_{50} = 3.9 µM	hERG IC_{50} = 7.5 µM

Figure 2-2: Amodiaquine regioisomeres that cannot form toxic quinoneimine metabolites

Amodiaquine compared to its regioisomeres isoquine and tert-butyl isoquine that have the metabolic soft spots to toxic metabolites blocked show similar efficacy, but increasing hERG activity. Note: P. berghei ED_{50}; effective dose for median 50% of cohort against *Plasmodium berghei* infected mice, hERG IC_{50}; concentration showing 50% inhibition of Ether-à-go-go-Related Gene (hERG) channel activity.

Isoquine showed promising *in vivo* efficacy in *Plasmodium berghei* infected mice. Further optimisation identified tert-butyl isoquine as a promising drug lead that was subsequently progressed to phase 1 human trials. However, this candidate did show a potential cardiotoxicity risk due to its *in vitro* activity against the human Ether-à-go-go-Related Gene (hERG) channel and was ultimately discontinued due to inadequate drug exposure in humans.[69,70]

Our research group has continued similar investigation into synthesising improved amodiaquine analogues aimed at preventing the formation of toxic reactive metabolites. Chemical series to circumvent metabolism have included benzoheterocyclic 4-aminoquinolines, with the most promising being based on the benzoxazole amodiaquine scaffold, Figure 2-3.[71,72]

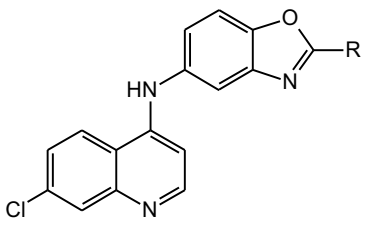

Figure 2-3: Benzoxazole amodiaquine scaffold

2.2 Rationale

The benzoxazole amodiaquine analogues shown in Figure 2-4, displayed good antiplasmodial activity and the most active compounds with favourable selectivity indexes were carried forward for *Plasmodium berghei* efficacy evaluation in mice, carried out by Dr Sergio Wittlin and colleagues at the Swiss Tropical and Public Health Institute (Basel, Switzerland). In Table 2-1 are displayed the results of three dosing regimens. These *in vitro* equipotent compounds showed greater diversity *in vivo* with compound **DS23B** having the best efficacy and showing complete cure at 4 x 10 mg/kg oral dosing. It was hypothesised that this diversity in efficacy could be due to differences in pharmacokinetic properties of the series, resulting in different exposures. The pharmacokinetics of these analogues were therefore investigated with the aim of explaining the observed differences in efficacy and accordingly compared these results to the pharmacokinetics of amodiaquine to evaluate if they were more beneficial.

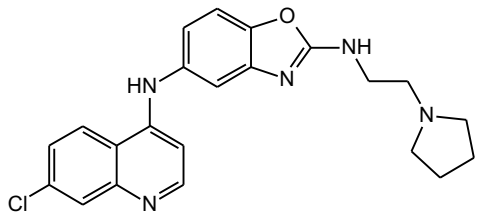

DS23B

NF54 IC_{50} : 15.0 nM

K1 IC_{50} : 56.0 nM

CHO IC_{50} : 4900 nM

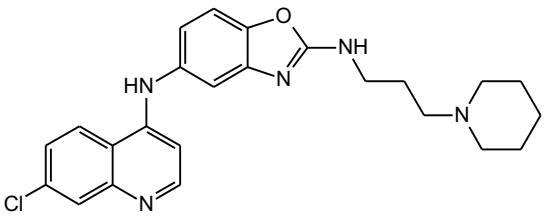

DS48B

NF54 IC_{50} : 10.0 nM

K1 IC_{50} : 39.0 nM

CHO IC_{50} : 671 nM

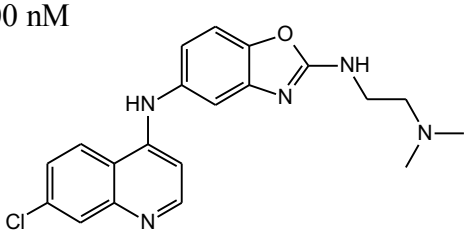

DS50B

NF54 IC_{50} : 11.5 nM

K1 IC_{50} : 41.9 nM

CHO IC_{50} : 7590 nM

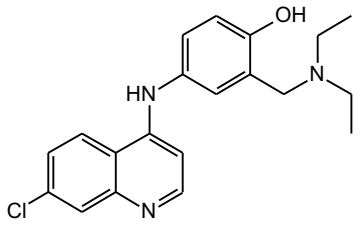

Amodiaquine

NF54 IC_{50} : 4.00 nM

K1 IC_{50} : 10.0 nM

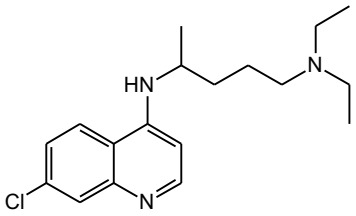

Chloroquine

NF54 IC_{50} : 10.0 nM

K1 IC_{50} : 275 nM

Figure 2-4: Benzoxazole amodiaquine analogues and their respective activity and cytotoxicity values

Note: NF54 IC_{50}; antiplasmodial activity showing 50% inhibition in drug sensitive *Plasmodium falciparum* strain NF54, K1 IC_{50}; antiplasmodial activity showing 50% inhibition in multi-drug resistant *Plasmodium falciparum* K1 strain, CHO IC_{50}; cytotoxicity concentration showing 50% inhibition in Chinese hamster ovarian cells.

Table 2-1: Efficacy of benzoxazole analogues of amodiaquine *in vivo* against *Plasmodium berghei* infected mice

Compound	% Reduction in parasitemia (MSD)		
	4×50 mg/kg	1×50 mg/kg	4×10 mg/kg
DS23B	99.83 (>30)	99.54 (23.3)	99.82 (>30)
DS48B	99.76 (>30)	99.54 (14.0)	99.76 (15.7)
DS50B	99.82 (29.3)	99.54 (13.7)	99.88 (24.0)
Amodiaquine	99.88 (>30)	n.d.	100 (>30)
Chloroquine[73]	99.70 (9.00)	n.d.	99.90 (16.0)

Efficacy experiments performed by Dr Sergio Wittlin and colleagues at the Swiss Tropical and Public Health Institute (Basel, Switzerland) using an adapted method based on the Peter's 4 day suppressive test.[72,74] MSD = mean survival time (in days); n.d. = not done.

2.3 Methodology overview

Figure 2-5 shows the approach and experiments undertaken for the pharmacokinetic evaluation of the three amodiaquine analogues. LC/MS/MS method development for accurate quantification of the compounds in mouse blood preceded animal experiments. An initial 7 hr pharmacokinetic experiment for **DS50B** and **DS23B** showed slow elimination and that the compounds had not yet reached their terminal half-life, making pharmacokinetic calculations inaccurate. A 24 hr experiment for **DS48B** showed a complete profile and calculated parameters are shown in Section 2.5.1. The 56 hr repeat experiments for **DS50B** and **DS23B** showed variability in the internal standard that appeared to be a result of ion suppression from the dosage formulation. The LC/MS/MS method was reassessed and improved. The unaffected final time points of this experiment were used to design a 15-day experiment for both **DS50B** and **DS23B**. This experiment showed acceptable pharmacokinetic profiles with parameters calculated by NCA and NLME modelling. Mouse pharmacokinetic data for amodiaquine from a previous experiment was reanalysed using the same NCA and compartmental approach to compare with the novel series. Additional *in vitro* assays including blood plasma partitioning, plasma protein binding, kinetic solubility and permeability ($logP_e$) and lipophilicity ($logD_{7.4}$) to describe the observed pharmacokinetic differences and fully characterise the compounds are shown in section 2.4.8. Section 2.4.6 contains additional simulations to examine potential PK/PD relationships.

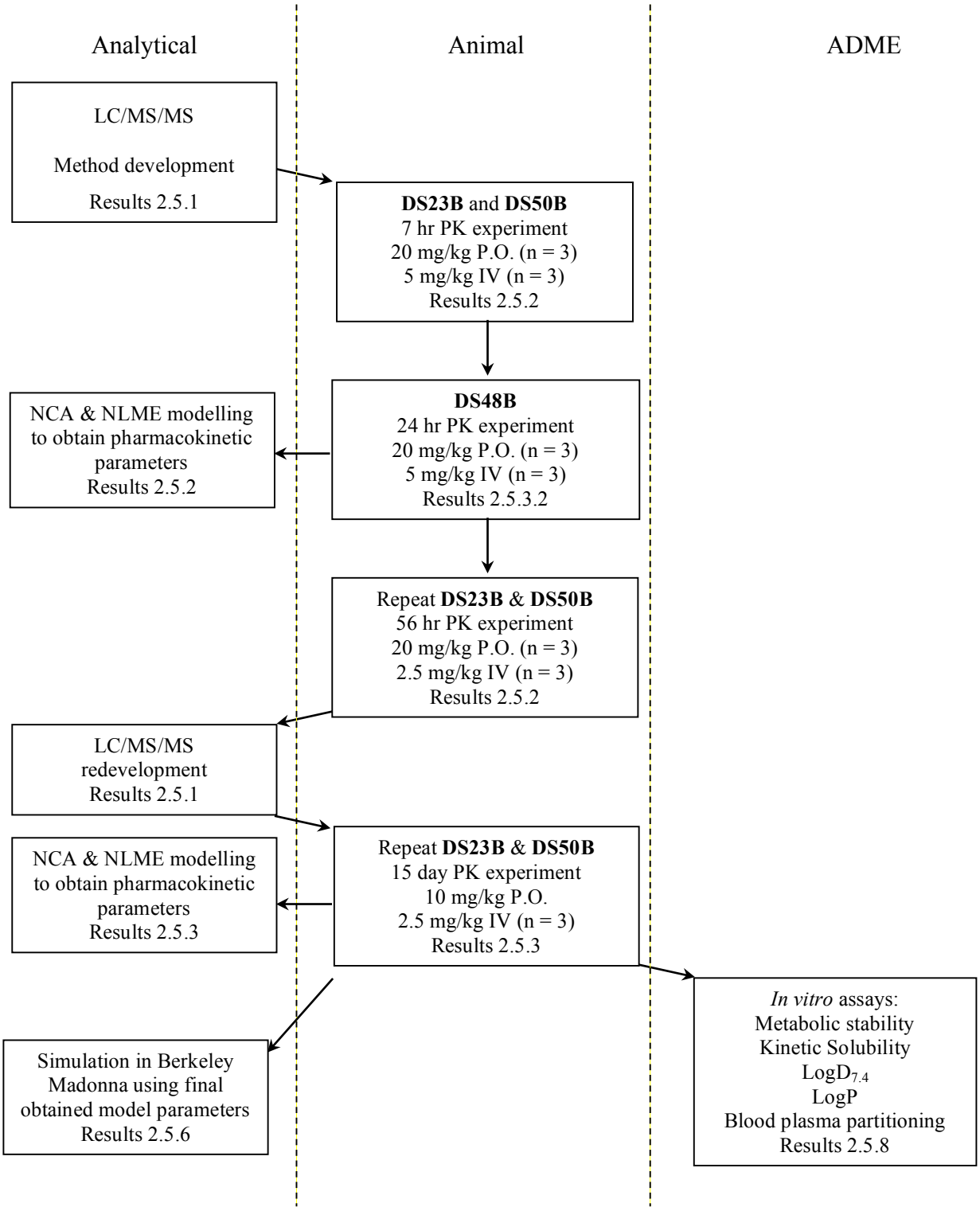

Figure 2-5: Overview of methods used for evaluation of benzoxazole analogues of amodiaquine

2.4 Methods

2.4.1 In vivo antimalarial efficacy testing

In vivo antimalarial efficacy testing was carried out by Dr Sergio Wittlin and colleagues at the Swiss Tropical and Public Health Institute (Basel, Switzerland) and followed a similar protocol recommended by Fidock *et al*.[75] This includes the adapted method of the classical 4-day suppressive test of Peters[74,76] to evaluate initial efficacy of compounds. Specific modifications included; experimental groups of three mice instead of five and a GFP-transfected *P. berghei* ANKA strain (donated by A. P. Waters and C. J. Janse, Leiden University, The Netherlands) to easily determine parasitaemia using flow cytometry with a detection limit of 1 parasite in 1000 erythrocytes instead of Giemsa stained blood smears that require manual counting. Additionally, intravenous infection was used as opposed to intraperitoneally for improved and more consistent infection rates.

The procedure was as follows; on day one, experimental groups (n = 3) NMRI Swiss-type mice were inoculated intravenously in the tail vein with 2 x 10^7 GFP-transfected *P. berghei* ANKA parasitised red blood cells. Treatment with a dose of 50 mg/kg commenced 4 hrs after infection. The experimental mice were orally administered with the selected compound first dissolved or suspended in 70% Tween 80 and 30% ethanol (v/v), and then further diluted ten times in water, while the untreated control group received the suspension vehicle alone. Treatment occurred 4, 24, 48 and 72 hrs after infection. Blood samples for the quadruple-dose regimens were collected 96 hrs after infection. Activity expressed as percentage reduction in parasitaemia was calculated as the difference between the mean percent parasitaemia for the untreated control and treated groups expressed as a percent relative to the untreated control group.

$$\%\ Reduction\ in\ Parasitaemia = 100 - \left(\frac{mean\ parasitaemia\ treated}{mean\ parasitaemia\ control}\ x\ 100\right)$$

Mice were monitored for 30 days post-infection and survival days recorded. Mice that survived to 30 days are considered completely cured. As is the norm for this specific screening protocol, compounds exhibiting a cure at 4 x 50 mg/kg were carried forward to examine lower dosing of 4 x 10 mg/kg and 1 x 50 mg/kg regimes.[72,77] An exception was made for compound **DS50B** which showed a cure in 2 out of the 3 mice, with the third mouse surviving to 29 days. It was decided that its inclusion remained relevant in this series considering its initial reduction in parasitaemia was more than **DS48B** that managed to cure all 3 mice. These published results shown in Table 2-1 warranted further *in vivo* pharmacokinetic investigation as discussed in Section 2.2 Rationale.

2.4.2 Final LC/MS/MS quantification

An LC/MS/MS quantification method preceded animal studies and showed accuracy within 93.6 – 108%. As discussed in the methodology overview, after this validation and animal work the final whole blood sample analysis encountered unforeseen column expiration and ion suppression on a differently selected column, leading to a repeat animal experiment. The LC/MS/MS reinvestigation is presented in the results and discussion section 2.5.1, page 67 of this chapter.

Briefly, the final reinvestigated LC/MS/MS method used for the final samples were performed as follows. Whole blood concentrations of the compounds were quantified by an LC/MS/MS assay developed for a range of 10 – 5000 ng/ml. The samples were extracted by protein precipitation using 20 µl whole blood and 240 µl acetonitrile containing a structurally similar internal standard. Gradient chromatography was performed on a Waters Xterra™ MS C_{18} (2.1 x 30 mm, 3.5 µm) reverse phase column at a flow rate of 600 µl/min with mobile phases 0.03% ammonium hydroxide (v/v) in water and acetonitrile. Transition 436.3→351.2 was monitored for **DS48B** on an AB Sciex API 3200® mass spectrometer operated at unit resolution in multiple reaction-monitoring mode. Similarly, transitions 408.1→98.0 and 382.2→72.0 were monitored for **DS23B** and **DS50B** respectively, on an AB Sciex API 4000Q® for increased sensitivity. Chromatograms showing retention times of each analyte according to the described methods are shown in Figure 2-6. Column carry-over was present for these compounds. A carry-over peak below 20% of a blank control sample after injecting a high-quality control sample is considered acceptable. Injecting 10 µl of blank methanol solvent between each sample reduced total carry-over to the accepted criteria. The highest carry over was 12.3% observed for **DS23B**. **DS48B** and **DS50B** showed carry-overs of 8.41% and 5.30% respectively. The accuracies (%Nom) for low (10 ng/mL for **DS48B**, and 19.3 ng/ml for **DS23B** and **DS50B**), medium (2000 ng/mL) and high (4000 ng/mL) quality controls ranged between 95.1 – 117%, 90.0 – 102.0% and 99.0 – 113%, and percentage coefficient (%CV) below 28.0, 33.6 and 12.0% for **DS48B**, **DS23B** and **DS50B** respectively. In depth final quantification statistics, expended extraction method, mass spectrometer conditions, mobile phase gradient, integrated peaks of low quality controls, blank samples and their respective internal standards for each compound are presented in Chapter 7: Experimental, section 7.2, page 197.

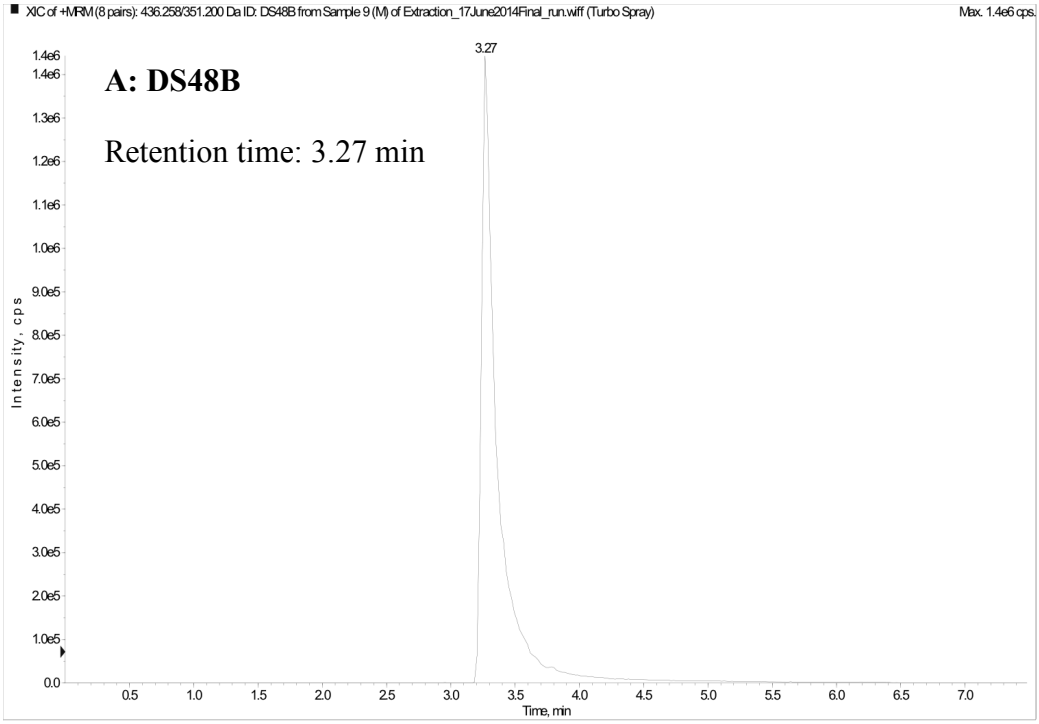
XIC of +MRM (8 pairs): 436.258/351.200 Da ID: DS48B from Sample 9 (M) of Extraction_17June2014Final_run.wiff (Turbo Spray)
Max. 1.4e6 cps.
3.27
A: DS48B
Retention time: 3.27 min
Intensity, cps
Time, min

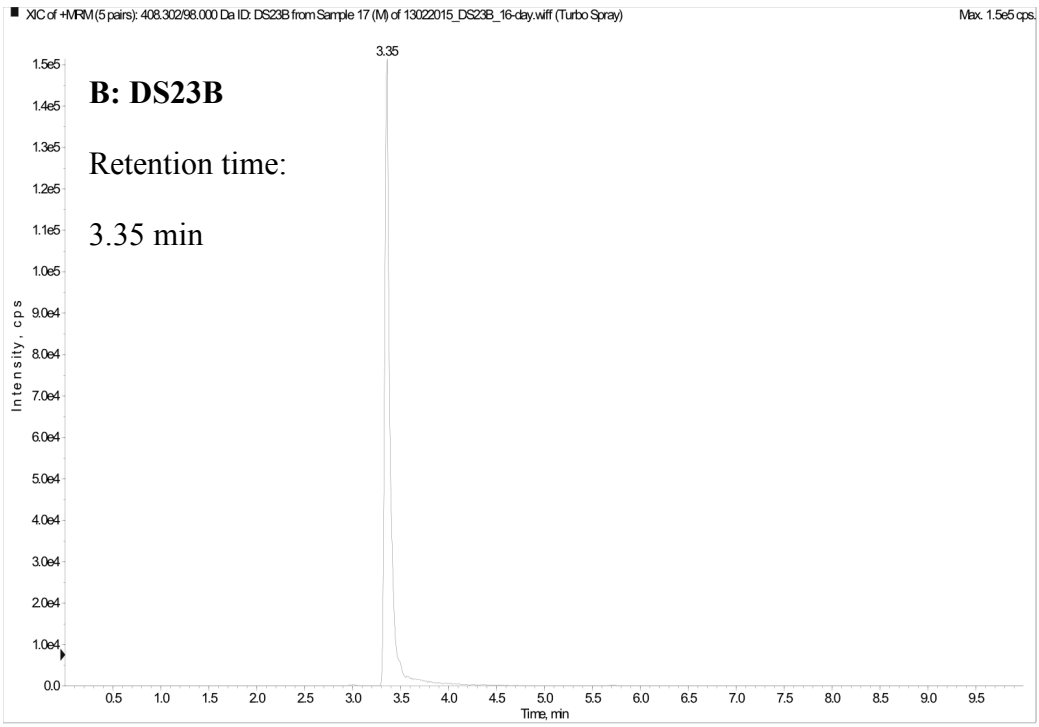
XIC of +MRM (5 pairs): 408.302/98.000 Da ID: DS23B from Sample 17 (M) of 13022015_DS23B_16-day.wiff (Turbo Spray)
Max. 1.5e5 cps.
3.35
B: DS23B
Retention time:
3.35 min
Intensity, cps
Time, min

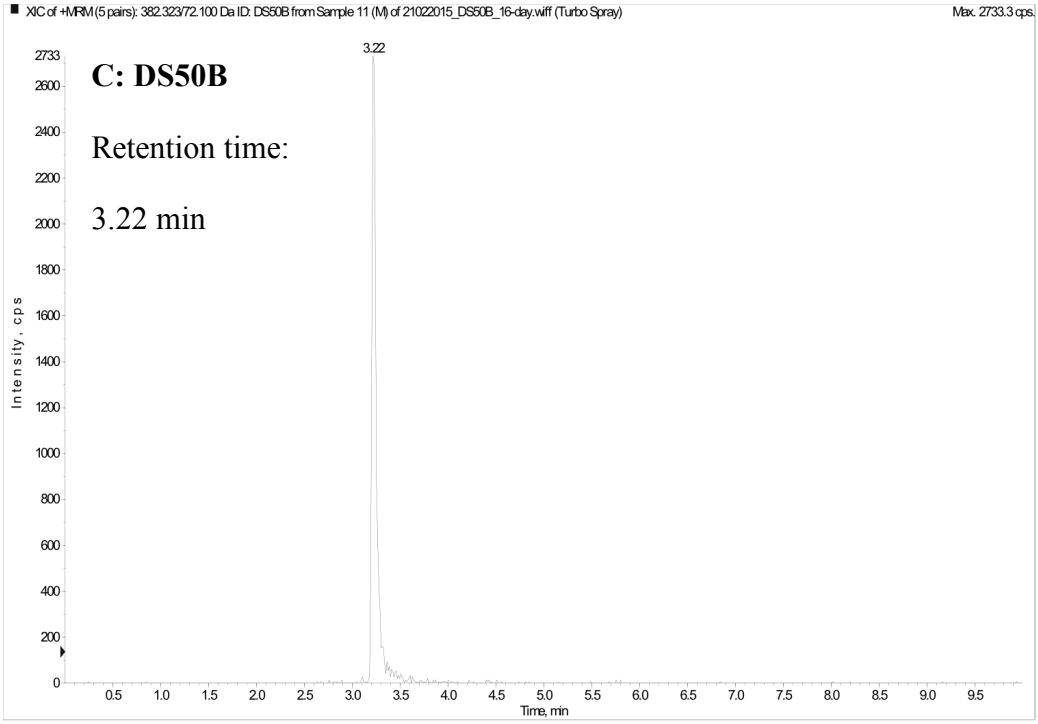

Figure 2-6: Representative chromatogram of benzoxazole analogues of amodiaquine.

Chromatograms for medium quality controls (4000 ng/ml) for **A**: **DS48B**, **B**: **DS23B** and **C**: **DS50B**.

2.4.3 In vivo pharmacokinetic experiment

2.4.3.1 Animals

All animal studies and procedures were conducted with prior approval of the Ethics Committee of University of Cape Town, approval number 013/028, in accordance with the National Code for animal use in research, education, diagnosis and testing of drugs and related substances in South Africa. The pharmacokinetic animal experiment used healthy 8-week-old C57BL/6 mice maintained at the University of Cape Town animal facility. Mice were housed in 27 x 21 x 28 cm cages under controlled environmental conditions including a maintained temperature of 26 ± 1°C and 12 hr light/dark cycle. Food and water were available *ad libitum.*

2.4.3.2 Compound preparation and administration

The author of this thesis prepared compounds for administration. Mr Trevor Finch from the Division of Pharmacology, University of Cape Town (South Africa) performed all animal handling, administration of compounds and blood collection under direct supervision of the author, with the author always present.

On the day of the experiment, a predetermined mass of the test compound was weighed for oral and intravenous groups based on the average mass of the animal experimental groups determined

that morning. Initial experiments used a 2.5 mg/kg intravenous dose and 20 mg/kg oral dose. The second repeat experiment for **DS23B** and **DS50B** was reduced to an oral dose of 10 mg/kg.

For each compound, the intravenous groups consisted of three males and weighed approximately 30 g, while oral groups consisted of three females and weighed approximately 25 g.

For oral administration, the weighed compound was suspended in 1000 µl of aqueous 0.5% hydroxypropyl methylcellulose (HPMC) (w/v) and vortexed for 1 minute. Drug administration followed by oral gavage of 250 µl total volume of suspension. Based on previous experience this excess is needed to accurately draw up and administer the required volume during the animal procedure. Administration occurred within 30 minutes of suspension preparation.

For intravenous administration, the weighed compound was prepared in an organic vehicle of 10% dimethyl sulfoxide (DMSO), 10% ethanol, 50% polypropylene glycol and 30% polyethylene glycol 400. The compound was dissolved in DMSO first, vortexed, followed by addition of other vehicle constituents and vortexing for at least 1 min. Solubility was confirmed by visual inspection of the dosage solution before administration. Intravenous injection into the penile dorsal vein of 60 µL total volume was performed under microscope. The organic vehicle required a slow push over 1 minute to prevent shock to the mice. The approximate final dose for the males weighing approximately 30 g contained 0.2 ml/kg DMSO, 0.2 ml/kg ethanol, 1 ml/kg polypropylene glycol and 0.6 ml/kg polyethylene glycol 400, which is considered safe in mice.[78]

Formulation stability could be performed to ensure the expected dose considering the compound could be unstable, but formulation preparation right before administration was found to be sufficient at this preclinical stage.

Whole blood samples were collected *via* tail bleeding at predetermined time points in 0.5 ml lithium microvials and vortexed for 30 seconds to prevent coagulation. The samples were stored at -80°C. For the first **DS23B** and **DS50B** experiment whole blood collection occurred at time intervals predose, and 0.5, 1, 3, 5 and 7 hrs for the oral and intravenous groups. Additionally, the intravenous group included sample collection at 5 minutes after dosing. As discussed in the methodology overview, the time-concentration profiles of **DS23B** and **DS50B** showed incomplete pharmacokinetic profiles. This led to additional whole blood sample collections of **DS48B** at 24 hrs for both groups. The animal experiments for **DS23B** and **DS50B** were repeated and sample collection extended to include 24, 32, 48 and 56 hrs. Experimental error during analysis of the blood samples unfortunately required another repeat experiment. Time intervals for the second **DS23B** and **DS50B** repeat experiment were extended for the oral group to include daily sample collection after the 48 hr sample for an additional 13 days.

The animal experimental record containing specific mouse weights, exact sample times and compound weights are included in Table 7-5 to Table 7-7, in Chapter 7: Experimental Records.

2.4.4 Non-compartmental analysis

Non-compartmental analysis was performed using PK Solutions, version 2.0 (Summit Research Services, Montrose, CO, USA). The analysis used individual whole blood concentrations vs sample times. Parameters calculated from the intravenous data included clearance (Cl) in ml/min/kg, initial central compartment volume (Vc) and volume at steady state (Vss) in L/kg, and elimination half-life ($t_{1/2}$) in hrs. Maximum concentration (C_{max}) in µM and time to maximum concentration (T_{max}) were taken directly from the individual oral profiles. Area under the curve from time zero to infinity ($AUC_{0-\infty}$) was calculated for both intravenous and oral profiles and used to calculate absolute oral bioavailability (F) expressed as a percentage. Parameters were normalised by individual mouse weights.

AUC for oral and intravenous data was calculated as the sum of the observed area under the curve (calculated by the trapezoidal rule) and extrapolated area (calculated by C/k_e where k_e is the elimination rate constant). The k_e was estimated as the log-linear slope of the final time points that were manually chosen to represent terminal phase. Half-life was calculated according to $t_{1/2} = \ln 2/k_e$.

Clearance was calculated according to fraction of dose absorbed divided by $AUC_{0-\infty}$. For intravenous administration fraction absorbed is equal to 1. To calculate Vc, the initial intravenous whole blood concentration (C_0) is calculated by extrapolation of the concentration-time curve to time zero. The equation then follows that Vc equals the dose amount divided by C_0. Vss was calculated according to dose multiplied by the area under the first moment curve ($AUMC_{0-\infty}$) divided by $AUC_{0-\infty}$ squared. This equation is commonly expressed as

$$Vss = Cl\ x\ MRT$$

Where MRT is mean residence time and can be calculated as follows:

$$MRT = \frac{AUMC_{\infty}}{AUC_{0-\infty}}$$

As mentioned, clearance from intravenous data is calculated as:

$$Cl = \frac{Dose}{AUC_{0-\infty}}$$

Therefore;

$$Vss = \frac{Dose\ x\ AUMC_{0-\infty}}{AUC_{0-\infty}{}^{2}}$$

Results are reported as the mean of the final individual parameters and standard error of the mean (s.e.) estimated by the sample estimate of the population standard deviation divided by the square root of the sample size.

2.4.5 Non-linear mixed effects modelling

Modelling was performed using Monolix® version 4.3.0 (LIXOFT, Antony, France). To aid in understanding the model-building process and criteria that was followed, an in-depth example of the approach is explained here with criteria results from compound **DS50B**. In subsequent chapters, brief overviews of the methods are given, but the same fundamental methodology applies.

2.4.5.1 The data input

The analysis used the same individual whole blood concentrations vs sample times used for NCA with the addition of time points that were measured below the lower limit of quantification (BLQ). The extra time points were input as their concentrations being unknown and censored as BLQ with the BLQ concentration stipulated. The model could then estimate the likelihood that the concentration was somewhere between zero and the BLQ.

Intravenous and oral group data were pooled in the same model and the data file specified the compartment of dose input as either the absorption compartment for oral data or central compartment for intravenous data. All units used were converted to mg/L for concentration and hrs for time. These are the units that would be used for human data from pharmacokinetics, which simplified the output data and the final parameters were converted to the same units as NCA for comparison.

The masses of the individual mice were included as a covariate in kg and transformed to log centred around the median. The transformed mass values were fixed within the covariate model using allometric scaling of volume and clearance.[79] This allowed the model to normalise clearance and volumes to the mass of individual mice and the final values were calculated and then reported for the median value of weight in the cohort.

2.4.5.2 The structural models

Three pharmacokinetic models were developed sequentially to be used as a "library" of one-, two-, and three- compartment models. The models were adapted for intravenous or oral administration, with an intravenous dose considered as instantaneous into the central compartment, and an oral dose absorbed *via* a fist-order process, possibly preceded by an absorption delay (T_{lag}) if applicable. Model building was guided by physiological plausibility, significant improvements in -2 the log-likelihood (-2LL), and evaluation of goodness of fit plots, including visual predictive plots (VPC) and individual plots.

In this sequential approach models were built up from the simplest model and complexity added stepwise. Development started with a one-compartment model and parameter data and diagnostics collected. The order of complexity was then increased to a two-compartment model. If the additional complexity was deemed statistically significant when reviewed with the simpler model (described in more depth in sections 2.4.5.2.1- 2.4.5.2.3), the model was again progressed to a more complex model and similarly reviewed.

The one-compartment model in the designed library where all model attempts started is shown in Figure 2-7.

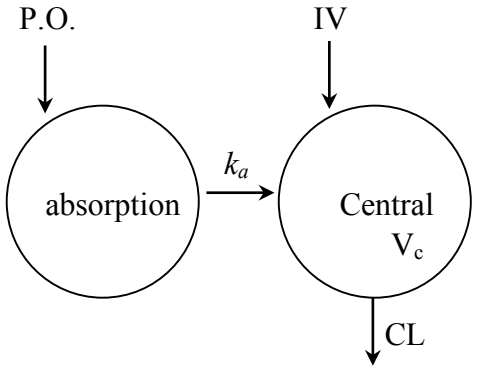

Figure 2-7: One-compartment model

Structurally the model follows that the compound can be introduced P.O. (per os, by oral administration) into the absorption compartment. An absorption rate (k_a) following first order kinetics allows one-way transfer of the compound from the absorption compartment to the central compartment. The central compartment is defined as the whole blood concentrations observed and where intravenous (IV) input occurs *via* instantaneous bolus introduction. Clearance (CL) occurs from the central compartment defined as rate of elimination (k_e) multiplied by volume of the central compartment (Vc).

For this model, the input of the dose administered in mg was defined using the assumption that the dose was instantaneous into the central compartment (V_c), with units in litres. In the case of oral

administration, the dose was introduced into an absorption compartment, with dose amount in mg represented by A_a. The rate of absorption followed first-order kinetics (k_a) into the V_c, where the amount of drug is described by A_c in mg. Whole blood concentration (C_c) is equal to A_c divided by V_c. Whole blood clearance (CL) was measured in L/h and followed CL = k_e x V_c where k_e is the rate of elimination. Initialisation of all compartments were set to zero i.e. no compound was present in circulation. Bioavailability (Foral) was also calculated, described in Monolix® as the proportion of the oral dose that reached V_c.

Using these terms, the differential equations describing this one-compartment model are as follows:

Given:

$$C_c = \frac{A_c}{V_c}$$

For an intravenous dose:

$$\frac{dA_c}{dt} = Dose - CL\ x\ \left(\frac{A_c}{V_c}\right)$$

For an oral dose, the addition of the absorption compartment results in the following modification:

$$\frac{dA_a}{dt} = Dose - k_a\ x\ A_a$$

$$\frac{dA_c}{dt} = k_a\ x\ A_a - CL\ x\ \left(\frac{A_c}{V_c}\right)$$

After modelling reached satisfactory parameters, the next sequential step was to increase complexity of the model to a two-compartment model and review if the diagnostics showed a significant statistical improvement. In Figure 2-8 is shown the two-compartment model used.

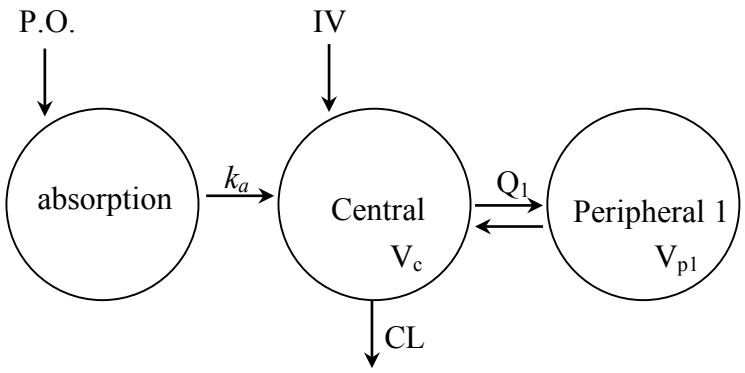

Figure 2-8: Two-compartment model

Structurally the model follows the same input and clearance as the previous one-compartment model with the addition of a peripheral compartment. Transfer between the central and peripheral compartments are defined by the inter-compartmental clearance (Q_1) allowing redistribution of the compound. Q_1 is defined by the rate of transfer from the central compartment to the peripheral compartment (k_{cp}) multiplied by the volume of the central compartment (Vc). The volume of the peripheral compartment is calculated by the rate of transfer from central to peripheral compartments divided by the rate of transfer back to the central compartment (k_{cp}/k_{pc}) multiplied by Vc.

The two-compartment model follows the same principles as described for the one-compartment model with the addition of a peripheral compartment where drug amount A_c can move in and out of the secondary compartment, becoming A_{p1} in mg with volume of distribution V_{p1}, described *via* inter-compartmental clearance Q_1 (L/h). The differential equations to describe this are shown below.

Given:

$$C_c = \frac{A_c}{V_c}$$

If the dose is intravenous:

$$\frac{dA_c}{dt} = Dose - CL\ x\ \left(\frac{A_c}{V_c}\right) - Q_1\ x\ \left(\frac{A_c}{V_c} - \frac{A_{p1}}{V_{p1}}\right)$$

$$\frac{dA_p}{dt} = Q_1\ x\ \left(\frac{A_c}{V_c} - \frac{A_{p1}}{V_{p1}}\right)$$

If the dose is oral:

$$\frac{dA_a}{dt} = Dose - k_a\ x\ A_a$$

$$\frac{dA_c}{dt} = k_a\ x\ A_a - CL\ x\ \left(\frac{A_c}{V_c}\right) - Q_1\ x\ \left(\frac{A_c}{V_c} - \frac{A_{p1}}{V_{p1}}\right)$$

$$\frac{dA_p}{dt} = Q_1\ x\ \left(\frac{A_c}{V_c} - \frac{A_{p1}}{V_{p1}}\right)$$

After modelling, the diagnostics for the test compound are compared to that of the one-compartment model and if found statistically more significant by the addition of the parameters Q_1 and V_{p1}, a three-compartment model was then attempted, Figure 2-9.

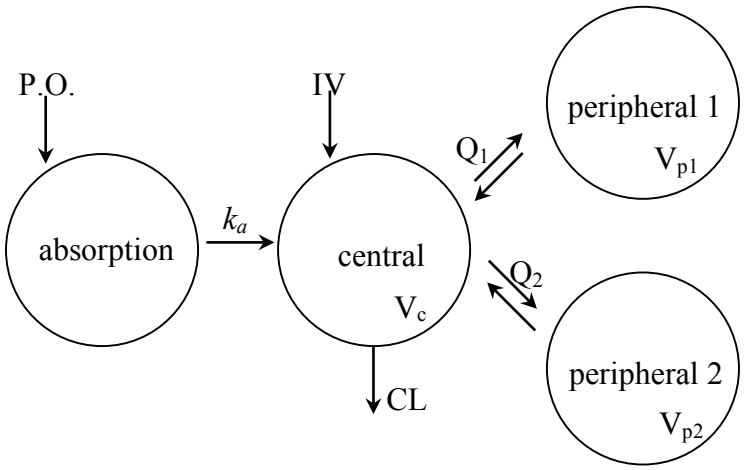

Figure 2-9: Three compartment model

Structurally the model follows the same input and clearance as the previous one-compartment model with the addition of two peripheral compartments. Transfer between the central and peripheral compartments are defined by the inter-compartmental clearances, Q_1 and Q_2, allowing redistribution of the compound. Q_1 and Q_2 are defined by the rate of transfer from the central compartment to the peripheral compartments, k_{cp1} or k_{cp2} respectively multiplied by the volume of the central compartment (Vc). The volumes of the peripheral compartments are then calculated by the rate of transfer from central to respective peripheral compartments divided by rate of transfer back to the central compartment k_{cp1}/k_{p1c} or k_{cp2}/k_{p2c}, multiplied by Vc.

The same principles as the two-compartment model apply and similarly, drug amount A_c can now move in and out of a third compartment, becoming A_{p2} in mg with volume of distribution V_{p2}, described *via* inter-compartmental clearance Q_2 (L/h). The differential equations to describe this are shown below.

If the dose is intravenous:

$$\frac{dA_c}{dt} = Dose - CL\ x\ \left(\frac{A_c}{V_c}\right) - \left(Q_1\ x\ \left(\frac{A_c}{V_c} - \frac{A_{p1}}{V_{p1}}\right) + \ Q_2\ x\ \left(\frac{A_c}{V_c} - \frac{A_{p2}}{V_{p2}}\right)\right)$$

$$\frac{dA_{p1}}{dt} = Q_1\ x\ \left(\frac{A_c}{V_c} - \frac{A_{p1}}{V_{p1}}\right)$$

$$\frac{dA_{p2}}{dt} = Q_2\ x\ \left(\frac{A_c}{V_c} - \frac{A_{p2}}{V_{p2}}\right)$$

If the dose is oral:

$$\frac{dA_a}{dt} = Dose - ka\ x\ A_a$$

$$\frac{dA_c}{dt} = ka\ x\ A_a - CL\ x\ \left(\frac{A_c}{V_c}\right) - \left(Q_1\ x\ \left(\frac{A_c}{V_c} - \frac{A_{p1}}{V_{p1}}\right) + \ Q_2\ x\ \left(\frac{A_c}{V_c} - \frac{A_{p2}}{V_{p2}}\right)\right)$$

$$\frac{dA_{p1}}{dt} = Q_1\ x\ \left(\frac{A_c}{V_c} - \frac{A_{p1}}{V_{p1}}\right)$$

$$\frac{dA_{p2}}{dt} = Q_2\ x\ \left(\frac{A_c}{V_c} - \frac{A_{p2}}{V_{p2}}\right)$$

After modelling the -2 the log-likelihood (-2LL), evaluation of goodness of fit plots, including visual predictive plots (VPC) and individual plots were reviewed again against the simpler two-compartment model.

A brief overview of the -2LL and goodness of fit plots' purpose and interpretation are described below.

2.4.5.2.1 A description of -2 the log-likelihood value

The -2LL, also often referred to as the objective function value (OFV), and is the sum of the squared residuals, and a mathematical optimisation tool that aims to quantify how well the observed data fits with the model. It considers fixed effects parameters, inter-individual variability and unexplained variability. In Figure 2-10 is shown a 3D graphic representation of the objective function surface (or the sum of the squared residuals surface) for a model exploring the best values of two parameters. As the software explores the optimal parameters of the model, it is guided by this surface to find the lowest point considered convergence of the best fitting parameters. The

minimum or lowest -2LL value is the maximum likelihood of the parameters fitting to the observed data.

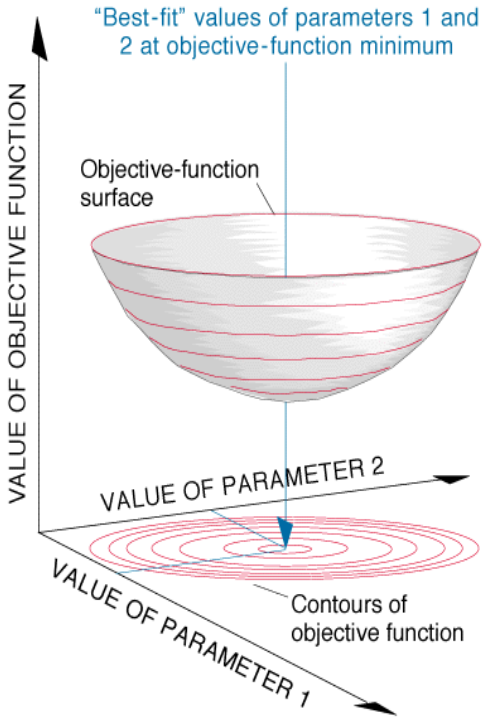

Figure 2-10: Objective function surface of two parameters

The -2 log likelihood (-2LL) or objective function value illustrated as a surface which the model can trace to the lowest point of convergence to obtain the best-fit values of two parameters.

The -2LL is therefore a vital criterion to determine which model parameters from the structural, covariate and statistical models are best for the observed data. However, as stated in Chapter 1, simplicity in model building is key, and to quote economist Ronald Coase[80]:

> *"If you torture the data long enough, it will confess (sic) to anything"*

Adding a parameter to the model will often result in a lower -2LL due to the added variability allowing an additional degree of freedom in the model. In other words, the more complex a model is, the more flexible it becomes at fitting data. It is therefore necessary to have a threshold in the decrease of -2LL to justify the inclusion of additional complexity and prevent over-parameterisation. The criteria stated a decrease of at least 3.84 points as the threshold of significance for the inclusion of one additional parameter. This correlates to a *p*-value of 0.05

based on the assumption that the residuals are chi-square distributed.[81] This criteria is well accepted in model building.[51,82–91]

A large concern when dealing with the -2LL is the occurrence of a local minima, Figure 2-11. This occurs when the model explores the objective function value surface and finds a decreasing -2LL pocket that does not correlate to the global optimised values. This occurs when the initial starting estimates of the model are out of place and allows the model to get "lost". This occurs more frequently in complicated models. To prevent this, it is the responsibility of the modeller to input feasible initial parameter values where the model will start searching for the optimised parameters. It is also the modeller's responsibility to understand the final parameters and whether they are plausible, and re-estimate the initial parameters to guide the model out of a local minima, when the parameters are nonsensical or implausible.[92]

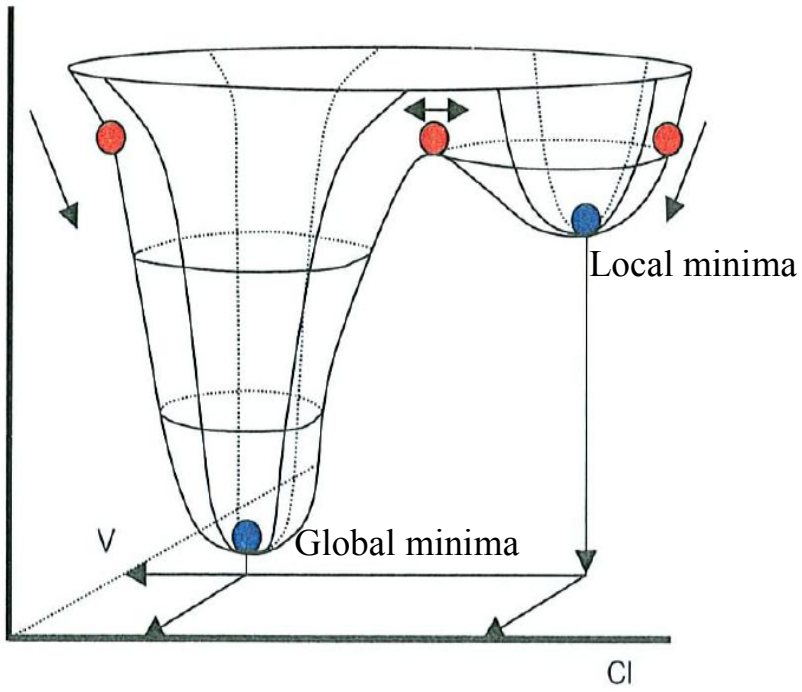

Figure 2-11: Local vs global minima[92]

A limitation in modelling when using the -2 log likelihood surface is that the exploration of the surface can be caught in a cavity of the surface known as a local minimum. This cavity is not the optimised parameters and is a result of the model diverting into this surface due to the initial estimated parameters being too far away from the global minima. In the figure the blue dots represent convergence and final parameter estimates. The red dots represent the initial parameter estimates.

For **DS50B** and all other analyses, model building started with the parameters obtained from NCA. In Figure 2-12 is shown a screenshot of the graphical feedback in Monolix® using observed data from **DS50B** in a two-compartment model as an example when predicting initial parameters.

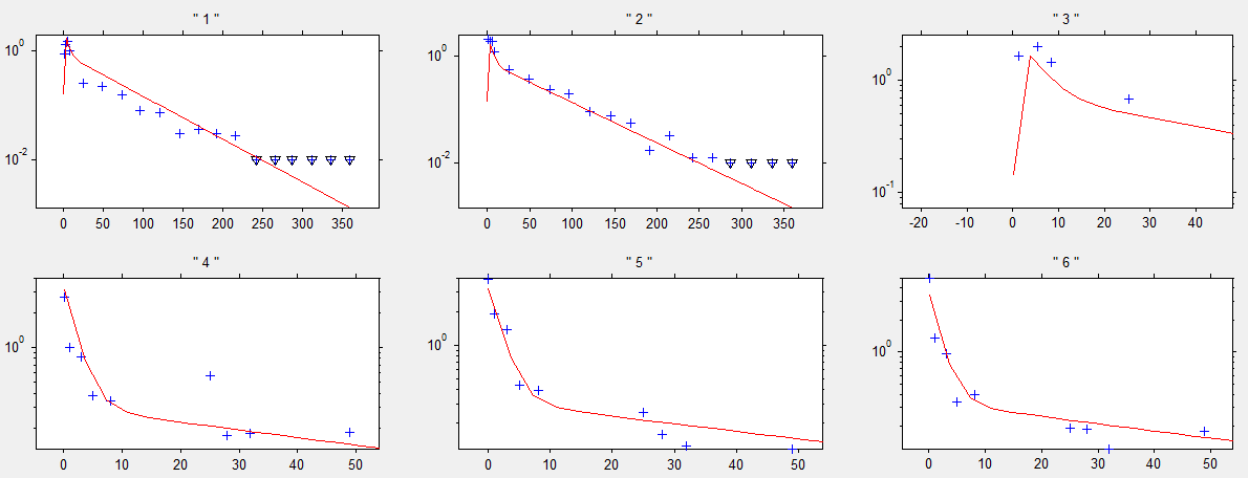

Figure 2-12: Selecting initial parameters

Initial parameter selection for **DS50B** defined by a two-compartment model with parameters; bioavailability (Foral), absorption rate (ka), central volume (V), clearance (Cl), inter-compartmental clearance (Q) and peripheral volume (Vp) manually chosen. The graphic feedback allows visualisation of the best population fit (represented by the red line) to the observed data (blue crosses) and below limit of quantification time points (triangular blue crosses). The plot for individual mouse "3" is a mouse from the oral group and has been zoomed in as example to confirm if the rate of absorption (ka) and bioavailability (Foral) is a close approximation.

The model is run and the -2LL examined for improvement. If a significant improvement in -2LL occurs with the same model, but different initial parameter estimates occur, a local minimum was likely present.

An important consideration when dealing with -2LL values is that the values are abstract when viewed by themselves. They can only be used to compare models and support whether one model is statistically more significant than the other. This comparison must also only occur for nested models that fit within each other. A nested model is considered as a smaller, simpler model fitting into a larger more complex model, described by their structure and equations. The structural models are nested as can be seen from the structure diagram and their differential equations. For example, comparing the two-compartment to the one compartment model, if the inter-compartmental clearance (Q) were fixed to zero, it would again be a one-compartment model. The -2LL values themselves differ greatly between non-nested models and are not an indication of their importance. The -2LL value therefore only serves to guide the backwards and forwards development of the inclusion and exclusion of parameters.

2.4.5.2.2 A description of the visual predictive check graphic

A visual predictive check (VPC) is a simulation-based diagnostic used to visualise how the distribution of the experimental data compares with the model predictions. In a VPC, simulations

from the model are used to obtain confidence intervals for where the model predicts several percentiles of the incomplete data to be. The corresponding percentiles from the original data are then checked for consistency against the model-based confidence intervals, highlighting data points or sections of the profile that are not well represented by the model.[93–97] In the studies that use three subjects per group, only the 50th confidence percentile was used to assess whether the model could account for the observed data. In Figure 2-13 is shown the A: intravenous and B: oral VPC of the **DS50B** model respectively.

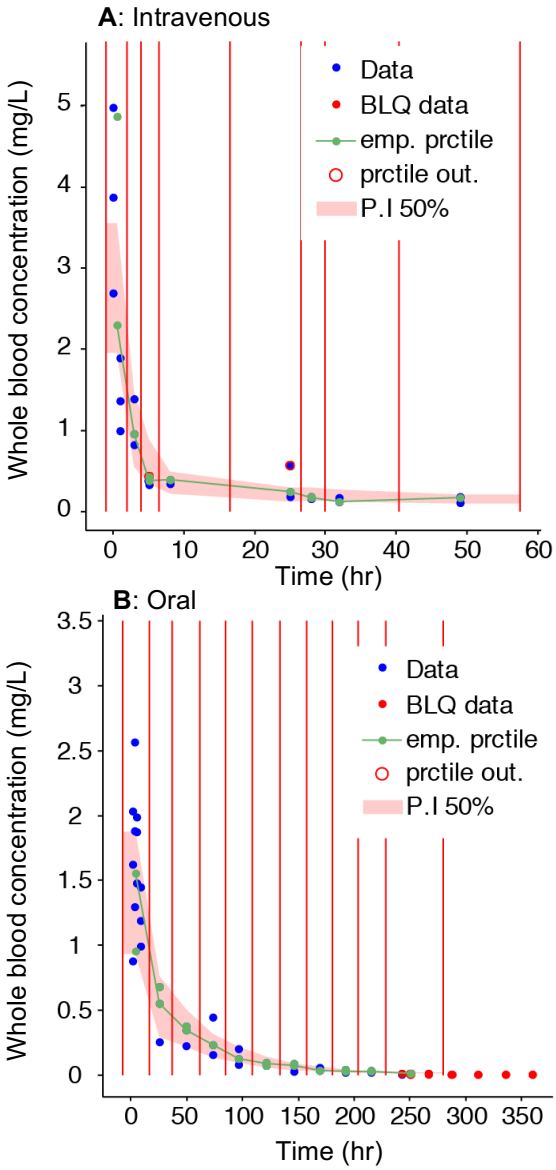

Figure 2-13: Visual predictive check of A: DS50B intravenous data and B: DS50B oral data. The graphical diagnostic plot shows the simulated output of the A: intravenous observed data vs the B: oral observed data (blue dots) of the **DS50B** *in vivo* pharmacokinetic experiment modelled as a two-compartment model. The red dots represent simulated concentration time points below the limit of quantification (BLQ = 10 ng/ml) data. The data input consisted of pooled oral and intravenous data. The oral and intravenous visual predictive checks were stratified to compare the two experimental groups. The green line represents the empirical percentile of the observed data and the shaded pink area represents the median of the population estimate. Ideally, this empirical percentile should fit within the pink shaded area.

In the oral profile, the BLQ data represented by red dots are simulated BLQ data, meaning the values that the model estimated are shown and can be seen decreasing to zero. The red vertical lines represent bins, which correspond to the data distribution. In this case, a minimum bin number was set to the experimental group number of three i.e. every bin as denoted by the space between the red vertical lines contain at least three data points. Where the red lines are closer, more sampling occurred and, for example, as can be seen for the intravenous data between 8 and 24 hrs, sampling was sparser. Importantly, the empirical percentile represented by the green line and the median percentile represented by the pink shaded area changes according to the bin number to best represent the distribution of the data and should be appropriately changed. Setting a high bin number can manipulate a VPC to appear better than the actual observed data and all presented VPC's were set to a minimum bin number of three, except for amodiaquine that evaluated a group size of 10.

2.4.5.2.3 A description of the individual fits

Additionally, individual fits were used to assess if there were major outliers in the group and if the model could approximate well for all individuals in the cohort. Figure 2-14-A and B show the individual fits for the most deviating individual oral and intravenous mice in the **DS50B** experiment respectively.

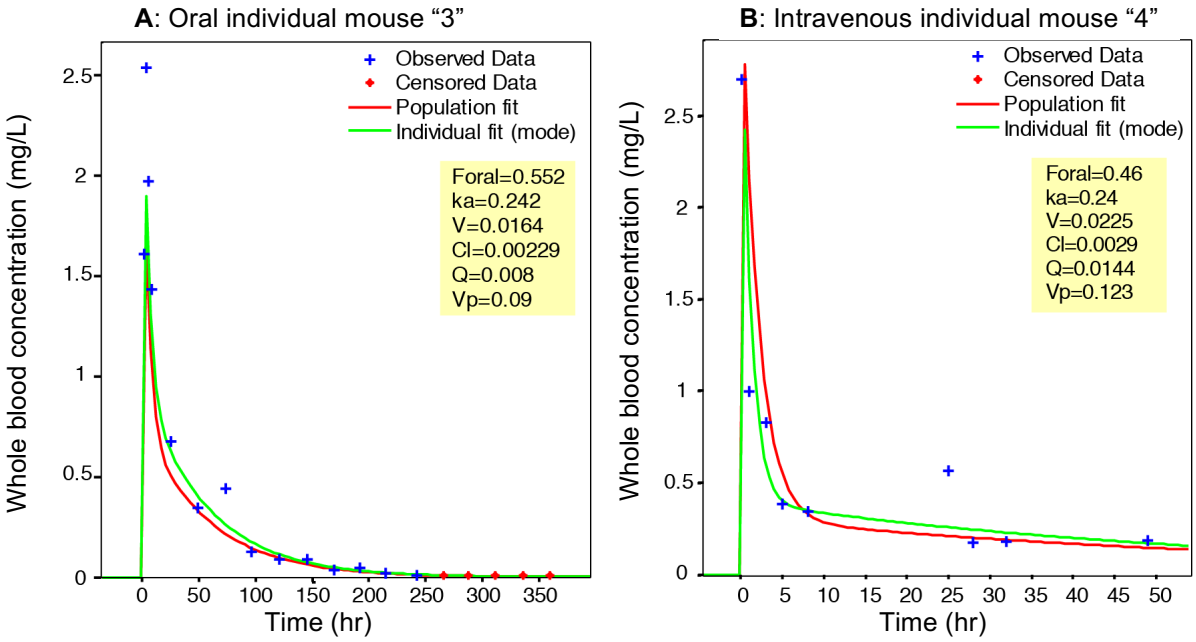

Figure 2-14: Individual fit of DS50B experiment A: Oral mouse "3" and B: Intravenous mouse "4"

The graphical diagnostic individual fit output of individual mouse "3" that was in the oral experimental group and individual mouse "4" that was in the intravenous group. The blue crosses represent the observed concentration data points from the experiment, the red stars represent the "censored" or below limit of quantification (BLQ) data and the green line represents the individual fit after parameter variability for respective individual mice are included. The population fit represented by the red line, is the median of the cohort of both the oral and intravenous groups. The individual parameters of each mice are shown in the yellow legend.

The Foral and ka for the intravenous plot is not factored in the final simulation, and represents the median values as determined by the population model. In these plots, outlying data points at 56 hrs for the oral group, and 25 hrs for the intravenous group can be seen. These were likely due to experimental error during extraction, and explain these individual plots resulting in the most deviation.

*2.4.5.3 Example of **DS50B** structural model results*

Starting with the one-compartment model, initial fixed effects equal to the NCA results were introduced and the model allowed to optimise the values. Optimisation struggled and results and diagnostic outputs proceeded with errors, meaning the model could not accurately find convergence of the parameters. The final -2LL was recorded as -22.47. As stated previously, this is an arbitrary value and can only be used in comparison with another nested model. In Figure 2-15 and Figure 2-16 is shown the intravenous VPC and the individual fit of intravenous mouse "4"

respectively. The difficulty in modelling was unsurprising considering the linear-log plot of **DS50B**'s intravenous data showed non-linearity that a one-compartment model would likely not be able to account for. Nevertheless, in modelling it is important to build up from the simplest foundation and not allow bias in observational data.

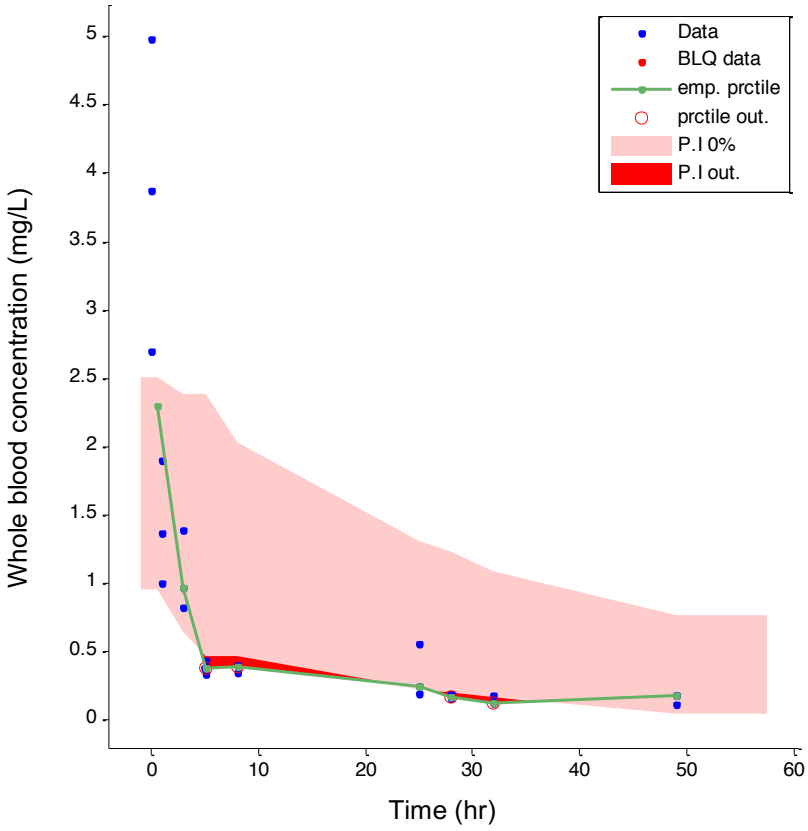

Figure 2-15: DS50B one-compartment model intravenous visual predictive check

The graphical diagnostic plot shows the simulated output of the intravenous observed data of the **DS50B** *in vivo* pharmacokinetic experiment modelled as a one-compartment model. The data input consisted of both the oral and intravenous data. The visual predictive check (VPC) was divided to see how the two experimental groups compare to the model and the intravenous plot shown here. The green line represents the empirical percentile of the observed data and the shaded pink area represents the median of the population estimate. Ideally, this empirical percentile should fit within the pink shaded area. As can be seen in this VPC, the structural model could not account for the rapid decrease in concentration to hour 8 and then slower elimination over time. The prediction interval that falls out of the simulation is represented by the red area and individual observed data points that cannot be predicted for circled in red.

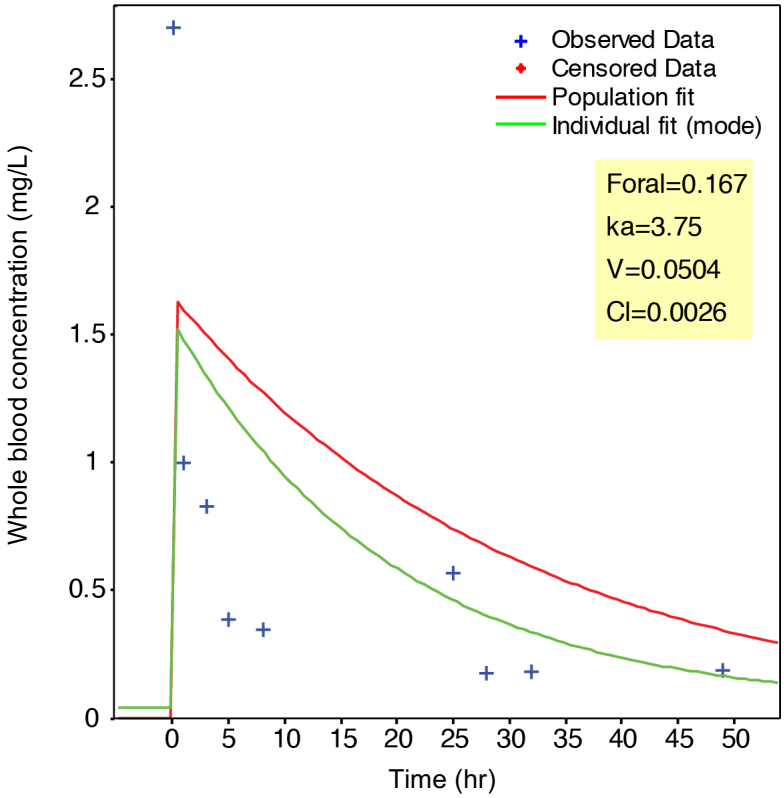

Figure 2-16: DS50B one-compartment model individual fit

The graphical diagnostic individual fit output of individual mouse "4" that was in the intravenous group. The blue crosses represent the observed concentration data points from the experiment and the green line represents the individual fit after parameter variability for the individual mouse is included. The population fit represented by the red line, is the median of the cohort of both the oral and intravenous groups. The individual parameters of each mice are shown in the yellow legend. The population fit is unable to account for the individual data and the individual fit poorly corresponds to the observed data.

Next a two-compartment model was attempted and initial fixed parameters from the previous one-compartment model used and parameters altered significantly according to the graphical output, shown previously in Figure 2-12 to find the best starting point for parameter optimisation. The model could converge and find the optimised parameters and a reduction in -2LL of 105.26 points. Considering the two additional degrees of freedom due to parameters, Vp and Q would require a reduction of 5.88 points in -2LL, the two-compartment structural model was deemed a statistically significant improvement.

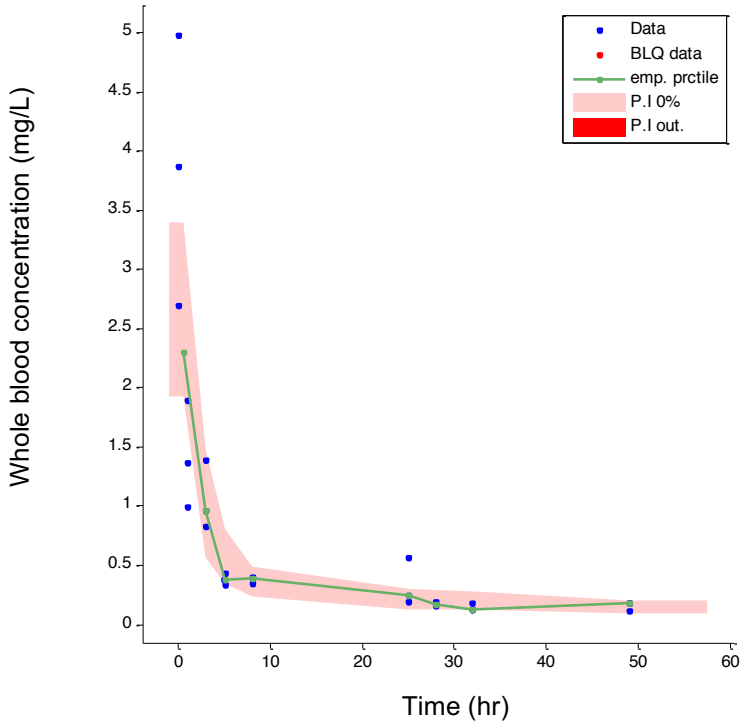

Figure 2-17: DS50B two-compartment model intravenous visual predictive check

The graphical diagnostic plot shows the simulated output of the intravenous observed data of the **DS50B** *in vivo* pharmacokinetic experiment modelled as a two-compartment model. The data input consisted of both oral and intravenous data. The visual predictive check (VPC) was divided to see how the two experimental groups compare to the model, with the intravenous VPC shown here. The green line represents the empirical percentile of the observed data and the shaded pink area represents the median of the population estimate. Ideally, this empirical percentile should fit within the pink shaded area. Individual observed data points that cannot be predicted for are circled in red.

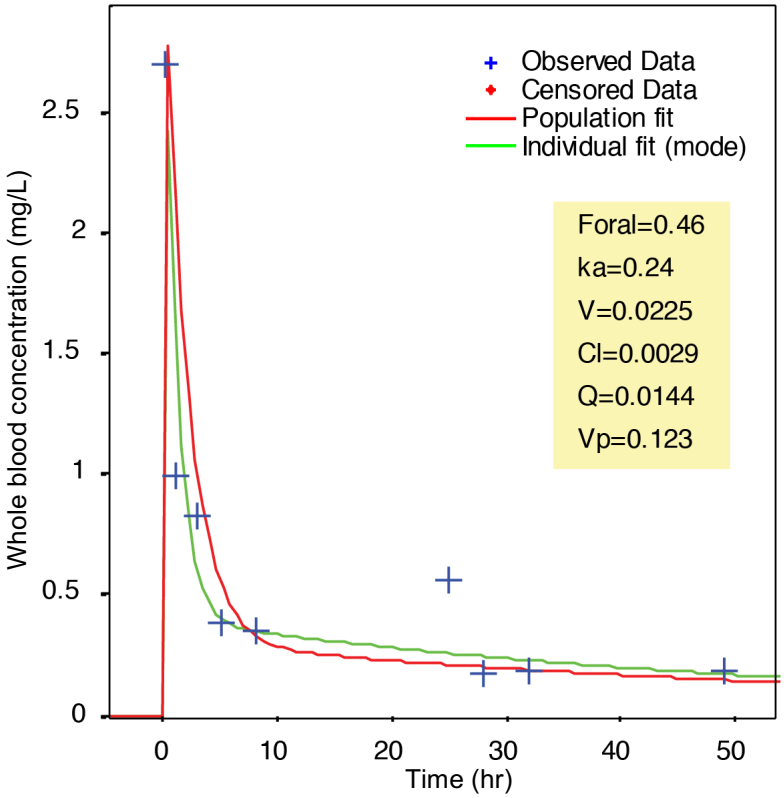

Figure 2-18: DS50B two-compartment individual fit

The graphical diagnostic individual fit output of individual mouse "4" that was in the intravenous group. The blue crosses represent the observed concentration data points from the experiment and the green line represents the individual fit after parameter variability for the individual mouse is included. The population fit represented by the red line, is the median of the cohort of both the oral and intravenous groups. The individual parameters of each mice are shown in the yellow legend. The population and individual fit lines are better able to correspond to the observed data.

A three-compartment model was then attempted to observe if it could provide significantly better estimates of the parameters. Again, the initial fixed effects results from the previous model were used and adapted to best fit the graphical output. The model could converge on optimised parameters and the reduction in -2LL was 2.43 points. This was deemed an insignificant statistical improvement on the previous structural model and the graphical outputs confirmed improved results seen in corresponding VPC and individual plots, Figure 2-19 and Figure 2-20.

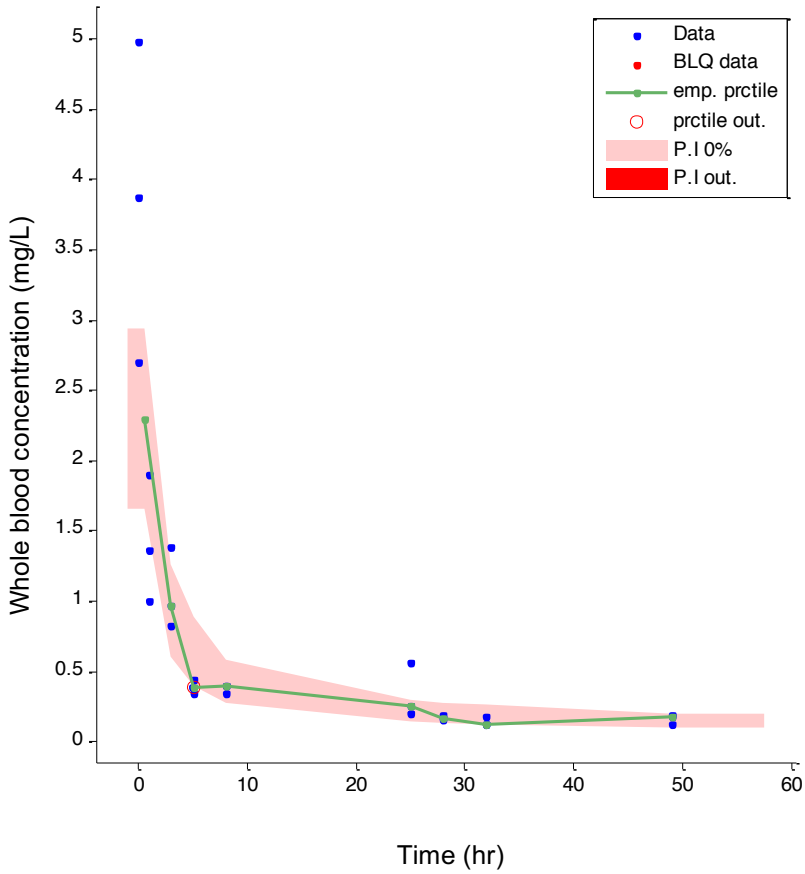

Figure 2-19: DS50B three-compartment model intravenous visual predictive check

The graphical diagnostic plot shows the simulated output of the intravenous observed data of the **DS50B** *in vivo* pharmacokinetic experiment modelled as a three-compartment model. The data input consisted of both oral and intravenous data. The visual predictive check (VPC) was divided to see how the two experimental groups compare to the model, with the intravenous VPC shown here. The green line represents the empirical percentile of the observed data and the shaded pink area represents the median of the population estimate. Ideally, this empirical percentile should fit within the pink shaded area. Individual observed data points that cannot be predicted for are circled in red.

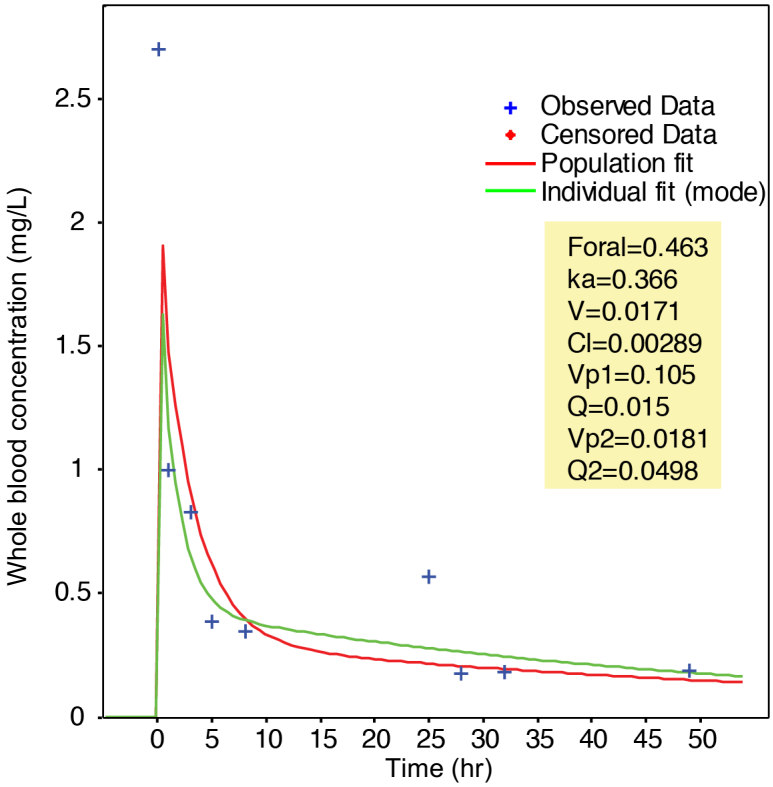

Figure 2-20: DS50B three-compartment individual fit

The graphical diagnostic individual fit output of individual mouse "4" that was in the intravenous group. The blue crosses represent the observed concentration data points from the experiment and the green line represents the individual fit after parameter variability for the individual mouse is included. The population fit represented by the red line, is the median of the cohort of both the oral and intravenous groups. The individual parameters of each mice are shown in the yellow legend. The population and individual fit lines are better able to correspond to the observed data, but shows no significant improvement on the two-compartment model.

Structural model choice then regressed back to the more appropriate two-compartment model. In the simulations, it could be seen that the ka value was able to accurately account for absorption. To satisfy expectations, a Tlag function was added to the two-compartment model to review if it could significantly improve model outputs. In Figure 2-21 is shown the structural model used. The -2LL increased by 0.10 point and the Tlag was estimated to be 0.0062 hrs with relative standard error recorded at 117171%, meaning the model could not make sense of this parameter. This additional parameter was not only statistically insignificant, but caused great difficulty for the model to predict as the absorption amount by the rate of absorption needed to be present instantaneously in the absorption compartment as the concentration in the central compartment shows. Physiologically this fits due to the oral gavage that is used on the mice. The dose amount is instantaneously deposited in the absorption compartment (gut) in suspension form where the particles either are already in solution or finely distributed. The Tlag function is important for

dosing where a lag in transit time to the absorption compartment is expected, such as transit to the absorption site, disintegration of a tablet or capsule, deaggregation of particles and dissolution in the surrounding environment to be available for absorption.[21,98]

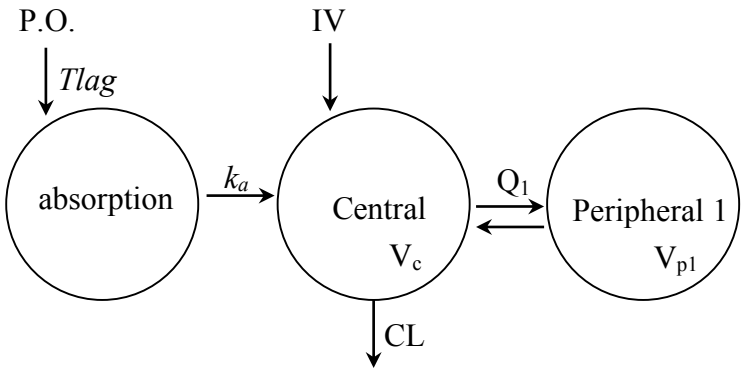

Figure 2-21: Two-compartment model with Tlag function

The Tlag function was therefore excluded and with the structural model firmly established, the statistical model could be addressed.

2.4.5.4 Statistical model

Each fixed effect parameter of the two-compartment model **DS50B** (Foral, ka, CL, Vc, Q and Vp) has its own variability parameter in the model described as omega parameters. This encompasses between subject variability, distribution variance and any variability found specific to the parameter in question. Additionally, there is also the residual or unexplained variability that cannot be accounted for and form the sigma parameters. The same process of simplifying the model as much as possible applies to these statistical models as well. Originally, during the model building process, all omega and sigma variables were included, meaning each fixed parameter had its own omega value and the sigma model allowed combined residual variability allowing constant or proportional error on the concentration values. The significance of these parameter inclusions to the final model was assessed by removing the parameters stepwise and similarly as explained for the structural model, observing notable decreases in -2LL, VPC and individual plots. For **DS50B**, omega parameters of clearance and volume fixed effects were low enough to be eliminated, and constant sigma variability was deemed statistically insignificant in the final model. Elimination of all these parameters resulted in a mere increase in -2LL of 1.44, showing they did not add value to the final model.

In Table 2-2 is shown the final parameters of the **DS50B** model.

Table 2-2: DS50B two-compartment model results

	Parameter	s.e. (lin)	r.s.e.(%)
Fixed effects:			
Foral	0.46	0.074	16
ka (hr^{-1})	0.24	0.06	25
V (L)	0.0186	0.0028	15
Cl (L/h)	0.00251	0.00016	6
Q (L/h)	0.0072	0.0017	23
Vp (L)	0.102	0.007	7
Covariate model:			
Beta Vp (tWEIGHT)	1	-	-
Beta V (tWEIGHT)	1	-	-
Beta Cl (tWEIGHT)	0.75	-	-
Parameter variability:			
Omega Foral	0.253	-	-
Omega ka	0.0603	0.65	1.09E+03
Omega V	0	-	-
Omega Cl	0	-	-
Omega Q	0.461	-	-
Omega Vp	0	-	-
Sigma model			
Proportional	0.308	0.0094	3
Constant	0	-	-

Note: Foral; bioavailability, ka; rate of absorption, V; central volume, Cl; clearance, Q; inter-compartmental clearance, Vp; peripheral volume. Standard error (s.e.) and relative standard error (r.s.e) expressed as a percentage of the population estimate were estimated by linearization of the Fisher information matrix. The covariate tWEIGHT is defined as the transformed log individual mass of each mouse centred around the median of the cohort mass. Parameter values equal to 0, such as Omega V are parameters that were excluded from the model based on their statistical insignificance as determined by -2LL.

The beta parameters denoted results from the covariate model as explained in the data input section, where clearance and volumes were allometrically scaled by the transformed weight of each individual mouse.

Standard error values were calculated by linearization of the Fisher Information Matrix. This is a way of measuring the amount of information that all observable random variables carry around the distribution of the population models. It includes the fixed effect parameters, the covariate model, omega variables and sigma variables.

Subsequent compound NLME modelling fixed parameters and statistical model results, such as that shown in Table 2-2 are presented in Chapter 7, page 197.

In subsequent chapters the results of only the VPC without bins marked are shown. As stated previously all VPC output settings were described as a minimum bin number of 3, except amodiaquine which used 10 animals per group and therefore used a minimum bin number of 10. All individual fits are presented in the experimental chapter. The -2LL values are not included because as described they are abstract values and only guide model building and specific reduction or increase are quoted in the results section.

2.4.5.5 Comparing methods

To compare NLME results to NCA, all parameters and standard errors were converted to the units commonly used for preclinical pharmacokinetic data. Additionally for the NLME parameters, C_{max} values were estimated from the individual plots and the half-life calculated by the PK Parameter Conversion Excel spreadsheet from S.L Shafer.[99] AUC for the oral profiles were determined using the pharmacokinetic equation:

$$AUC = \frac{Dose\ x\ Bioavailability}{Clearance}$$

Standard error in the case of AUC and half-life, were estimated by the square root of the summed squared relative standard errors of the relevant parameters. The new calculated relative standard errors were then converted to standard error.

In subsequent chapters, the NLME data alongside the NCA parameter estimation with their respective standard errors is tabulated. The parameter estimates should be compared, but the standard errors cannot be compared. The NCA standard errors are merely calculated as the deviation from the mean divided by the square root of the group number. As mentioned the standard error calculation for NLME includes the structural model, the covariate model, the omega model and sigma model around the population fit. The standard error has no bearing on the quality of the model or parameter estimated, but rather just the data as observed in the final model.

When comparing NCA and NLME results it is important to remember that the NLME results are fundamentally more appropriate than NCA on both physiological and mathematical grounds. In the case of **DS50B**, the fact that non-linear elimination occurred means modelling will obtain the best parameter estimates. The objective of comparing the NCA and NLME results is to observe how significant the deviations are in a preclinical setting. Here the school of thought remains that

the ease of NCA implementation compared to NLME is more valuable than accuracy gained in pharmacokinetic parameters at this early screening stage.

Additionally, to refine the project objectives and evaluate the least amount of days that would result in an accurate estimation of the pharmacokinetic results, the data sets were reduced to 1, 2 and 5 days and the model allowed to predict the parameter estimates.

2.4.6 PK/PD simulation

To compare the modelling pharmacokinetic results to the efficacy results obtained by the Swiss Tropical and Public Health Institute (Basel, Switzerland), additional simulations were run in Berkeley Madonna version 8.3.18 (Berkeley Madonna Inc., Berkeley, CA, USA). Berkeley Madonna is a differential equation solver that allows simulations to be performed in milliseconds. It is a very useful tool that allows instantaneous feedback for pharmacometric analysis requiring simplicity and ease of implementation.[100] The pharmacokinetic population parameters calculated by the most appropriate model, were input with coded differential equations describing the structural model.

The dose amount and frequencies were changed according to the efficacy experiment and their respective AUC, C_{max} and time above antiplasmodial NF54 IC_{50} ($T>IC_{50}$) values extracted for a 30 day simulation, equal to that of the efficacy experiment.

2.4.7 Data subset analysis

While NCA could not calculate the pharmacokinetic parameters of the compounds that had incomplete elimination data, NLME modelling might. To investigate the robustness of NLME modelling for extrapolating parameters from incomplete data, the final 15-day dataset was reduced to 24 hrs, 48 hrs and 120 hrs and input in Monolix® and re-estimated. The same model building progression as previously described was used to assess the smallest dataset for which NLME could still accurately predict parameters.

2.4.8 In vitro ADME methods

Following the pharmacokinetic results obtained, investigation of the *in vitro* absorption, distribution, metabolism, elimination (ADME) properties of the compounds were performed with the aim to clarify the great differences in clearance, and volumes observed for **DS48B** in relation to those of **DS50B** and **DS23B**.

Under supervision of the author of this thesis, the compounds were submitted to the Drug Discovery and Development Centre (H3D), University of Cape Town (South Africa). Ms Nina Lawrence and colleagues at H3D, performed the technical portion of the parallel artificial membrane assay (PAMPA), kinetic solubility [evaluated at pH 2 and pH 6.5 in phosphate-buffered saline, and pH 6.5 in fasted state simulated intestinal fluid (FaSSIF) buffer], lipophilicity assay and a 5-point microsomal stability assay for each compound. The author of this thesis performed the blood plasma partitioning assay.

2.4.8.1 Parallel artificial membrane assay (PAMPA)

For the PAMPA assay, the permeation of the test compounds across an artificial hexadecane membrane first introduced by Kansy *et al* (1998)[101] was examined as quantified by LC-MS/MS. The assays were performed in triplicate in 96-well MultiScreen Filter plates (Millipore, 0.4μM PCTE Membrane). Membrane filters were pre-coated with 5% hexadecane in hexane and allowed to dry prior to the assay. A membrane integrity marker, Lucifer yellow was added to the pre-coated MultiScreen plate donor/drug solution wells meant to measure integrity of the membrane. Phosphate buffer at a pH of 7.4 was added to the 96-well acceptor plate. The test compound previously dissolved in DMSO at a concentration of 10 mM, and stored at -20°C prior to use was spiked into the donor buffer at physiologically relevant pH's (pH4, 6.5 and 8) at a final concentration of 1 μM. The donor plate was then slotted into the acceptor plate and incubated for 4 hours at 25°C with gentle shaking (40 – 50 rpm). Following the incubation, samples from the acceptor wells and theoretical equilibrium wells were transferred to the analysis plate and the matrix matched with donor buffer. Acetonitrile containing the internal standard carbamazepine at a concentration of 0.0236 μg/mL was added to all samples. The samples were analysed by LC/MS/MS (Agilent Rapid Resolution HPLC, AB SCIEX 4000 QTRAP MS). The instrument response of analyte to internal standard peak areas were used to calculate the apparent permeability (P_{app}) in cm/s as follows:

$$P_{app} = Constant - \left(\ln\ 1 - \frac{I_{acceptor}}{I_{equilibrium}} \right)$$

Where:

$$Constant = \frac{V_D\ x\ V_A}{(V_D + V_A)\ x\ A\ x\ time}$$

The analyte to internal standard peak area ratio of the test compound in the acceptor compartment represents the instrument response for the acceptor compartment test compound amount ($I_{acceptor}$) and similarly the test compound to internal standard ratio of the combined total donor and acceptor compartments represent the Instrument response for samples at equilibrium ($I_{equilibrium}$).

The constant used is calculated by the acceptor compartment volume equal to 0.25 cm^3 (V_A) and the donor compartment volume (V_D) equal to 0.15 cm^3. The accessible filter surface area (A) is equal to 0.24 cm^2 and time is equal to the total incubation time represented in seconds.

Membrane integrity was assessed by calculating the P_{app} of Lucifer Yellow with acceptable criteria values less than 50 nm/s evaluated by a Modulus microplate reader with excitation 490 nm/emission 510 – 570 nm values used.[102]

2.4.8.2 Kinetic solubility

Kinetic solubility assays were performed using the miniaturised shake flask method.[103,104] The same 10 mM stock solutions of each of the test compounds prepared in DMSO described previously were used to prepare calibration standards ranging from 10 to 220 µM in DMSO. The 10 mM stock solution was spiked at a volumetric ratio of 1 to 50 in phosphate buffered saline at pH 6.5, 0.01M hydrochloric acid equal to pH 2 and FaSSIF at a pH of 6.5. This was done in duplicate and resulted in a final DMSO concentration of 2%. The samples were slowly shaking for 2 hours at 25°C and were then filtered and analysed by means of HPLC-DAD (Agilent 1200 Rapid Resolution HPLC with a diode array detector). The aqueous samples' solubility concentrations were calculated by the best fit calibration curves constructed using the calibration standards.

2.4.8.3 Metabolic stability assay

The metabolic stability assay used a 5-point liver metabolic stability method. The assays were performed in duplicate in 96-well micro titre plates. The test compounds diluted from their stock solution to 0.1 µM were incubated individually in mouse, rat and pooled human liver microsomes (0.4 mg/mL) at 37 °C in the presence and absence of the cofactor nicotinamide adenine dinucleotide phosphate (NADPH) at a concentration of 1 mM. The predetermined time wells were quenched by adding 300 µL of ice cold acetonitrile containing internal standard (carbamazepine, 0.0236 µg/mL) at either 0 min, 5 min, 10 min, 30 min or 60 min. Test compounds in the supernatant were quantified by means of LC/MS/MS (Agilent Rapid Resolution HPLC, AB SCIEX 4000 QTRAP MS).

The quantified concentrations vs time points were used to determine the Obach intrinsic clearance (Cl_{int}) using the substrate depletion approach.[105,106] The rate of elimination (k) was determined from the negative linear regression of the log concentration profile. Intrinsic clearance could then be calculated as follows

$$Cl_{int} = k\ x\ \frac{incubation\ volume}{mass\ microsomal\ protein}\ x\ (45\ microsomes/liver) x\ Z$$

The incubation volume for these experiments were 0.1 ml, while the mass of microsomal protein per well was 0.036 mg. The expression Z refers to the liver organ mass in mg per species body weight in kg, which used the following constants from Richmond *et al* (2010) shown in Table 2-3.[107]

Table 2-3: Constant Z that represents liver organ mass in mg per kg of species body weight

Species	Z (Liver mass mg per kg body weight)
Human	25.7
Rat	40
Mouse	87.5

The *in vitro* half-life could then also be calculated by the negative elimination rate constant (k), $t_{1/2} = \ln(2)/k$.

Predicted hepatic extraction ratio (E_H) was calculated by

$$E_H = \frac{Cl_{int}}{Q + Cl_{int}}$$

With hepatic blood flow in ml/min/kg (Q) determined by constants calculated from Davies & Morris (1993), shown in Table 2-4.[108]

Table 2-4: Q constant representing hepatic blood flow

Species	Q (Hepatic blood flow in ml/min/kg)
Human	20.7
Rat	55.2
Mouse	90

2.4.8.4 Lipophilicity

The lipophilicity assays were performed using a shake-flask procedure from a modified method from Alelyunas *et al* (2010).[109] The previously mentioned 10 mM stock solutions of each test compound were spiked into a 1:1 mixture of phosphate buffer (pH 7.4) and *n*-octanol to a final concentration of 100 µM. The solutions were shaken vigorously (1500 rpm) on an orbital shaker for 3 hours at 25°C. Thereafter the samples were centrifuged in order to fully separate the aqueous and organic layer. The samples were analysed by HPLC-DAD (Agilent 1200 Rapid Resolution HPLC with a diode array detector) and the peak areas used to determine the partition coefficient, ($LogD_{7.4}$) as follows:

$$Log\ D_{7.4} = Log_{10}\left(\frac{peak\ area\ of\ octanol\ phase}{peak\ are\ of\ the\ buffer\ phase}\right)$$

2.4.8.5 Plasma protein binding

Plasma protein binding was measured using an ultracentrifugation method. The assays were performed in a 96-well microtiter plate with pooled human plasma, spiked with the previously mentioned stock solutions of test compound to a final concentration of 1 µg/ml and the assays performed in duplicate. A volume of 40 µl of the spiked plasma was immediately removed and quenched using 200 µl of ice-cold acetonitrile, containing 0.0236 µg/ml internal standard carbamazepine and stored at -20°C. This served as the total compound amount reference samples. After incubating the remaining plasma samples at 37°C for 1 hr, the samples were transferred to ultracentrifugation tubes and ultracentrifuged for 4 hrs at 37°C (42,000 rpm) (Optima L-80XP; Beckman). A volume of 40 µL supernatant was extracted and quenched with the internal standard containing ice-cold acetonitrile. Analyte concentrations of all compounds and sample types were determined by means of LC/MS/MS (Agilent Rapid Resolution HPLC and AB Sciex 4000 QTRAP MS). The peak area ratios of compound to internal standard were used to determine

instrument response for the reference and supernatant samples. Plasma protein binding could then be calculated as follows:

$$\%Plasma\ Protein\ Bound = \frac{I_{ref} - I_{SN}}{I_{ref}}\ x\ 100$$

Where: I_{ref} = Instrument response from the total compound amount; and I_{SN} = Instrument response from the supernatant.

2.4.8.6 Red blood cell to plasma partitioning coefficient

Blood plasma partitioning was evaluated by the author of this thesis. Using a LC/MS/MS based depletion method adopted from Yu *et al*. (2005)[110] with slight modification. Atenolol, propranolol, and chloroquine were used as controls and a structurally similar compound from the **DS** series was used as internal standard.

Blood plasma partitioning ratio was determined by measuring the concentration of the drug from centrifuged whole blood plasma after equilibration to a carefully defined plasma control incubated at the same time (reference plasma), thus eliminating the use of different matrices. Since both the equilibrating plasma and reference plasma are identical, the instrument response factors from both aliquots were the same. Therefore, the analyte peak area ratio to the internal standard could be used as follows:

$$K_{RBC/PL} = \frac{1}{H} \times \left(\frac{I_{RefPl}}{I_{Pl}} - 1\right) + 1$$

Where: $K_{RBC/PL}$ = Blood plasma partitioning, H = haematocrit; I_{RefPl} = Instrument response from the reference plasma; and I_{Pl} = Instrument response from the equilibrating plasma.

Briefly the assay was performed as follows; freshly drawn heparinized human whole blood was divided into a reference plasma control group and an equilibrating group. The reference plasma control volume was centrifuged, haematocrit measured and the plasma collected. The whole blood and reference plasma groups were divided into appropriate aliquots per compound. A 1 mg/ml DMSO primary stock solution of each compound was serially diluted in water to obtain a final spiking solution that resulted in less than 0.1% DMSO in the final sample, ensuring haemolysis did not take place. Both the whole blood and plasma reference groups were spiked with this diluted test compound solution to obtain a final concentration of 500 nM and mixed gently. The samples were then incubated at 37°C for 1 hr. After incubation the whole blood samples were immediately centrifuged and 50 µl plasma collected. The same volume of the reference plasma control group aliquots was taken and the plasma samples extracted with 200 µl ice-cold acetonitrile containing

the structurally similar internal standard. The samples were analysed by LC/MS/MS (Agilent Rapid Resolution HPLC and AB Sciex 4000 QTRAP MS) and the peak areas obtained. All controls passed within 20% of the literature values from Yu *et al*. (2005).[110]

2.5 Results & Discussion

2.5.1 Reinvestigation of the LC/MS/MS method

Analysis of the repeat 56 hr experiments of **DS23B** and **DS50B** showed a rapid increase in pressure on the HPLC system while injecting the initial system check samples to measure instrument response. The peaks of the internal standard **DS48B** had started to tail, Figure 2-22, and showed the column was no longer viable for the extracted batch.

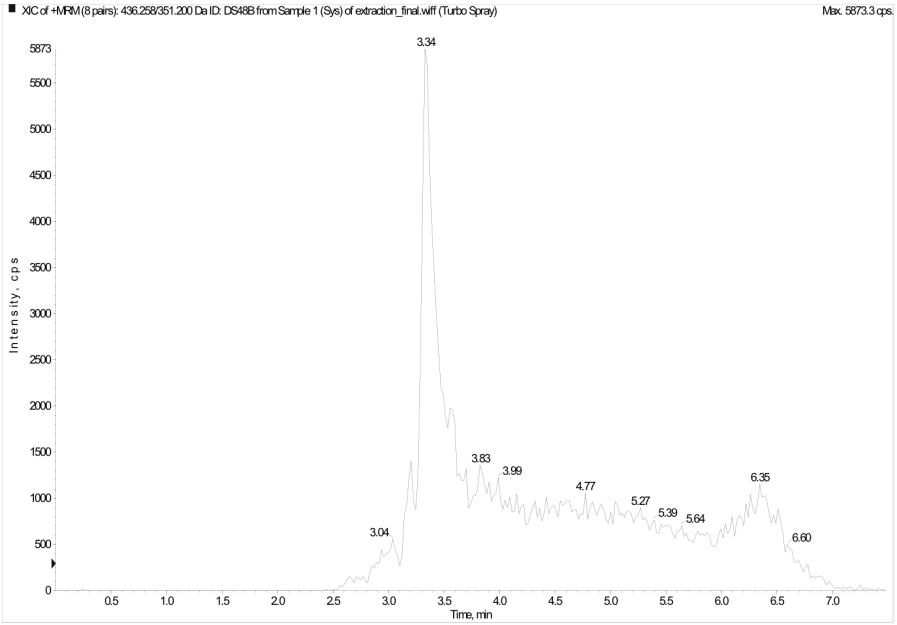

Figure 2-22: Internal standard peak tailing

Internal standard response on Waters Xterra™ MS C18 column used for previous method development showed severe peak tailing, probably due to expiration.

Replacing the Waters Xterra™ MS C_{18} column with a Phenomenex® Kinetex C_{18} (2.1 x 50 mm, 2.6 µm) column showed better chromatography and suitable pressure and the final batch was analysed. Quantitation showed a severe drop in internal standard response for 5 minute intravenous samples in both the **DS23B** and **DS50B** batches, and a mismatch between experimental, and calibration samples was observed. The calibration standards did have acceptable accuracy and precision statistics, but the inconsistent internal standard response required further investigation. Figure 2-23 shows the internal standard peak area over the course of sample injection for the **DS50B** batch.

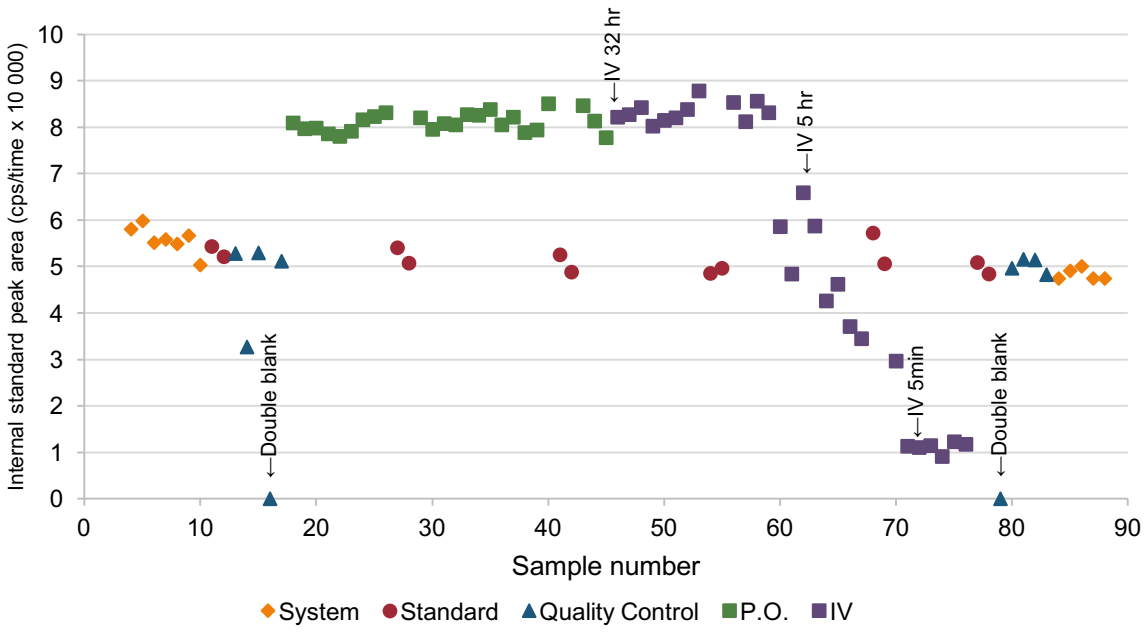

Figure 2-23: Internal standard drop

A drop in internal standard peak area was observed for intravenous(IV) samples in the **DS50B** batch and a general mismatch between experimental and calibration samples.

Following the trend in Figure 2-23, the internal standard response decreased for intravenous samples from injection number 60 as pharmacokinetic sample time increased and was lowest for the 5 minute intravenous samples. The samples were reinjected to ensure the instrument did not lose sensitivity during the batch, but the same trend was observed and the samples were discarded. The oral dosage formulation which hydroxypropyl methylcellulose and intravenous oral formulation, which contained polyethelyne glycol, polypropylene glycol, dimethyl sulfoxide and ethanol, could cause ion suppression of the analytes and internal standard, and would explain the observed trend of increased suppression occurring at the time of dosing and decreasing as the formulation vehicle was eliminated. Excluding the internal standard showed that the intravenous group's concentration increased over time, meaning that the internal standard did compensate for the suppression and had to be included. However, the pharmacokinetic results presented in section 2.5.3 showed that the analyte and internal standard were not suppressed proportionally resulting in **DS23B** being overcompensated and had higher concentrations than expected, namely 5 uM higher intravenous concentration at half the dose of the 7 hr experiment. **DS50B** was undercompensated resulting in a 2-fold lower C_{max} at the same 20 mg/kg oral dose. Table 2-5-A shows reinvestigation of the chromatography using quality control samples spiked with the intravenous formulation at an equal volume ratio as the original injection. Blood containing the

intravenous formulation had a lower response than quality controls spiked with Millipore water to the same expected concentration of the dosage formulation. Redeveloped chromatography that avoided this suppression on a new Waters Xterra™ MS C_{18} (2.1 x 30 mm, 3.5 µm) column with slight modifications to the gradient used in the initial 7 hr pharmacokinetic showed acceptable precision of the peak areas, Table 2-5-B.

Table 2-5: Improving chromatography after discovering ion suppression

A. Ion suppressed Kinetex chromatogram

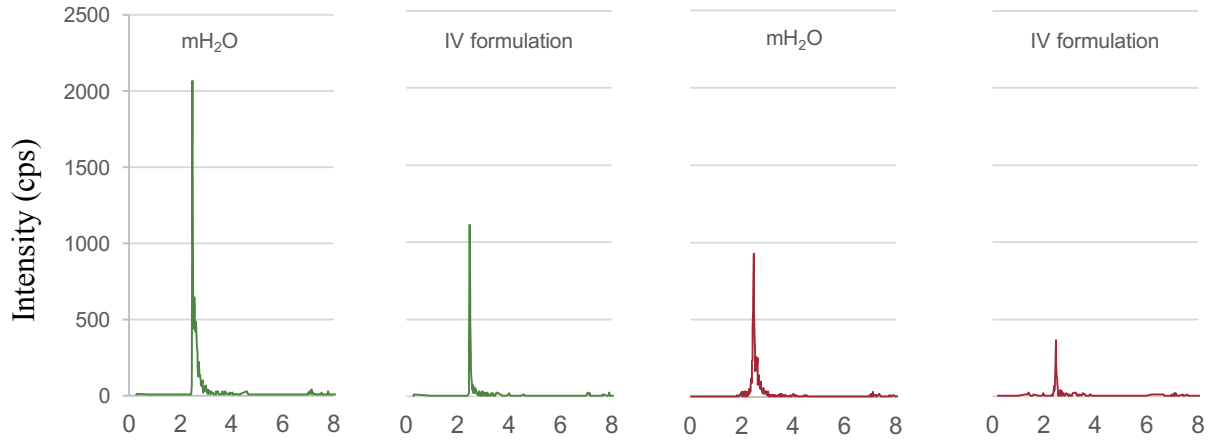

	DS23B	DS23B	DS50B	DS50B
Peak area	9540	2840	6620	1120

B. Improved Xterra chromatogram

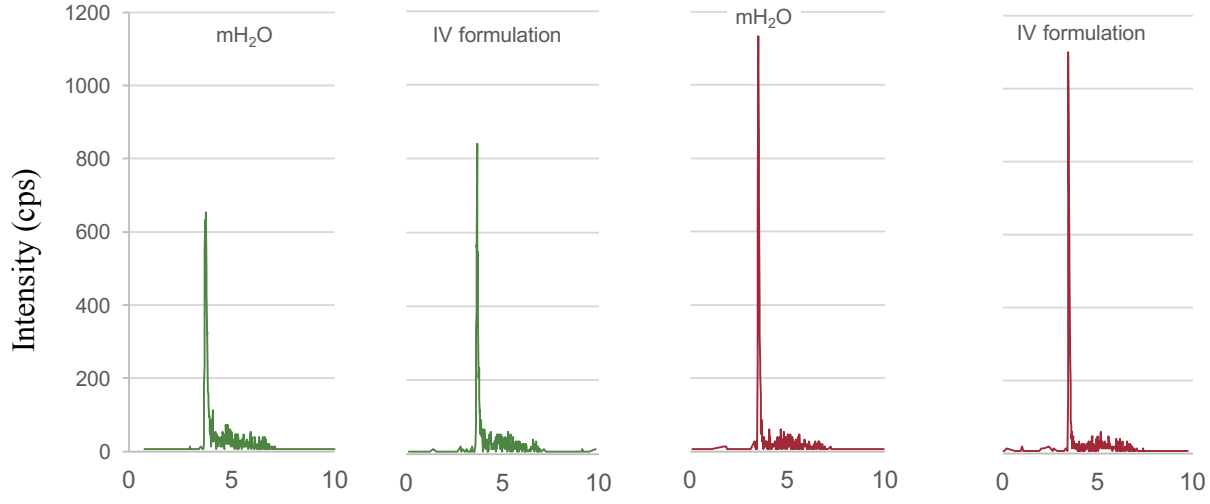

	DS23B	DS23B	DS50B	DS50B
Peak area:	4960	5150	5240	4920

A: Using the same chromatography as the failed 56 hr pharmacokinetic batch, ion suppression from competing formulation background decreased peak area significantly, 29.8% and 16.9% of expected response for **DS23B** (green line) and **DS50B** (red line) respectively. **B**: Changing to a new Xterra column showed improved precision of 96.3% for **DS23B** and 93.8% for **DS50B** between the intravenous formulation and blank matrix.

2.5.2 Incomplete pharmacokinetic profiles

In Figure 2-24 is shown the incomplete pharmacokinetic profiles of **DS23B A**; 7 hour pharmacokinetic experiment after an intravenous dose, **B**; 7 hour experiment after an oral dose, **C**; repeat intravenous experiment and **D**; oral experiment over 56 hrs. Similarly, Figure 2-25 shows the incomplete profiles for **DS50B**. The repeat 56 hrs experiments showed ionisation interference as described in previous Results Section 2.5.1, page 67.

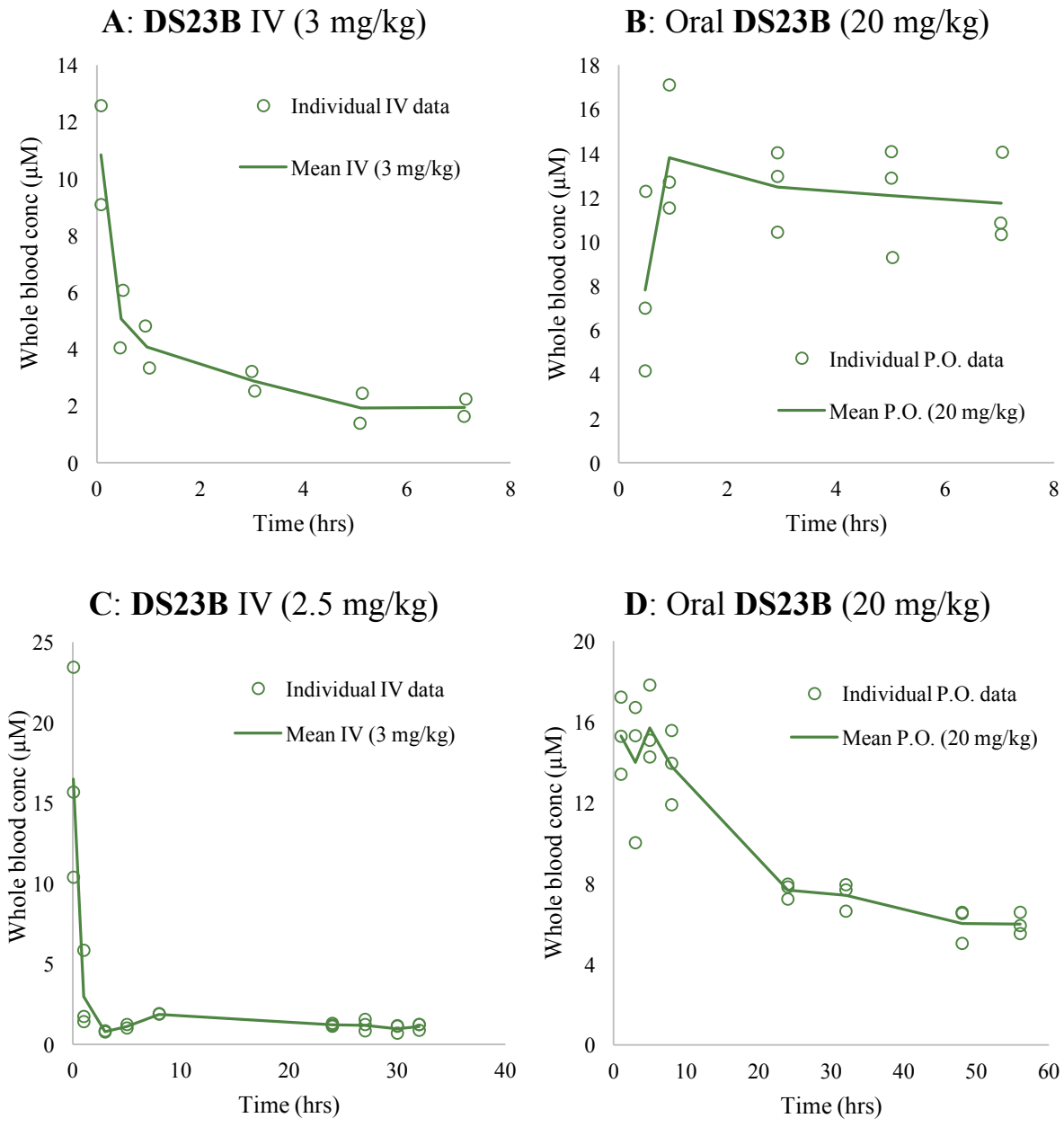

Figure 2-24: Incomplete pharmacokinetic profiles of DS23B

Whole blood concentrations (µM) against time profiles of compound **DS23B** after **A**: 3 mg/kg intravenous (IV) dose, **B**: 20 mg/kg oral dose evaluated over 7 hours. **C**: 2.5 mg/kg intravenous dose evaluated over 32 hours and **D**: 20 mg/kg oral dose evaluated over 56 hours with loss of LC/MS/MS signal and unreliable concentration results for these two profiles. Open circles and the green line respectively represent individual data and the mean concentration data.

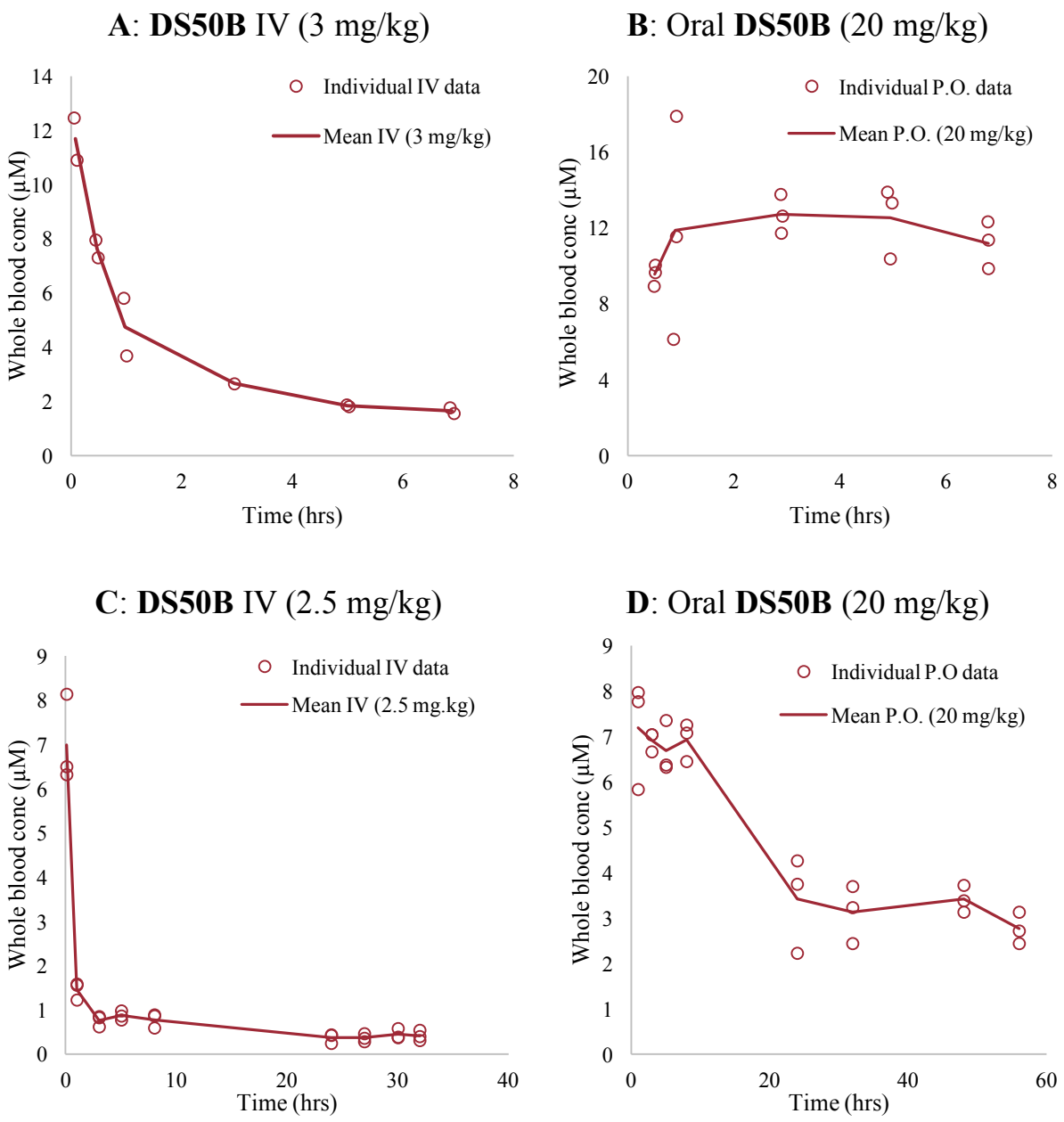

Figure 2-25: Incomplete pharmacokinetic profiles of DS50B

Whole blood concentrations (µM) against time profiles of compound **DS50B** after **A**: 3 mg/kg intravenous (IV) dose, **B**: 20 mg/kg oral dose evaluated over 7 hours. **C**: 2.5 mg/kg intravenous dose evaluated over 32 hours and **D**: 20 mg/kg oral dose evaluated over 56 hours with loss of LC/MS/MS signal and unreliable concentration results for these two profiles. Open circles and the red line respectively represent individual data and the mean concentration data.

Unfortunately, the loss in ionisation described in section 2.5.1, page 67, necessitated another repeat experiment. Linear extrapolation of the natural log concentrations on the final 3 samples of **DS23B** and **DS50B** was done to plan an experiment with the objective of obtaining a full pharmacokinetic profile after a 10 mg/kg dose that could be followed to the lowest level of quantification (LOQ) of 10 ng/ml. In Figure 2-26 is shown the log-linear extrapolation of **A**: **DS23B** and **B**: **DS50B**.

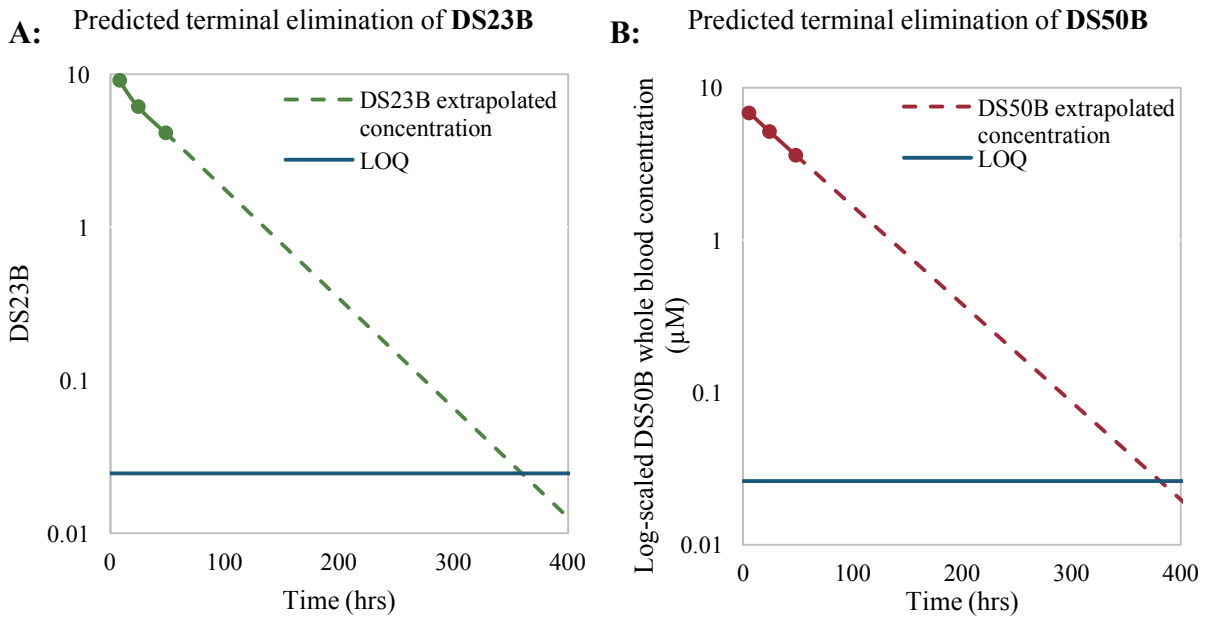

Figure 2-26: Extrapolated concentration data of DS23B and DS50B

Extrapolated semi-log plots of the terminal phase points of **A**: **DS23B** and **B**: **DS50B** from their respective 56 hr experiments. Filled circular data points (green for **DS23B** and red for **DS50B**) represent the mean of the last three measured concentrations and the dashed line represents the extrapolated concentration from these three points. The blue line in both plots represent the lowest level of quantification (LOQ = 10 ng/ml).

The extrapolated data predicted that **DS23B** would reach an LOQ concentration after approximately 360 hrs or 15 days, and for **DS50B** it was predicted that LOQ would be reached at approximately 384 hrs or 16 days. In a rigorous drug discovery setting, a 15 day pharmacokinetic experiment would be impractical. Nevertheless, in this academic setting, it was of interest to see how accurate the extrapolation would be. The repeat experiment, though unfortunate, provided an appealing opportunity to assess if simulated extrapolations were valid. Rarely on a preclinical level is there the opportunity to plan a prospective study of this nature. A 15 day pharmacokinetic study was therefore pursued for the oral groups with sampling occurring every day.

The final results showed that compound **DS50B** was over predicted and reached LOQ at day 10, not 15, and compound **DS23B** reached a concentration of 9.02 ng/ml (s.e. 0.376) on day 15 considered to be a successful prediction.

2.5.3 Final pharmacokinetic results

2.5.3.1 Amodiaquine

In Figure 2-27 is shown the raw data of amodiaquine with observed concentration-time points for 10 mice represented by open circles and a mean solid line added for A: Intravenous and B: Oral experiments. In Table 2-6 is shown the final calculated parameters of Amodiaquine for both NCA and NLME analysis for a side-by-side comparison. A visual predictive check of the final model used is shown in Figure 2-28 and stratified by oral and intravenous groups. The model best fit a 2-compartment model as described in section 2.4.5.

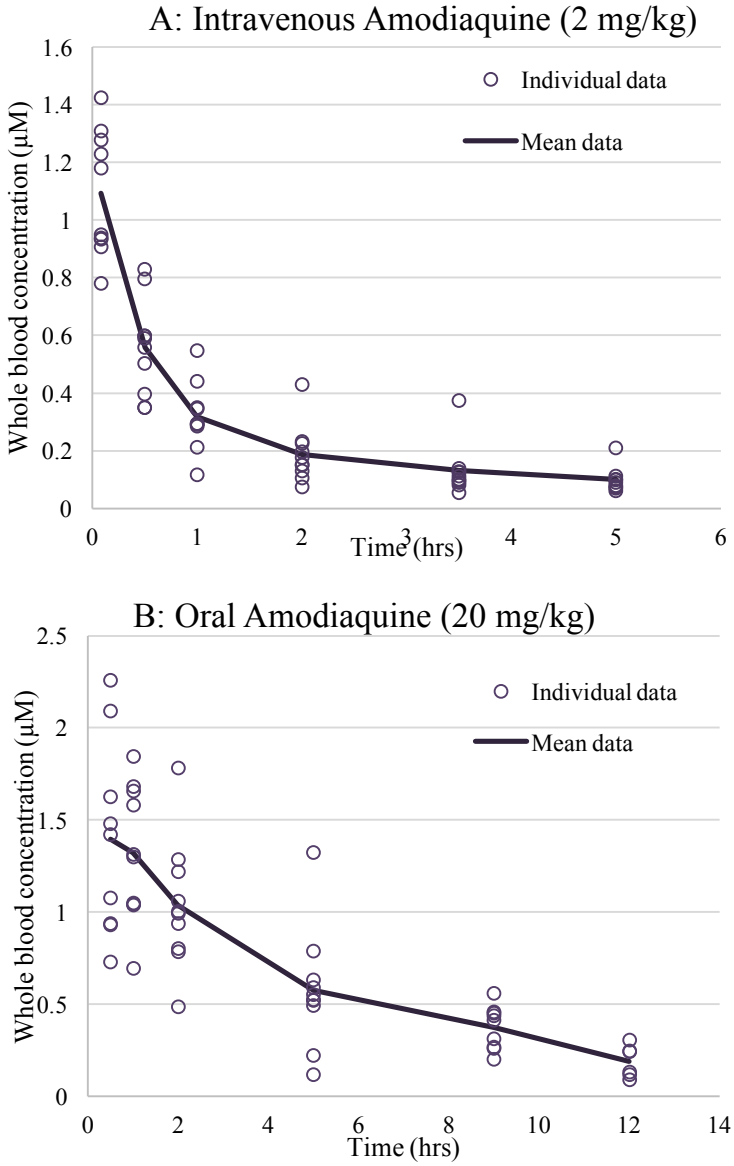

Figure 2-27: Observed pharmacokinetic data for amodiaquine in mice

Individual observed concentration-time points from the amodiaquine pharmacokinetic experiment in 10 mice for A: Oral and B: Intravenous experiments. Observed data are represented by purple open circles and the mean data represented by a solid purple line.

Table 2-6: Calculated pharmacokinetic parameters for amodiaquine in mice

	Amodiaquine		
Parameter	*a. Oral NCA*	*b. IV NCA*	*c. Two compartment*
Blood Cl (ml/min/kg)	-	54.3 (6.54)	55.9 (7.27)
Vc (L/kg)	-	3.34 (0.483)	4.40 (0.572)
Vss (L/kg)	-	12.1 (2.14)	14.0 (1.82)
$t_{1/2}$ *(hr)*	3.88 (0.434)	2.95 (1.50)	3.78 (0.619)
$AUC_{0\text{-}inf}$ *(µM.min)*	514 (26.6)	109(16.0)	489 (80.2) *
T_{max} *(hr)*	1.35 (0.429)	-	-
C_{max} *(uM)*	1.42 (0.127)	-	1.35 (0.001) *
F (%)	47.2 (2.45)	-	48.6 (6.03)
ka (hr^{-1})	-	-	0.735 (0.140)

Standard error of parameters is represented in parenthesis next to final median value for 10 mice. F; bioavailability, ka; rate of absorption, Vc; central volume, Blood Cl; whole blood clearance, Q; inter-compartmental clearance, Vss; steady state volume. Standard error (s.e.) of the population estimate were estimated by linearization of the Fisher information matrix. The parameters calculated by NCA used SummitPK solutions™ and the NLME modelling was performed in Monolix®. Individual mouse weights were included as a covariate and allometrically scaled for clearance and volumes. Individual plots and final parameters with variability values are presented in Chapter 7: Experimental, section 7.2.3, page 224.

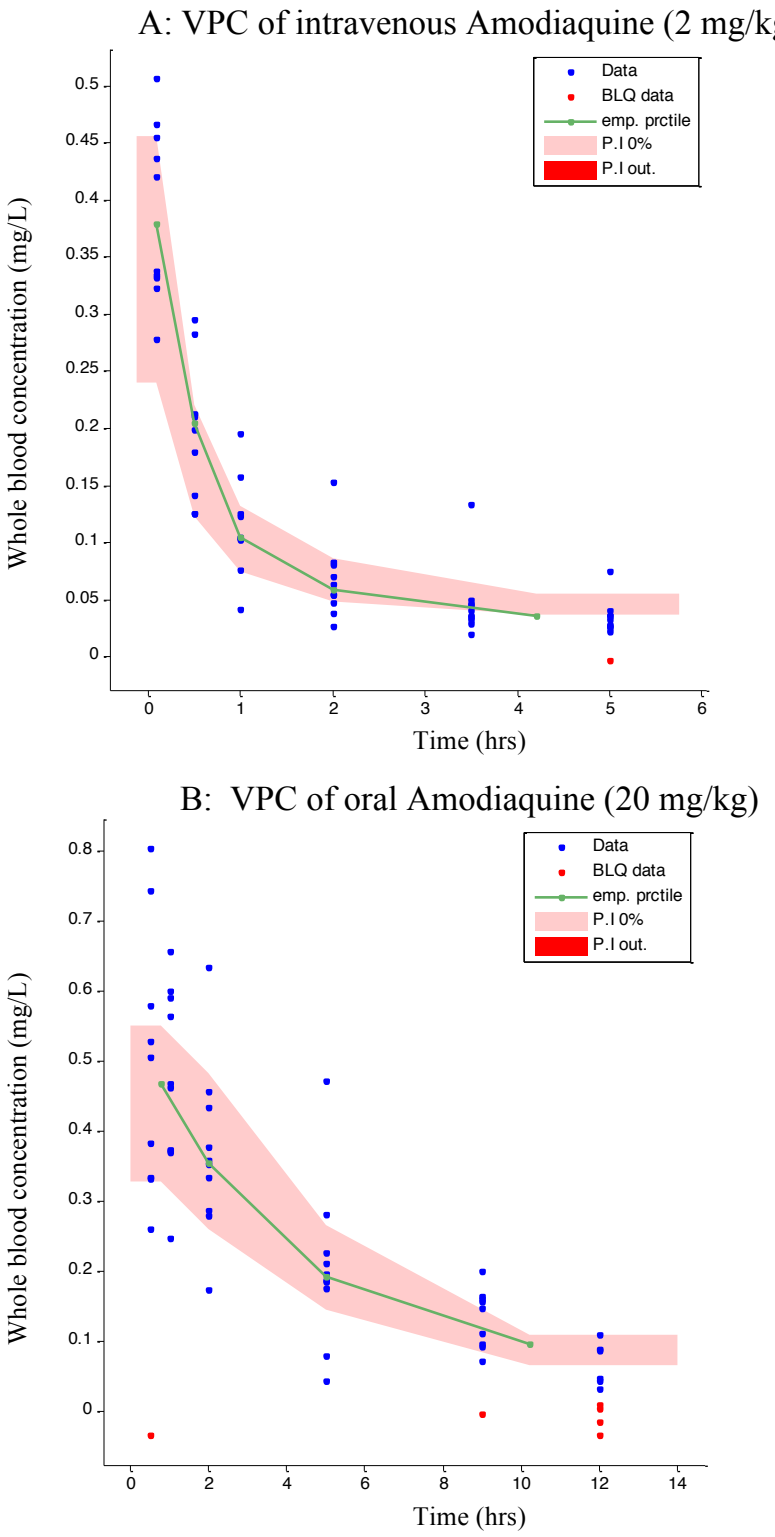

Figure 2-28: Visual predictive check of the final model used for Amodiaquine

The graphical diagnostic plot shows the simulated output of the amodiaquine two-compartment model for the A: intravenous and B: oral pharmacokinetic experiments. The final model was established from the pooled oral and intravenous data and the diagnostic plots stratified according to dosing. Observed data above the limit of quantification is represented by blue dots and concentrations measures below the limit of quantification represented by red dots. The green line represents the empirical percentile of this observed data and the shaded pink area represents the median of the population estimate. Ideally, this empirical percentile should fit within the pink shaded area.

2.5.3.1.1 Summary of amodiaquine results

Amodiaquine showed non-linear elimination hinting that a possible two-compartment model would be more appropriate. This was confirmed with a significant 74 point drop in objective function compared to a one-compartment model. In mice, the half-life of amodiaquine was a moderate 3.75 hrs after oral dosing. Whole blood clearance was moderate at 55.9 ml/min/kg and amodiaquine showed a high steady state volume of 14 L/kg. Amodiaquine has good bioavailability greater than 70% in mice. Unfortunately, the more active DEAQ metabolite of amodiaquine was not included during the original analysis of the pharmacokinetic experiment, because it was not available to us.

The final two-compartment model of amodiaquine captured the observation well as seen by the visual predictive checks for both the oral and intravenous experiment. Comparing NLME results to NCA showed indiscernible results for all parameters, concluding that NCA captured the pharmacokinetic parameters very well for this dataset.

2.5.3.2 DS48B

In Figure 2-29 is shown the raw data of **DS48B** with observed concentration-time points for 3 mice represented by open shapes representing each individual mouse and a mean line of the 3 mice added for A: Intravenous and B: Oral experiments. In Table 2-7 is shown the final calculated parameters of **DS48B** for both NCA and NLME analysis for a side-by-side comparison. A visual predictive check of the final model used is shown in Figure 2-30 and stratified by oral and intravenous groups. The model best fit a 2-compartment model.

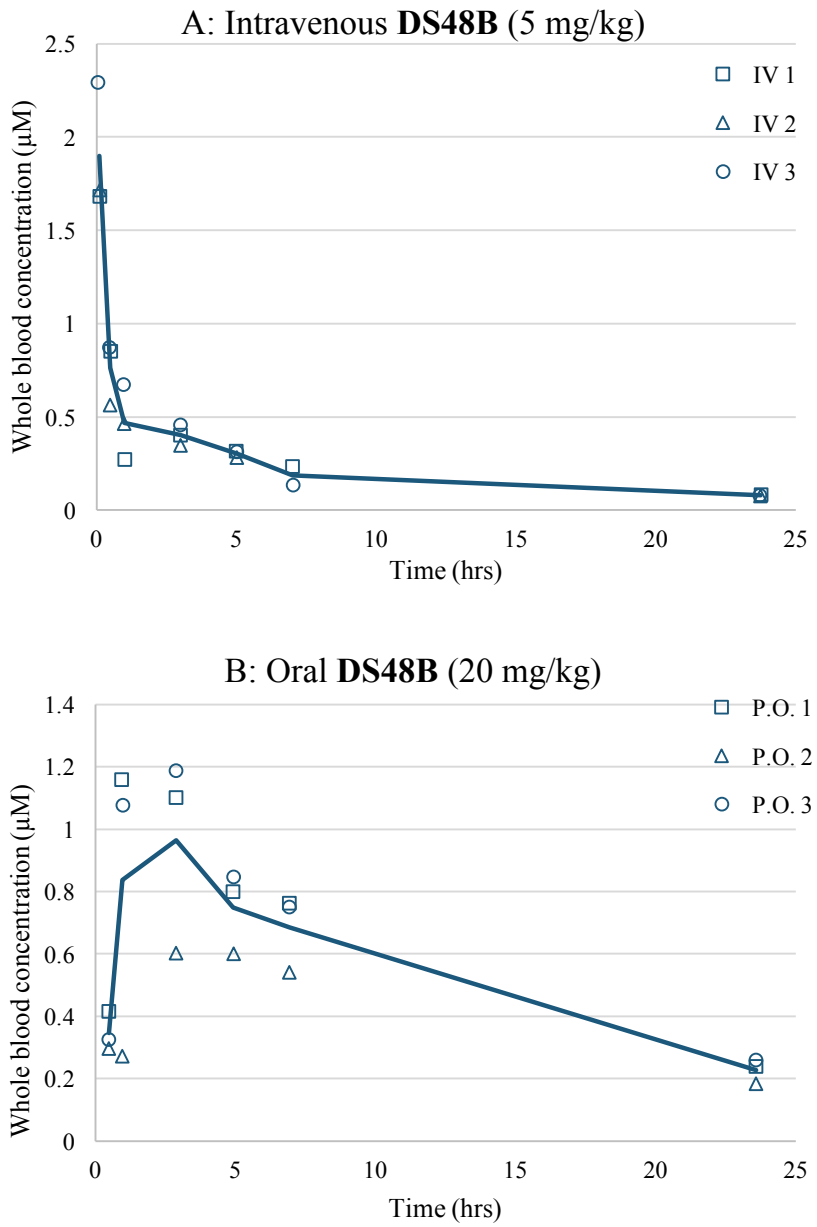

Figure 2-29: Observed pharmacokinetic data for DS48 in mice

Individual observed concentration-time points from the **DS48B** pharmacokinetic experiment in 3 mice for A: Intravenous and B: Oral experiments. Each individual animal is represented by its respective open blue shape, and the mean data of the group is represented by a solid blue line.

Table 2-7: Pharmacokinetics of amodiaquine analogue DS48B in mice

	DS48B		
Parameter	*a. Oral NCA*	*b. IV NCA*	*c. Two compartment*
Blood Cl (ml/min/kg)	-	31.1 (1.45)	38.1 (3.43)
Vc (L/kg)	-	5.68 (1.21)	7.12 (1.57)
Vss (L/kg)	-	24.2 (0.122)	28.4 (3.98)
$t_{1/2}$ *(hr)*	10.5 (0.498)	9.51 (0.153)	9.40 (2.50)
$AUC_{0\text{-}inf}$ *(µM.min)*	983 (122)	435 (17.2)	893 (134) *
T_{max} *(hr)*	2.24 (0.644)	-	-
C_{max} *(uM)*	0.983 (0.190)	-	0.782 (0.004) *
F (%)	57.6 (7.13)	-	61.3 (0.066)
ka (hr^{-1})	-	-	0.434 (0.110)

Standard error of parameters is represented in parenthesis next to final median value for 3 mice. F; bioavailability, ka; rate of absorption, Vc; central volume, Blood Cl; whole blood clearance, Q; inter-compartmental clearance, Vss; steady state volume. Standard error (s.e.) of the population estimate were estimated by linearization of the Fisher information matrix. The parameters calculated by NCA used SummitPK solutions™ and the NLME modelling was performed in Monolix®. Individual mouse weights were included as a covariate and allometrically scaled for clearance and volumes. Individual plots and final parameters with variability values are presented in Chapter 7: Experimental, section 7.2.3, page 224.

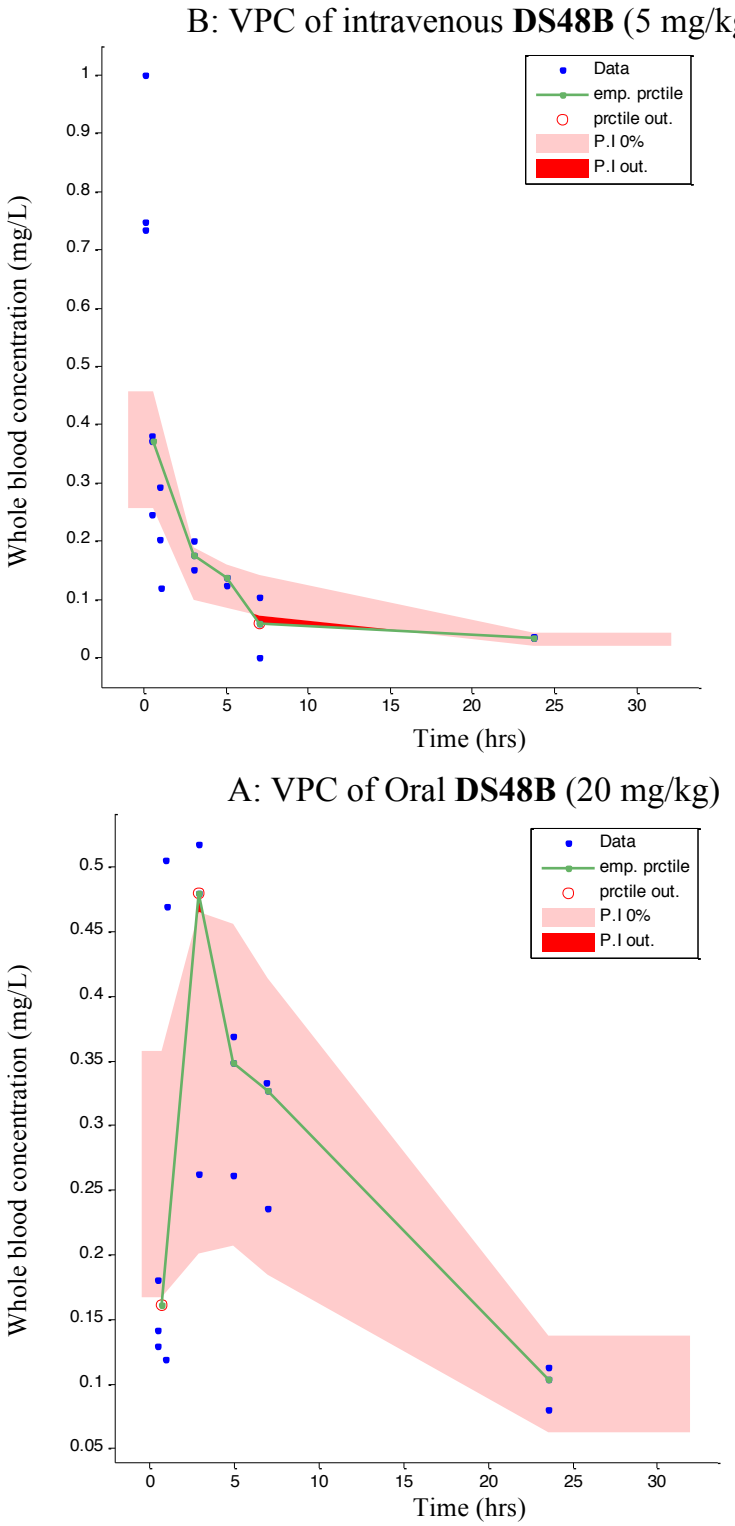

Figure 2-30: Visual predictive check of the final model used for DS48B

The graphical diagnostic plot shows the simulated output of the **DS48B** two-compartment model for the A: oral and B: intravenous pharmacokinetic experiments. The final model was established from the pooled oral and intravenous data and the diagnostic plots stratified according to dosing. Observed data above the limit of quantification is represented by blue dots. The green line represents the empirical percentile of this observed data and the shaded pink area represents the median of the population estimate. Ideally, this empirical percentile should fit within the pink shaded area.

2.5.3.2.1 Summary of **DS48B** results

Like amodiaquine, **DS48B** showed non-linear elimination and a two-compartment model was found to be most appropriate with a significant 38 point drop in objective function compared to a one-compartment model. In mice, the half-life was high at 9.40 hrs after oral dosing, 2-fold greater than amodiaquine. Whole blood clearance was moderate at 38 ml/min/kg and a high steady state volume of 28 L/kg was observed. **DS48B** had good bioavailability greater than 60% in mice from modelling results. As mentioned the more active metabolite of amodiaquine was not included; this metabolite would have been more appropriate for pharmacokinetic comparison with **DS48B**.

The **DS48B** final two-compartment model captured the oral observations better than intravenous observations. The model struggled to fully capture the non-linear elimination process seen at 8 hours and over predicted the population distribution for this time point. NCA and NLME results were comparable and NCA captured the pharmacokinetics parameters for this dataset.

2.5.3.3 DS50B

In Figure 2-31 is shown the raw data of **DS50B** with observed concentration-time points for 3 mice represented by open shapes, each representing an individual mouse and a mean line added for A: Intravenous and B: Oral experiments. In Table 2-8 is shown the final calculated parameters of **DS50B** for both NCA and NLME analysis for a side-by-side comparison. A visual predictive check of the final model used is shown in Figure 2-32 and stratified by oral and intravenous groups. The model best fit a 2-compartment model.

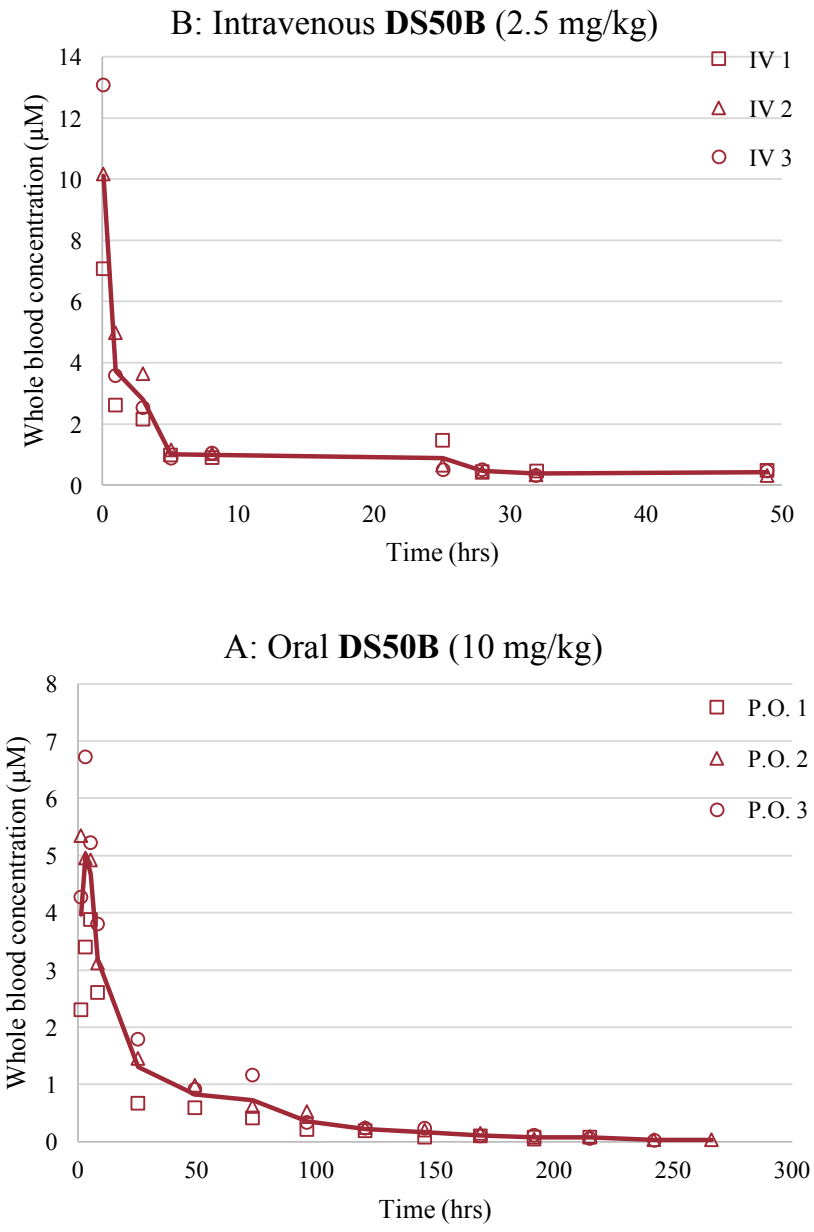

Figure 2-31: Observed pharmacokinetic data for DS50B in mice

Individual observed concentration-time points from the **DS50B** pharmacokinetic experiment in 3 mice for A: Intravenous and B: Oral experiments. Each individual animal is represented by its respective open red shape, and the mean data of the group is represented by the solid red line.

Table 2-8: Pharmacokinetics of amodiaquine analogue DS50B in mice

	DS50B		
Parameter	*a. Oral NCA*	*b. IV NCA*	*c. Two compartment*
Blood Cl (ml/min/kg)	-	1.24 (0.256)	1.64 (0.098)
Vc (L/kg)	-	0.020 (0.011)	0.744 (0.112)
Vss (L/kg)	-	0.27 (0.216)	4.82 (0.338)
$t_{1/2}$ *(hr)*	39.21 (2.78)	30.1 (4.12)	41.9 (3.94)
$AUC_{0\text{-}inf}$ *(µM.min)*	9050 (1420)	6570 (1880)	9870 (1690) *
T_{max} *(hr)*	3.28 (0.007)	-	-
C_{max} *(uM)*	5.02 (0.566)	-	7.61 (0.029) *
F (%)	41.0 (6.44)	-	44.8 (6.90)
ka (hr^{-1})	-	-	0.240 (0.060)

Standard error of parameters is represented in parenthesis next to final median value for 3 mice. F; bioavailability, ka; rate of absorption, Vc; central volume, Blood Cl; whole blood clearance, Q; inter-compartmental clearance, Vss; steady state volume. Standard error (s.e.) of the population estimate were estimated by linearization of the Fisher information matrix. The parameters calculated by NCA used SummitPK solutions™ and the NLME modelling was performed in Monolix®. Individual mouse weights were included as a covariate and allometrically scaled for clearance and volumes. Individual plots and final parameters with variability values are presented in Chapter 7: Experimental, section 7.2.3, page 224.

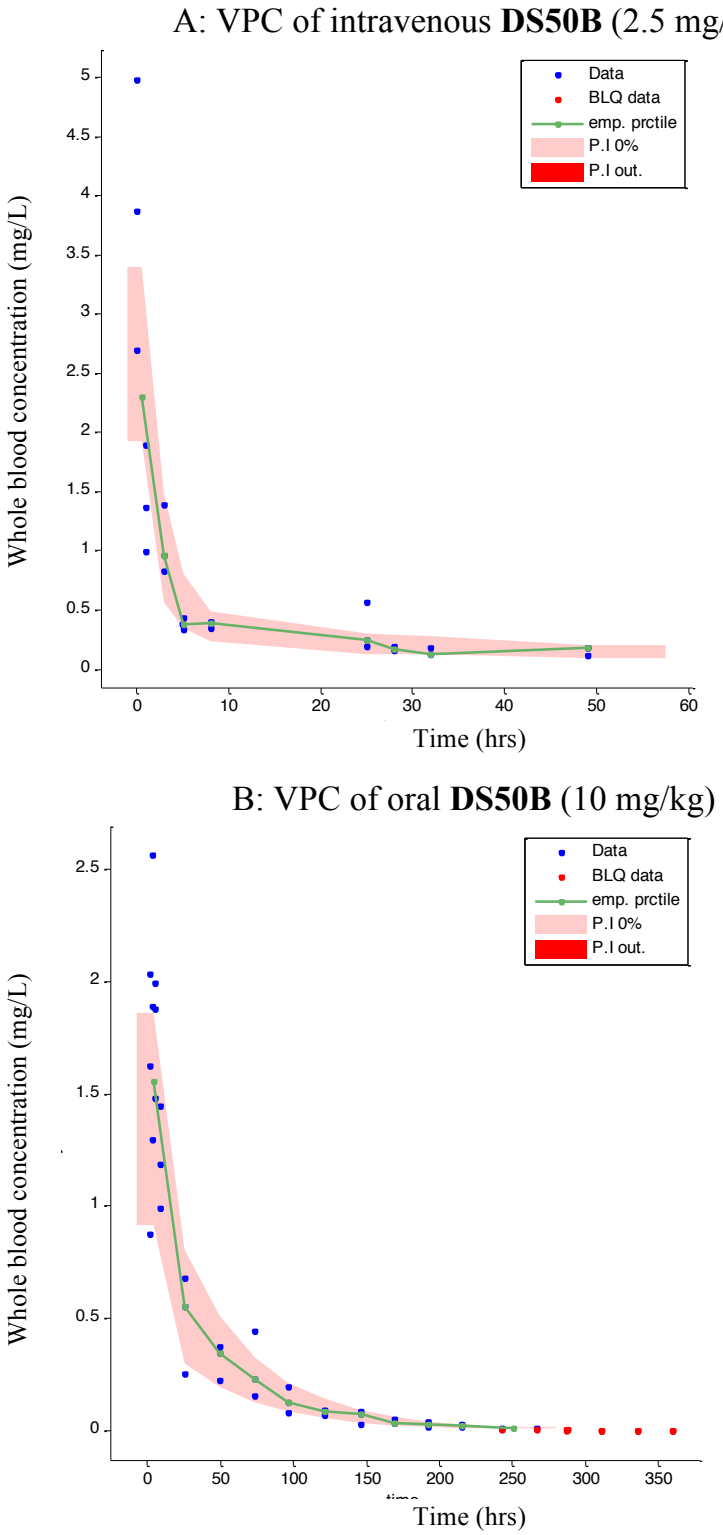

Figure 2-32: Visual predictive check of the final model used for DS50B

The graphical diagnostic plot shows the simulated output of the **DS50B** two-compartment model for the A: intravenous and B: oral pharmacokinetic experiments. The final model was established from the pooled oral and intravenous data and the diagnostic plots stratified according to dosing. Observed data above the limit of quantification is represented by blue dots and concentrations measures below the limit of quantification represented by red dots. The green line represents the empirical percentile of this observed data and the shaded pink area represents the median of the population estimate. Ideally, this empirical percentile should fit within the pink shaded area.

2.5.3.3.1 Summary of **DS50B** results

Overall **DS50B** had an excellent pharmacokinetic profile. Clearance was calculated to be a low 1.64 ml/min/kg resulting in a long half-life of approximately 42 hrs. A moderate 4.82 L/kg volume at steady state was observed. The bioavailability of **DS50B**, calculated to be 45%, was the lowest observed of the amodiaquine analogues in this series, but is still considered adequate for further progression. Even with the lowest bioavailability, the slow clearance of **DS50B** and moderate steady state volume resulted in a calculated oral C_{max} and $AUC_{0\text{-}inf}$ of 5 and 10-fold more than **DS48B** and amodiaquine.

Like all the amodiaquine series compounds, **DS50B** best fits a two-compartment model, apparent from its multi-exponential elimination and a 106 point drop in objective function compared to a one-compartment model. The intravenous concentration-time profile of **DS50B** showed an unexpected drop in concentration, decreasing the linearity of the profile too far reaching for NCA to cope with. The possibility of sample swaps or possible instrument error were investigated, but no error was found. Other experimental errors could still be responsible for this observation as an actual physiological/pharmacological explanation is not possible. Pharmacokinetic parameter calculations first attempted to include all sample points, but one outlier at 8 hrs was eventually excluded during NCA to avoid emphasis of this concentration-time point during calculation of the elimination phase. NLME included all observations without needing to exclude time points at 8 hrs. It is evident from the presented visual predictive check that the proportional error and variability included on inter-hepatic clearance (Q) (see section 7.2.3.2, page 217 for complete summary table of model parameters) captured even the 8 hr observations well. NCA failed to accurately calculate central and steady state volumes with a 17-fold under prediction of steady state volume for the compound when compared to NLME, resulting in an under predicted intravenous half-life of 70% compared to NLME.

2.5.3.4 DS23B

In Figure 2-33 is shown the raw data of **DS23B** with observed concentration-time points for 3 mice represented by open shapes representing 3 individual mice respectively and a mean line added for A: Intravenous and B: Oral experiments. In Table 2-9 below is shown the final calculated parameters of **DS23B** for both NCA and NLME analysis for a side-by-side comparison. A visual predictive check of the final model used is shown in Figure 2-34 and stratified by oral and intravenous groups. The model best fit a 2-compartment model as described in section 2.4.5.

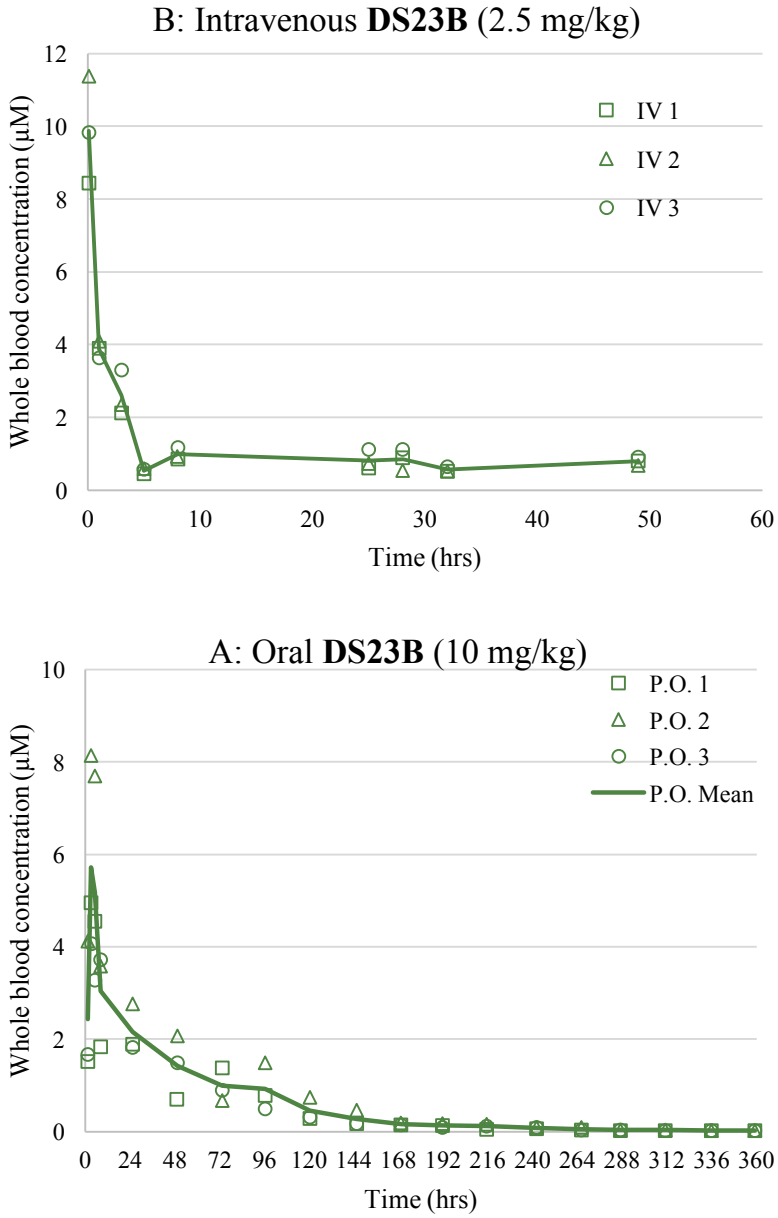

Figure 2-33: Observed pharmacokinetic data for DS23B in mice

Individual observed concentration-time points from the **DS23B** pharmacokinetic experiment in 3 mice for A: Intravenous and B: Oral experiments. Each individual animal is represented by its respective open green shape, and the mean data of the group is represented by the solid green line.

Table 2-9: Pharmacokinetics of amodiaquine analogue DS23B in mice

	DS23B		
Parameter	*a. Oral NCA*	*b. IV NCA*	*c. Two compartment*
Blood Cl (ml/min/kg)	-	4.51 (2.26)	1.18 (0.083)
Vc (L/kg)	-	0.639 (0.576)	0.716 (0.122)
Vss (L/kg)	-	14.5 (4.08)	4.59 (0.322)
$t_{1/2}$ *(hr)*	48.9 (1.27)	82.8 (0.686)	51.4 (5.09)
$AUC_{0\text{-}inf}$ *(µM.min)*	13000 (2120)	14100 (5190)	10400 (1721) *
T_{max} *(hr)*	3.17 (0.096)	-	-
C_{max} *(uM)*	5.72 (1.24)	-	7.04 (0.016) *
F (%)	30.5 (6.49)	-	54.4 (8.16)
ka (hr^{-1})	-	-	0.244 (0.085)

Standard error of parameters is represented in parenthesis next to final median value for 3 mice. F; bioavailability, ka; rate of absorption, Vc; central volume, Blood Cl; whole blood clearance, Q; inter-compartmental clearance, Vs; steady state volume. Standard error (s.e.) of the population estimate were estimated by linearization of the Fisher information matrix. The parameters calculated by NCA used SummitPK solutions™ and the NLME modelling was performed in Monolix®. Individual mouse weights were included as a covariate and allometrically scaled for clearance and volumes. Individual plots and final parameters with variability values are presented in Chapter 7: Experimental, section 7.2.3, page 224.

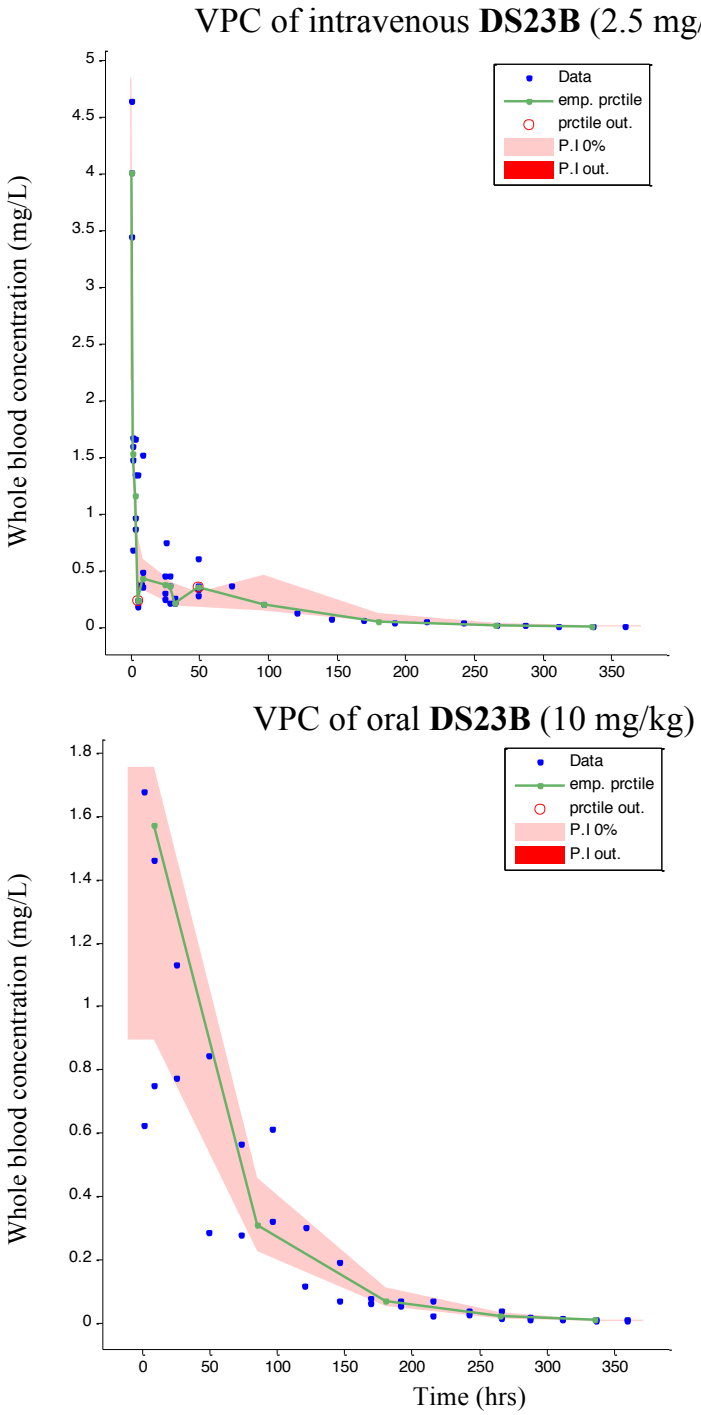

Figure 2-34: Visual predictive check of the final model used for DS23B

The graphical diagnostic plot shows the simulated output of the **DS23B** two-compartment model for the A: intravenous and B: oral pharmacokinetic experiments. The final model was established from the pooled oral and intravenous data and the diagnostic plots stratified according to dosing. Observed data above the limit of quantification is represented by blue dots. The green line represents the empirical percentile of this observed data and the shaded pink area represents the median of the population estimate. Ideally, this empirical percentile should fit within the pink shaded area.

2.5.3.4.1 Summary of **DS23B** results

Like **DS50B**, amodiaquine analogue **DS23B** had excellent pharmacokinetic results. An extremely low 1.18 ml/min/kg clearance with a resulting long half-life of approximately 54 hrs was observed, the highest half-life of the series. The volume at steady state was a moderate 4.59 L/kg. The bioavailability of **DS23B** was approximately 54%. Similar to the slow clearance of **DS50B** and moderate steady state volume, the calculated oral C_{max} and $AUC_{0\text{-}inf}$ of **DS23B** overshadowed that of **DS48B** and amodiaquine, by a 5 and 10-fold increase respectively.

Again, like the other amodiaquine series compounds, **DS23B** with its non-linear elimination best fit a two-compartment model, and model progression showed a 136 point drop in objective function compared to a one-compartment model. **DS23B** Had the same unexpected drop in its intravenous concentration-time profile at 8hrs. The exact reason for this remains inconclusive, but an experimental error of some kind for this time point is possible. NCA calculations had to exclude these sample points to avoid emphasis of this concentration-time profile during calculation of the elimination phase. NLME included all observations without needing to exclude time points at 8 hrs. The presented visual predictive show that the model that included proportional error and variability on clearance managed to capture the observations well (complete summary table of model parameters are presented in section 7.2.3.2, page 217). NCA over predicted steady state volume and whole blood clearance 4 and 3-fold respectively and the resulting intravenous half-life was over predicted by 50%.

2.5.4 Non-linear mixed effects modelling vs non-compartmental modelling

The non-linear elimination of amodiaquine analogues showed that NLME would better calculate the pharmacokinetic parameters of these compounds. However, NCA could correctly capture 2 of the 4 compounds, namely amodiaquine and **DS48B**. The amodiaquine dataset of 10 mice greatly improved NCA calculations. Regarding compounds **DS23B** and **DS50B** that NCA could not accurately calculate, it is important to re-emphasise the empirical methodology of NCA that estimates pharmacokinetic parameters using different sections of the pharmacokinetic curve and calculates the values separately for each individual subject, averages the results, and expresses uncertainty as the standard deviation seen between final individual parameters. For **DS23B** and **DS50B** the drop in concentration at 8 hrs could not be solved by NCA leading to over and underestimation of some parameters. NLME analyses all the observations from different test subjects collectively to find the most appropriate pharmacokinetic parameters with their level of variability that best explains all the data. In this case, the variance added to selective parameters

and more importantly random effects that aid in estimating error could account for the likely experimental error encountered at the 8hr mark. Another advantage of the variability added was seen with samples that approached the lower range of quantification, which inherently have higher variability as the concentration decreases to the lowest limit of quantification. Here random effects can allow the concentrations to be considered with leeway as to what the actual concentration was with proportional and/or constant error to account for the accuracy and precision deficits a LC/MS/MS method may have. NCA simply cannot do this and at most observations can be deemed outliers and removed from the dataset if they are considered detrimental to the final parameters. The NLME analysis also had the advantage of being able to include samples that were below the limit of quantification for **DS50B**. The software can stipulate that at a specific time point a sample less than 10 ng/ml was observed rather than a data point that has no value in NCA calculations.

2.5.5 Efficacy comparison

Correlating the pharmacokinetic results with the respective efficacy evaluation in *Plasmodium berghei* infected mice, the most effective compound was **DS23B** with 30 mean survival days at a 4 x 10 mg/kg oral dose. It also had the best pharmacokinetic properties with the lowest clearance rate and highest exposure. The intermediate half-life compound **DS50B** was the second most effective with 24 mean survival days at a 4 x 10 mg/kg oral dose, while the fastest clearing compound, **DS48B,** had the lowest survival rate of 16 days at the 4 x 10 mg/kg oral dose. **DS48B** may be more potent than **DS50B** as the 1 x 50 mg/kg dose showed similar efficacy, while **DS48B** had a 26-fold lower exposure than **DS50B**. Compounds **DS50B** and **DS23B** at multiple oral dosing of 4 x 10 mg/kg experienced higher accumulation, possibly increasing their concentration above IC_{50} and improving mean survival days longer and more effectively than the less successful **DS48B** compound.

2.5.6 PK/PD simulation

To assess trends in the PK/PD results of the compounds investigated, the models of each compound were used to simulate AUC, C_{max} and $T>IC_{50}$ with input dosing matching the efficacy experiments. An example of a simulated population average profile for **DS48B** following a 4 x 50 mg/kg oral dose is shown in Figure 2-35. Table 2-10 shows the results of all compound simulations in comparison with their respective efficacy evaluation to observe potential PK/PD relationships. An important limitation to emphasise is that the C57Bl/6 mice are not the same strain as the NMRI Swiss-type strain used in the efficacy experiment. The NMRI Swiss-type strain was not available

at the University of Cape Town animal unit. As per the project's ethics agreement C57Bl/6 mice were used for the pharmacokinetic evaluation and have been used by the Division of Pharmacology animal lab since 2008. Therefore, they were chosen as they are readily available to the lab and the previous amodiaquine pharmacokinetic study was performed in C57Bl/6 mice.

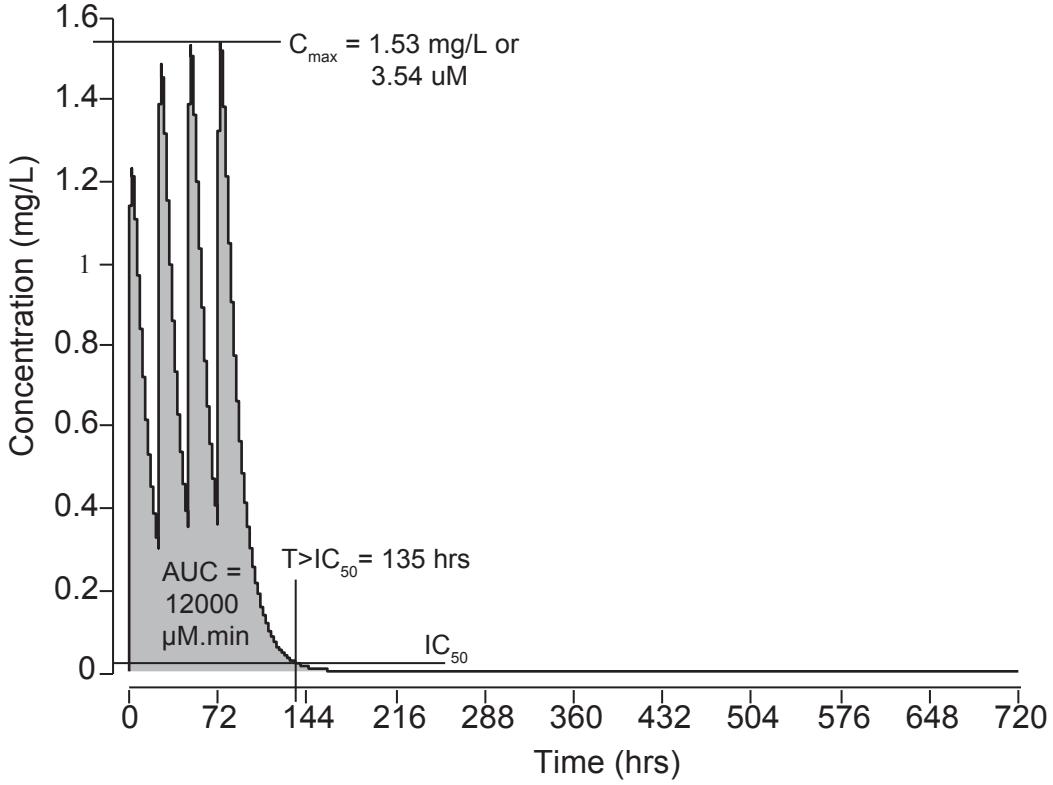

Figure 2-35: Simulated profile of DS48B after 4 x 50 mg.kg dosing

DS48B was simulated over 30 days or 720 hrs using typical population parameters determined from a two-compartment model. The plot annotates area under the curve (AUC) represented in grey calculated from the integral of the concentration-time profile, maximum concentration (C_{max}) and time above IC_{50}.

Table 2-10: PK/PD simulations of benzoxazole amodiaquine analogues

DS48B	1 x 50 mg/kg	4 x 10 mg/kg	4 x 50 mg/kg
AUC(μM.min):	3020	2410	12000
C_{max} (μM):	2.84	0.708	3.54
T>IC_{50} (hrs):	83.3	135	158
%P (MSD):	99.54(14.0)	99.76(15.7)	99.76(>30)
DS50B	1 x 50 mg/kg	4 x 10 mg/kg	4 x 50 mg/kg
AUC (μM.min):	79600	63600	318000
C_{max} (μM):	44.7	14.0	69.4
T>IC_{50} (hrs):	452	478	668
%P (MSD):	99.54(13.7)	99.88(24.0)	99.82(29.3)
DS23B	1 x 50 mg/kg	4 x 10 mg/kg	4 x 50 mg/kg
AUC (μM.min):	104000	83200	414000
C_{max} (μM):	38.8	14.6	73.3
T>IC_{50} (hrs):	536	560	680
%P (MSD):	99.54(23.3)	99.82(>30)	99.83(>30)

Note: AUC; Area under curve (μM.min), C_{max}; Maximum concentration (uM); T>IC_{50}; Time above *in vitro* antiplasmodial activity NF54 IC_{50} (hrs), %P; Percentage reduction in parasitemia and MSD; Mean mouse survival days after treatment.

Comparing simulated AUC, time above antiplasmodial NF54 IC_{50}, and C_{max} against the *in vivo* efficacy of the compounds only showed a trend between an increase in time above IC_{50} relative to an increase in mean survival days for all compounds. There was no correlation of efficacy with AUC and C_{max} simulated values. Important limitations of this approach include that this experiment was not designed for PK/PD evaluation, which would require more diverse dosing (including dose amount and frequency) and have the final data scattered around each compound's ED_{50}. The simulation is also based on the assumption that no saturation occurs at the higher concentration reached with 50 mg/kg doses or repeated dosing. If these assumptions are not true, the simulated pharmacokinetics would underestimate the exposure and overestimate efficacy. However, it is interesting that at this early stage of preclinical screening, simulations using NLME already showed useful trends that could benefit dose optimisation in future efficacy experiments.

2.5.7 Robustness of NLME with subset data

For compounds **DS23B** and **DS50B** all data subsets fit a two-compartment model. The final parameter results for **DS23B** and **DS50B** are shown in Table 2-11 and Table 2-12. Fixed effects parameter values that were greater or smaller by 30% of the 15-day experiment are highlighted in bold.

Table 2-11: DS23B subset data analysis results

	24 hrs	48 hrs	120 hrs	360 hrs
Fixed Effects				
Foral	0.692	0.629	0.556	0.51
ka (hr^{-1})	0.182	0.205	0.243	0.244
V (L)	0.0184	0.0185	0.0184	0.0173
Cl (L/h)	**0.000541**	**0.000943**	0.00166	0.00177
Q (L/h)	0.0104	0.0101	0.01	0.00932
Vp (L)	**0.17**	**0.15**	0.0971	0.0908
Sigma				
Proportional	0	0	0	0
Constant	0.323	0.314	0.325	0.335

Foral; bioavailability, ka; rate of absorption, V; central volume, Cl; whole blood clearance, Q; inter-compartmental clearance. NLME modelling was performed in Monolix® and individual mouse weights were included as a covariate and allometrically scaled for clearance and volumes.

Table 2-12: DS50B subset data analysis results

	24 hrs	48 hrs	120 hrs	144 hrs	360 hrs
Fixed Effects					
Foral	0.541	0.469	0.461	0.500	0.510
ka (hr^{-1})	0.243	0.272	0.288	0.308	0.244
V (L)	0.0190	0.0181	0.0189	0.0185	0.0173
Cl (L/h)	**0.00005**	**0.00286**	**0.00254**	0.00229	0.00177
Q (L/h)	0.0102	0.00792	0.0079	0.0103	0.0093
Vp (L)	**0.238**	0.0831	0.0931	0.0894	0.0908
Sigma					
Proportional	0.115	0.0568	0.706	0	0
Constant	0.237	0.243	0.285	0.337	0.335

Foral; bioavailability, ka; rate of absorption, V; central volume, Cl; whole blood clearance, Q; inter-compartmental clearance. NLME modelling was performed in Monolix® and individual mouse weights were included as a covariate and allometrically scaled for clearance and volumes.

As expected the shorter terminal phase has the highest misinterpretation of the clearance parameter and for both 24 hrs and 48 hrs subsets of each compound Monolix® could not converge on the correct value. For **DS23B** a 120 hrs data subset was enough to come within a 30% margin of the final results. However, **DS50B** needed an additional 144 hr experiment. Therefore, a minimum 5- and 6-day experiment for **DS23B** and **DS50B** respectively could have captured the pharmacokinetics of these compounds.

2.5.8 In vitro assay results

Table 2-13 shows the performed *in vitro* ADME assays, performed by Ms Nina Lawrence and colleagues at H3D. The blood plasma partitioning experiment was performed by the author. The results of the assays are discussed in sections 2.5.8.1 to 2.5.8.6 that follow.

Table 2-13: ADME results of amodiaquine analogues

General structure 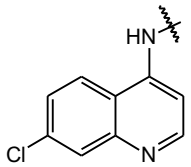

Compound		DS23B 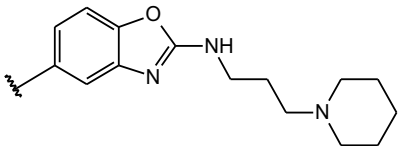			DS48B 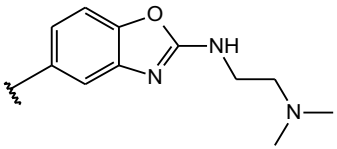			DS50B 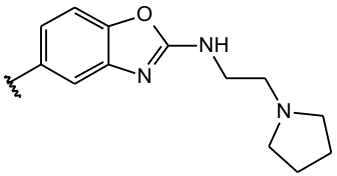			Amodiaquine 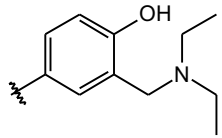		
Solubility (uM)	pH 2	198.5 (high)			198.8 (high)			195.9 (high)			200.0 (high)		
	pH 6.5	179.3 (high)			174 (high)			154.5 (high)			194.2 (high)		
	FASSIF pH 6.5	183 (high)			170.7 (high)			160.4 (high)			177.9 (high)		
Microsome species		HLM	RLM	MLM	HLM	RLM	MLM	HLM	RLM	MLM	HLM	RLM	MLM
Half-life (min)		123.2	68.2	52.5	104.8	76.3	58.3	52.2	14	14.4	<10[111]	n.d.	<10[111]
CL(int) (mL/min/kg)		16.3	45.7	129.9	19.1	40.9	117.1	38.4	223.6	474.8	n.d.	n.d.	n.d.
Predicted E_H		0.4	0.5	0.6	0.5	0.4	0.6	0.6	0.8	0.8	n.d.	n.d.	n.d.
Metabolic stability class		(moderate)			(moderate)			(low)			(low)[111,112]		
$LogD_{7.4}$		2.56 (optimal)			1.01 (optimal)			0.93 (low)			1.57 (optimal)		
Log P_e (cm/s)		-5.9 (moderate)			-5.7 (moderate)			-5.7 (moderate)			-6.4 (moderate)		
% Plasma protein binding		98.8 (high)			98.7 (high)			98.8 (high)			>90[112] (high)		
Blood plasma partitioning		2.9 (high)			1.8 (high)			1.9 (high)			2.5 (high)		

ADME classification shown in parenthesis, n.d.; not done. All experiments performed under supervision of Ms Nina Lawrence and colleagues at the Drug Discovery and Development Centre (H3D), except blood to plasma partitioning performed by the author of this thesis.

2.5.8.1 Parallel artificial membrane assay (PAMPA)

The PAMPA assay is based on passive diffusion across an artificial membrane. Passive diffusion is involved in processes such as absorption from the gastrointestinal tract, penetration over the blood brain barrier, and transport across cells; all important factors for predicting drug like properties of compounds.[102] The experiment was quantified by LC/MS/MS after a 4-hr incubation at room temperature using PBS pH 6.5 (pH is a large factor in final $LogP_e$ results), which compares more closely to the pH of the small intestine where majority of passive diffusion takes place across the gastrointestinal wall.[113–115] Permeability of the respective compounds were classified according to ranges per manufacturer Biofocus instructions (based on Kansy *et al*., 1998)[101] provided in Table 2-14. The reference compound amodiaquine had the best $LogP_e$ value of -6.4 at pH 6.5 and similarly all three compounds were classified as having moderate permeability which supports the *in vivo* bioavailability results, calculated greater than 40% for all compounds. This shows decent absorption across the gastrointestinal tract. Of course, passive diffusion is not the only pathway for compounds to be absorbed. Transcellular passive diffusion, as well as active and paracellular transport are also possible permeability pathways for drugs. Assays such as Caco-2, which consist of monolayer cultured human colon epithelial cancer cells to assess permeability with, can predict the mentioned pathways,[116,117] and can provide more mechanistic detail. In this case, however, the PAMPA assays were sufficient to address permeability and correlated well with bioavailability.

Table 2-14: PAMPA classification

Permeability class	**$LogP_e$**
High	>-5.5
Moderate	-6.5 to -5.5
Low	<-6.5

2.5.8.2 Plasma protein binding

Human plasma protein binding data of compounds were obtained by incubation in human plasma. Plasma stability was assessed during the procedure against buffer samples to ensure correct interpretation of the binding data. Compound **DS23B** was the only compound to show a degradation of 1.5%. Binding was very high for the compounds at more than 98% for all three

amodiaquine analogues. Literature predicts amodiaquine protein binding greater than 90%[112] much alike to the analogues.

Plasma protein binding has continued to gain importance as the free-drug theory has proved useful in describing pharmacokinetic/pharmacodynamics relationships. The free-drug theory states that only unbound drug can interact and elicit an effect on its target receptor, and the unbound drug in tissue (intracellular space) is equal to the unbound drug in plasma (extracellular space).[118] Plasma protein binding has become useful in predicting distribution, metabolism, elimination as well as possible toxicity and drug-drug interactions of drugs.[119,120]

For distribution, tissue distribution (related to volume of distribution at steady state) was specifically considered to be proportional to the free fraction drug in plasma and inversely proportional to the tissue free fraction of a drug. To simplify, it is expected that high plasma protein binding will result in low steady state volume as highly plasma bound compounds are not available to move into tissues.[118–122] However, for amodiaquine and **DS48B**, high steady state volume was observed and **DS23B** and **DS50B** showed moderate steady states volumes. Here it is important to consider that the plasma protein binding assay exists in an isolated environment and cannot account for the altered equilibrium that may exist with other binding sites. Changes in the unbound plasma fraction of a drug therefore do not always predict distribution of drugs as a low unbound drug does not mean no drug will move into tissue[120] and the amodiaquine and the analogues presented here are a good example of this.

The expected influence of higher plasma protein binding decreasing *in vivo* clearance was observed. This is due to less drug being available for elimination and metabolism. An example of this is renal excretion by glomerular filtration and/or active secretion that depend on free fraction drug, and metabolism that depends on an enzyme's ability to interact with unbound drug.[119,121,123,124] The very low clearance of this series and related long half-lives may well be due to their high plasma protein binding.

There is concern for possible toxicity and drug-drug interactions when plasma protein binding is high. Antimalarial drugs are given in combination to prevent resistance and the high plasma protein binding of these compounds could have higher toxic incidents or wide population variability as small changes in protein binding (due to factors including drug-drug displacement or population factors such ethnicity) can lead to significant fluctuations in free fractions. This series was designed to limit toxicity due to reactive metabolite formation and this might prevent issues related to this type of toxicity.

2.5.8.3 Kinetic solubility

Kinetic solubility at pH 2, pH 6.5 in phosphate-buffered saline and pH 6.5 in FaSSIF buffer, which contains a mixture of lecithins (phospholipids) and bile salts (sodium taurocholate) were evaluated at 25°C for 2 hrs. The different buffers were chosen to best simulate the pH gradient of the gastrointestinal tract environment, where a drug will encounter low pH stomach acid, to a more neutral environment in the small intestine.[125] Table 2-15 shows solubility classification used according to Kerns & Di.[126]

Kinetic solubility testing is important in early drug discovery screening as compounds that do not possess good solubility properties will have poor absorption and bioavailability as compounds need to be in solution to cross the gastrointestinal tract.[111] Poor kinetic solubility can also negatively affect the quality of other in vitro ADME assays.

Amodiaquine and its analogues all showed high kinetic solubility, measured between 155 and 200 µM in all media. The excellent kinetic solubility results support the *in vivo* bioavailability values observed greater than 40% for all compounds.

Table 2-15: Solubility classification

Solubility Class	Concentration (µM)
High	≥150
Moderate	50 – 150
Low	5 – 49
Very Low	<5

2.5.8.4 Metabolic stability assay

Metabolic stability data of amodiaquine analogues **DS23B**, **DS48B** and **DS50B** in human, rat and mouse liver microsomes were performed in a five-time point assay over 60 minutes to establish predicted half-life, *in vitro* clearance (CL) and hepatic extraction (E_H). Amodiaquine was not available to the lab at the time and was therefore not evaluated.

Microsomal stability related to liver metabolism is a very advantageous assay in drug screening as the liver is the largest site of metabolism.[127] Liver microsomes are prepared by liver homogenization and consists of subcellular fractions from the endoplasmic reticulum of hepatic cells.[128] They are used specifically for phase I oxidation evaluation and contain enzymes such as

cytochrome P450, flavin monooxegenase, carboxyl esterase, epoxide hydrolase and Uridine 5'-diphospho-glucuronosyltransferase (UDP glucuronyl transferase).[129–131]

The metabolic stability classes for the amodiaquine analogues were classified as low for **DS50B** and moderate for **DS23B** and **DS48B**. The calculated intrinsic clearance values were not corrected for plasma protein or microsomal binding or blood plasma partitioning. Comparing the observed *in vivo* clearance values of the compounds there was a disconnect between **DS23B** and **DS50B**, which both showed very slow clearance and reasonable bioavailability's which would suggest microsomal stability would be favourable.

The high plasma protein binding discussed in section 2.5.8.2 can account for the mismatch as a small unbound fraction of free drug would be available for first pass effects. Additionally, non-specific microsomal binding was not measured and can similarly account for the poor translation between the *in vitro* assay and *in vivo* observation.

Amodiaquine is considered to have low metabolic stability according to literature[111,112] which is beneficial as it is quickly metabolised to its more active metabolite DEAQ. To ensure that the compounds did not have any possible concealed metabolites with similar retention times as their respective parent compound, the extracted mouse blood samples were sent for additional metabolite identification by Dr Mathew Njoroge from the Department of Chemistry, University of Cape Town (South Africa). No significant metabolites were detected in the final samples, showing that the compounds were indeed metabolically stable when administered in mice.

2.5.8.5 Lipophilicity

Experiments to examine the lipophilicity of the compounds were performed at physiological pH of 7.4. The lipophilicity of a compound is related to whether a compound favours partitioning into a non-polar (organic) or aqueous phase, and has a major effect on absorption, distribution, and pharmacological activity.[132]

Ideally, the lipophilicity expressed as LogD value should be between 1 and 3, as too aqueous (<1) limits absorption from the gastrointestinal tract and too high (>3) can cause the compound to adhere to lipophilic membranes and not be available target interaction. Therefore, a moderate LogD between 1 and 3 is considered optimal for gastrointestinal tract absorption by passive diffusion after oral dosing (which the moderate PAMPA results indicate can still be an important route of absorption for this series) shows potential for increased oral bioavailability of a drug.[109,132]

Like amodiaquine, compounds **DS23B** and **DS48B** showed optimal LogD values and all had good bioavailability to support this. The LogD value of 0.93 for **DS50B** is considered poor and

comparing the series bioavailability results, compound **DS50B** did have the lowest bioavailability of the compounds analysed.

2.5.8.6 Blood to plasma partitioning

The blood plasma partitioning value to describe distribution between red blood cells and plasma was determined by a modified LC/MS/MS-based depletion method.[110] A blood plasma partitioning value great than 1 is usually a consequence of the compounds distributing into red blood cells.[133] Distribution into red blood cells for antimalarial compounds can be viewed as advantageous as they are able to reach their target site well.

All three compounds showed high blood plasma partitioning values ranging from 1.8 to 2.9, in the same range as the reference amodiaquine that had a partitioning value of 2.5. A proportional relationship has been observed with blood plasma partitioning ratios and volume at steady state. Higher blood plasma partitioning also correlates with lower clearance as drug is not available to certain metabolism and elimination processes inside erythrocytes.[133,134] This together with the high plasma protein binding observed correlates well with the low *in vivo* whole blood clearance observed for these compounds.

2.6 Conclusion

The *in vivo* properties of the three compounds are summarized in Table 2-16. The three amodiaquine analogues show considerable potential as antimalarial drugs.

Table 2-16: Summary of efficacy and pharmacokinetic parameters for benzoxazole analogues of amodiaquine in mice

General Structure	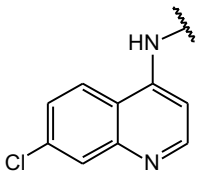			
Compound	**DS48B** 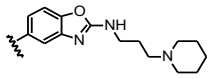	**DS50B** 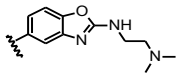	**DS23B** 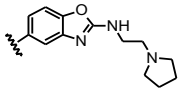	Amodiaquine 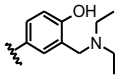
Oral	20 mg/kg	10 mg/kg	10 mg/kg	20 mg/kg
Blood Cl (ml/min/kg)	38.1	1.64	1.18	55.9
Plasma Cl (ml/min/kg)				
Vss (L/kg)	28.4	4.82	4.59	14.0
$t_{1/2}$ *(hr)*	9.40	41.9	51.4	3.78
Bioavailability (%)	61.3	44.8	54.4	48.6
$AUC_{0\text{-}inf}$ *(µM.min)* *	893	9870	10400	489
C_{max} *(uM)*	0.782	7.61	7.04	1.35
NF54 IC50 nM	10.0	11.5	15.0	4.00
P. berghei efficacy 4 x 50 mg/kg (MSD)	99.76 (>30)	99.82 (29.3)	99.83 (>30)	99.88 (>30)

Note: NLME calculated pharmacokinetic parameters were obtained at a dose of 20 mg/kg for **DS48B** and Amodiaquine and 10 mg/kg for **DS23B** and **DS50B**

The analogues were metabolically stable *in vivo*, had very attractive pharmacokinetic properties that coincide well with their observed efficacy. The pharmacokinetic properties of the analogues could explain their differences in *in vivo* activity against *Plasmodium berghei*, which follows the

trend of improved efficacy with increased concentration time above IC_{50}. **DS23B** performed exceptionally well, rivalling the efficacy of amodiaquine and chloroquine. Analysis by NLME was greatly beneficial considering NCA would have incorrectly predicted better pharmacokinetic properties for **DS50B** compared to **DS23B**. Possible reasons for this include the lack of a mechanistic approach, missing elimination phase data and sample concentrations close to the lower limit of quantification. Accurate and precise results are vital in early drug discovery as compounds are progressed and eliminated through a resource limited screening cascade. NLME was also able to include data below the lower limit of quantification and samples affected by large variability, possibly due to experimental error.

3 ANTIMALARIAL AMINOPYRIDINE IN THE FORM OF ITS CYCLODEXTRIN INCLUSION COMPLEX

3.1 Introduction

The 3,5-diaryl-2-aminopyridine class of molecules show great promise as antimalarial drug candidates.[135] The class was identified as promising selective antiplasmodial hits using an image-based[136] high throughput screen of the BioFocus DPI SoftFocus library.[137] Through hit to lead optimisation, *in vitro* potency, absorption, distribution, metabolism and elimination (ADME) properties were addressed. Compound **MMV017007** from this series was able to successfully cure mice infected with *Plasmodium berghei* at a dose of 50 mg/kg using the Peters test.[138] This promising *in vivo* efficacy inspired hit to lead and lead optimisation campaigns, to continue improving activity, ADME, *in vivo* potency in the *Plasmodium berghei* infected mouse model and safety within the series. These efforts culminated in the discovery of the now clinical candidate **MMV390048**, Figure 2-1.[135,139] To expand on viable clinical candidates and continue efforts to optimise this promising class, earlier leads were re-examined for risk properties that could be addressed. A physicochemical disadvantage associated with MMP is its poor solubility [0.021mg/mL in water/ethanol (99:1, v/v) at 25 °C]. One of the primary reasons high attrition of drugs are seen is due to the common issue with lipophilic drug candidates.[140] This led to attempts

to improve solubility properties and rescue **MMV017007** (hereafter referred to as **007**) by supramolecular beneficiation.

Hit Compound	**MMV017007**	**MMV390048**
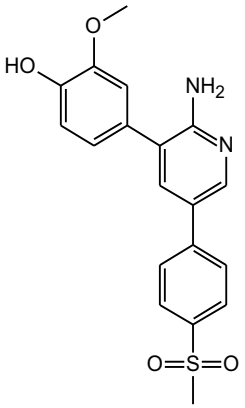	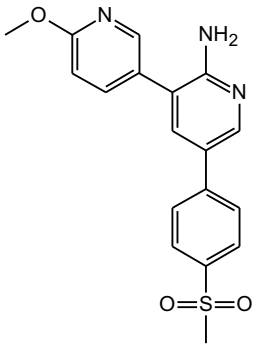	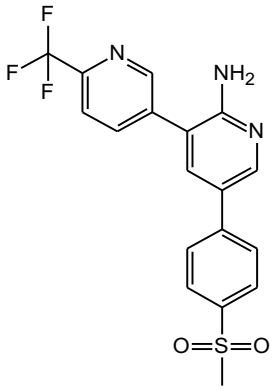
	K1 IC_{50}: 0.051 µM	K1 IC_{50}: 0.025 µM
K1 IC_{50}: 0.049 µM	NF54 IC_{50}: 0.051 µM	NF54 IC_{50}: 0.051 µM
NF54 IC_{50}: 0.049 µM	hERG: 3.00 µM	hERG: >10 µM
	Cytotox (L6): >146 µM	Cytotox (L6): 251 µM

Figure 3-1: Selected 3,5,-diaryl-2-aminopyridines

The original hit compound from the BioFocus DPI SoftFocus kinase library compared to optimised lead structures MMV017007 and MMV390048. Note: NF54 IC_{50}; antiplasmodial activity showing 50% inhibition in *Plasmodium falciparum* drug sensitive strain NF54, K1 IC_{50}; antiplasmodial activity showing 50% inhibition in a *Plasmodium falciparum* multi-drug resistant K1 strain, Cytotox (L6) cytotoxicity concentration in L6 muscle cell line.

The benefits of crystalline forms of compounds include increased reproducibility in manufacturing, increased stability and less effort to purify crystalline forms.[141] One of the approaches attempted included an extrinsic strategy of a cyclodextrin inclusion complex formulated between heptakis(2,6-di-*O*-methyl)-β-cyclodextrin (DMB) and **007.** The structure of the host DMB molecule is shown in Figure 3-2.

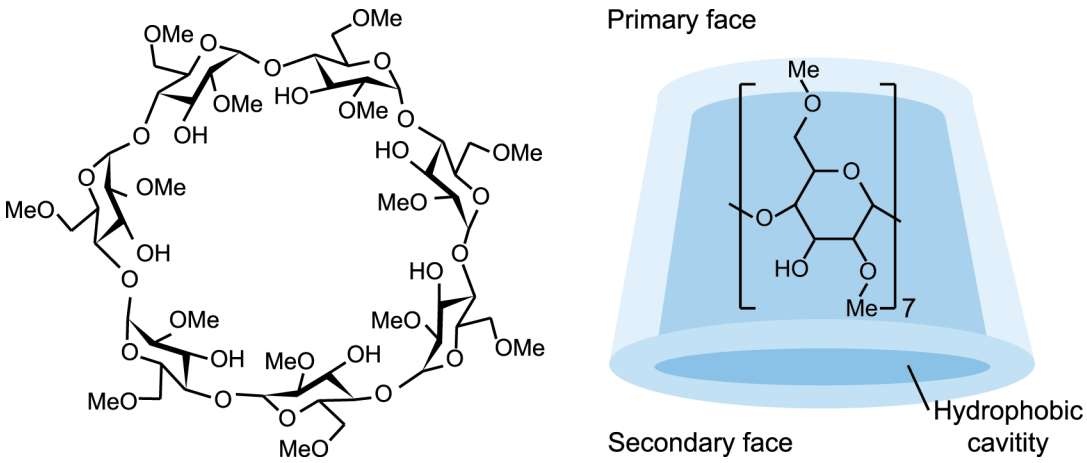

Figure 3-2: Chemical structure of the host DMB molecule

Heptakis(2,6-di-*O*-methyl)-β-cyclodextrin (DMB) structure as seen from the front and side to show the hydrophobic cavity and outer surface groups that can aid in hydrogen bonding and solubility in aqueous solutions.

Cyclodextrins are oligosaccharides that have a hydrophilic exterior and lipophilic cavity that can form inclusion complexes with lipophilic guest molecules to improve their aqueous solubility.[142] Cyclodextrins are found as white crystalline powders. The crystal lattice is formed by hydrogen bonding on the secondary phase. Crystallization in aqueous medium causes some molecules of water to be included in the cyclodextrin cavity. Water molecules are also present as an integral part of the crystal structure (crystal water). The cyclodextrin-inclusion complexes are formed by the substitution of included water from the cyclodextrin cavity by the appropriate guest molecule.[143,144] The guest molecule is not covalently linked with the host but associated with the lipophilic cavity, allowing for easy detachment. Solubility is improved by favourable hydrogen bonding between the outer surface hydroxyl groups of the cyclodextrin and water.[145] The complex is in dynamic equilibrium with its guest molecule and host cyclodextrin, Figure 3-3. The equilibrium shifts to the free fraction by competitive displacement from endogenous bile salt and cholesterol in the stomach, change in temperature and drug uptake in tissues.[146] Absorption of cyclodextrins themselves has been estimated at about 2 – 4% from the small intestine, with the remaining being degraded by amylase and absorbed as glucose.[147,148]

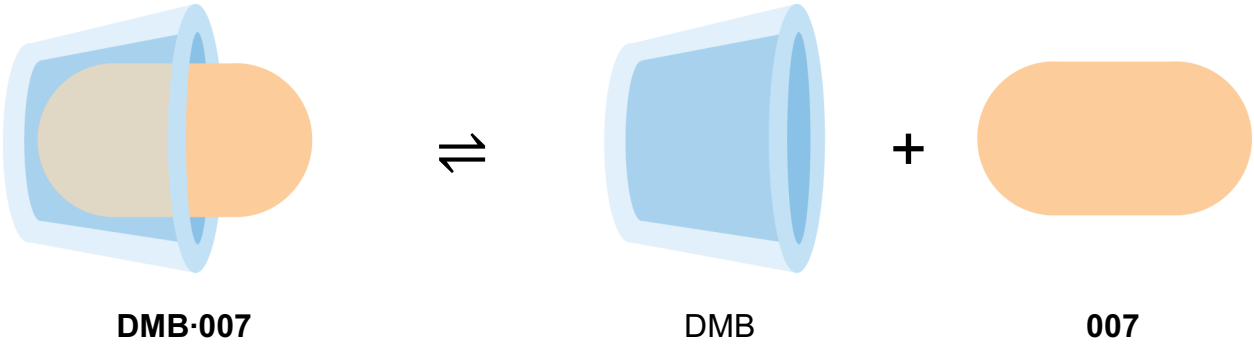

Figure 3-3: Dynamic equilibrium of DMB complex

Simplified schematic of MMV017007 (**007**) represented in orange and Heptakis(2,6-di-*O*-methyl)-β-cyclodextrin (DMB) represented as the blue cone. The guest compound can move in and out of the DMB structure and an equilibrium takes place between these two forms.

Ms. Laurelle Joseph at the Centre for Supramolecular Chemistry Research, University of Cape Town, (South Africa) attempted derivatisations of cyclodextrins, with namely, β-cyclodextrin, (2-Hydroxypropyl)-β-cyclodextrin, heptakis(2,6-di-O-methyl)-β-cyclodextrin (DMB), heptakis(2,3,6-tri-O-methyl)-β-cyclodextrin (TRIMEB) and hexakis(2,3,6-tri-O-methyl)-α-cyclodextrin (TRIMEA) to produce a co-crystal. Only the DMB derivatization was successful and yielded a 1:1 host-guest inclusion complex.

Further examination of the apparent solubility of **007** in DMB at the highest host concentration employed (namely 20 mM) was 0.0592 mM, hence a 65-fold compared to **007**. Using the hosts β-CD (AN-type behaviour) and HP-β-CD (AL-type behaviour) as solubilisers yielded association constant values of 1620 M-1 and 2872 M-1 respectively. The solubility enhancement factors and respective highest concentrations employed were 17-fold for 20 mM β-CD and 49-fold for 23 mM HP-β-CD. The 1:1 host-guest inclusion complex between DMB and **007** (hereafter **DMB·007**) was deemed the most successful and was progressed to antimalarial screening.

Ms. Joseph further characterised the **DMB·007** complex to confirm its successful derivatisation and purity. This included thermogravimetric analysis (TGA) to quantify the water content as well as 1H NMR to determine the host-guest stoichiometry leading to the correct chemical formula for the inclusion complex, which could be reported with total confidence. Single crystal X-ray diffraction was used to solve the structure of the inclusion complex at atomic resolution, Figure 3-4. The mode of guest inclusion, the role of the water molecules as well as the crystal packing could all be modelled unambiguously. Scale-up of the inclusion complex was performed to provide the necessary material for the antimalarial and further pharmacokinetic testing. The purity of the inclusion complex was confirmed using powder X-ray diffraction.[149]

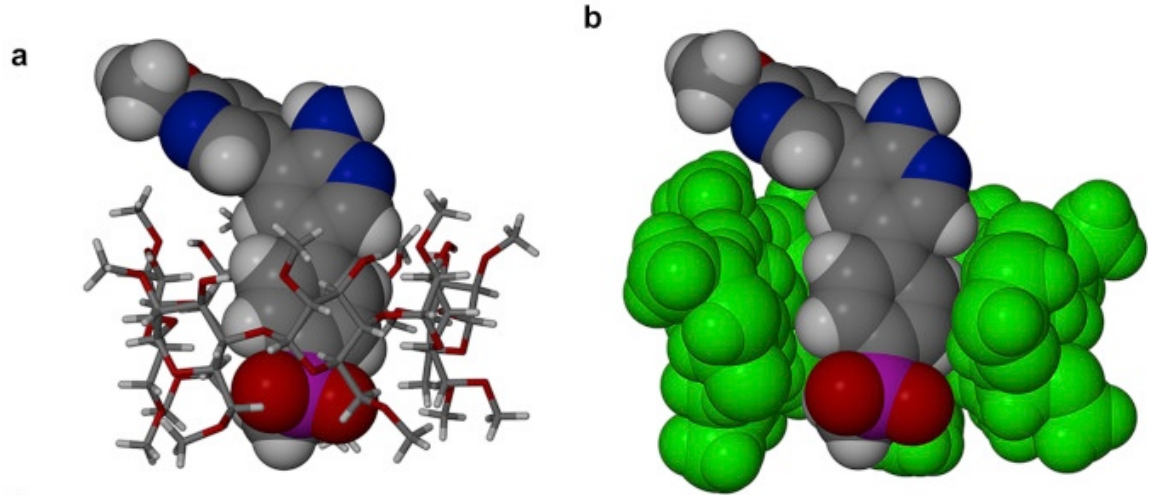

Figure 3-4 X-ray structure of the DMB·007 complex

The host drawn is in stick representation and the guest is in space-filling mode (a) and a sectioned space-filling view to illustrate the mode of guest inclusion (b).[149]

This **DMB·007** complex and reference active ingredient, **007** were tested *in vivo* at 30, 10 and 3 mg/kg in the *Plasmodium berghei* model, carried out by Dr Sergio Wittlin and colleagues at the Swiss Tropical and Public Health Institute (Basel, Switzerland). **DMB·007** showed a 30% improvement in efficacy at 3 mg/kg over **007**, Table 3-1.

Table 3-1: Efficacy of DMB·007 complex

Dose (mg/kg)	**007** %P (MSD)	**DMB·007** %P (MSD)
1 x 30	98.7 (8.33)	99.36 (9.00)
1 x 10	97.8 (8.00)	98.6 (6.00)
1 x 3	20.8 (3.00)	54.4 (7.00)

Experiments using a single dose suppressive test performed by Dr Sergio Wittlin and colleagues at the Swiss Tropical and Public Health Institute (Basel, Switzerland). Note: Active pharmaceutical ingredient **007** as reference. heptakis (2,6-di-O-methyl)-β-cyclodextrin (DMB) complex with **007**. %P: Reduction in percentage parasitaemia in the *Plasmodium berghei* mouse model (n = 3). MSD: Mean survival days after ending treatment.

Examination of the original data from the efficacy experiment (Table 3-2) indicated that results from mice treated with 3 mg/kg of reference compound **007** had a much higher variance (standard

error 10.2) compared to the standard error of 2.20 of the **DMB·007** group. Further, the mouse survival days were not an improvement on the control groups.

Table 3-2: DMB·007 and 007 efficacy in *Plasmodium berghei* infected mice

		Control Vehicle	**007**	**DMB·007**
Dose (mg/kg)		-	3	3
% Parasitaemia (Survival days)	M1	8.13 (3)	41.1 (3)	58.7 (7)
	M2	8.77 (3)	12.3 (3)	53.3 (7)
	M3	33.1 (3)	9.09 (3)	51.3 (7)
Mean		20.8 (3)	16.7 (3)	54.4 (7)
Standard error		10.2 (0)	8.22 (0)	2.20 (0)

Individual values for the efficacy experiment using a single 3 mg/kg dose suppressive test performed by Dr Sergio Wittlin and colleagues at the Swiss Tropical and Public Health Institute (Basel, Switzerland). Note: Active pharmaceutical ingredient **007** as reference. heptakis (2,6-di-O-methyl)-β-cyclodextrin (DMB) complex with **007**. %P: Reduction in percentage parasitaemia in the *Plasmodium berghei* mouse model (n = 3). MSD: Mean survival days after ending treatment.

Closer examination of the original efficacy experiment's raw data showed that the **007** group had much higher variance (standard error 10.2) with two mice having no effect with comparable reduction in parasitaemia to the vehicle control group. Further, their mouse survival days were not an improvement on the control groups. The **DMB·007** group did have low variance (standard error 2.20) and consistent results in reduction on parasitaemia leading to improved mouse survival days over the control and **007** groups.

3.2 Rationale

It was hypothesised that an increase in solubility due to the complexation increased exposure and efficacy of **007** against *Plasmodium berghei* in infected mice. The kinetic solubility and pharmacokinetics at the lower dose range in mice were therefore examined to understand the improvement in efficacy.

In a drug discovery and development setting, the 33.6% improvement in efficacy may not be sufficient to warrant further investigation. However, for the academic project undertaken, the

complex that showed modest improvement was the best available. The **DMB·007** complex also showed a 65-fold increase in aqueous solubility which was deemed intriguing for further development.

3.3 Methodology overview

In Figure 3-5 is shown the approach and experiments undertaken for the pharmacokinetic evaluation of the active pharmaceutical ingredient **007** as reference and **DMB·007**. A LC/MS/MS quantification method was first developed in mouse blood for **007**, section 3.4.2. The absorption of the DMB saccharide alone and **DMB·007** are negligent due to their large size[148,150] and the final quantification method only included **007** and a structurally similar internal standard. A 24 hr pharmacokinetic experiment in mice was performed for oral **DMB·007** and **007** administered groups (n = 3) at 5 mg/kg equivalent **007** dose in solid form using mouse sized capsules. A third group consisted of **007** dosed intravenously at 2.5 mg/kg as reference for clearance, volume of distribution and bioavailability calculations. The final concentration time points after LC/MS/MS quantification were analysed by NCA and NLME modelling. Two approaches of NLME modelling were attempted with results obtained placing different emphasis on the parameters responsible for the change in exposure, section 3.4.5. Additional kinetic solubility experiments were performed to evaluate the pH related effect of complex solubility.

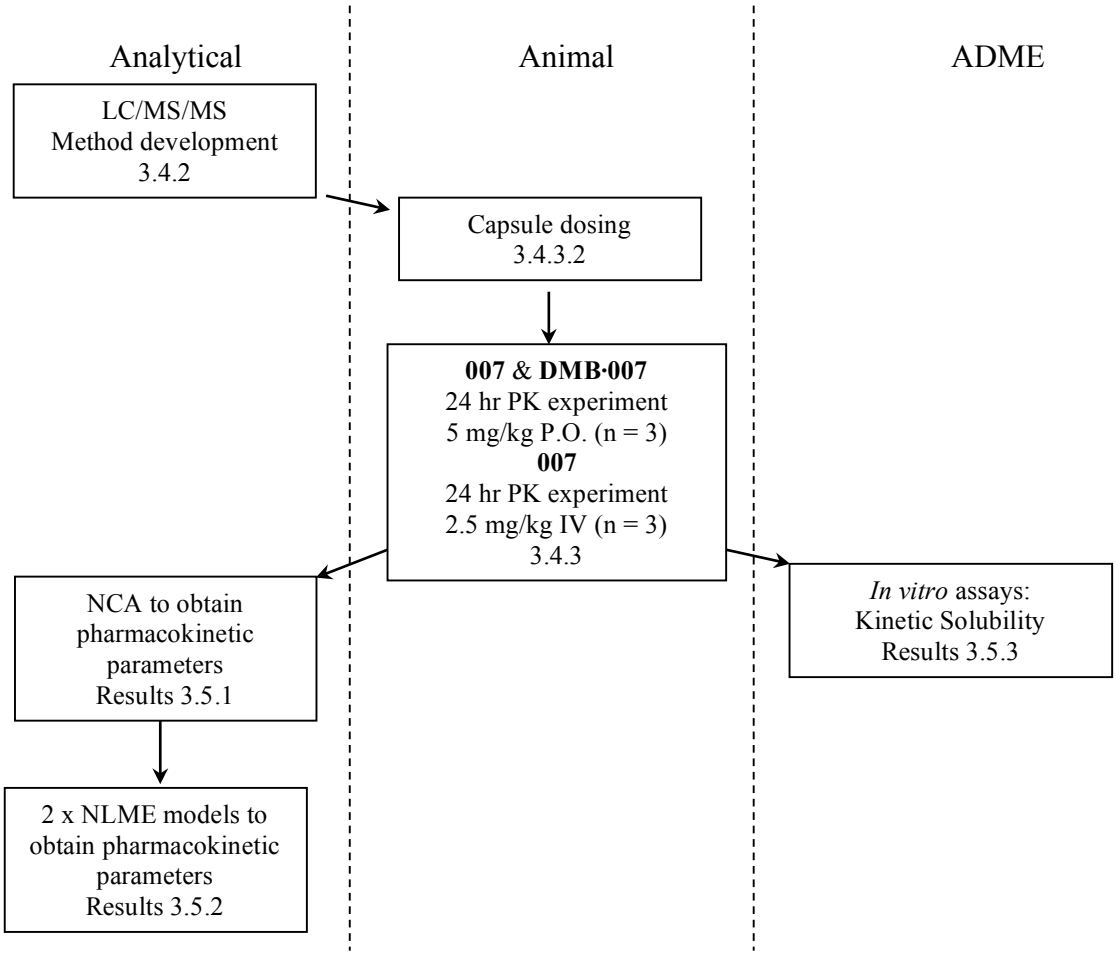

Figure 3-5: DMB·007 evaluation methodology overview

3.4 Methods

3.4.1 In vivo antimalarial efficacy

In vivo antimalarial efficacy testing was carried out by Dr Sergio Wittlin and colleagues at the Swiss Tropical and Public Health Institute (Basel, Switzerland) and followed a similar protocol recommended by Fidock *et al*.[75] This includes the adapted method of the classical 4-day suppressive test of Peters[74,76] to evaluate initial efficacy of compounds. Specific modifications were the same as described in section 2.4.1, page 33. The method only differed in dosing regimens and the animals were treated at 1 x 30 mg/kg, 1 x 10 mg/kg and 1 x 3 mg/kg of the **007** and **DMB·007** compounds, similarly suspended in 70% Tween 80 and 30% ethanol (v/v). Analysis of efficacy was carried out the same as mentioned previously, with mean reduction in parasitaemia and mean survival days measured.

3.4.2 LC/MS/MS quantification

Whole blood concentrations of **007** were quantified by an LC/MS/MS assay developed for a range of 4.1 – 3000 ng/ml. The samples were extracted by protein precipitation using 20 µl whole blood and 240 µl methanol containing a structurally similar internal standard. Gradient chromatography was performed on a Phenomenex® Kinetex PFP (2.1 x 50 mm, 2.6 µm) reverse phase column at a flow rate of 200 µl/min with mobile phases 0.1% formic acid (v/v) in water and acetonitrile. Transition 355→277 was analysed for the compound on an AB Sciex API 4000Q® mass spectrometer operated at unit resolution in multiple reaction-monitoring mode. The compound ionised well and method development proceeded without challenges. The accuracies (%Nom) for low (10 ng/mL), medium (2000 ng/mL) and high (4000 ng/mL) quality controls ranged between 95.5% – 97.3% and the percentage coefficient (%CV) was below 4.9%. In Figure 3-6 is shown the peak of a medium quality control. For further discussion on the analytical method used, see Chapter 7: Experimental, section 7.3.1, page 224.

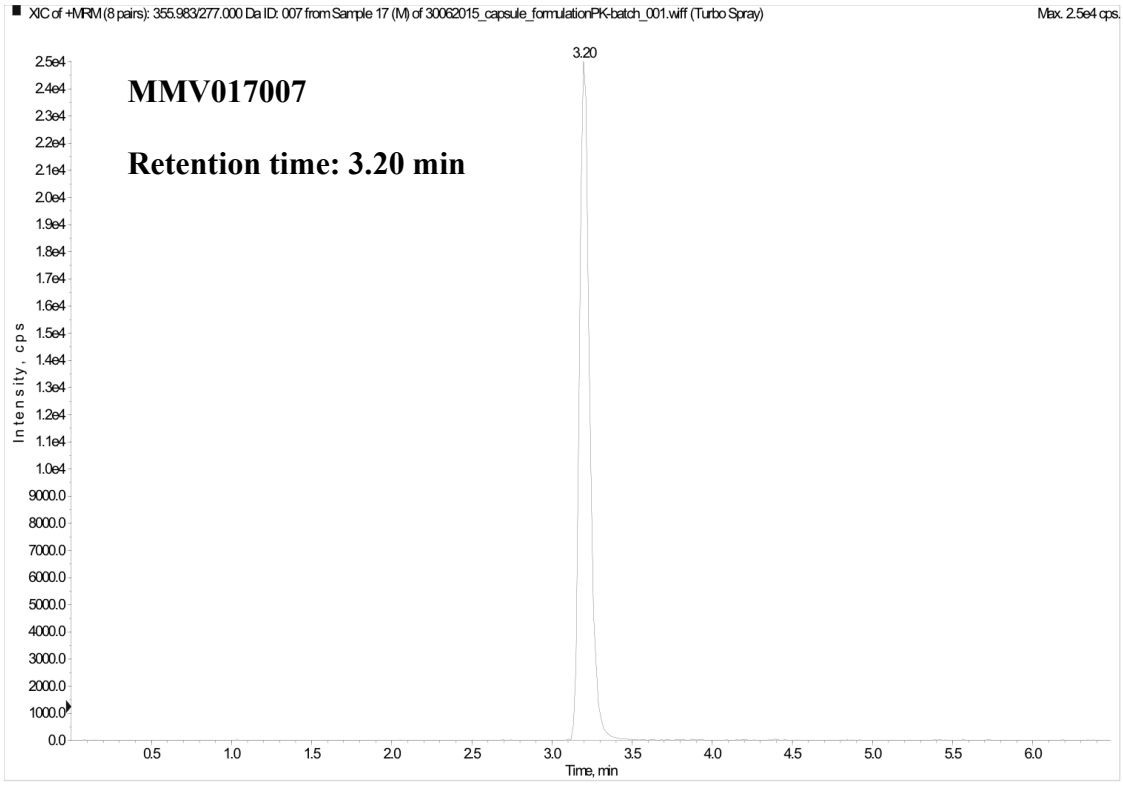

Figure 3-6: Representative chromatogram of MMV017007

3.4.3 In vivo pharmacokinetic experiment

3.4.3.1 Animals

All animal studies and procedures were conducted with prior approval of the Ethics Committee of University of Cape Town (approval number 013/028) in accordance with the National Code for animal use in research, education, diagnosis and testing of drugs and related substances in South Africa. The pharmacokinetic animal experiment used healthy six-week-old C57BL/6 mice maintained at the University of Cape Town animal facility and housed as previously described in Section 2.4.3.1, page 36.

3.4.3.2 Compound preparation and administration

All animal handling, administration of compounds and blood collection were performed by Mr Trevor Finch from the Division of Pharmacology, University of Cape Town (South Africa) under direct supervision of the author, with the author present at all procedure times.

The nine, 6-week-old C57BL/6 mice were divided into one intravenous group consisting of three males weighing approximately 30 g and two oral dosage groups, each consisting of three females weighing between 23 and 24.5 g. For intravenous administration, test compound **007** weighed that morning was prepared by the author in an organic vehicle of 10% DMSO, 10% ethanol, 50% polypropylene glycol and 30% polyethylene glycol 400.

The formulation was vortexed for 1 minute and solubility was confirmed by visual inspection of the dosage solution before administration, which took place within 30 minutes of weighing the compound. Intravenous injection required a slow push over 1 minute into the penile dorsal vein of 60 µL total volume and was performed under microscope resulting in a 5 mg/kg dose. A volume of 20 µl of whole blood was collected from the tail tip at 0.08, 0.5, 1, 3, 8 and 24 h.

For the oral groups the filled Torpac® capsules were prepared by Ms Laurelle Joseph at the Centre for Supramolecular Chemistry Research, University of Cape Town, (South Africa) under the guidance of the author of this thesis. The solid-state material was passed through a 100-micron sieve to ensure consistent particle size and surface area and filled in respective capsules using the Torpac® Profunnel capsule filler. The final mass coincided with a 5 mg/kg **007** dose, and **DMB·007** dose equivalent to 5 mg/kg of **007** for a 25 g mouse.

Fasting the animals before pharmacokinetic evaluation to improve the issue of variability in absorption of these compounds was considered. However, this was decided against due to the inconvenience and discomfort of the animals, and the ability to see variability and accordingly flag solubility issues was deemed an advantage at this early stage in drug discovery and development.

The capsules, Figure 3-7, were dosed with a modified method designed by Mr. Trevor Finch. The dosing procedure gavaged anesthetised mice with a venous catheter, depositing the capsule in the oesophagus, which was then pushed into the stomach with a rounded tip stainless steel gavage needle. On average, the entire gavage procedure took 90 seconds, which compared well with the efficiency of gavaging a suspension, which averages 20 seconds in the experiments.

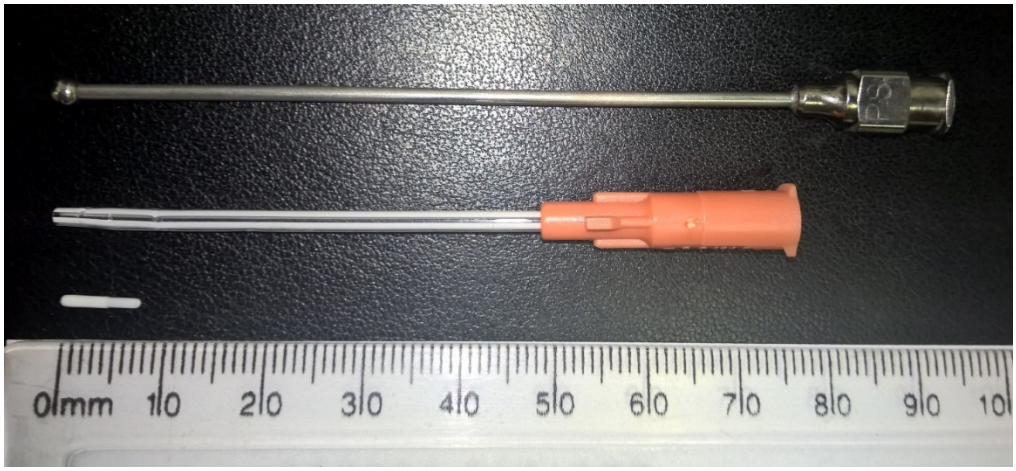

Figure 3-7: Torpac® capsule and modified apparatus used for gavage

Apparatus used by Mr Trevor Finch to gavage the capsules in C57/Bl6 mice. Mouse capsule size of 8.4 mm length and maximum 1.27 mm diameter. The capsule placed in the end of the venous catheter was gavaged in anesthetised mice. Measured polyetheretherketone (PEEK) tubing, not pictured here, was inserted and pushed to the end of the catheter, depositing the capsule. After removing the catheter and PEEK tubing, the oral gavage needle was used to push the capsule into the stomach.

Blood samples from oral groups were collected at 0.5, 1, 3, 5, 8 and 24 h.

All samples from the oral and intravenous groups were collected in 0.5 ml lithium heparin microvials and briefly vortexed to prevent blood coagulation and immediately put on ice at time of collection and stored at -80°C until extraction.

The animal experimental spreadsheet listing animal weights and individual capsule masses is presented in Table 7-18, section 7.3.2, page 230 in Chapter 7: Experimental.

3.4.4 Non-compartmental analysis

NCA was performed using PK Solutions, version 2.0 (Summit Research Services, Montrose, CO, USA). The analysis used individual whole blood concentrations vs sample times and were analysed as described in section 2.4.4, page 38.

3.4.5 Non-linear mixed effects modelling

Following the general sequential approach described in section 2.4.5, page 39, two modelling approaches were attempted using the same concentration-time data as the NCA calculations. Individual mouse weights were included as a covariate and allometrically scaled for clearance and volume. The first approach included first estimating the best structural model based on the intravenous data alone. The intravenous data of the compound best fit a one-compartment model, with first-order elimination. These parameters were fixed and the oral data of **007** and **DMB·007** evaluated separately. The oral dose allowed for a lag in transit (T_{lag}) time to the absorption compartment and absorption *via* a first-order process (k_a) from this compartment to the central compartment. The parameters were estimated separately. The second modelling approach involved pooling all data from the three groups as a single data set to be analysed in the same model. The **007** and **DMB·007** groups were designated in the covariate model as a categorical variable and the model allowed to determine the optimised estimates from all nine mice. Again, a one-compartment model with first-order rate of absorption (k_a) and a lag-time (T_{lag}) to account for the delay in the onset of absorption best fit the data. Model building was guided by physiological plausibility, significant improvements in -2 the log-likelihood (-2LL), and evaluation of goodness of fit plots, including visual predictive plots (VPC) and individual plots. The structure of the model is shown in Figure 3-8 below. Variability was included for all parameters and eliminated if statistically insignificant, as determined by changes in the -2LL. Individual plots and final parameters with statistical model parameters are presented in Chapter 7: Experimental, section 7.3.4, page 230.

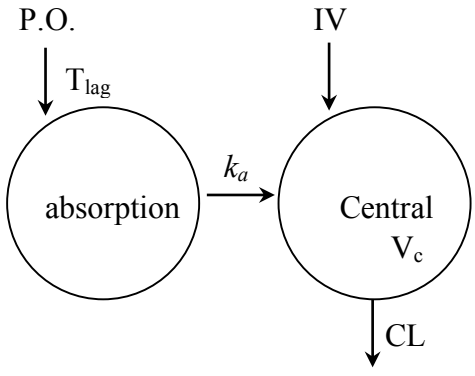

Figure 3-8: One compartment model with T_{lag} function

Structurally the model follows that the compound can be introduced P.O. (per os, by oral administration) into the absorption compartment followed by a lag in transit time (T_{lag}). One-way transfer of the compound from the absorption compartment to the central compartment proceeds *via* absorption rate (k_a) following first order kinetics. The central compartment is defined as the whole blood concentrations observed and where intravenous (IV) introduction of the dose occurs *via* instantaneous bolus. Clearance (CL) occurs from the central compartment defined as rate of elimination (k_e) by volume of the central compartment (Vc).

3.4.6 Kinetic Solubility

Kinetic solubility was determined by the miniaturised shake flask method[103,104] with modification. The experiment was performed by Mr Lloyd Tanner from the Division of Pharmacology, University of Cape Town (South Africa) under direct supervision of the author of this thesis. The method used a 10 mM stock solution of **007** and a 37.8 mM stock solution of **DMB·007**, equivalent to an equal amount of **007** in both solutions, prepared in acetonitrile. The stock solutions of **007** were used to prepare calibration standards ranging from 11 to 220 µM in acetonitrile. The stock solutions were added to a 96 well plate and dried using a Mivac© drying apparatus. Respective buffers that included phosphate buffered saline at pH 7.4, 0.01 M hydrochloric acid equal to pH 2 and FaSSIF buffer at a pH of 6.5 were then added to this dried material to a final concentration of 200 µM to simulate a dissolution step as opposed to the traditional method that spikes stock DMSO solution in relevant buffer. The aqueous samples and calibration standards prepared in phosphate buffer at a range of 11 – 220 µM were then slowly shaken for 2 hours at 25°C using a plate shaker. The solutions were then filtered and analysed by means of HPLC-DAD (Agilent 1200 Rapid Resolution HPLC with a diode array detector). The aqueous samples' solubility concentrations were calculated by the best fit calibration curves constructed using the calibration standards.

3.5 Results and discussion

At the time of the experiment, the capsules were still on a trial basis, but performing this experiment in mice rather than rats or dogs had the advantage of needing less of **DMB·007** for the smaller animals and matching the animal species of the efficacy model. The mouse-sized capsules have since been introduced commercially.

The Tocris® mouse sized capsules are designed to disintegrate within 10 minutes in the stomach. High variance was expected with the added disintegration and dissolution steps and per the approved ethics agreement it was necessary to stay within a group number of 3.

3.5.1 Pharmacokinetic profiles and calculated parameters

In Figure 3-9 is shown the observed concentration-time points raw of the aminopyridine intravenous and oral capsule experiments, each using n = 3. In Table 3-3 are shown the final calculated parameters for both NCA and NLME attempts for a side-by-side comparison. Visual predictive check of the final models attempted are shown and stratified by oral and intravenous groups in Figure 3-10. The model best fits a 1-compartment model with a T_{lag} function.

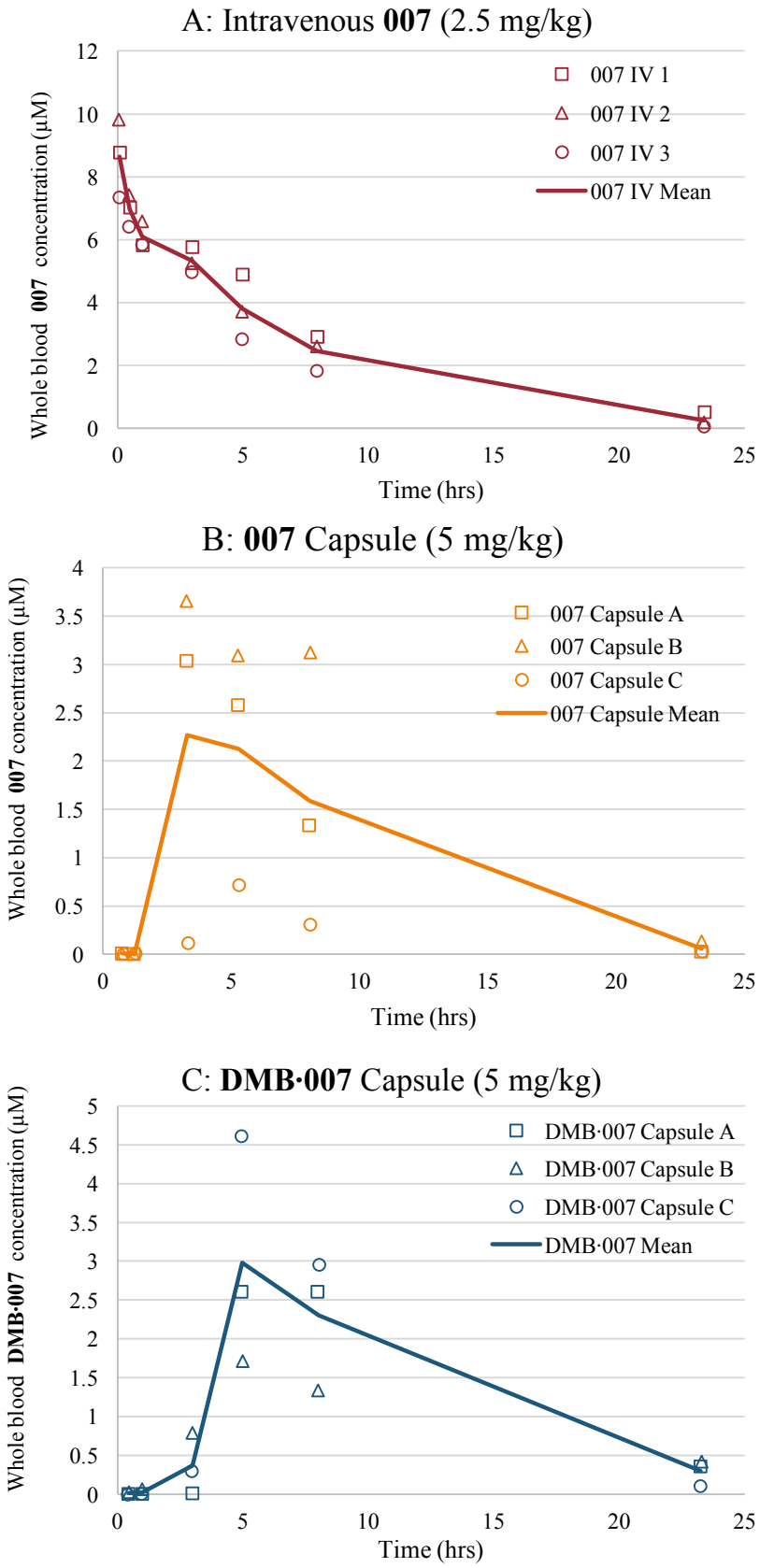

Figure 3-9: Observed pharmacokinetic data for aminopyridine experiment in mice

Individual observed concentration-time points from the A: **007** pharmacokinetic intravenous experiment, B: **DMB·007** oral experiment and C: **007** oral experiment (n = 3). Each individual animal is represented by its respective open shape, and the mean data of the group is represented by a solid line of corresponding colour.

Table 3-3: Comparison of parameter values by method

Parameter	*DMB·007*	*007*	*IV*
Non-compartmental analysis			
Blood Cl (ml/min/kg)	-	-	1.94 (0.236)
Vd (L/kg)	-	-	0.74 (0.058)
$t_{1/2}$ *(hr)*	6.12 (1.79)	3.82 (0.516)	4.58 (0.787)
$AUC_{0\text{-}inf}$ *(µM.min)*	2131 (241)	1548 (715)	3666 (442)
T_{max} *(hr)*	4.96 (0.011)	3.93 (0.683)	-
C_{max} *(uM)*	2.98 (0.856)	2.47(0.898)	-
F (%)	29.3 (3.53)	22.1 (9.47)	-
Conc 24 hr (µM)	0.295 (0.096)	0.061 (0.0354)	0.25 (0.135)
NLME modelling as combined data set			
Blood Cl (ml/min/kg)	-	-	2.34 (0.304)
Vd (L/kg)	-	-	0.82 (0.025)
$k_a(hr^{-1})$	0.815 (0.230)	1.76 (1.10)	-
$t_{1/2}$ *(hr)*	-	-	4.05 (1.05)
$AUC_{0\text{-}inf}$ *(µM.min)*	1970 (335)	1360 (585)	5330
T_{lag} *(hr)*	2.83 (0.210)	2.76 (0.350)	-
C_{max} *(uM)*	2.96 (0.776)	2.84 (1.11)	-
F (%)	24.9 (11.0)	21.5 (0.99)	-
NLME modelling as separate data sets			
Blood Cl (ml/min/kg)	2.68 (fixed)	2.68 (fixed)	2.68 (0.080)
Vd (L/kg)	1.06 (fixed)	1.06 (fixed)	1.06 (0.032)
$k_a(hr^{-1})$	0.926 (0.38)	1.58 (1.2)	-
$t_{1/2}$ *(hr)*	4.59 (fixed)	4.59 (fixed)	4.59 (0.138)
$AUC_{0\text{-}inf}$ *(µM.min)*	1940 (279)	1310 (542)	5240
T_{lag} *(hr)*	2.88 (0.13)	2.59 (0.47)	-
C_{max} *(uM)*	2.91 (0.571)	2.85 (1.09)	-
F (%)	30.1 (8.70)	22.7 (13.0)	-

Standard error of parameters is represented in parenthesis next to final median value for 3 mice. F; bioavailability, ka; rate of absorption, Vd; volume of distribution, Blood Cl; whole blood clearance, T_{max}; time of maximum concentration, C_{max}, maximum concentration. The parameters calculated by NCA used SummitPK solutions™ and the NLME modelling was performed in Monolix®. Individual plots and final parameters with variability values are presented in Chapter 7: Experimental, section 7.3.3.1, page 232.

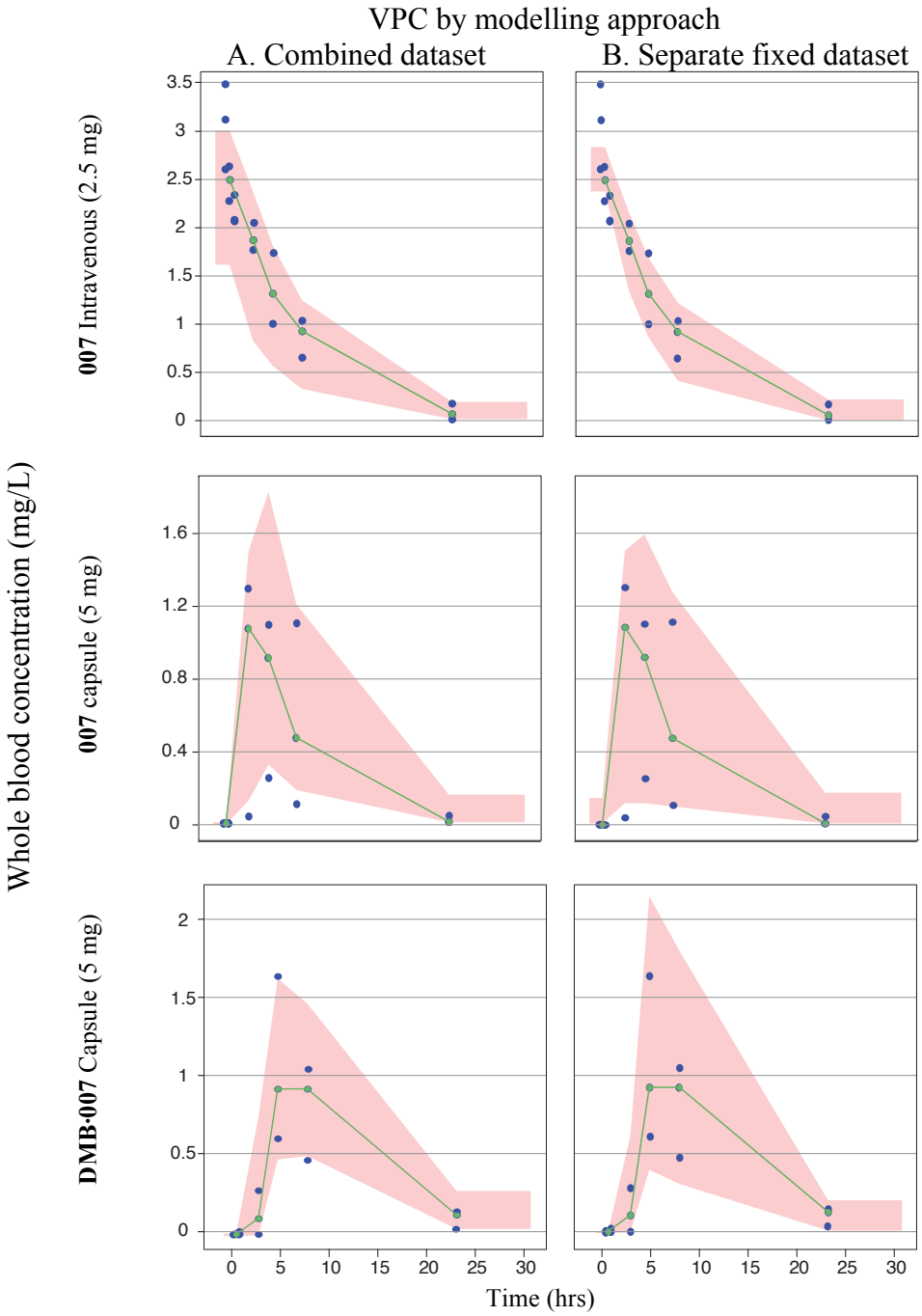

Figure 3-10: Visual predictive check of the final model used for 007

The graphical diagnostic plots of the aminopyridine dosage forms by method used. Observed data above the limit of quantification is represented by blue dots and concentrations measures below the limit of quantification represented by red dots. The green line represents the empirical percentile of this observed data and the shaded pink area represents the median of the simulated population estimate. Ideally, this empirical percentile should fit within the pink shaded area. The combined approach is a single model using data pooled from both oral and intravenous data, and the diagnostic plots here are stratified according to dosing. The separate approach consists of three separate models for each dosing group. First a robust model for the intravenous data was established to accurately determine clearance and volume which was fixed in the next two respective models for each dosing form.

3.5.1.1.1 Comparison of results for aminopyridine dosing

Examining the pharmacokinetic profiles of the three experiments, **007** was detectable for the entire duration of 24 hrs in all groups. As expected parameters calculated by NCA showed the capsule dosage form had higher variability in absorption due to the added variability of capsule and compound dissolution. The rate of absorption for **DMB·007** from the concentration-time profile appeared slower with a significant lag in absorption and a longer time to maximum concentration (T_{max}) of 5 hours compared to 4 hours for **007**. Mean bioavailability suggests higher exposure was observed for **DMB·007**, which also showed less variability in pharmacokinetics, suggesting its absorption to be more consistent and predictable. Apparent terminal half-life was higher for **DMB·007** and at 24 hours after the dose, an average concentration of 0.3 µM was observed, much higher than the average concentration of **007**, which was only 0.06 µM.

The pharmacokinetic profile of the **007** compound appeared to show linear elimination with an initial α-slope, distribution phase, of higher magnitude during the first 2 hours compared to the β-slope, elimination phase, Figure 3-11. This initially suggested a two-compartment model may best fit the data.

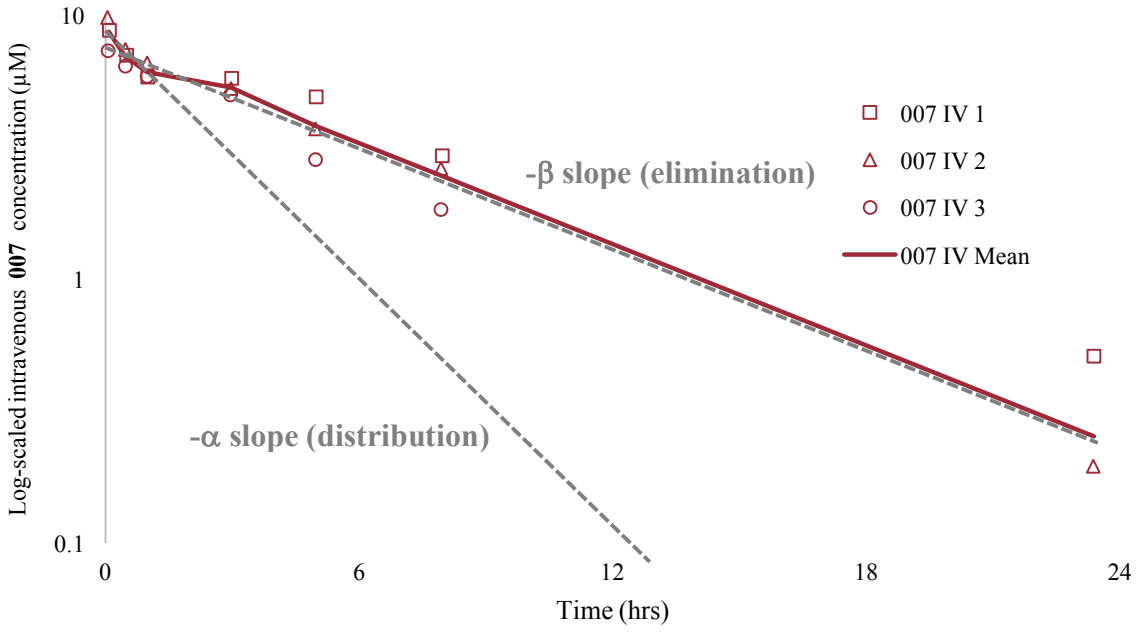

Figure 3-11: Pharmacokinetic profile of intravenous 007

The log-scaled intravenous profile of **007** (n = 3) with observations shown in open shapes respective of individual animal and the mean intravenous concentration shown by solid red line. The α and β slope related to distribution and elimination respectively are illustrated next to the mean line as dashed grey lines.

Model building proceeded with the general approach as described in section 2.4.5, page 39 and started with a one compartment model, in this case starting with just the intravenous reference data. Changing the structural model to a two-compartment model with two added parameters namely, inter-compartmental clearance and peripheral volume resulted in the log-likelihood function dropping only 3 points, which was not statistically significant for the additional two parameters included. There was also no striking improvement in diagnostic plots showing that a one-compartment model was statistically relevant to capture the intravenous dataset. Whole blood clearance was calculated to be low at 2.68 ml/min/kg (38% higher than NCA calculations) and volume of distribution was low at only 0.74 L/kg confirming that the compound did not greatly move into peripheral space and stayed in the measured central compartment. The half-life was moderate at 4 hrs.

Model building for the oral groups used these clearance and volume parameters as fixed values and necessary oral bioavailability and rate of absorption parameters added in each dosing groups' respective oral model. A delay in absorption was clear from the oral profiles and inclusion of a T_{lag} parameter caused a significant drop in objective function, together with improved diagnostic plots, confirming its inclusion. Both the **007** dosing group and **DMB·007** had similar lag in absorption times, calculated close to 3 hrs. This was different from the initial NCA impression, showing that NLME could "fill-in" the individual profiles compared to the empirically observed T_{max} and C_{max} values from NCA that can be misleading if sampling does not occur at exactly T_{max}. This concluded that both dosage forms had similar transit times from capsule to compound available for absorption.

Further the modelling approach using separate datasets result showed a 9% increase in bioavailability for **DMB·007** and though variance was high in both models, **DMB·007** showed less variance supporting the results of the NCA. When clearance and volume of distribution were unfixed and re-estimated to assess the stability of the model, a significant increase in objective function did occur for both models. Unfixing parameters should not cause an increase in objective function value, so this was interpreted as a sign that a local minimum of the objective function value was encountered during the search for the optimal parameter values, possibly indicating that the model was not stable and over-parameterised for such a small data set. The differences in the final parameter estimates of the freed models were a lower clearance of **DMB·007** and 11% increase in bioavailability in favour of **DMB·007** compared to **007**.

A joint model for both **007** and **DMB·007** with separate estimates for k_a, bioavailability and T_{lag} of the two compounds was also attempted and showed slightly different results compared to the

separate analyses. In this model, no significant increase in bioavailability was observed and the model showed a faster rate of absorption (k_a) for **007** when compared to **DMB·007** (1.7 and 0.8 hr^{-1} respectively), and larger variability observed for **007** than **DMB·007**.

3.5.2 Modelling attempts and limitations

It is not straightforward to decide what modelling approach is the most suitable to interpret this data. The argument for developing a joint model is mathematical/statistical in nature as the model gains power in sample size and is expected to be more robust. The argument against this asserts that the introduced dose is fundamentally different in chemical nature, so a separate or more flexible structural model may be necessary to account for the complexity of the absorption and the differences between the two compounds. Adding complexity to the model such as using a mixed-order absorption or transit compartment model was attempted but not feasible, as the added complexity could not be supported by the data and was prone to lead to more bias than solid answers.

NLME relies on finding parameters that best fit all the data, and even separating the absorption parameters of **DMB·007** and **007** as a categorical covariate could not robustly identify significant differences. The model could not reliably attribute the differences to either T_{lag}, k_a, or bioavailability, and the results were found to be mostly driven by the choice of initial parameter estimates rather than solid differences in the data.

Despite this uncertainty, results from both the separate or joint modelling approach provide similar results to the kinetic solubility and final efficacy results. Of course, it is an important limitation to note that a direct comparison between the efficacy experiment that used suspension formulations cannot be directly compared to the pharmacokinetic study that used a solid-state formulation in this case. The separate models approach suggested higher bioavailability, while the joint model proposed more consistent, slower absorption from the duodenum. Both results are consistent with increased concentration observed at 24 hours and improvement in **DMB·007** efficacy *in vivo* over **007.**

3.5.3 Kinetic Solubility

In Table 3-4 is shown the solubility experiment results performed by Mr Lloyd Tanner from the Division of Pharmacology, University of Cape Town (South Africa) under supervision of the author of this thesis. The concentration of **007** (the guest molecule able to cross the intestinal wall) was measured.

Table 3-4: Kinetic solubility of DMB·007 and 007

	Concentration of **007** measured (μM)	
	DMB·007	**007**
pH 2 in 0.01 M HCl solution	198 (1.75)	170 (0.261)
pH 6.5 in FaSSIF media	65.5 (2.24)	23.1 (0.568)
pH 7.4 phosphate buffer	52.9 (1.36)	22.0 (0.569)

The solubility experiment was performed by Mr Lloyd Tanner from the Division of Pharmacology, University of Cape Town (South Africa) under direct supervision of the author and used a miniaturised shake flask method. The concentration of **007** was measured for comparison. FaSSIF: 25°C for 2 hrs. n = 2

Improved kinetic solubility was observed for **DMB·007** at all pH's with a two-fold increase at FaSSIF pH 6.5 and pH 7.8, and a slight improvement at pH 2. As expected, comparing the acetonitrile dried method to DMSO spiked concentrations had lower solubility results. Ideally, the best practice to evaluate the dissolution would be an exact mass of pre-weighed complex with buffer added to the solid mass, but the low yield and high effort required to produce **DMB·007** required conservative efforts in evaluation. The assays were kept at 2 hrs to best simulate transit times through the stomach and were in line with the final pharmacokinetic results.

The increase in solubility at pH 2 for both **DMB·007** and **007** due to partial ionisation of the amine group is problematic as absorption should ideally take place in the higher pH environment of the duodenum where there is a larger surface area and longer transit times to allow for complete absorption. Stomach emptying could cause great variance as early emptying after dosing could lead to inadequate time for dissolution and subsequent absorption, and could even lead to dissolved compound crashing out in the higher pH duodenum. Previous pharmacokinetic studies show that

cyclodextrins are capable of delayed release due to a pH-dependent shift in dynamic equilibrium, releasing the guest molecule in intestinal, rather than gastric fluid and improving absorption and bioavailability from the small intestine.[113–115] The **DMB·007** complex did show improved solubility of 2.8-fold at pH 6.5 FaSSIF media and 5.3-fold in pH 7.4 phosphate buffer compared to **007**.

3.6 Conclusion

Table 3-5 compares the final results of **DMB·007** and **007** with the acetonitrile dried solubility method and separate modelling approach.

Table 3-5: Summary of DMB·007 and 007 results

		DMB·007	**007**
Bioavailability (%)		30.1	22.7
T_{lag} (hr)		2.88	2.59
k_a (hr^{-1})		0.926	1.58
Solubility pH (μM)	2 (Fassif)	198	170
	6.5	65.5	23.1
	7.8	52.9	22.0
%P (MSD) 1 x 3 mg/kg		54.4 (7)	20.8 (3)

Note: Pharmacokinetic parameter assessed at 5 mg/kg oral dose. %P: Reduction in parasitaemia (%), MSD: Mean Survival Days.

To draw a single conclusive reason for the difference observed in efficacy of **DMB·007** and **007** remains challenging. Speculatively, a pH dependent change in dissolution for **DMB·007** and **007** resulting in increased absorption from the duodenum would explain the decreased variance and change in apparent half-life of the NCA results for **DMB·007**, and improved final exposure. Either the joint or separate modelling approaches that respectively showed improved bioavailability or improved rate and consistency in absorption support the narrative of higher and more consistent absorption for **DMB·007**. However, the emphasis on which parameter is responsible remains unknown. Decreasing variance in absorption supports the known drug discovery paradigm that a compound's reproducibility *in vivo* is as significant if not more important than an improved increase in absorption.[151] However, it is important to maintain that the experiments used to evaluate the expected pharmacokinetic improvements all show small and possibly insignificant differences.

Criticism of the modelling used in this study rightly observe it as a "hit-and-miss" approach that is noteworthy. Although variance in the capsule dosing form was assumed to be higher, it was thought that modelling could overcome this, but this was not possible. To keep in line with the

objectives of the study it needed to exhaust all possible modelling options to compare NCA and NLMA. One school of thought believes that modelling even to ascertain variability within the dosing forms is a positive outcome and speaks to current knowledge of the experiment and where improvements need to be made Future experiments to evaluate the effect of **DMB·007** complexation on pharmacokinetics would benefit from higher animal numbers and more sample times at the expected absorption phase. In contrast, another school of thought believes that modelling already adds a level of difficulty that lacks efficiency at this preclinical stage.

Further criticism of the technique used include the capsule use and that it is a flawed design and an over complication of a mouse pharmacokinetic study that was unlikely to lead to any meaningful results. Notwithstanding this, it is noteworthy that the quality of the material that showed a 65-fold increase in aqueous solubility provided by the Supramolecular group warrants further progression. This would ideally include dissolution studies. Therefore, progressing to animal studies was the simplest approach in the lab repertoire at the time. Rats and dogs are commonly used in capsule dosing where the material tested needs to stay in a solid-state to assess its improvement in dissolution.[152–161] Mice capsule provided a unique advantage here as they were more similar to the mice used for efficacy studies and considering their smaller size their greatest advantage was that less of **DMB·007** needed to be synthesised.

4 FUSIDIC ACID PRODRUGS FOR POTENTIAL REPOSITIONING IN TUBERCULOSIS

4.1 Introduction

Fusidic acid is a well-characterised antibacterial drug that shows favourable *in vitro* antimycobacterial activity, Figure 4-1.[162–164] Introduced clinically in the 1960s for the management of gram-positive infections including methicillin resistant *Staphylococcus aureus* (MRSA),[165–168] fusidic acid possesses favourable pharmacokinetic properties and a well-tolerated safety profile.[169,170] The naturally occurring fusidane antibiotic acts by inhibiting protein synthesis through stabilisation of the elongation factor G – GDP complex, preventing peptide elongation, Figure 4-2.[171,172]

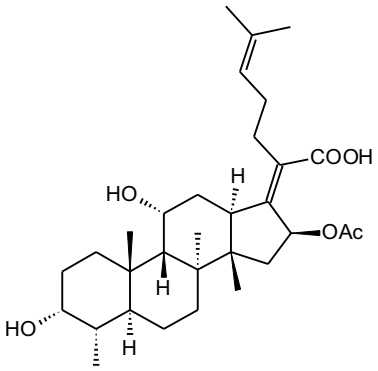

Fusidic acid

Activity MIC_{99}: 1.25 µM

Cytotoxicity in CHO IC_{50}: >194 µM

Figure 4-1: Structure and activity of fusidic acid

MIC_{99}; minimum inhibitory concentration to inhibit 99% of mycobacterial growth, CHO IC_{50}; cytotoxicity concentration showing 50% inhibition in Chinese hamster cell ovarian cells.

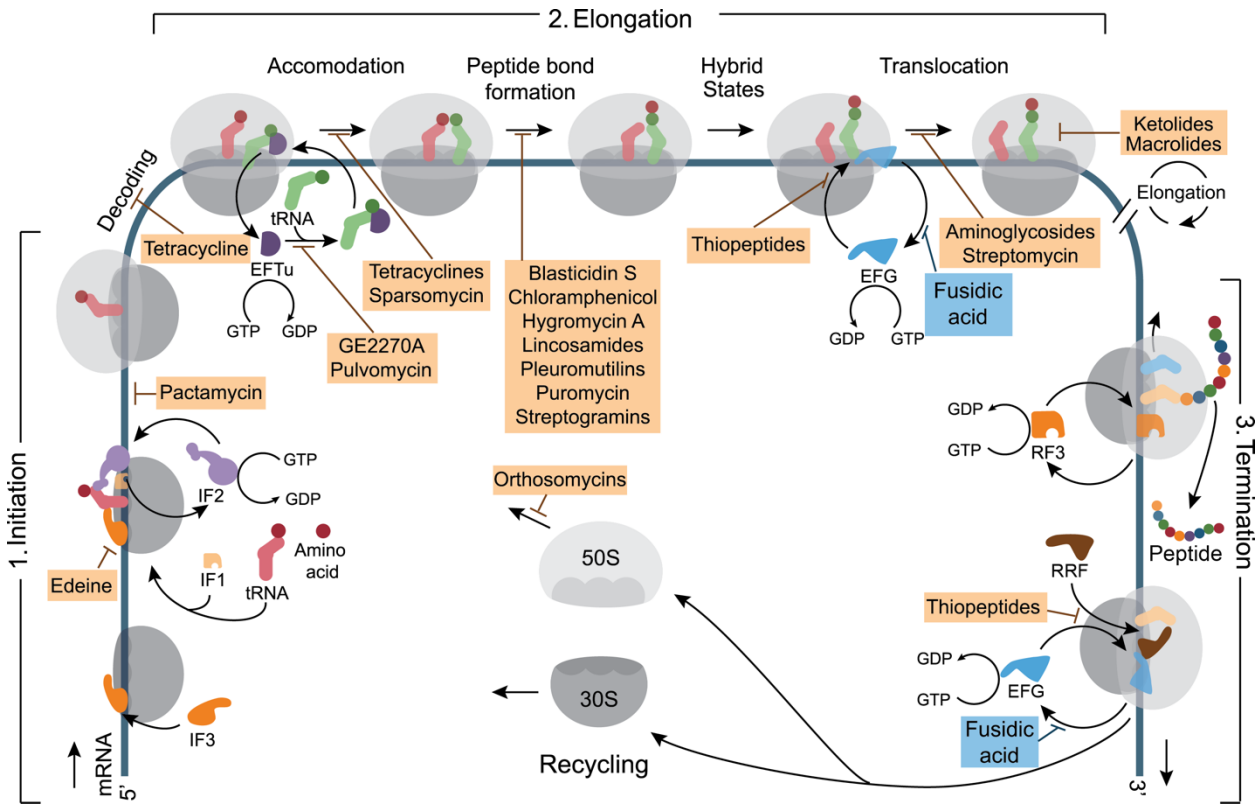

Figure 4-2: Sites of antibiotic action during protein synthesis. Adapted from Wilson, 2009.[173]

During initiation, initiation factors (IF) 1, 2 and 3 assist ribosome complexation and incorporate messenger RNA (mRNA) at its 5' cap position and insert coded transfer RNA (tRNA) carrying its appropriate amino acid. Elongation factor thermo-unstable (EFTu) assists additional tRNA to move into the free ribosome site where peptide elongation can occur. Elongation factor G (EFG) assists in translocating mRNA and tRNA as the ribosome complex moves along the mRNA sequence to insert coded tRNA carrying amino acids that form peptide bonds with the lengthening peptide chain. Finally, when the mRNA reaches its terminal stage, release factor 3 (RF3) reads the stop codon, signalling termination where EFG and ribosome recycling factor (RFF) assist in removing mRNA and tRNA, and split the ribosome complex that can return to the initiation phase of a new peptide synthesis. Fusidic acid stabilises EFG-GTP in the ribosome complex, thereby preventing turnover, which disrupts the translocation and termination stages of this sequence.

The antimycobacterial activity of fusidic acid, including activity against resistant clinical strains,[163] unique mode of action and well-tolerated clinical profile made it an attractive compound to repurpose for the potential treatment of tuberculosis. The Global Alliance for Tuberculosis Drug Development initiated efficacy evaluation of fusidic acid in mice at Colorado State University in the laboratory of Dr Anne Leanerts. Two models were used to evaluate efficacy; an acute interferon-gamma knockout (GKO) mouse model to test against actively replicating bacteria representing early bactericidal activity, and a chronic Balb/c mouse model to test against more slowly replicating bacteria. Both models showed fusidic acid had no effect against tuberculosis in

mice at 100 mg/kg oral dosing. To increase exposure, repeat experiments using subcutaneous dosing at 100 and 200 mg/kg were performed, but three experiments had to be halted and animals sacrificed early due to severe toxicity. A cyclodextrin formulation, 30% Captisol®, was used to aid in buffering the acidic drug for a repeat experiment and improved tolerability, and the experiment could be performed to 4 week completion. All subcutaneous experiments similarly showed no effect in the selected tuberculosis mouse models. In Table 4-1 is shown the log colony forming unit (CFU) reduction results with appropriate positive controls for comparison. This lack of *in vivo* efficacy in a tuberculosis mouse model is consistent with other findings such as the study by Payne *et al*.,[174] that found fusidic acid to be active *in vitro*, but not *in vivo* in mice against toxoplasmosis and listeria.

Table 4-1: Tuberculosis efficacy of fusidic acid in mice

GKO knockout mouse (fast replicating bacteria)				
			log CFU reduction	
Drug	Dose (mg/kg)	Route	Lung	Spleen
Isoniazid	25	Oral	3.02	4.52
Fusidic Acid	100	Oral	0.15	0.18
Isoniazid	25	Oral	2.99	5.04
Fusidic Acid	100	SQ	-0.18	-0.25
Fusidic Acid	200	SQ	0.78	0.62

Chronic Balb/c (slow replicating bacteria)					
				log CFU reduction	
Drug	Dose (mg/kg)	Route	Duration	Lung	Spleen
Rifampicin	10	Oral	4 weeks	3.44	1.79
Fusidic acid	100	PBS SQ	2 weeks*	0.21	0.14
Fusidic acid	200	PBS SQ	2 weeks*	0.01	-0.04
Fusidic acid	100	Captisol® SQ	4 weeks	-0.13	0.05

Anti-tuberculosis efficacy experiments performed at Colorado State University in the laboratory of Dr Anne Leanerts
Note: * experiment halted early due to signs of toxicity. SQ; subcutaneous, PBS; phosphate buffered saline, CFU; colony forming units. Negative values represent an increase in mycobacterial burden compared to controls.

4.2 Rationale

It was hypothesised that the reasons for the lack of fusidic acid efficacy in mice could include poor exposure of fusidic acid at the site of infection. To test this hypothesis, a prodrug strategy was considered. The definition of a prodrug includes any compound that must undergo

biotransformation *in vivo* to exhibit its pharmacological effect. It has become an advanced field with strategies that can improve a pharmacologically active compound's physiochemical, biopharmaceutical or pharmacokinetic properties. Potential compound properties that can be improved through a prodrug approach can include:[175–179]

1. Poor aqueous solubility
2. Chemical instability
3. Insufficient oral absorption
4. Rapid pre-systemic metabolism
5. Inadequate blood brain barrier penetration
6. Poor tissue distribution
7. Toxicity and/or local irritation

Esters are the most common prodrugs used, accounting for approximately 49% of all prodrugs on the market.[178] Other derivatisation options include synthesis of the compound to form carbonates, ethers, phosphates, amides, carbamates, N-Mannich bases, oximes and imines.[180]

For this study, it was expected that fusidic acid would already have sufficient oral absorption and good bioavailability, based on its well documented clinical profile. The initial aim for a prodrug design was to see if prodrug modification could improve tissue distribution at expected drug target sites, which in tuberculosis pathology can be difficult to reach. Prodrugs designed to interact with carboxylic esterase is a common strategy as carboxylic esterase is functionally prominent and ubiquitously distributed.[181] This is advantageous as a prodrug metabolised by carboxylic esterase is unlikely to become saturated or show high population variance. Carboxylic esterase is distributed in lungs[182] and macrophages,[183] which make them an attractive prodrug strategy in tuberculosis as they could potentially deliver compounds closer to the site of mycobacterial infection. Accordingly, a series of C-3 ester prodrugs of fusidic acid was designed and synthesised by Dr Gurminder Kaur from the Department of Chemistry, University of Cape Town (South Africa). In Figure 4-3 is shown the two of the prodrugs, **GKFA16** and **GKFA17**, considered for further investigation due to their inherent antimycobacterial and low cytotoxicity giving a favourable selectivity index.[184]

GKFA16

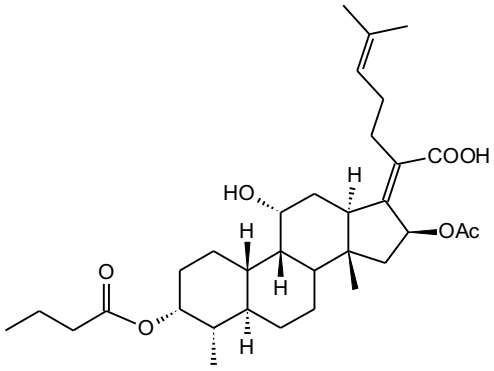

MIC_{99}: 1.25 µM

CHO IC_{50}: 170 µM

GKFA17

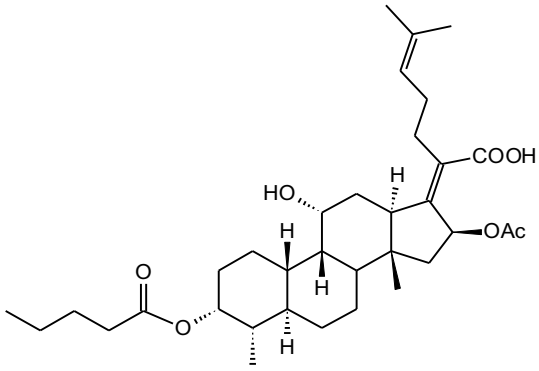

MIC_{99}: 2.5 µM

CHO IC_{50}: 74 µM

Figure 4-3: C-3 ester fusidic acid prodrugs, GKFA16 and GKFA17[184]

The C-3 ester fusidic acid prodrugs were designed and synthesised by Dr Gurminder Kaur from the Department of Chemistry, University of Cape Town (South Africa). Note: MIC_{99}; minimum inhibitory concentration to inhibit 99% of mycobacterial growth, CHO IC_{50}; cytotoxicity concentration showing 50% inhibition in Chinese hamster cell ovarian cells.

In parallel to the *in vivo* studies undertaken, metabolite identification studies of fusidic acid were being conducted by Dr Mathew Njoroge at the Department of Chemistry, University of Cape Town (South Africa). It showed metabolism of fusidic acid to a metabolite with a shorter retention time exclusively in mouse and rat liver microsomes, but this metabolism did not occur in human liver microsomes. This metabolite was suspected to be 3-epifusidic acid.[185] To our knowledge, this metabolite has not been observed in a clinical setting. In Figure 4-4 is shown the selected prodrugs and their assumed metabolite route in rodents accompanied by individual antimycobacterial activity and cytotoxicity data.

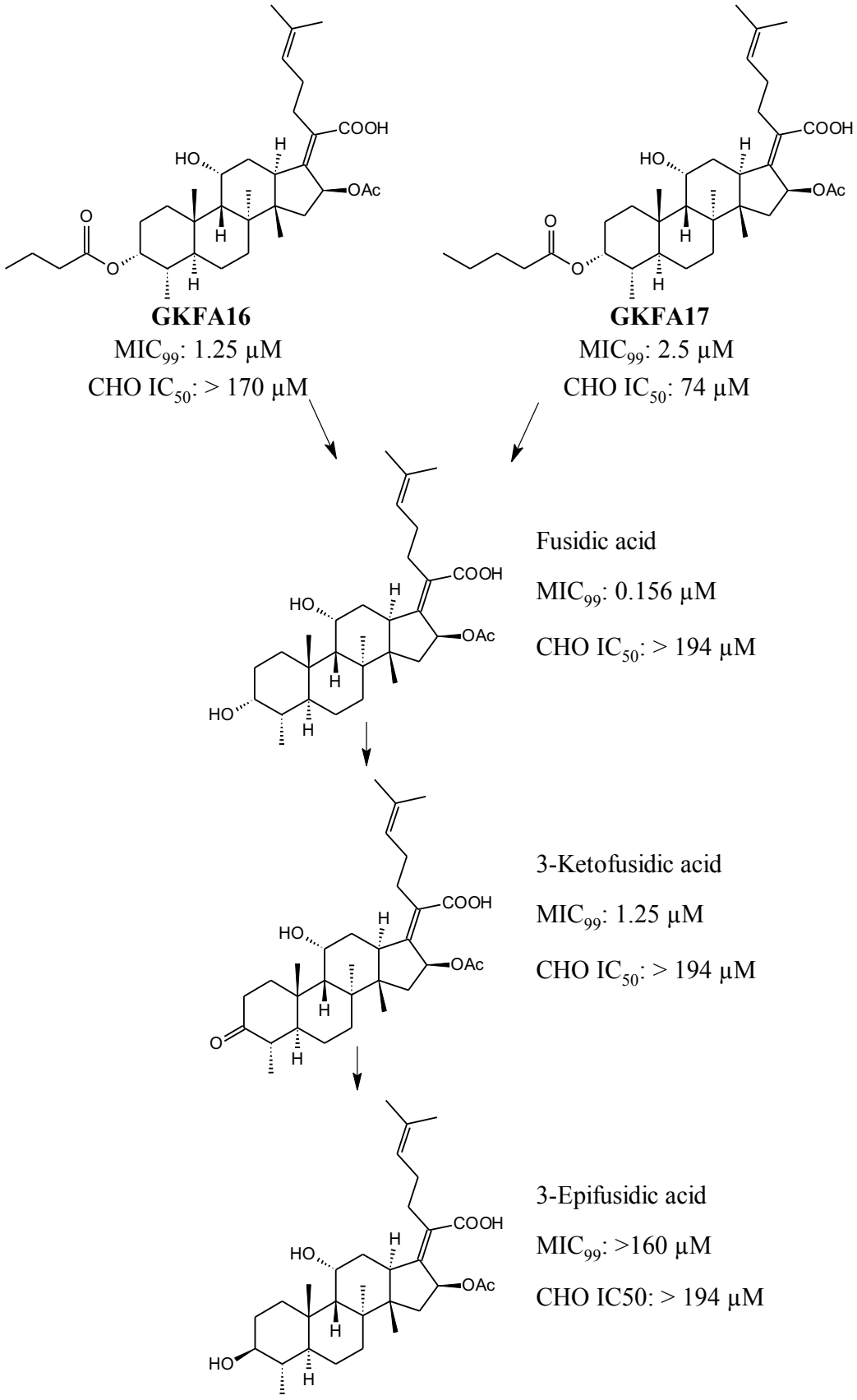

Figure 4-4: Metabolic pathway of C-3 ester prodrugs GKFA16 and GKFA17 in mice

Note: MIC_{99}; minimum inhibitory concentration to inhibit 99% of mycobacterial growth, CHO IC_{50}; cytotoxicity concentration showing 50% inhibition in Chinese hamster cell ovarian cells.

To rationalise the lack of fusidic acid efficacy in mice, full pharmacokinetics, organ distribution (discussed in Chapter 5, page 167) was performed and relevant metabolites in mice were monitored to evaluate compound exposure closer to the site of infection for these fusidic acid C-3 ester prodrugs, fusidic acid and its 3-keto- metabolite.

4.3 Methodology overview

Figure 4-5 shows the approach and experiments undertaken for the pharmacokinetic evaluation of two fusidic acid C-3 ester prodrugs and their respective known metabolites as reference. A multiplex LC/MS/MS assay was developed to quantify the selected metabolites efficiently in one method, section 4.4.2. The initial pharmacokinetic experiments of **GKFA16**, **GKFA17** and fusidic acid where run over 7 hours and 3-ketofusidic acid over 24 hours. An intense peak matching the transition and retention times of the suspected 3-epifusidic acid was observed. This information motivated the synthesis of 3-epifusidic acid, and a recovery experiment to retrospectively quantify the metabolite was performed, section 4.5.1. Quantified 3-epifusidic acid and metabolites were included in NCA, but NLME modelling attempts to include metabolite concentrations as separate compartments were unstable with the small datasets. NLME was used to exclusively model parent compounds for comparison with their respective NCA results. The compounds were progressed to organ distribution studies, discussed in Chapter 5, page 167.

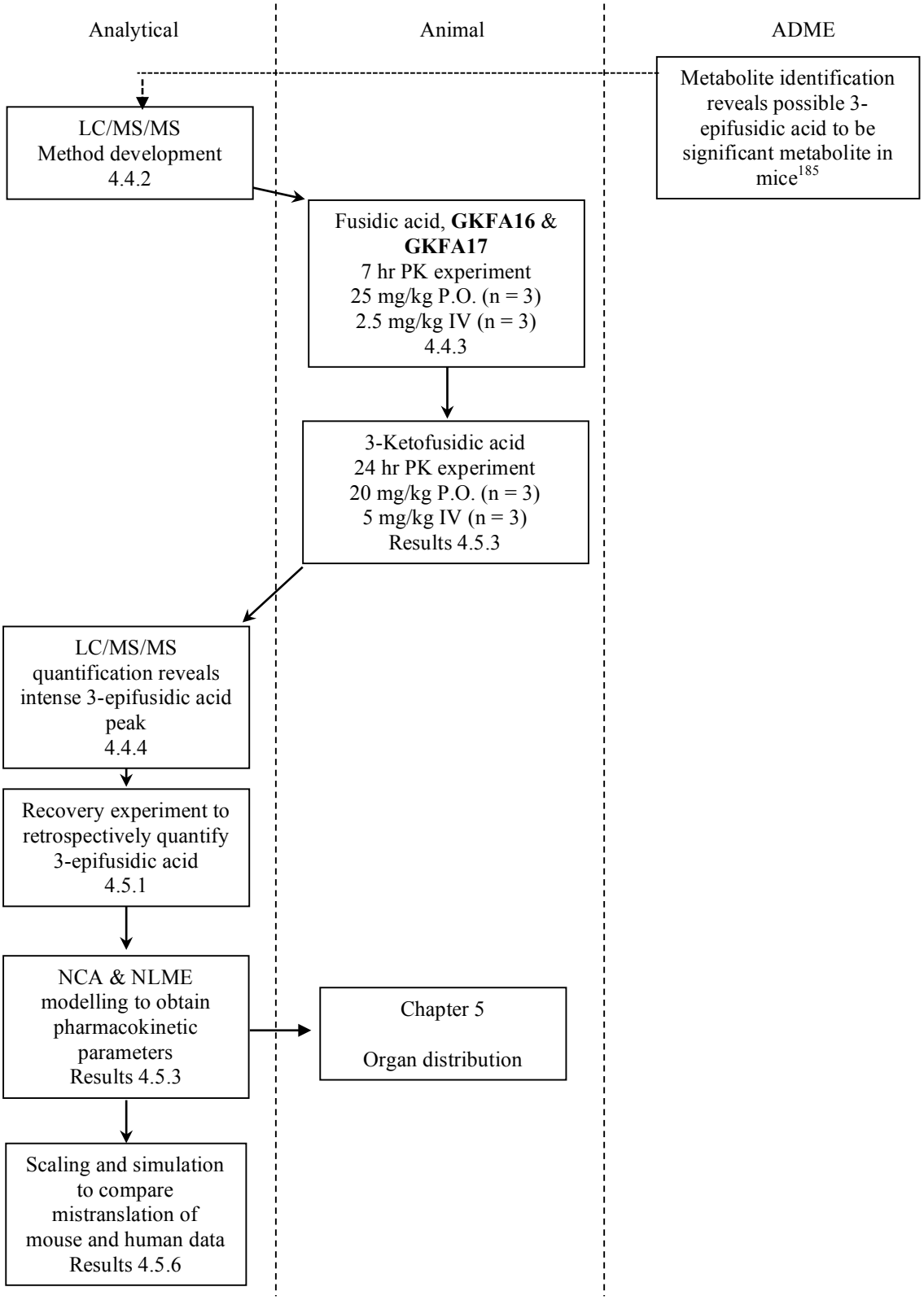

Figure 4-5: Fusidic acid evaluation methodology overview

4.4 Methods

4.4.1 In vivo anti-tuberculosis efficacy

4.4.1.1 Testing site

In vivo efficacy trials were performed by Dr Anne Lenaerts at Colorado State University according to standardised methods[186–188] approved by the Colorado State University Institutional Animal Care and Use Committee (IACUC).

4.4.1.2 In vivo efficacy model of acute tuberculosis infection

Efficacy of fusidic acid was tested by the method from Lenaert *et al*. (2003).[187] Briefly, 8 week female C57BL/6-IFNγ knockout mice, also known as interferon-gamma knockout mice (GKO) from Jackson Laboratories were infected with a low dose aerosol of approximately 100 colony forming units (CFU)'s of *Mycobacterium tuberculosis* Erdman strain per mouse. A total of three mice were sacrificed on day one to verify bacterial uptake. On day 13, 5 mice were sacrificed to quantify pre-treatment bacterial load in lungs and spleen. Treatment by oral gavage of fusidic acid at 100 mg/kg in aqueous 0.5% methylcellulose commenced in the remaining five mice on the same day. The drug was given daily for nine consecutive days. On day 10 post-initiation of treatment, lungs and spleens were harvested and bacterial loads determined by enumeration of CFU.

4.4.1.3 In vivo efficacy model of chronic tuberculosis infection

Fusidic acid was also evaluated in a chronic infection, using female Balb/c mice (Charles River Labs, Wilmington, MA) infected with a low dose aerosol infection.[186,189–191] Similarly on the day of infection three mice were sacrificed to verify bacterial uptake. At 21 days post-infection, 5 mice were sacrificed as controls and the remaining 5 mice per experimental group were treated with fusidic acid at 100 and 200 mg/kg, given in sterile phosphate buffered saline by subcutaneous injection for 4 weeks of treatment. Alternatively, fusidic acid was dosed at 100 mg/kg in 30% Captisol, also given subcutaneously. Lungs and spleens were harvested after the 28 days of treatment and bacterial loads determined by enumeration of CFU.

4.4.2 LC/MS/MS method

Whole blood concentrations of the compounds were quantified by an LC/MS/MS assay developed for a range of 2 – 5000 ng/ml. The samples were extracted by protein precipitation using 20 µl whole blood and 240 µl methanol containing a structurally similar internal standard. Gradient chromatography was performed on a Phenomenex® Kinetex C_{18} (2.1 x 50 mm, 2.6 µm) reverse

phase column at a flow rate of 400 µl/min with mobile phases 0.03% ammonium hydroxide (v/v) in water and acetonitrile. The ammonium adducts of all compounds ionised best and Table 4-2 shows final transitions for the selected compounds analysed on an AB Sciex API 4500® mass spectrometer operated at unit resolution in multiple reaction-monitoring mode. Quantification accuracy and precision were measured for high (4000 ng/ml), medium (2000 ng/ml) and low (6 ng/ml) quality controls of all analytes. The quantification statistics of each compound's respective batch with highest and lowest accuracy (%Norm) and highest percentage coefficient (%CV) of all parent and metabolite compounds are shown in Table 4-2.

Table 4-2: Fusidic acid analogues transition and statistics

Compound	Transition	%Norm	CV
GKFA16	604 → 527	93.5 – 123	9.42%
GKFA17	618 → 541	95.6 – 112	22.2%
Fusidic acid	534 → 458	97.7 – 116	30.5%
3-ketofusidic acid	532 → 455	94.6 – 104	17.8%

Figure 4-6 shows a chromatogram of the multiplex method and an inset zoomed axis of the chromatogram with labelled peaks. The integrated peaks of low quality controls and their respective internal standards for each compound from selected batches, quantification statistics of individual analytes of each batch, expanded extraction method and mass spectrometer conditions are presented in Chapter 7: Experimental, section 7.4, starting on page 240.

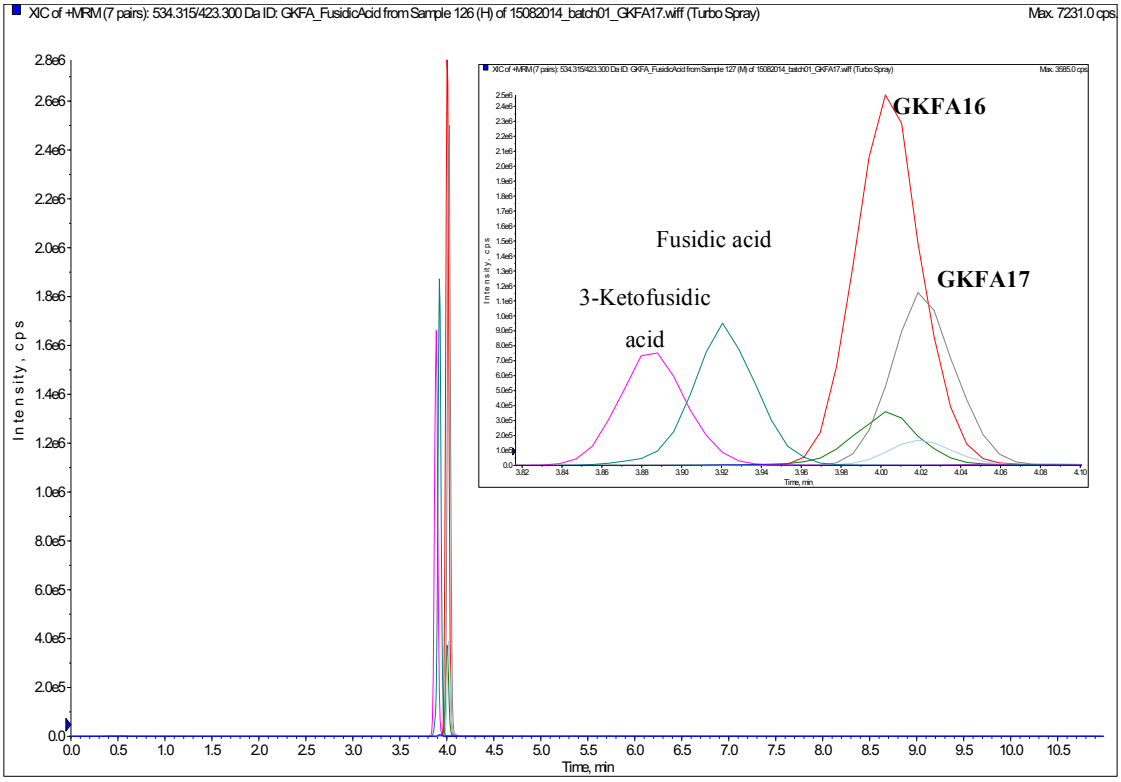

Figure 4-6: Chromatogram of fusidic acid analytes

Multiplex assay to quantify **GKFA16** and **GKFA17** and respective metabolites in the same method. Cut-out presents the zoomed in time axis between 3.82 and 4.10 min to better view the separation.

4.4.3 In vivo pharmacokinetic experiment

4.4.3.1 Animals

All animal studies and procedures were conducted with prior approval of the Ethics Committee of University of Cape Town (UCT) (approval number 013/032) in accordance with the National Code for animal use in research, education, diagnosis and testing of drugs and related substances in South Africa. The pharmacokinetic animal experiment used healthy 6 - 8-week-old C57BL/6 mice maintained at the University of Cape Town animal facility. Mice were housed in 27 x 21 x 28 cm cages under controlled environmental conditions including a maintained temperature of 26 ± 1°C and 12 hr light/dark cycle. Food and water was available *ad libitum.*

4.4.3.2 Compound preparation

The author of this thesis prepared compounds for administration. Mr Trevor Finch from the Division of Pharmacology, University of Cape Town (South Africa) performed all animal handling, compound administration and blood collection under direct supervision of the author, with the author present for all animal procedures and responsible for samples and record keeping.

On the day of the experiment, a predetermined mass of the test compound was weighed for oral and intravenous groups based on the average mass of the animal experimental groups determined that morning.

For the 3-ketofusidic acid compound, the intravenous group consisted of three males that weighed approximately 30 g, while the oral group consisted of three females that averaged approximately 22 g.

For oral administration, the weighed compound was suspended in 1000 µl of aqueous 0.5% HPMC (w/v) and vortexed for 1 minute. Drug administration followed by oral gavage of 200 µl total volume of suspension. Administration occurred within 30 minutes of suspension preparation. For intravenous administration, the weighed compound was prepared in an organic vehicle of 10% dimethyl sulfoxide (DMSO), 10% ethanol, 50% polypropylene glycol and 30% polyethylene glycol 400. The compound was first dissolved in DMSO, vortexed, followed by addition of other vehicle constituents and then vortexing for at least 1 min. Solubility was confirmed by visual inspection of the dosage solution before administration. Intravenous injection into the penile dorsal vein of 60 µL total volume was performed under microscope. The organic vehicle required a slow push over 1 minute to prevent shock to the mice.

For fusidic acid, **GKFA16** and **GKFA17**, both the oral and intravenous groups consisted exclusively of males, averaging 26 g. Oral and intravenous dosing followed the same procedure, and in all experiments dosage occurred within 30 minutes of formulation preparation.

Whole blood samples were collected *via* tail bleeding at predetermined time points in 0.5 ml lithium microvials and vortexed for 30 seconds to prevent coagulation. The samples were stored at -80°C. For the 3-ketofusidic acid experiment whole blood collection occurred at time intervals predose, and 0.5, 1, 3, 5, 8 and 24 hrs for the oral and intravenous groups. Additionally, the intravenous group included sample collection at 5 minutes after dosing. Fusidic acid, **GKFA16** and **GKFA17** had whole blood collected at 5 min, 0.5, 1, 3, 5 and 7 hrs for intravenous groups and 0.5, 1, 3, 5, and 7 hrs for oral groups.

The animal experimental records are presented in Table 7-29 to Table 7-32, section 0, starting from page 251.

4.4.4 Metabolite identification

4.4.5 Non-compartmental analysis

NCA was performed using PK Solutions, version 2.0 (Summit Research Services, Montrose, CO, USA). The analysis used individual whole blood concentrations vs sample times and were analysed as described in section 2.4.4, page 38. Additionally, AUC values for the metabolite data were calculated by the sum of the observed AUC (calculated by the trapezoidal rule) and extrapolated area (calculated by final concentration divided by k_e where k_e is the elimination rate constant). Individual whole blood concentration vs time data, individual NCA results are presented in section 7.4.3, page 264.

4.4.6 Non-linear mixed effects modelling

As previously described in section 2.4.5, page 39, model development occurred sequentially starting with one-, two-, and three- compartment structural models. The models were adapted for intravenous or oral administration, with the intravenous dose considered as instantaneous into the central compartment, and an oral dose absorbed *via* a fist-order process from an absorption compartment. Model building was guided by physiological plausibility, significant improvements in -2 the log-likelihood (-2LL), and evaluation of goodness of fit plots, including visual predictive plots (VPC) and individual plots.

At the time of the design, the 3-epifusidic acid metabolite was unknown. The model would start with the concentration-time data for the 3-ketofusidic acid and parameter estimates recorded and fixed into the next model using the data obtained from fusidic acid. These estimates would then similarly be fixed in the prodrug models. Finally, the model would be freed to check the robustness of the model and again fixed where necessary and the statistical model approached sequentially. After discovering and quantifying the 3-epifusidic acid metabolite data, this was included as an extra compartment within the designed model. The accented section below represents the envisioned structural model approach.

Step 1: Model 3-ketofusidic acid's intravenous data to obtain clearance and volume values.

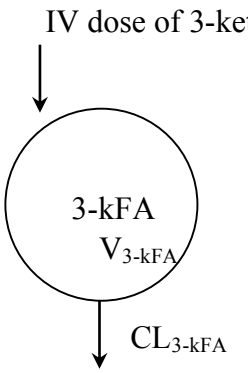

Step 2: Fix previously obtained 3-ketofusic acid (3-kFA) clearance and volume values and estimate addition of intravenous fusidic acid (FA) and its metabolite values to obtain rate of fusidic acid metabolism to 3-ketofusidic acid ($k_{FA/3\text{-}FA}$) and the clearance and volume values of fusidic acid.

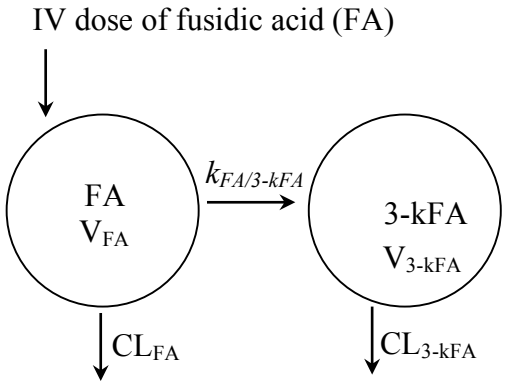

Step 3: Fix previously obtained 3-ketofusic acid (3-kFA) and fusidic acid (FA) clearance and volume values and rate of fusidic acid metabolism to 3-ketofusidic acid ($k_{FA/3\text{-}FA}$). Estimate addition of intravenous prodrugs **GKFA16** and **GKFA17**, and its metabolite values to obtain rates of metabolism and the clearance and volume values of **GKFA16** and **GKFA17**.

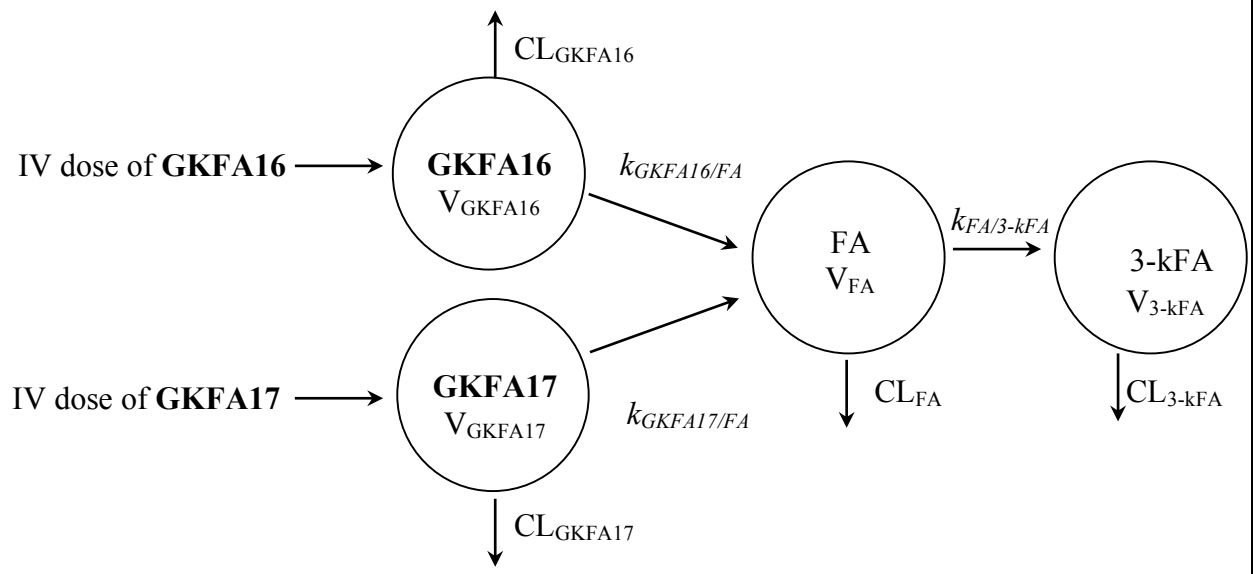

Step 4: Using the last estimates, free previously fixed parameters and analyse robustness of the model.

4.5 Results and discussion

4.5.1 Quantification of rodent specific metabolite, 3-epifusidic acid

Previous metabolite identification studies highlighted a possible metabolite of interest that appeared to be 3-epifusidic acid. This metabolite was exclusively observed in mouse and rat, but not human liver microsomes.[185] During analysis of the pharmacokinetic samples, an intense chromatographic peak matching the expected transitions and retention time of the 3-epifusidic acid metabolite was observed in all experimental samples. A representative pharmacokinetic sample chromatogram to view the then suspected 3-epifusidic acid peak is shown in Figure 4-7.

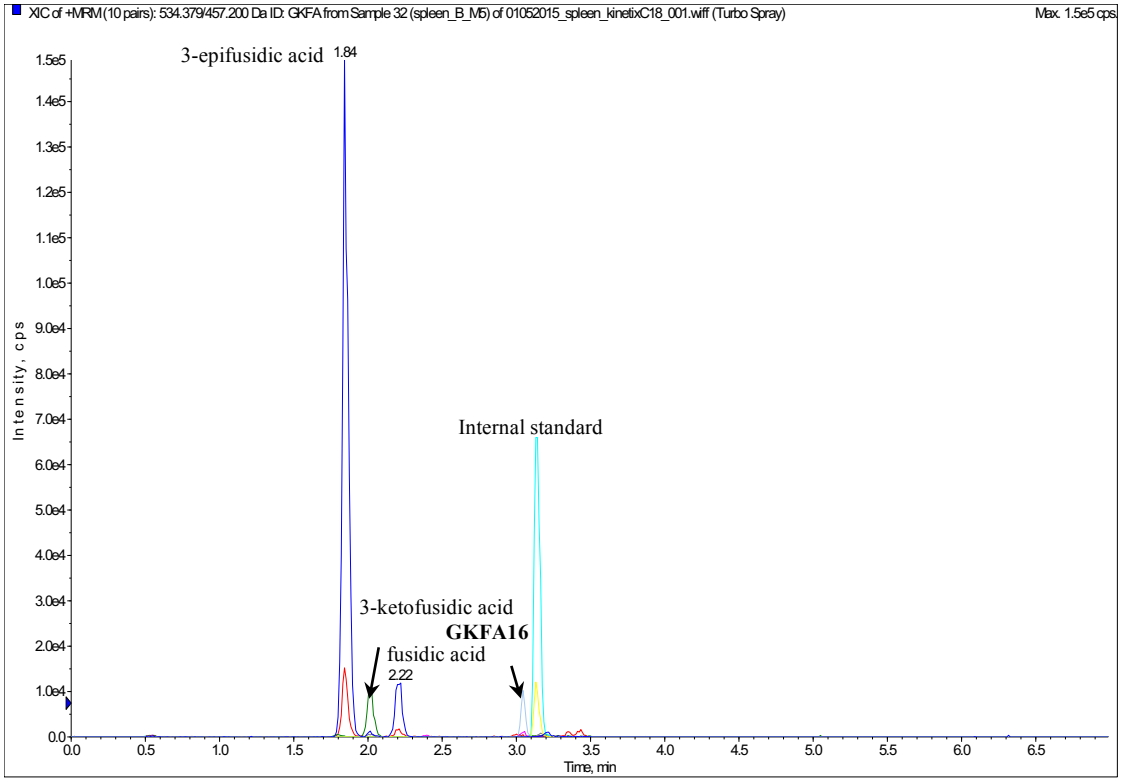

Figure 4-7: Chromatogram including 3-epifusidic acid metabolite

Due to the significant peak, Dr Gurminder Kaur proceeded to synthesise 3-epifusidic acid and Dr Mathew Njoroge confirmed that the metabolite identification correctly predicted 3-epifusdic acid. Since metabolite 3-epifusidic acid has the same transitions as fusidic acid, and due to their stereoisomerism, it was hypothesised that a recovery experiment to account for potential ionisation, extraction and matrix effect changes in the final instrument response, and resulting peak area could be used for quantification. The synthesised 3-epifusidic acid metabolite was subsequently used in a recovery experiment designed to obtain a suitable correction factor to quantify 3-epifusidic acid retrospectively with the calibration curve of fusidic acid. Equal concentrations of fusidic acid and 3-epifusidic acid were spiked at high (5000 µg/ml), medium (2500 µg/ml) and low (10 µg/ml) concentrations in appropriate matrix such as blood or organ tissue, and extracted under the same conditions as the pharmacokinetic and organ distribution studies. By comparing the peak area of 3-epifusidic acid to fusidic acid within the dynamic range of the quantification method, it was possible to calculate a correction factor to account for potential changes in ionisation, extraction and matrix effect. The results in Table 4-3 showed that protein precipitation extraction in blood had lower recovery and that the 3-epifusidic acid had a higher response than fusidic acid. This is likely due to more endogenous background being present after protein precipitation, interfering with ionisation at the retention time of fusidic acid. Liquid-liquid

extractions had very consistent analyte to internal standard areas between fusidic acid and 3-epifusidic acid in the different matrices with high recovery. Percentage recovery was compared to reference controls spiked in Millipore® water due to the scarce amount of organ tissue available as percentage recovery is usually performed in blank extracted matrix to match the background of the final extraction. Percentage recovery did not match across the investigated range with a lower extraction recovery observed at the low range and higher than expected recovery occurring at the medium range. This is likely due to a more linear response in Millipore® water, while the endogenous background of the tissue extractions caused saturation, resulting in a more quadratic curve that could not be accurately compared to the Millipore® water peak areas. Quantification of 3-epifusidic acid used a final correction factor of 1.0 for liquid-liquid extracted samples and 2.3 for protein-precipitated samples. The concentrations of 3-epifusidic acid were included in subsequent data analysis.

Table 4-3: Recovery experiment of 3-epifusidic acid

Chromatogram showing integration of one low conc quality control (10 ng/ml)

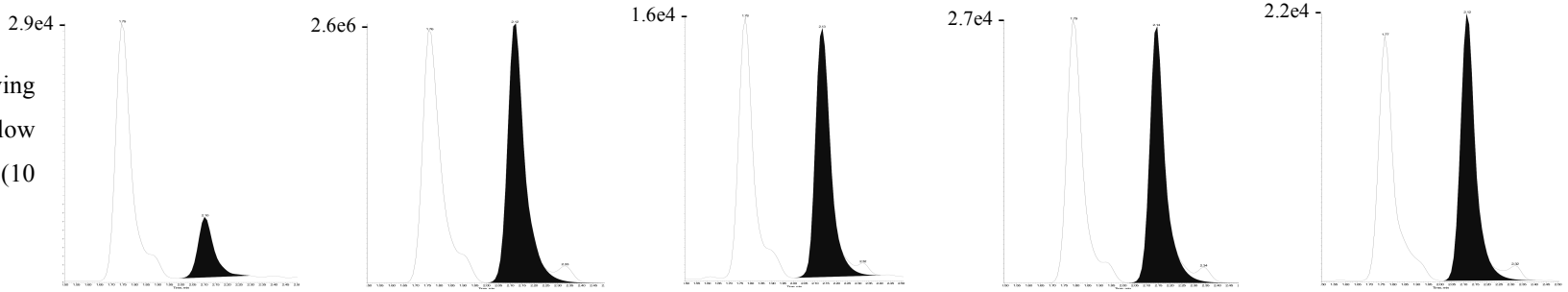

Quality control	H	M	L	H	M	L	H	M	L	H	M	L	H	M	L
FA area ratio mean	40.0	18.7	0.466	195	103	0.984	33.2	17.0	0.229	32.2	13.7	0.142	44.5	21.3	0.323
e-FA area ratio mean	95.3	42.3	1.09	204	109	1.08	35.2	18.2	0.247	33.6	14.6	0.152	43.7	21.4	0.336
FA Recovery (%)	20.5	29.0	24.9	117	166	115	108	121	44.3	92.2	99.1	39.0	116	136	58.8
e-FA Recovery (%)	61.9	79.5	49.6	243	294	138	129	155	50.1	108	127	52.1	129	164	62.9
Correction factor	2.34	2.27	2.38	1.09	1.06	1.05	1.08	1.07	1.06	1.07	1.06	1.04	1.04	1.01	0.981

Note: (FA) fusidic acid, (e-FA) 3-epifusidic acid at 5000 ng/ml (H), 2500 ng/ml (M) and 10 ng/ml (L) concentrations using protein precipitation (Protein ppt) and liquid-liquid extraction (Liq-Liq). Calculated recovery used analytes spiked at same concentrations in Millipore water as reference.

4.5.2 Importance and limitations of retrospective quantification of 3-epifusidic acid

Increased sensitivity and precision of LC/MS/MS technology has led to the use of microsampling in mice to offer the benefit of several blood samples collected from the same mouse over the course of a pharmacokinetic experiment. The major disadvantage is that the smaller blood volume only allows enough sample for one extraction, meaning if a batch fails, a repeat animal experiment is necessary.

By applying a rational screening cascade to the study design, previous metabolite identification studies showed the likely transitions and retention time window of the suspected metabolite, 3-epifusidic acid. The final samples showed that the metabolite peak was prevalent and warranted further investigation. Subsequent synthesis of the 3-epifusidic acid confirmed that the metabolite identification was correct and a recovery experiment to provide a correction factor could quantify 3-epifusidic acid in all mouse pharmacokinetic samples.

Some have argued that a repeat animal experiment would have provided the necessary information to answer this question up front, thereby avoiding the need for a retrospective analysis. However, this would have required an animal study and additional LC/MS/MS analysis. A simple bioanalytical recovery experiment only required one set of LC/MS/MS analysis. Additionally, a very small amount of compound (less than 1 mg used from an existing stock solution) was necessary for the recovery experiment, whereas for an animal study approximately 10 mg of an already difficult to synthesise compound would be necessary. Finally, the LC/MS/MS batch of an animal experiment would also require more sample preparation and time than samples from a recovery experiment.

A limitation of this approach is that the original LC/MS/MS method was not optimised to include 3-epifusidic acid and matrix effects from the change in retention time could lead to a decrease in the accuracy and precision of this quantification. However, the data gained without a repeat animal experiment greatly outweighs this limitation and the results support the pharmacokinetic parameters of the other analytes.

4.5.3 Pharmacokinetic profiles and calculated parameters

4.5.3.1 Fusidic acid

In Figure 4-8 is shown the raw data of fusidic acid with observed concentration-time points for 3 mice with different open shapes representing individual mice and individual colours representing individual analytes for A: Intravenous and B: Oral experiments. In Table 4-4 is shown the final calculated parameters of fusidic acid for both NCA and NLME analysis for a side-by-side comparison. A visual predictive check of the final model used is shown in Figure 4-9 and stratified by oral and intravenous groups. The model best fit a 2-compartment model.

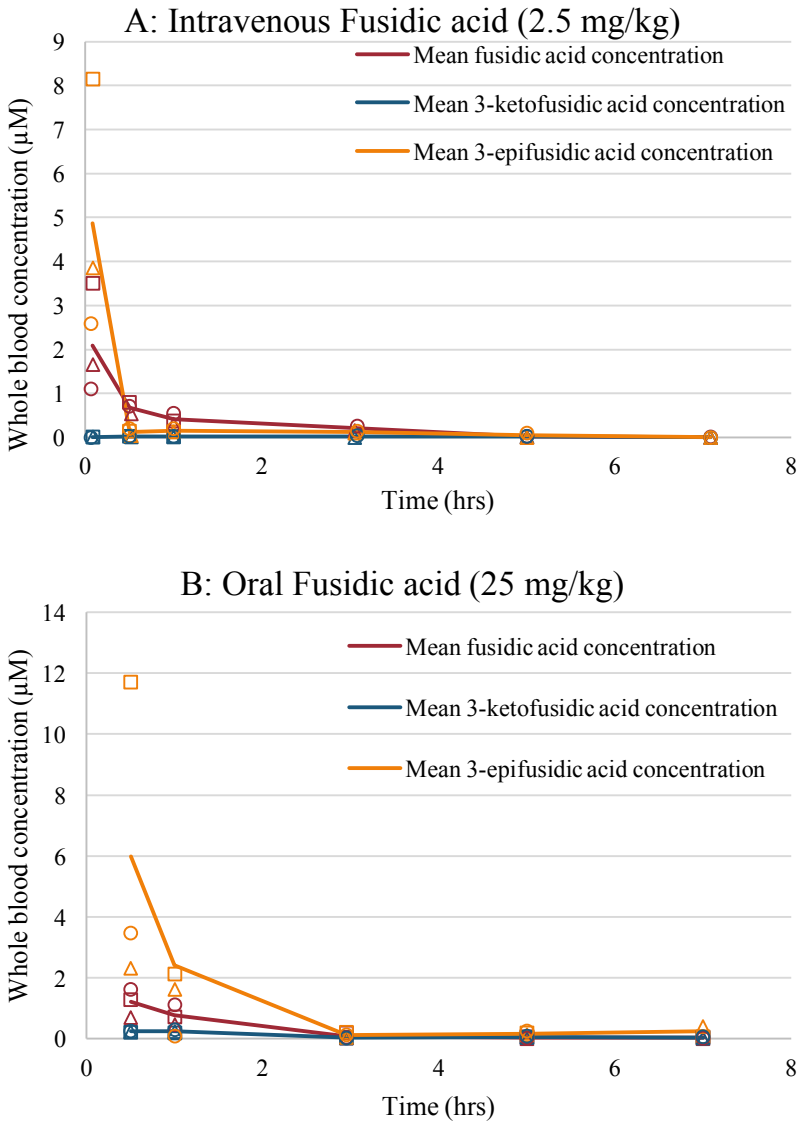

Figure 4-8: Observed pharmacokinetic data for fusidic acid in mice

Individual observed concentration-time points from the fusidic acid pharmacokinetic experiment in 3 mice for A: intravenous and B: oral experiments. Each individual animal is represented by a respective open shape. Each metabolite is represented by a different colour, namely fusidic acid (red), 3-ketofusidic acid (blue), 3-epifusidic acid (yellow).

Table 4-4: Pharmacokinetics of fusidic acid in mice

	Fusidic acid		
Parameter	*a. Oral NCA*	*b. IV NCA*	*c. Two compartment*
Blood Cl (ml/min/kg)	-	47.9 (4.22)	58.0 (15.1)
Vc (L/kg)	-	2.99 (0.817)	2.12 (0.550)
Vss (L/kg)	-	6.38 (0.686)	5.12 (1.12)
$t_{1/2}$ *(hr)*	1.27 (0.106)	0.819 (0.267)	1.80 (0.644)
$AUC_{0\text{-}inf}$ *(µM.min)*	116 (25.1)	101 (7.02)	94.5 (26.7) *
T_{max} *(hr)*	0.5	-	-
C_{max} *(uM)*	1.20 (0.256)	-	1.05 (0.042) *
F (%)	12.1 (2.02)	-	12.4 (0.032)
ka (hr^{-1})			3.06 (1.90)

Standard error of parameters is represented in parenthesis next to final median value for 3 mice. F; bioavailability, ka; rate of absorption, Vc; central volume, Blood Cl; whole blood clearance, Q; inter-compartmental clearance, Vs; steady state volume. Standard error (s.e.) of the population estimate were estimated by linearization of the Fisher information matrix. The parameters calculated by NCA used SummitPK solutions™ and the NLME modelling was performed in Monolix® Individual mouse weights were included as a covariate and allometrically scaled for clearance and volumes. Individual plots and final parameters with variability values are presented in Chapter 7: Experimental, section 7.4.3, page 264.

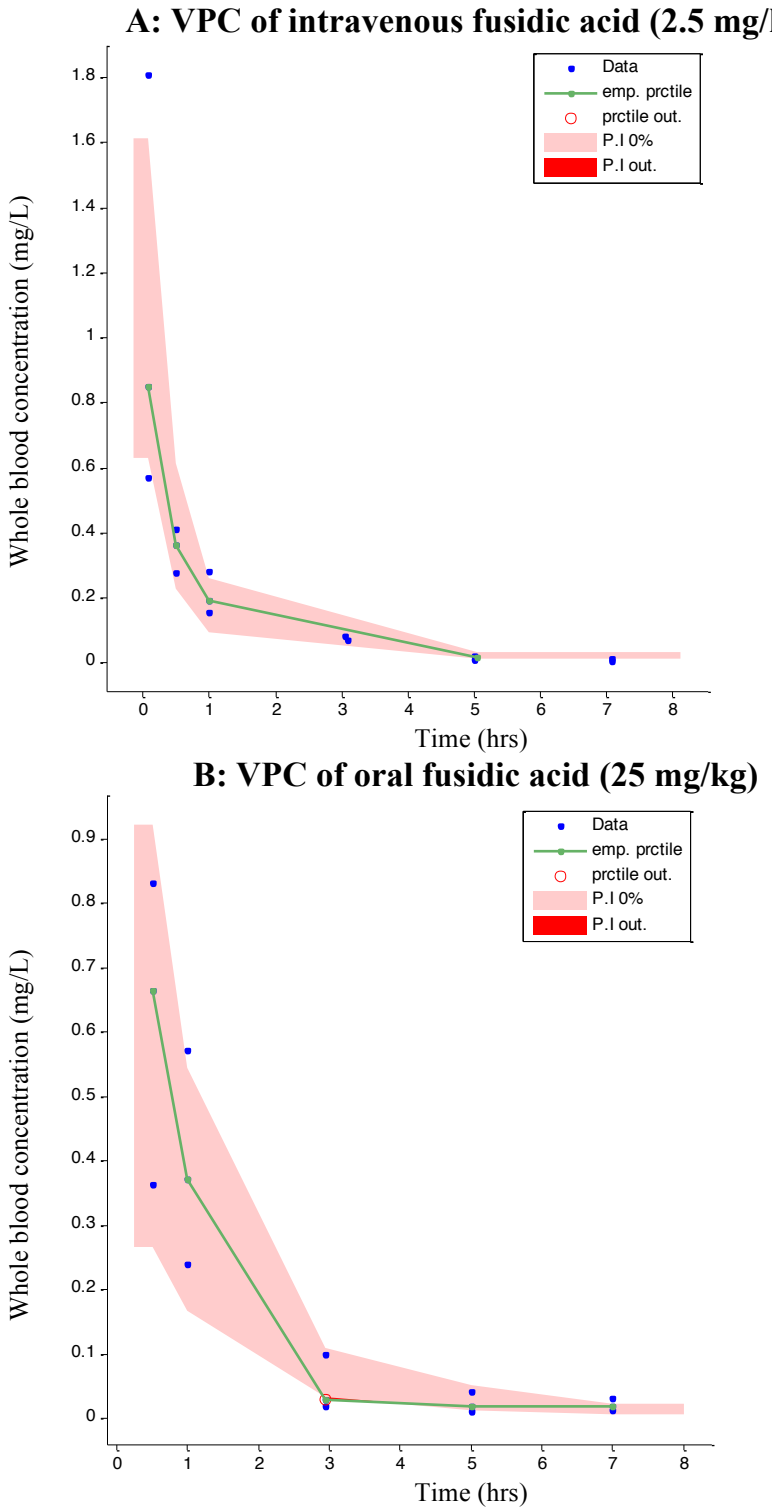

Figure 4-9: Visual predictive check of the final model used for fusidic acid

The graphical diagnostic plot shows the simulated output of the fusidic acid two-compartment model for the A: intravenous and B: oral pharmacokinetic experiments. The final model was established from the pooled oral and intravenous data and the diagnostic plots stratified according to dosing. Observed data above the limit of quantification is represented by blue dots. The green line represents the empirical percentile of this observed data and the shaded pink area represents the median of the population estimate. Ideally, this empirical percentile should fit within the pink shaded area.

4.5.3.1.1 Summary of fusidic acid pharmacokinetics

Fusidic acid showed non-linear elimination meaning a one-compartment may not best fit the dataset. Proceeding with model building from a one-compartment model to a two-compartment model had a significant drop in objective function of 114 points compared to a one-compartment model. Intravenous and oral administration of fusidic acid in mice showed a moderate clearance of 48 ml/min/kg, low (12%) bioavailability and high levels of the inactive 3-epifusidic acid metabolite with a 200% higher AUC than fusidic acid. This suggests the low bioavailability was due to high hepatic extraction as opposed to low absorption.

The two-compartment model of fusidic acid captured the observations well as seen by the visual predictive checks for both the oral and intravenous experiment. NLME and NCA results were comparable and showed that NCA captured the pharmacokinetic parameters well for this dataset.

4.5.3.2 3-Ketofusidic acid

In Figure 4-10 is shown the raw data of 3-ketofusidic acid with observed concentration-time points for 3 mice represented by respective open shapes, respective colours representing different analytes and mean lines added for A: Intravenous and B: Oral experiments. In Table 4-5 is shown the final calculated parameters of 3-ketofusidic acid for both NCA and NLME analysis for a side-by-side comparison. A visual predictive check of the final model used is shown in Figure 4-11 and stratified by oral and intravenous groups. The model best fit a 2-compartment model.

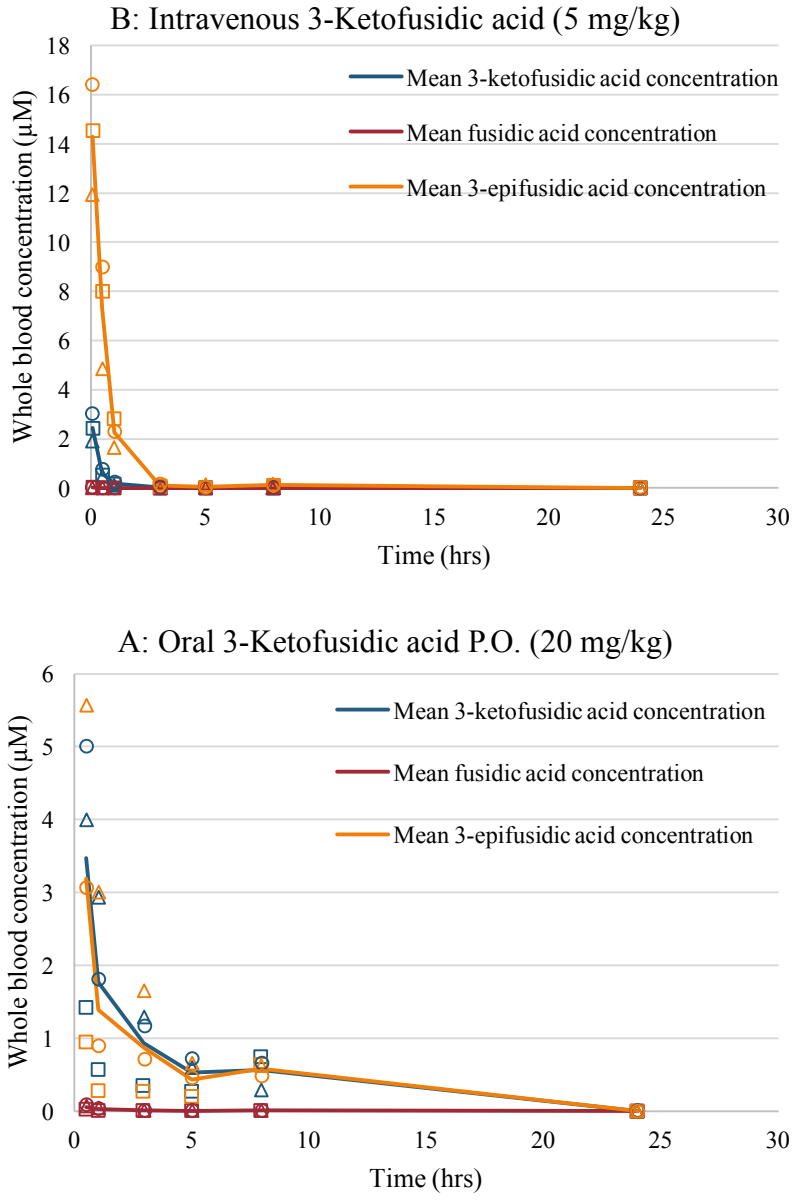

Figure 4-10: Observed pharmacokinetic data for 3-ketofusidic acid in mice

Individual observed concentration-time points from the 3-ketofusidic acid pharmacokinetic experiment in 3 mice for A: intravenous and B: oral experiments. Each individual animal is represented by a respective open shape. Each metabolite is represented by a different colour, namely fusidic acid (red), 3-ketofusidic acid (blue), 3-epifusidic acid (yellow).

Table 4-5: Pharmacokinetics of 3-ketofusidic acid in mice

	3-Ketofusidic acid		
Parameter	*a. Oral. NCA*	*b. IV NCA*	*c. Two compartment*
Blood Cl (ml/min/kg)	-	115 (16.6)	155 (26.3)
Vc (L/kg)	-	3.51 (0.192)	3.59 (1.08)
Vss (L/kg)	-	38.1 (3.79)	13.5 (3.92)
$t_{1/2}$ *(hr)*	2.51 (0.129)	3.45 (0.064)	2.74 (0.920)
$AUC_{0\text{-}inf}$ *(µM.min)*	752 (94.3)	89.7 (15.1)	867 (158) *
T_{max} *(hr)*	0.520	-	-
C_{max} *(uM)*	3.48 (1.07)	-	2.46 (0.033) *
F (%)	314 (39.4)	-	303 (68.0)
ka (hr^{-1})			0.408 (0.079)
Fusidic Acid AUC (µM.min)	6.57 (1.72)	3.10 (0.573)	-

Standard error of parameters is represented in parenthesis next to final median value for 3 mice. F; bioavailability, ka; rate of absorption, Vc; central volume, Blood Cl; whole blood clearance, Q; inter-compartmental clearance, Vss; steady state volume. Standard error (s.e.) of the population estimate were estimated by linearization of the Fisher information matrix. The parameters calculated by NCA used SummitPK solutions™ and the NLME modelling was performed in Monolix® Individual mouse weights were included as a covariate and allometrically scaled for clearance and volumes. Individual plots and final parameters with variability values are presented in Chapter 7: Experimental, section 7.4.3, page 264.

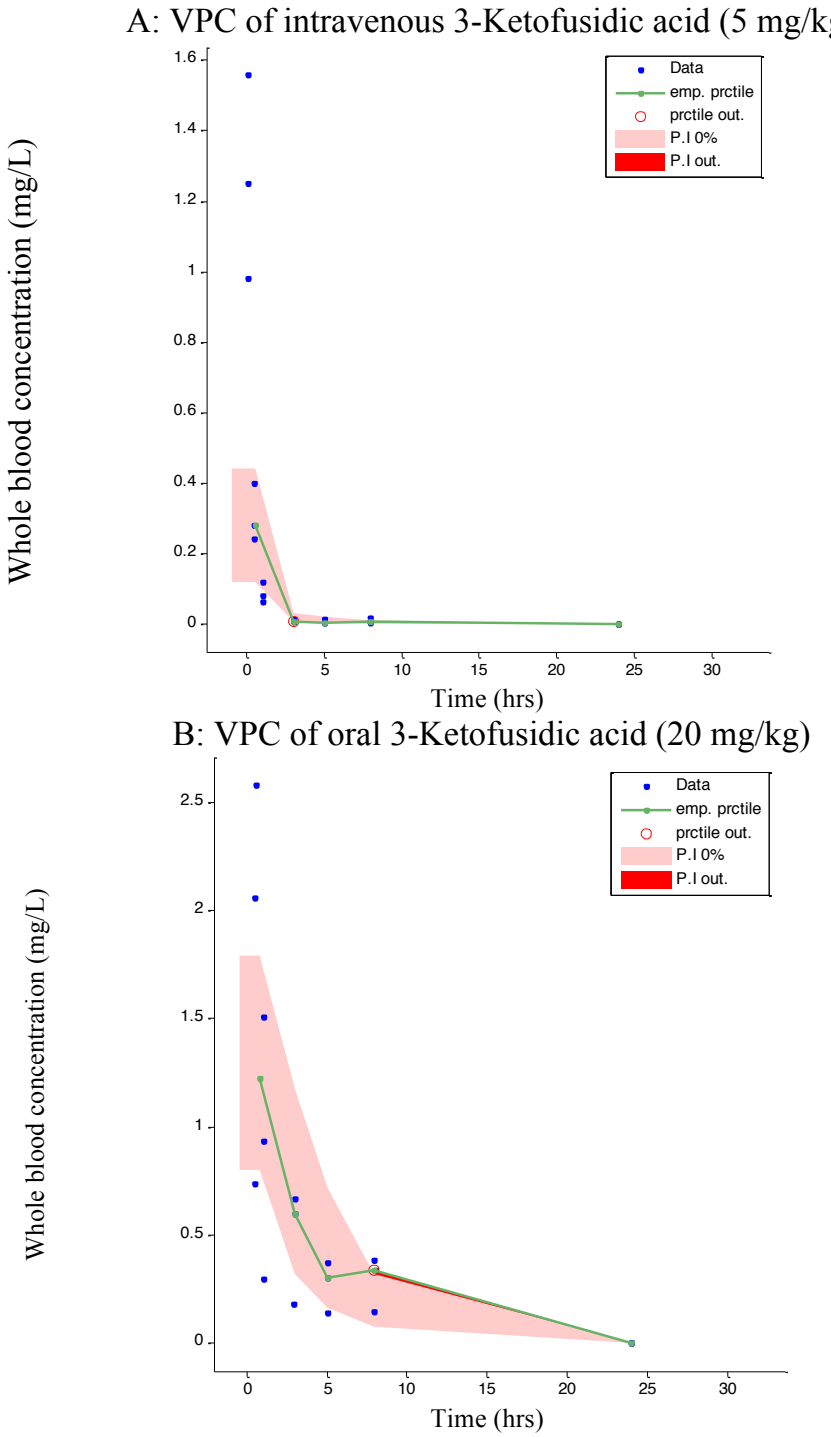

Figure 4-11: Visual predictive check of the final model used for 3-ketofusidic acid

The graphical diagnostic plot shows the simulated output of the 3-ketofusidic acid two-compartment model for the A: intravenous and B: oral pharmacokinetic experiments. The final model was established from the pooled oral and intravenous data and the diagnostic plots stratified according to dosing. Observed data above the limit of quantification is represented by blue dots. The green line represents the empirical percentile of this observed data and the shaded pink area represents the median of the population estimate. Ideally, this empirical percentile should fit within the pink shaded area.

4.5.3.2.1 Summary of 3-Ketofusidic acid

The oral and intravenous data from administration of the 3-ketofusidic acid yielded inconclusive results. Non-compartmental analysis and a two-compartment model estimated the bioavailability to be more than 300%. The metabolism of 3-ketofusidic acid had a nonsensical result showing a higher rate of metabolism to 3-epifusidic acid in the intravenous group compared to the oral group. Metabolism from the 3-ketofusidic acid to the more active fusidic acid was observed, but at negligible concentrations. Upon further investigation, it was noted that the genders of the oral and intravenous groups differed (as per agreement with the University of Cape Town Animal Research Ethics Committee to reduce discarded animals based on gender) and the rate of metabolism to 3-epifusidic acid was likely gender specific. Cempra Pharmaceuticals that developed a front loading dose for fusidic acid[170] reported higher clearance in female rats compared to males[192] and this finding should have been considered earlier in the design of the experiments. All other experiments exclusively used males. The results from this experiment were excluded from final data analysis and a repeat experiment decided against after careful consideration that further male vs female classification of rodent specific 3-epifusidic acid metabolism in mice are outside the scope of this study and unnecessary for the advancement of fusidic acid and its analogues in humans.

4.5.3.3 GKFA16

In Figure 4-12 is shown the raw data of **GKFA16** with observed concentration-time points for 3 mice graphed by open shapes representing individual animals and colours representing individual analytes and mean lines added for the A: oral and B: intravenous experiments. In Table 4-6 is shown the final calculated parameters of **GKFA16** for both NCA and NLME analysis for a side-by-side comparison. A visual predictive check of the final model used is shown in Figure 4-13 and stratified by oral and intravenous groups. The model best fit a 2-compartment model.

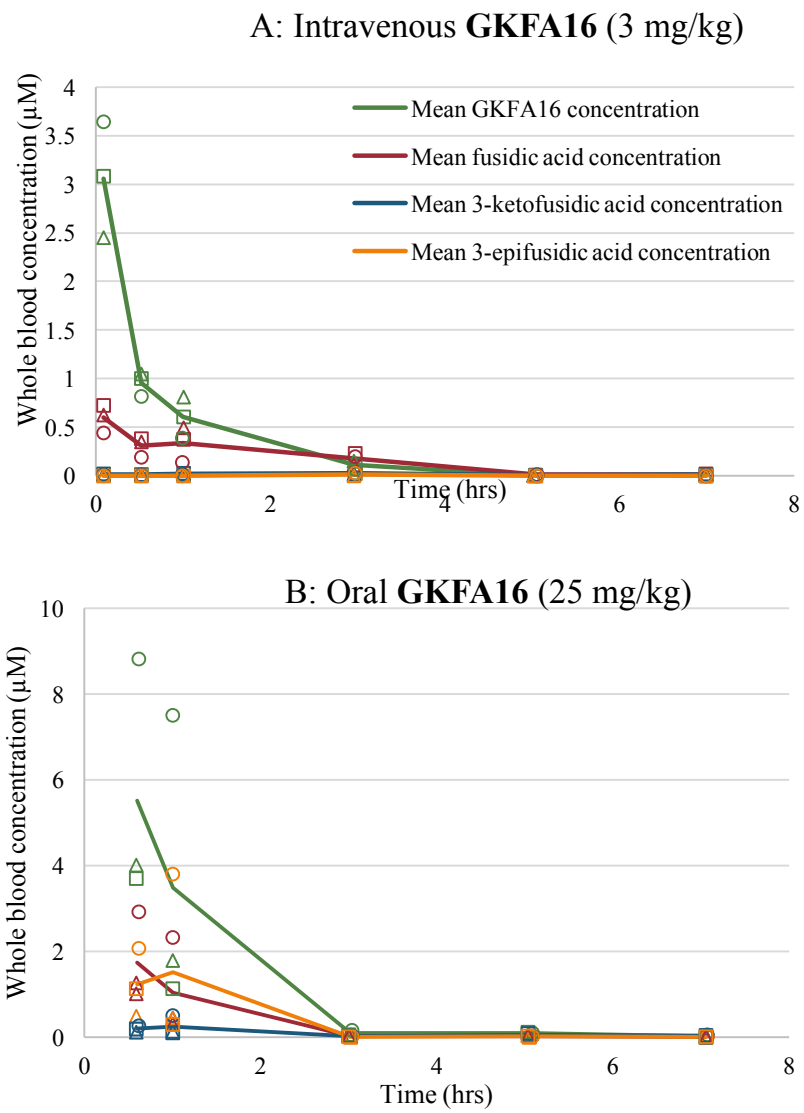

Figure 4-12: Observed pharmacokinetic data for GKFA16 in mice

Individual observed concentration-time points from the **GKFA16** pharmacokinetic experiment in 3 mice for A: intravenous and B: oral experiments. Each individual animal is represented by a respective open shape. Each metabolite is represented by a different colour, namely **GKFA16** (green), fusidic acid (red), 3-ketofusidic acid (blue), 3-epifusidic acid (yellow).

Table 4-6: Pharmacokinetics of GKFA16 in mice

	GKFA16		
Parameter	*a. Oral NCA*	*b. IV NCA*	*c. Two compartment*
Blood Cl (ml/min/kg)	-	19.2 (7.78)	40.3 (4.43)
Vc (L/kg)	-	0.611 (0.186)	1.34 (0.254)
Vss (L/kg)	-	1.28 (0.545)	2.30 (0.668)
$t_{1/2}$ *(hr)*	0.814 (0.209)	0.744 (0.092)	1.19 (0.368)
$AUC_{0\text{-}inf}$ *(µM.min)*	464 (215)	166 (18.2)	426 (156) *
T_{max} *(hr)*	0.500	-	
C_{max} *(uM)*	5.51 (1.66)	-	11.4 (1.11) *
F (%)	35.5 (16.5)	-	43.5 (15.2)
ka (hr^{-1})			3.18 (1.4)
Fusidic Acid AUC (µM.min)	134 (65.8)	63.8 (9.28)	-

Standard error of parameters is represented in parenthesis next to final median value for 3 mice. F; bioavailability, ka; rate of absorption, Vc; central volume, Blood Cl; whole blood clearance, Q; inter-compartmental clearance, Vss; steady state volume. Standard error (s.e.) of the population estimate were estimated by linearization of the Fisher information matrix. The parameters calculated by NCA used SummitPK solutions™ and the NLME modelling was performed in Monolix® Individual mouse weights were included as a covariate and allometrically scaled for clearance and volumes. Individual plots and final parameters with variability values are presented in Chapter 7: Experimental, section 7.2.3, page 264.

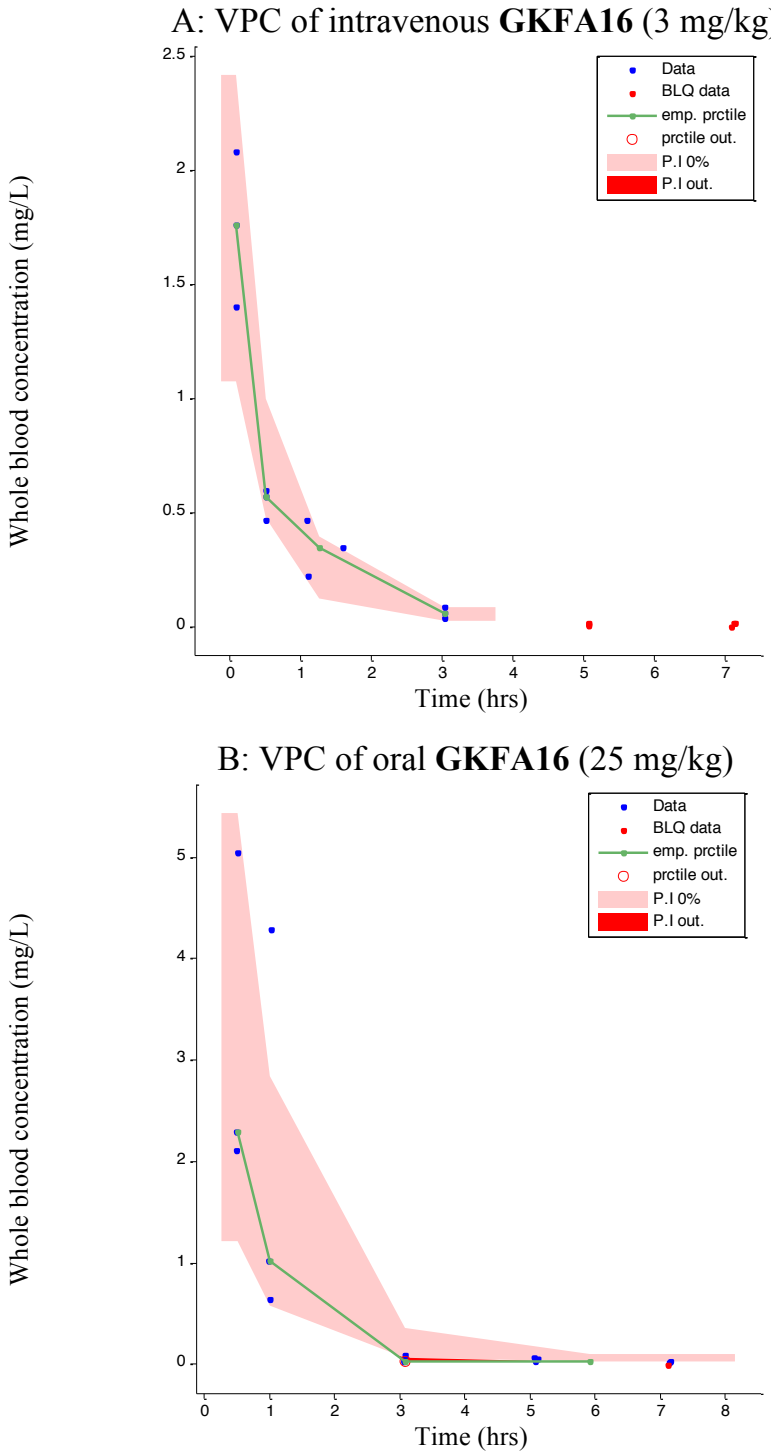

Figure 4-13: Visual predictive check of the final model used for GKFA16

The graphical diagnostic plot shows the simulated output of the **GKFA16** two-compartment model for the A: intravenous and B: oral pharmacokinetic experiments. The final model was established from the pooled oral and intravenous data and the diagnostic plots stratified according to dosing. Observed data above the limit of quantification is represented by blue dots and concentrations measures below the limit of quantification represented by red dots. The green line represents the empirical percentile of this observed data and the shaded pink area represents the median of the population estimate. Ideally, this empirical percentile should fit within the pink shaded area.

4.5.3.3.1 Summary of **GKFA16** results

Like fusidic acid, **GKFA16** best fit a 2-compartment model with a significant drop of 65 points in objective function compared to a 1-compartment model. From the observed pharmacokinetic profiles **GKFA16** was rapidly metabolised to the more active fusidic acid. Biotransformation of **GKFA16** to fusidic acid had similar exposure of fusidic acid compared to a single equivalent dose of fusidic acid with the bioavailability measured to be 43.5% compared to 12% for fusidic acid. The levels of 3-epifusidic were still observed at high concentration, of course detrimental to the pharmacokinetic profile of **GKFA16**, but **GKFA16** had much higher concentrations than 3-epifusidic acid during the first 3 hrs of the experiment. Clearance remained moderate for **GKFA16** (40 ml/min/kg), but all active metabolites were below their expected MIC concentrations before reaching 3 hours after the initial dose. Compound **GKFA16**, like fusidic acid, had very low half-lives in less than 2 hours.

Technically NCA failed to predict the pharmacokinetics of **GKFA16** with clearance calculated less than half of NLME calculations. Volumes were out by half as well but when considering final classification, both NCA and NLME values would be considered moderate volumes. The miscalculation on clearance and volume of course led to the half-life to be predicted less than half compared to NLME. For this compound, however, neither NLME nor NCA would classify **GKFA16** as having favourable pharmacokinetics, so though NCA was out by some margin, the conclusions remained the same.

4.5.3.4 GKFA17

In Figure 4-14 is shown the raw data of **GKFA17** with observed concentration-time points for 3 individual mice represented by respective open shapes and analytes represented by respective colours and mean lines added for A: Intravenous and B: Oral experiments. In Table 4-7 is shown the final calculated parameters of **GKFA17** for both NCA and NLME analysis for a side-by-side comparison. A visual predictive check of the final model used is shown in Figure 4-15 and stratified by oral and intravenous groups. The model best fit a 2-compartment model.

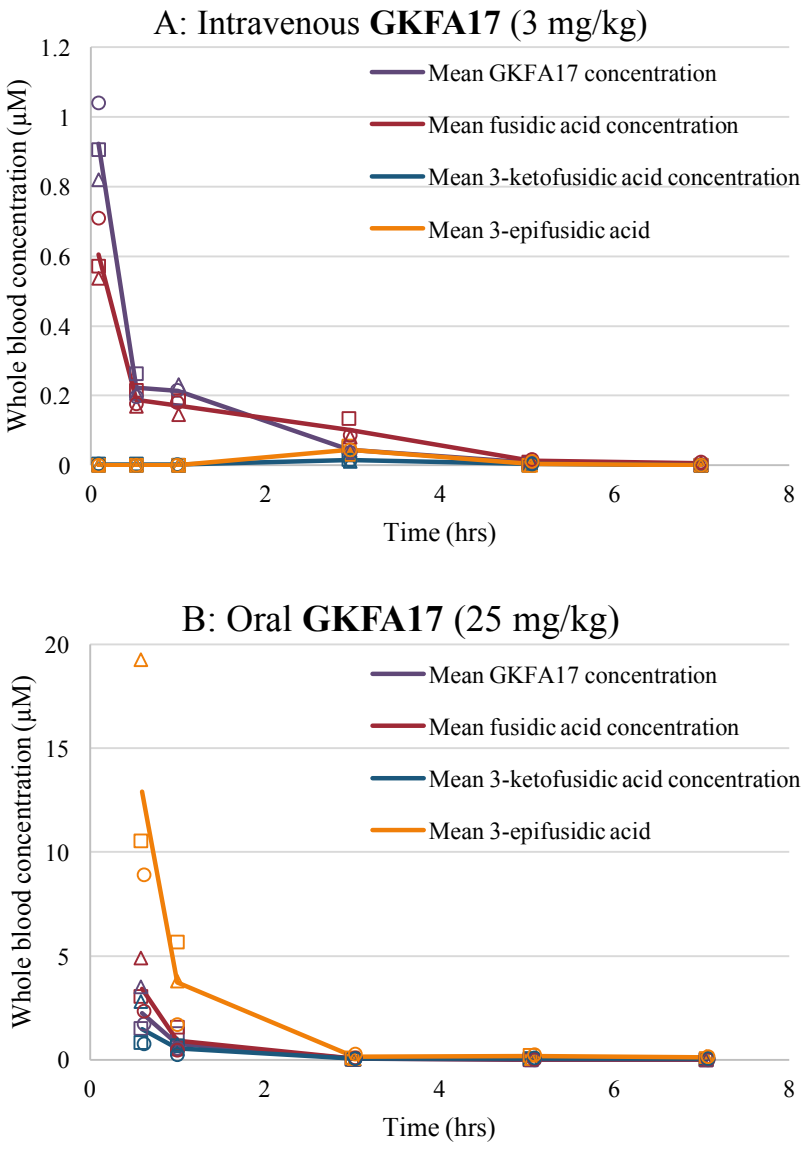

Figure 4-14: Observed pharmacokinetic data for GKFA17 in mice

Individual observed concentration-time points from the **GKFA17** pharmacokinetic experiment in 3 mice for A: Intravenous and B: Oral experiments. Each individual animal is represented by a respective open shape. Each metabolite is represented by a different colour, namely **GKFA17** (purple), fusidic acid (red), 3-ketofusidic acid (blue), 3-epifusidic acid (yellow).

Table 4-7: Pharmacokinetics of GKFA17 in mice

	GKFA17		
Parameter	*a. Oral. NCA*	*b. IV NCA*	*c. Two compartment*
Blood Cl (ml/min/kg)	-	71.6 (17.5)	134 (12.1)
Vc (L/kg)	-	0.903 (0.566)	3.88 (0.620)
Vss (L/kg)	-	2.10 (1.74)	8.36 (1.75)
$t_{1/2}$ *(hr)*	1.35 (0.206)	0.665 (0.114)	1.63 (0.373)
$AUC_{0\text{-}inf}$ *(µM.min)*	133 (12.2)	82.9 (26.4)	130 (21.6) *
T_{max} *(hr)*	0.583 (0.019)	-	-
C_{max} *(uM)*	2.85 (0.640)	-	2.28 (0.031) *
F (%)	22.3 (2.04)	-	44.5 (6.40)
ka (hr^{-1})			3 (fixed)
Fusidic Acid AUC (µM.min)	165 (30.6)	39.7 (2.80)	-

Standard error of parameters is represented in parenthesis next to final median value for 3 mice. F; bioavailability, ka; rate of absorption, Vc; central volume, Blood Cl; whole blood clearance, Q; inter-compartmental clearance, Vss; steady state volume. Standard error (s.e.) of the population estimate were estimated by linearization of the Fisher information matrix. The parameters calculated by NCA used SummitPK solutions™ and the NLME modelling was performed in Monolix® Individual mouse weights were included as a covariate and allometrically scaled for clearance and volumes. Individual plots and final parameters with variability values are presented in Chapter 7: Experimental, section 7.4.3, page 264.

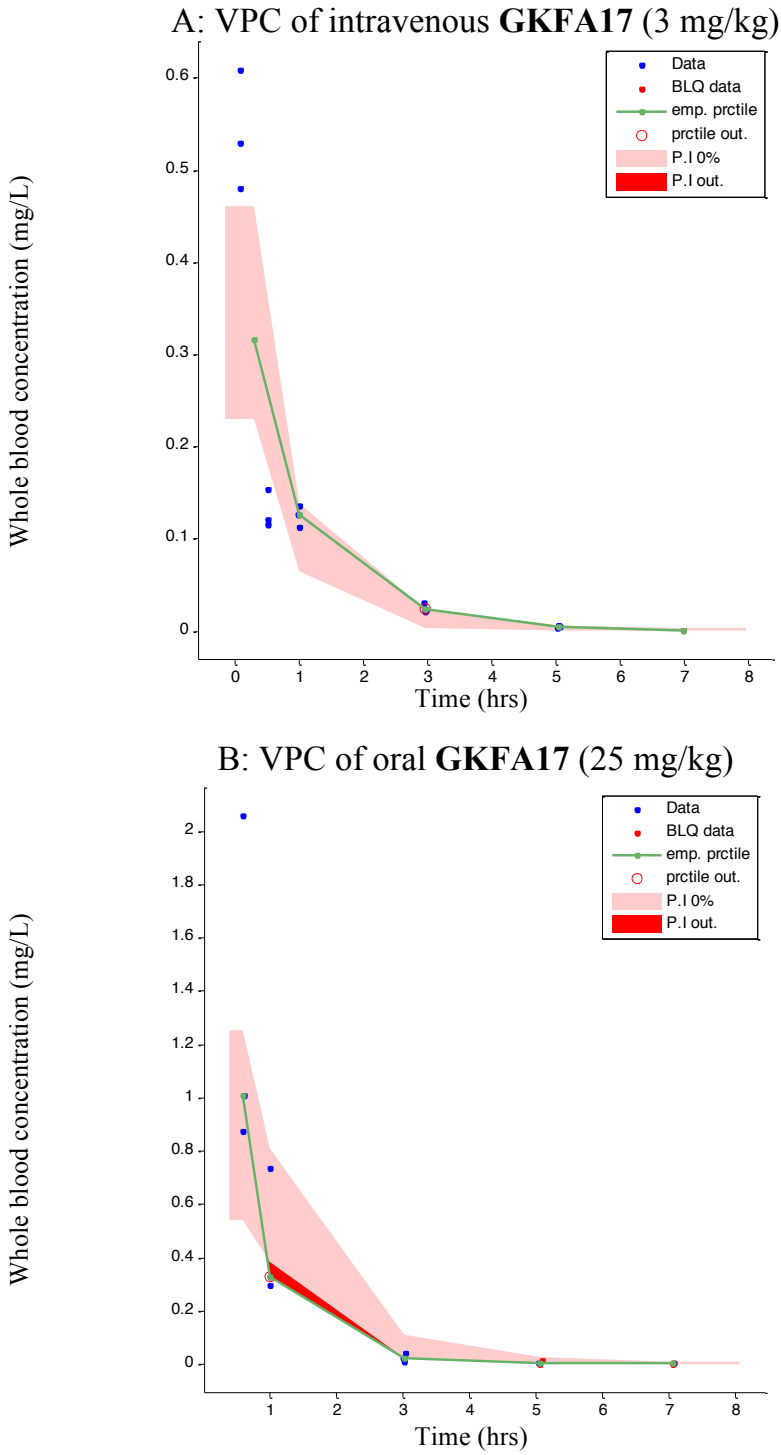

Figure 4-15: Visual predictive check of the final model used for GKFA17

The graphical diagnostic plot shows the simulated output of the **GKFA17** two-compartment model for the A: intravenous and B: oral pharmacokinetic experiments. The final model was established from the pooled oral and intravenous data and the diagnostic plots stratified according to dosing. Observed data above the limit of quantification is represented by blue dots and concentrations measures below the limit of quantification represented by red dots. The green line represents the empirical percentile of this observed data and the shaded pink area represents the median of the population estimate. Ideally, this empirical percentile should fit within the pink shaded area.

4.5.3.4.1 Summary of **GKFA17** pharmacokinetics

Similar to fusidic acid and **GKFA16**, **GKFA17** best fits a 2-compartment model. The objective function using a two-compartment model decreased by 80 points compared to a 1-compartment model, deemed statistically relevant for the additional two parameters. Examining the visual predictive checks of the model though, the model was unable to capture the elimination of **GKFA17** well and overpredicted concentrations during the distribution phase. A three-compartment model did not yield a significant improvement in model building. Like **GKFA16**, **GKFA17** was rapidly metabolised to the more active fusidic acid. **GKFA17** resulted in a 42% increase in fusidic acid exposure compared to single fusidic acid administration. The bioavailability of **GKFA17** was the same as **GKFA16** and measured 44.5%. Like all fusidic acid compounds tested, 3-epifusidic levels were apparent and negatively affected the pharmacokinetic outcomes of the fusidic acid series. Clearance of **GKFA17** was high at 1344 ml/min/kg with a corresponding low half-life less than 2 hrs.

The butyl ester **GKFA17** was more rapidly metabolised to fusidic acid than the propyl ester **GKFA16** and therefore did have higher initial concentrations of fusidic acid. This, however, also led to the higher clearance observed for **GKFA17** and exposed the fusidic acid 3-hydroxy soft spot to be metabolised to the inactive 3-epifusidic acid.

NCA performed poorly against NLME and clearance and half-life were under predicted less than 50% of NLME calculations. Bioavailability was also less than half of that predicted for NLME. NLME calculated central volume and volume at steady state 3-fold and 4-fold more than NCA. For the **GKFA17** dataset NCA performed worse than the **GKFA16**, but again for both compounds NCA would not recommend further evaluation of these compounds due to poor pharmacokinetics.

4.5.4 Comparison of metabolite exposure

A model to include the metabolite concentrations was attempted, but no robust model could be supported by the sparse data available and proved difficult and unstable in Monolix®. Comparing AUC of each metabolite calculated by simpler NCA was found to be a more suitable approach for the objectives of this study, and these results are shown in Figure 4-16.

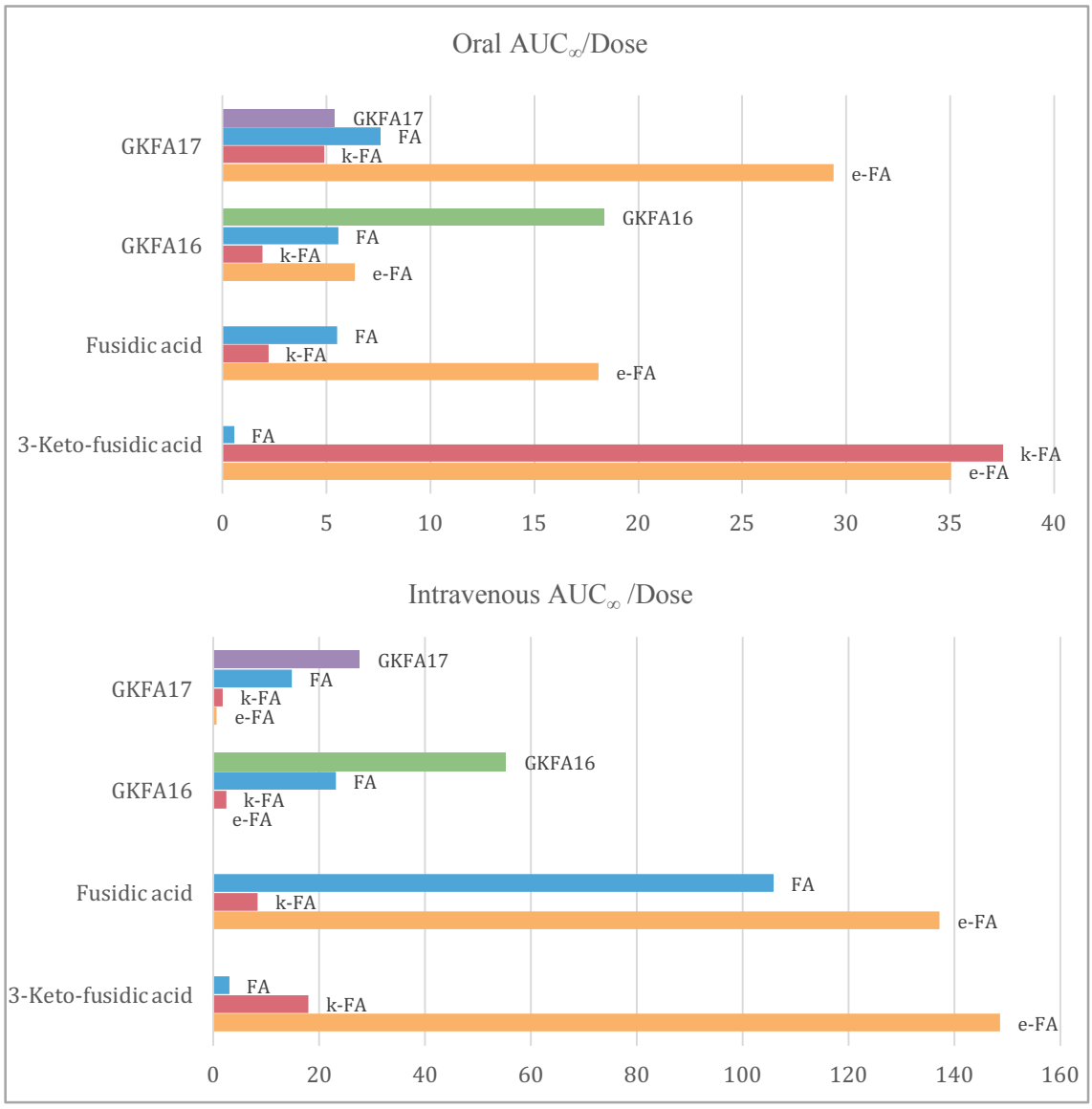

Figure 4-16: Parent and metabolite exposures

Note: Area under curve to infinity (AUC_∞) divided by dose given in respective experiment. Fusidic acid (FA), 3-ketofusidic acid (k-FA) and 3-epifusidic acid (e-FA) after oral and intravenous administration.

Examining the exposure levels presented in Figure 4-8, it is again apparent that the inactive 3-epifusidic acid greatly deterred active fusidic acid availability in mice. The low levels of 3-ketofusidic

acid exposures, showed a fast turnaround from fusidic acid to the final metabolite 3-epifusidic acid. It is striking to also see this and the ubiquitous nature of the 3-epifusidc acid metabolism after intravenous administration of male mice with 3-ketofusidic acid, which still showed 8 times higher levels of 3-epifusidic acid.

There is a lack of translation of carboxylic esterase between mice and humans due to higher expression of carboxylic esterase in mice compared to humans and across all tissues.[193] This in addition to the rodent-specific metabolism to inactive 3-epifusidic acid reveals that the mouse model is inappropriate for characterising fusidic acid and related analogues.

4.5.5 Non-compartment analysis vs non-linear mixed effects modelling

Due to the failed metabolite model, NLME modelling already showed limitations in implementation. The only comparisons that could be drawn were therefore between the parent compound NLME and parent compound NCA. This is important to consider for future preclinical studies hoping to make use of NLME modelling to predict metabolite profiles. In this case, better sampling would be required with more useful data points at the elimination phase. It would be wise to do a preliminary snapshot pharmacokinetic evaluation of the parent and metabolite to validate further animal studies that would provide more useful time points around the elimination phase. In this case, with the incredibly fast metabolism of fusidic acid to the 3-epifusidic acid, there was a limited elimination profile to explore.

NLME showed that the C-3 ester prodrugs had higher bioavailability than the NCA predicted, likely due to the elementary trapezoidal rule calculation that NCA uses to obtain reference AUC values and its sensitivity to the sampling schedule. If the sampling schedule was not optimal to characterise the absorption phase and maximum concentration peak of the curve, the resulting AUC as estimated by NCA can underestimate oral profiles. In contrast, poor sample scheduling during the elimination phase can lead to overestimation, illustrated in Figure 4-17. Together these incorrect predictions can lead to poor bioavailability estimates. NLME best describes a pharmacokinetic curve around observed sample points and accordingly calculates bioavailability by the integrated equation that best describes the data.

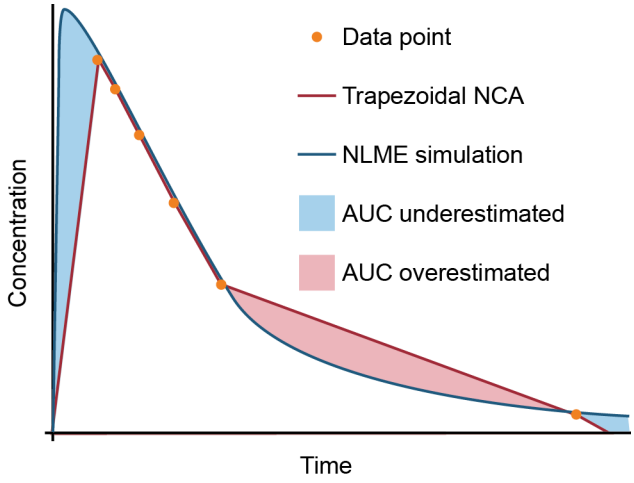

Figure 4-17: Trapezoidal NCA over and underestimation

The advantage of NLME analysis in this case provided a model that could be used for simulations. This was done using a scaling technique of the fusidic acid parameters as reference. This is discussed further in the next section.

4.5.6 Simulations to compare results with existing clinical data

To assess the impact of the rodent-specific 3-epifusidic acid, the mouse parameters were scaled using the well accepted power allometric equation,[79] Figure 4-18, to simulate what a human pharmacokinetic profile would look like if "translated" using conventional inter-species methods.

$$Cl_{human} = Cl_{mouse} \times \left(\frac{Wt_{human}}{Wt_{mouse}}\right)^{0.75} \qquad V_{human} = V_{mouse} \times \left(\frac{Wt_{human}}{Wt_{mouse}}\right)^{1}$$

Figure 4-18: Equation used for scaling clearance and volume based on weight.

The results comparing final parameters and simulated human pharmacokinetic plot versus actual observed clinical data is shown in Table 4-8. The parameter values were simulated in Berkeley Madonna to obtain the predicted pharmacokinetic profiles in a preclinical "translational" setting with a dose of 1650 mg, equivalent to the 23.6 mg/kg dose from the clinical data, which was most appropriate to compare with the original mouse experiments of 25 mg/kg. A possible limitation could include reported auto-inhibition of fusidic acid clearance in man leading to dose accumulation in plasma on multiple dosing.[169,194] This is, however, not observed in mice and rats,[192] and was therefore not included in the final simulation. It is doubtful that accounting for auto-inhibition could greatly improve the overall outcome of exposure when observing the single dose scaled parameters.

Knippenberg et al., 2016 reported a blood-plasma partitioning value of 0.9894[195] showing that comparison of whole blood to plasma in this case could be done 1:1.

Table 4-8: Simulated results compared to clinical parameters

A: Scaled Human **B: Clinical[170]**

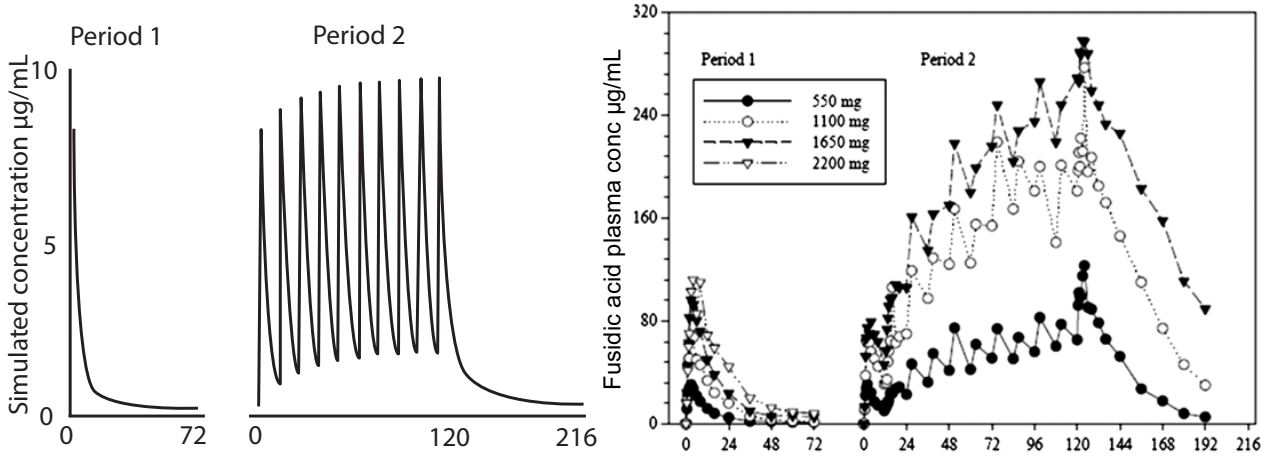

Time (hrs) for period 1 and 2

Parameter	*Mouse (25 g)*	*Scaled Human (70 kg)*	*Clinical[170] (>50 kg)*
Cl (L/h)	0.0865	33.3	1.10
Vss (L)	0.102	286	23.9
$t_{1/2}$ *(hr)*	1.80	5.95	16.1
Dose (mg)	0.571	1650	1650
Bioavailability (%)	12.1	12.1	91.0
AUC (mg.h/L)	0.818	5.95	1840
C_{max} *(mg/L)*	0.620	7.07	102

Cl; clearance, Vss; volume at steady state, AUC; area under the curve, C_{max}; maximum observed concentration. The two pharmacokinetic plots show a simulated profile from Berkeley Madonna™ with the Monolix® fusidic acid calculated parameters clearance and volume allometrically scaled by weight. The simulation used a 23.6 mg/kg dose to correspond to the clinical experiment of 1650 mg dose and input similar single dosing (Period 1) and multiple dosing over 216 hrs (Period 2).

Using this scaling technique to translate the mouse data to compare to existing clinical data, the extent of mismatch between species was seen. Simulated whole blood clearance compared to plasma clearance shows a 30-fold difference. Knippenberg et al., 2016 reported a blood-plasma partitioning value of 0.98 showing that comparison of whole blood to plasma in this case is appropriate. Similarly, the half-life of fusidic acid was 3 times faster in the simulated human outcome compared to clinical results. The simulated profile plot is juxtapositioned next to actual clinically observed profile, highlighting the higher clearance, shorter half-life and greatly diminished C_{max} that is 10 times less in a simulated human individual compared to observed clinical results.

4.5.7 Observed variability

The results showed high variance of all the compounds for oral and intravenous groups, likely due to poor solubility. Poor solubility causes two problems at a preclinical stage. Dosing becomes difficult as a homogenous suspension with uniform particle size is difficult to obtain and a highly organic intravenous vehicle, which requires a slow injection (usually 2- 3 min for 100 µl) to prevent a pH shock to the mice, is necessary. In a clinical setting fusidic acid is administered as a salt to aid in dissolution and this salt may have been more appropriate for this study. The high levels of 3-epifusidic acid and organ distribution studies, discussed in Chapter 5, did show that the liver concentrations were high and using the free base had a low impact on total absorption. Still, it is the variability in absorption that leads to inconsistent profiles between genetically similar mice as shown in the formulation study presented in Chapter 3.

4.6 Conclusion

In Table 4-9 is shown the final pharmacokinetic parameters of the fusidic acid analogues with their respective fusidic acid exposures.

Table 4-9: Final pharmacokinetic results of C-3 ester prodrugs in mice

General structure

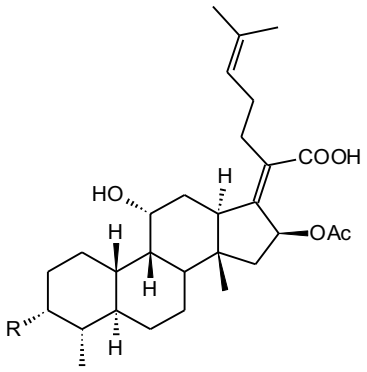

R =	Fusidic Acid 	**GKFA16** 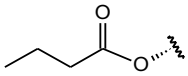	**GKFA17** 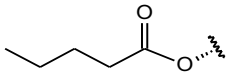
Blood Cl (ml/min/kg)	58.0	40.3	134
Vss (L/kg)	5.12	2.30	8.36
$t_{1/2}$ *(hr)*	1.80	1.19	1.63
F (%)	12.4	43.5	44.5
Fusidic Acid AUC (μM.min)	116	134	165
Increase in fusidic acid AUC	-	15.5 %	42.2 %

Blood Cl; whole blood clearance, Vss; steady state volume. Standard error (s.e.) of the population estimate were estimated by linearization of the Fisher information matrix. The parameters calculated by NCA used SummitPK solutions™ and the NLME modelling was performed in Monolix® Individual mouse weights were included as a covariate and allometrically scaled for clearance and volumes. Individual plots and final parameters with variability values are presented in Chapter 7: Experimental, section 7.4.3, page 264.

This investigation revealed a lack of pharmacokinetic translation of fusidic acid in mice and humans. The formation of 3-epifusidic acid in mice greatly lowered the exposure of fusidic acid, and explained the poor efficacy of fusidic acid in previous mouse models, despite good *in vitro* activity and well tolerated human clinical pharmacokinetics.

The ester prodrugs did display good fusidic acid exposure and are still promising to pursue for the potential repurposing and repositioning of fusidic acid against tuberculosis. Technically the two prodrugs, when considered without their metabolic mistranslation, do not possess the pharmacokinetic properties to advance to organ distribution studies in the screening cascade. However, the hypothesis that they could improve distribution and exposure at the site of infection by aiding in delivery was still intriguing enough to progress them. Chapter 5 discusses these results together with fusidic acid reference data.

Application of a mechanistic model to investigate the fusidic acid metabolites and prodrug delivery was not possible in this case and not recommended unless considering a preliminary snapshot pharmacokinetic study that can be expanded on with a repeat study containing optimised sampling times. NLME of the parent compound, however, improved AUC predictions and provided a tool to easily predict pharmacokinetic profiles using variable inputs and applying allometric scaling. This aided in assessing the distortion of the 3-epifusidic acid on final exposure and supports that earlier modelling of data can provide interesting translational capacity at a preclinical stage.

5 ORGAN DISTRIBUTION OF FUSIDIC ACID PRODRUGS

5.1 Introduction

The complex pathology of tuberculosis leads to poor drug exposure at the site of mycobacterial infection and is considered a major obstacle in current tuberculosis therapies and drug discovery. Drug access to the tuberculosis causing mycobacteria becomes increasingly difficult as the disease progresses from macrophage infection to diverse granuloma lesions, causing discrete microenvironments with poor vasculature that insulates the mycobacteria from the immune system and systemically available drugs, Figure 5-1.[196] Pharmacokinetic profiles that exclusively examine drug concentrations in plasma or whole blood therefore become inadequate to predict drug effectiveness and need to be refined to include target site concentrations, Figure 5-2.[197]

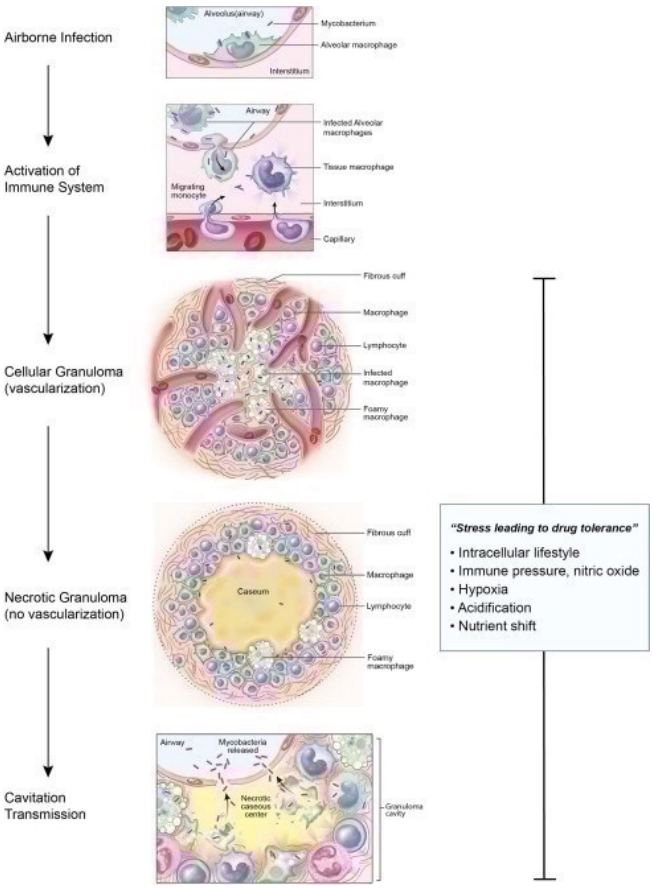

Figure 5-1: Tuberculosis disease progression[196]

Research into lung distribution and lesion pharmacokinetics of current therapies have shown diverse pharmacokinetic properties of tuberculosis drugs, suggesting an array of properties are necessary to target multiple mycobacteria environments, Figure 5-2. First line drugs; isoniazid, pyrazinamide and rifampicin partition rapidly into tissues, but cellular lesion concentrations of these three drugs are lower than plasma concentrations. Rifampicin does accumulate well in uninvolved lung tissue.[198,199] Matrix-assisted laser desorption ionisation mass spectrometry imaging (MALDI-MSI) revealed that sterilising agents, rifampicin and pyrazinamide penetrate well into necrotic caseum, suggesting this to be the site of persisting tolerant mycobacteria that are responsible for resistance.[200]

Tuberculosis is not exclusive to lung pathology and tuberculosis meningitis and pericarditis complications have high morbidity and mortality rates. Mortality of tuberculosis pericarditis is as high as one in every four patients dying within 6 months of diagnosis[201]. Tuberculosis meningitis carries morbidity higher than 50% with fatality rates as high as 10%.[202] Research shows first[203] and second line treatments[204] have poor permeation into the meninges infection space. Similarly, poor exposure of rifampicin, ethambutol and pyrazinamide was observed in patients suffering from tuberculosis pericarditis.[205]

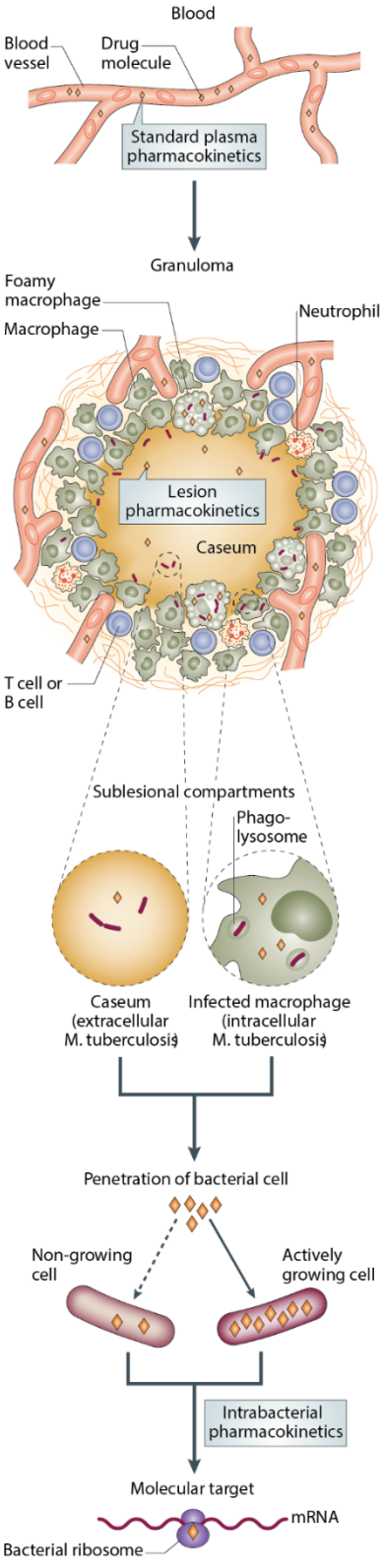

Figure 5-2: Pharmacokinetic challenges of reaching mycobacterial target[197]

5.2 Rationale

The research efforts mentioned above focused on the objective of shortening the treatment duration, preventing resistance and improving sterilising effects of existing tuberculosis therapies. The results showed diverse pharmacokinetic profiles of the existing first and second line drugs and the definition of what good pharmacokinetics for a tuberculosis drug is becomes troublesome. Considering the failure of many tuberculosis

therapies and emerging research searching for drug leads based on the properties of clinical candidates might only lead to the same inappropriate therapies. The need for new tuberculosis drug candidates is therefore vital with emphasis on novelty not only placed on activity, but on improved pharmacokinetic properties. It was hypothesised that refining the pharmacokinetic techniques to include organ distribution during early preclinical screening of drug leads with the aim of improving tissue distribution could improve drug discovery outcomes for tuberculosis.

Physiologically based pharmacokinetics (PBPK) provides the opportunity to build multi-compartment pharmacokinetic models, based on organ and tissue drug concentrations e.g. in Figure 5-3. They can be used to scale between species,[206] adult to paediatric dosing[207] and disease states where renal or hepatic function may be impaired.[208,209] In the past PBPK methods used animal tissue data to extrapolate to humans.[210–212] The choice of modelling approach is conditional on the data available, with existing observed data used in a "top down" pharmacokinetic approach and a broader understanding of human physiology and existing mechanisms used in a "bottom up" approach. These classifications have limitations on both sides, and the field has moved to a more "middle out" approach that utilises both paradigms.[210,213–215] This "middle-out" approach is sometimes classified within systems pharmacology.[215] Implementation of a tuberculosis aimed "middle out" systems model could assist in predicting drug concentrations more closely to the site of infection.[216–218]

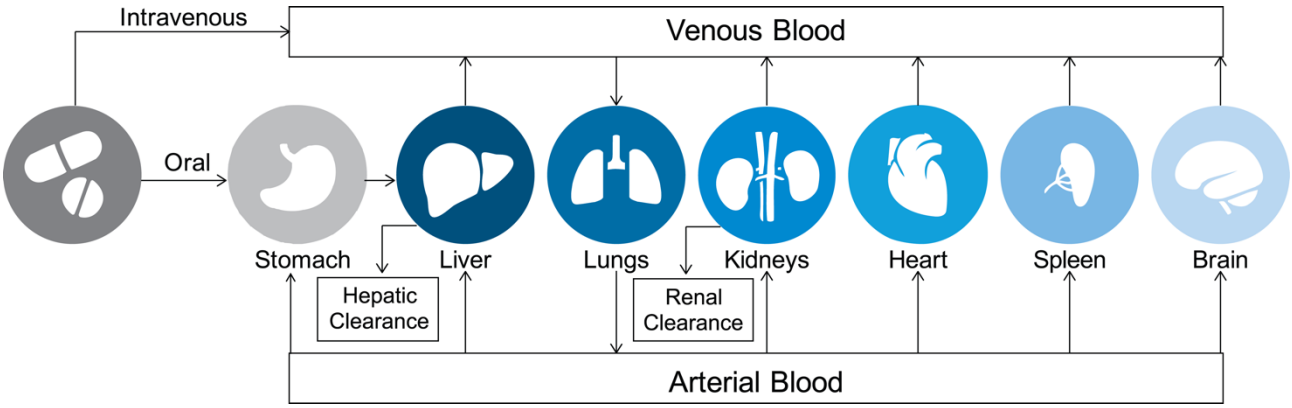

Figure 5-3: Physiologically based pharmacokinetic model

A traditional representation of a physiologically based pharmacokinetic model that shows drug distribution in organ specific compartments and their relation to one another. Both intravenous and oral pathways are shown.

Continuing the fusidic acid project, the prodrugs evaluated from Chapter 4 were further evaluated for organ distribution. However, a limitation of this study was that the C-3 ester fusidic acid prodrugs examined in Chapter 4, showed the rodent specific metabolite 3-epifusidic acid had the highest levels

of exposure and in turn negatively affected fusidic acid exposure. The C-3 ester prodrugs were still intriguing to assess if the C-3 ester prodrug strategy was useful in increasing exposure of the prodrugs and their respective metabolites in tissues compared to administration of unaltered fusidic acid. Drug concentrations were examined in the lungs and spleen due to the high bacterial burden at these sites, liver and kidneys due to their role as elimination sites, and the heart and brain due to tuberculosis pericarditis and meningitis complications.

5.3 Methodology overview

Figure 5-4 shows the process followed for the organ distribution evaluation of two C-3 ester fusidic acid prodrugs and fusidic acid as reference. Pharmacokinetic results discussed in Chapter 4 determined sampling time points for the organ distribution experiments. Sampling points were chosen to best represent the elimination phase of the compounds. **GKFA16**, **GKFA17** and fusidic acid were respectively dosed each at 10 mg/kg in 10 mice. Initial calibration curves of the organ homogenate used the same method as previously described for the whole blood pharmacokinetic experiments discussed in Chapter 4. Unfortunately, this method was imprecise and inaccurate with poor reproducibility of organ samples. LC/MS/MS methods were reinvestigated and the extraction improved to a liquid-liquid extraction method that likely reduced matrix effects from the complex organ tissue background.

The final data showed strong trends in pharmacokinetic results, but implementing a pharmacokinetic model in Monolix® proved unstable with the high number of compartments. Microsoft® Excel 2013 was used to calculate the respective AUC of the organ profiles to compare the exposure of the C-3 ester prodrugs, fusidic acid and their metabolites. These results were found to be sufficient for this fusidic acid repositioning project.

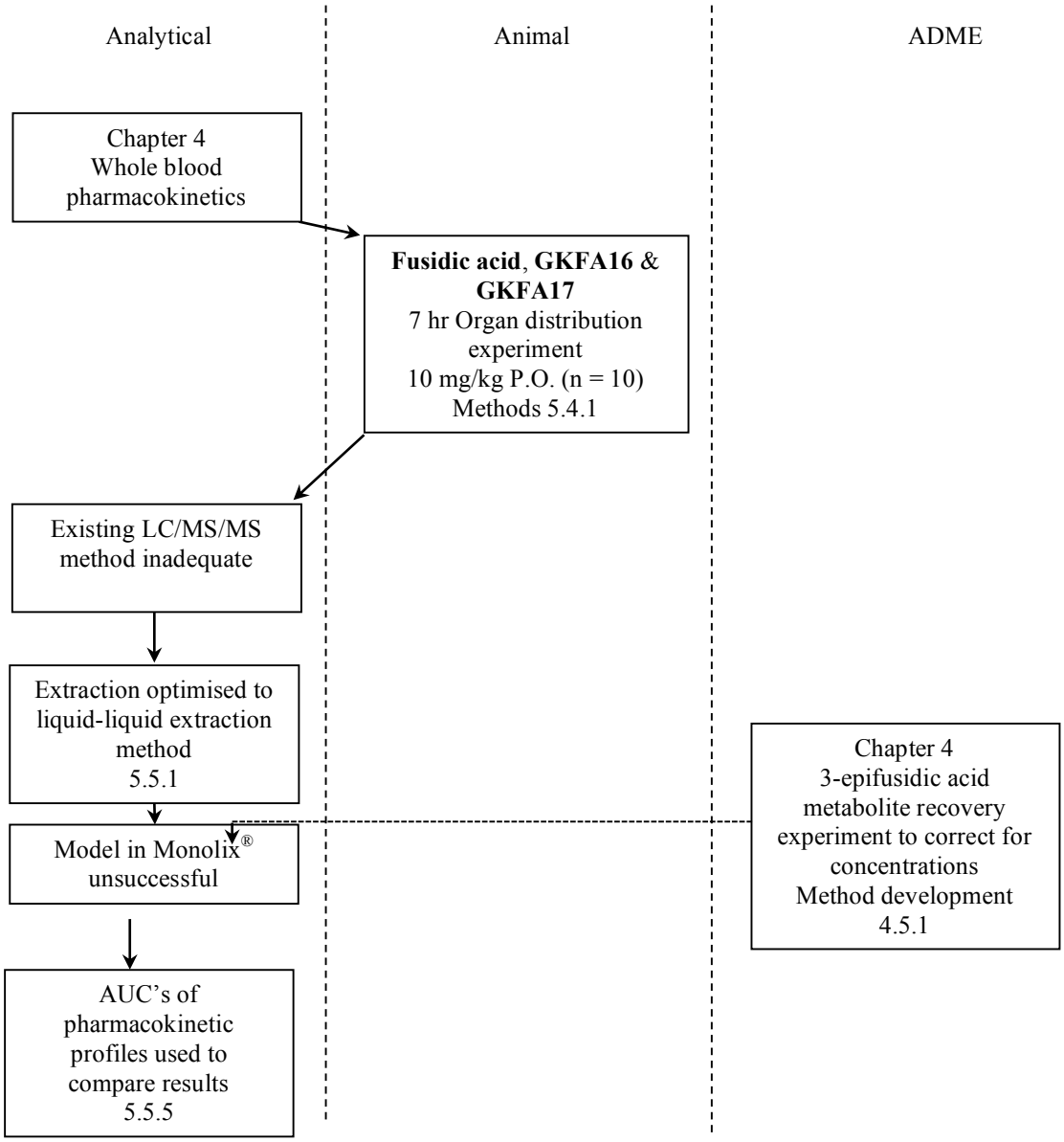

Figure 5-4: Methodology overview of organ distribution evaluation

5.4 Methods

5.4.1 In vivo tissue distribution experiment

5.4.1.1 Animals

All animal studies and procedures were conducted with prior approval of the Ethics Committee of University of Cape Town (UCT), approval number 013/032, in accordance with the National Code for animal use in research, education, diagnosis and testing of drugs and related substances in South Africa. The pharmacokinetic animal experiment used healthy eight-week-old male C57BL/6 mice maintained at the University of Cape Town animal facility. Mice were housed in 27 x 21 x 28 cm

cages under controlled environmental conditions including a maintained temperature of 26 ± 1°C and 12 hr light/dark cycle. Food and water was available *ad libitum*.

5.4.1.2 Compound preparation

On the day of the experiment, a predetermined mass of the test compound was weighed for the experimental group consisting of 10 males weighing approximately 30 g.

Right before oral administration the compound was suspended in 2000 µl of aqueous 0.5% HPMC (w/v) and vortexed for 1 minute. Drug administration followed by oral gavage of 150 µl total volume of suspension for a total dose of 10 mg/kg. Administration occurred within 30 minutes of suspension preparation. Mr Trevor Finch from the Division of Pharmacology, University of Cape Town (South Africa) performed the animal procedures.

5.4.1.3 Organ harvesting

Organ collection of 3 mice occurred at approximately 1, 3 and 5 hrs, and 1 mouse at 7 hrs to confirm elimination. Blood samples were collected every hour before sacrifice. Sacrifice was performed by cardiac puncture and removed most vascular blood, which was followed by dissection along the mid-ventral line of the animal to expose the organs. Both femoral arteries were cut and approximately 20 ml of saline injected into the right aorta to rinse the circulatory system of blood. This was continued until the organs experienced a pale colour change, and if additional rinsing was required, specific organs were isolated from the circulatory system to remove as much blood as possible. The organs were then dissected out. The author of this thesis was responsible for final inspection of blood, further rinsing if necessary and drying of the organs, weighing and flash freezing in liquid nitrogen, and sample storage at -80°C. The entire procedure was performed on average within 12 minutes. To obtain blank matrix for calibration curves, this process was repeated in three mice that did not receive any compound.

5.4.2 Tissue homogenation

The summarised procedure for tissue homogenation of each respective organ is shown in Table 5-1. Briefly a 1:1 or 2:1 mass of saline to mass of the thawed organ samples was added in a 2 ml reinforced microtube containing 5 x 2.8 mm ceramic beads. The large liver samples were first dissected into smaller sections and placed in different microtubes. The samples were then briefly vortexed on an

Omni Bead Ruptor™ instrument with settings according to the manufacturer's website. These settings could be optimised to a single method that can homogenise different organ samples in one batch. Homogenate liver samples were pooled for analysis and all samples stored at -80°C.

Table 5-1: Tissue homogenation settings

	Liver	Brain	Kidney	Lungs	Spleen	Heart
Saline:Organ (m/m)	1:1	2:1	1:1	2:1	2:1	2:1
Speed (m/s)	5.50	5.65	6.00	4.00	5.00	6.00
Time of Cycle (s)	30	30	30	40	30	30
Number of Cycles	2	2	1	1	1	2
Dwell (s)	5	5	0	0	0	20

The Omni bead ruptor has 4 adjustable settings namely the speed of pulsing/shaking (Speed), the time of sample shaking/pulsing (Time of cycle), the number of times the sample is pulsed (Number of cycles) and the time between pulse cycles (Dwell). Each organ sample was homogenised at their optimised settings with a specified amount of saline by mass to provide a homogenous liquid sample for accurate pipetting.

After analysis, the organ sample concentrations were corrected for by the saline dilution during homogenation and density of the homogenate. Table 5-2 contains the mean density values as determined for three different animal samples and rounded correction values used. The final concentration was expressed as nmol/mg. For reference, a solution of 1 nmol/mg in water would equal 1 uM.

Table 5-2: Organ densities and correction factor

	Density (g/ml)	Correction
Liver	0.954	1.0
Spleen	0.938	0.9
Kidney	0.853	0.9
Heart	0.969	1.0
Lung	0.975	1.0
Brain	0.862	0.9
Blood	0.985	1.0

5.4.3 Final LC/MS/MS method

Initial cross-validation of the method described in Chapter 4, section 4.4.2, page 133 in blank liver matrix showed that the extraction method and chromatography needed to be optimised due to increased background interference. The detailed results from the method optimisation is presented in Section 7.5.1, page 277. Briefly, the final liquid-liquid extraction method used 20 µl of homogenised organ sample with 20 µl of pH 3 universal buffer containing a structurally similar internal standard and 250 µl ethyl acetate. Gradient chromatography was performed on a Phenomenex® Kinetex C_{18} (2.1 x 50 mm, 2.6 µm) reverse phase column at a flow rate of 400 µl/min with mobile phases 0.03% ammonium hydroxide (v/v) in water and acetonitrile. The lung, brain and spleen samples were analysed on an AB Sciex API 4500® mass spectrometer, and the heart, liver and kidney samples on an AB Sciex API 5500® mass spectrometer, both operated at unit resolution in multiple reaction-monitoring mode.

Due to the small organ volume obtained from each mouse, conservative efforts were required for calibration standards and final analysis. Method development was performed in higher volume liver homogenate and the final method was then implemented for the other organs. Calibration standards for **GKFA16** and **GKFA17** were prepared together with their metabolites; fusidic acid and 3-ketofusidic acid. Each respective organ batch therefore contained all three experiments with one set of calibration standards to quantify **GKFA16** and **GKFA17**, and their metabolites. In Table 5-3 is shown the accuracies (%Nom) of each organ batch with highest and lowest accuracy of the calibration curves of all parent and metabolite compounds with their stipulated range.

Chapter 7: Experimental, section 7.5.3, page 277 presents the final quantification statistics of individual analytes of each batch, expanded extraction method and mass spectrometer conditions.

Table 5-3: Accuracy of calibration curves

	GKFA16	**GKFA17**	Fusidic acid	3-Ketofusidic acid	Range (ng/ml)
Whole blood	83.1 – 117%	85.8 – 106%	82.5 – 111%	88.5 – 110%	10 – 5000
Liver	83.5 – 115%	96.1 – 104%	94.2 – 107%	91.8 – 107%	50 – 2500
Lungs	86.9 – 113%	93.3 – 115%	93.5 – 115%	86.0 – 103%	10 – 2500
Spleen	91.0 – 106%	84.4 – 108%	87.4 – 104%	84.4 – 108%	10 – 2500
Kidney	93.8 – 112%	82.0 – 113%	90.0 – 115%	89.9 – 113%	10 – 2500
Brain	92.4 – 112%	93.9 – 111%	92.5 – 116%	94.0 – 112%	10 – 2500
Heart	83.3 – 115%	81 – 116%	88.0 – 111%	91.4 – 108%	10 – 2500

5.4.4 Area under the curve calculations

Concentration time profiles and area under the curve to infinity ($AUC_{0-\infty}$) were calculated in Microsoft Excel® 2013 by means of the linear trapezoidal rule from time 0 to the final concentration-time point, and to infinity estimated by assuming log-linear decline.

5.5 Results & Discussion

5.5.1 LC/MS/MS method optimisation

Organ concentrations of the compounds were quantified by a LC/MS/MS assay developed for a range of 10 – 2500 ng/ml, and liver tissue calibration curve for a range of 50 – 2500 ng/ml. Initial cross-validation of the method described in Chapter 4, section 4.4.2, page 133 in blank liver matrix showed that the extraction method and chromatography needed to be optimised due to increased background interference. A new Phenomenex® Kinetex C_{18} column with adjusted gradient chromatography decreased the run time and improved separation. The extraction method was optimised for a liquid-liquid extraction and improved separation. Figure 5-5 shows recovery of the analytes performed in triplicate, comparing methanol protein precipitation, liquid-liquid extraction using ethyl acetate and hexane as organic solvents followed by liquid-liquid extraction using ethyl acetate with universal buffer at different pH values to optimise best recovery and repeatability of extraction. The extraction trend of the two C-3 ester prodrugs showed better extraction at acidic pH while fusidic acid and the 3-ketofusidic acid metabolite showed higher extraction at basic pH. Liquid-liquid extraction to compare the best pH for extraction used pH 10 and pH 3 universal buffers and ethyl acetate as organic solvent. Their respective calibration curves had similar recovery rates. Figure 5-6 contains representative calibration curves of fusidic acid at pH 3 and pH 10. The final extractions used pH 3, due to slightly better regression values of the calibration curves compared to pH 10 and a lower background observed for blank samples. Figure 5-7 contains the blank chromatograms of the original protein precipitation double blank sample, and liquid-liquid extracted liver blank samples, extracted at pH 3 and pH 10.

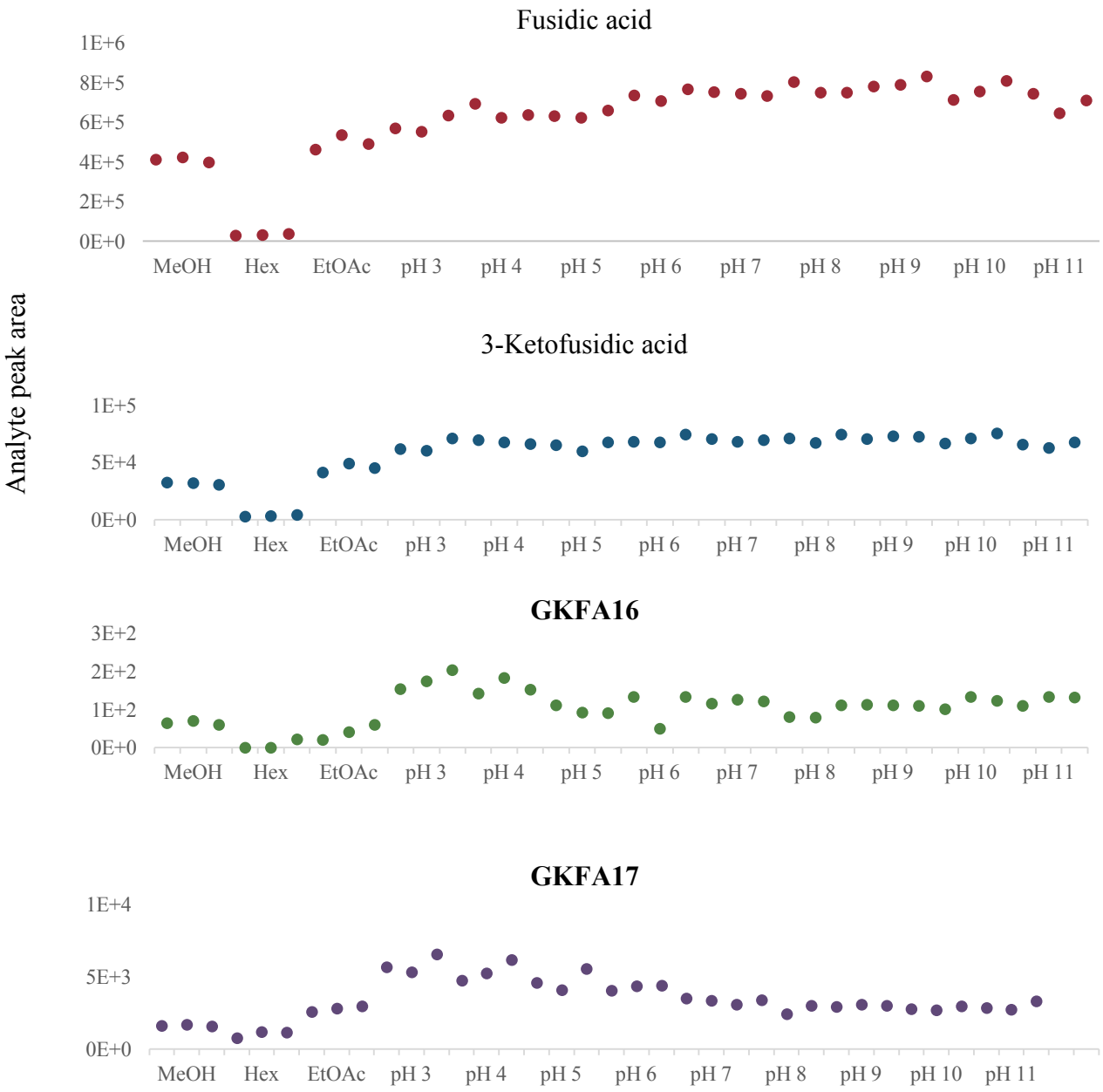

Figure 5-5: Organic solvent and buffer optimisation for liquid-liquid extraction

Extraction efficiency (related to an increase in analyte peak) of analytes extracted by protein precipitation extraction by MeOH (methanol), Hex (n-hexane) or EtOac (ethyl acetate) and liquid-liquid extraction using a range of acidic to alkali buffers.

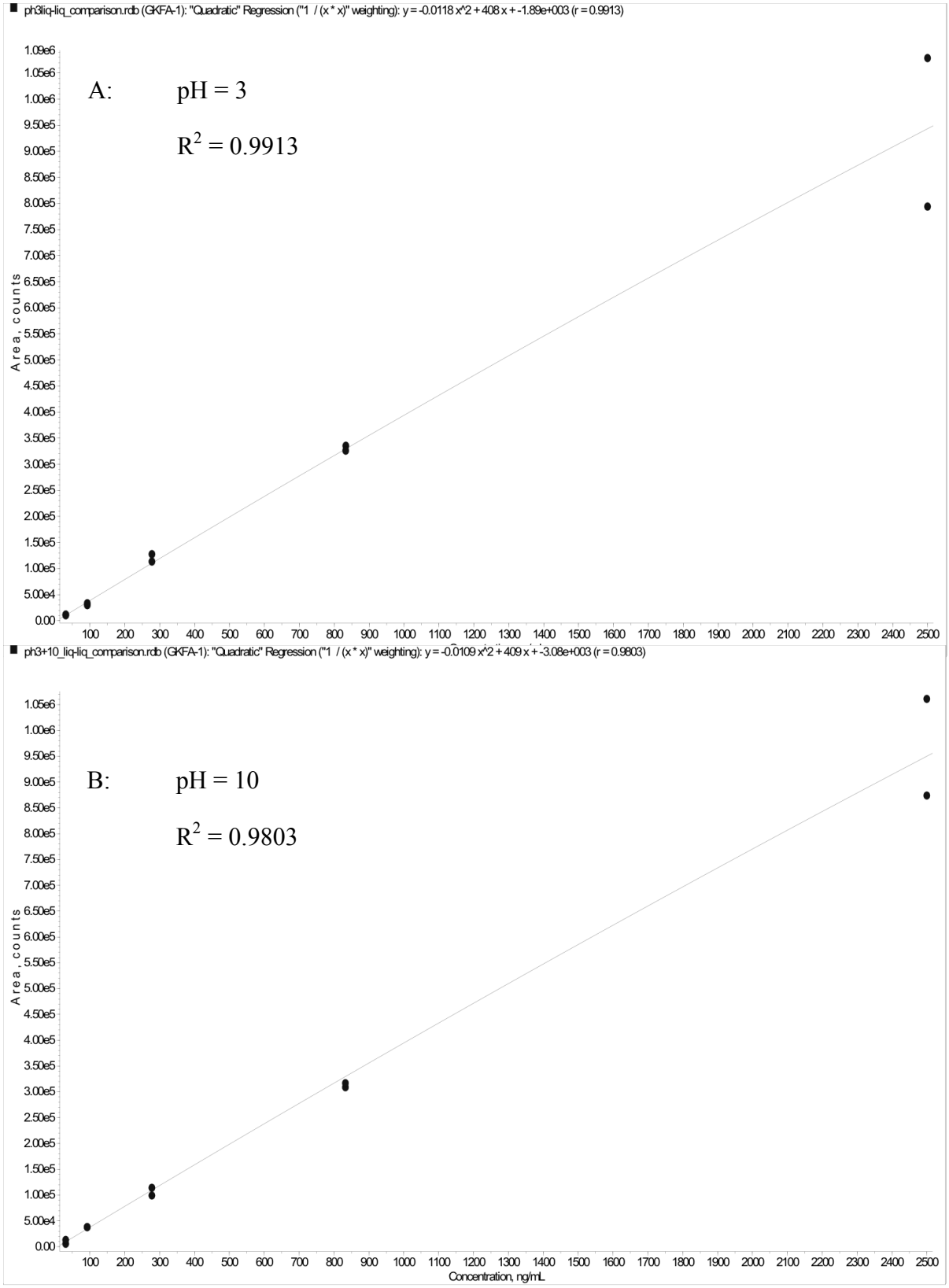

Figure 5-6: Calibration curves of pH 3 and pH 10 extraction

Area counts versus concentration of standards prepared by liquid-liquid extraction at A: pH 3 and B: pH10.

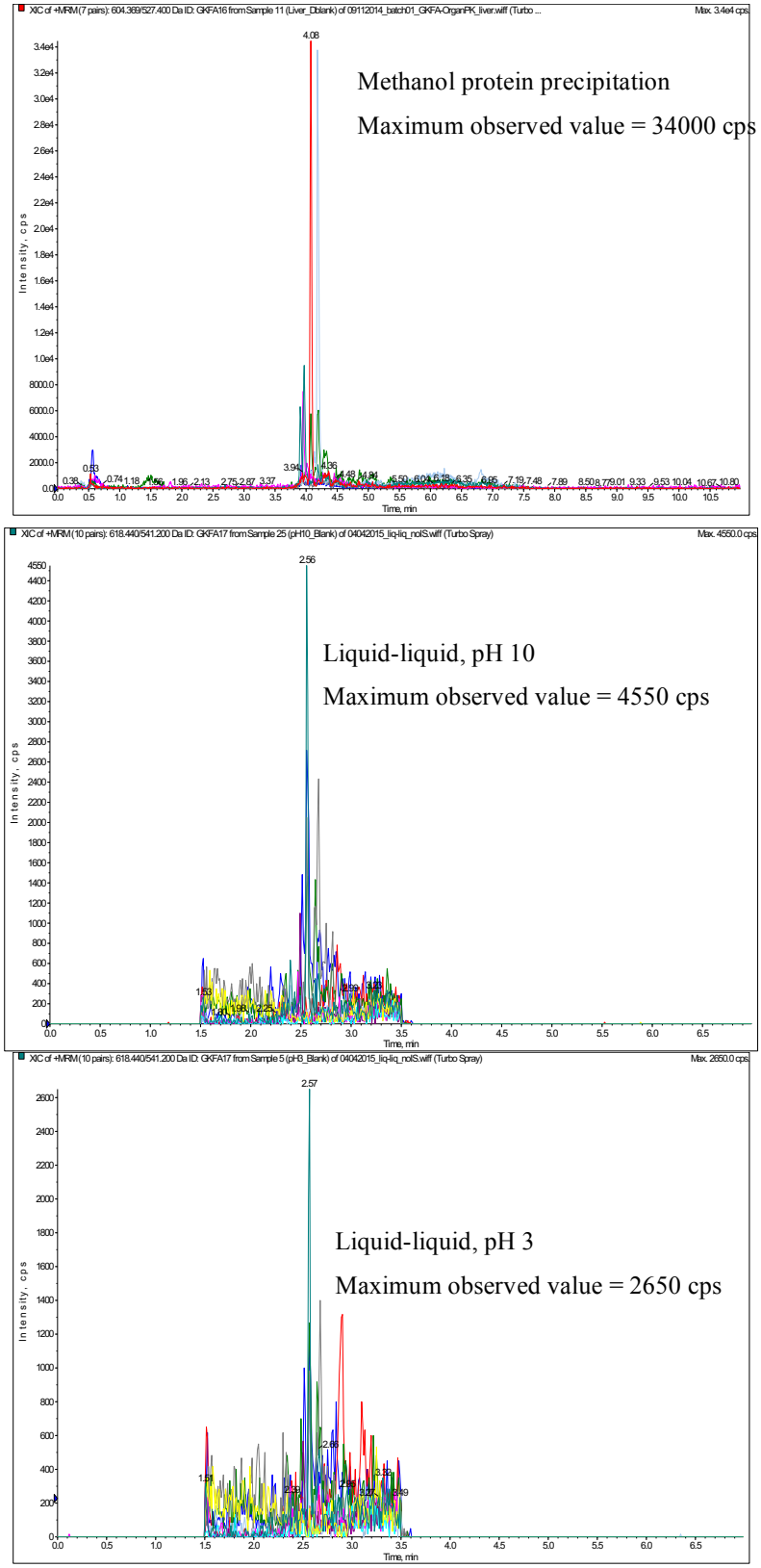

Figure 5-7: Double blank samples of different extraction methods

Comparison of extraction methods effect on carry over by examining the maximum observed value of a double blank sample after injecting a high concentration of the respective analytes. The lowest observed carry over was observed for a liquid-liquid extraction using a pH3 buffer.

5.5.2 Bioanalytical method

Developing an accurate LC/MS/MS method for the organ samples required an improved extraction method. A liquid-liquid extraction method was found to be sufficient for the samples, but could be refined to a solid phase extraction method as high background was still observed. Original expectations were that sensitivity would be the major challenge in quantification, but the lowest standard of these compounds still showed an intense peak at 10 ng/ml from a 20 µl diluted organ sample. More importantly, the greatest challenge for quantification was matrix effects from the organ samples that decreased precision and reproducibility. A known limitation of multiplex methods that evaluate a diverse polarity range of analytes and/or metabolites is that the gradient required to separate and elute analytes in an efficient run time increases the chances of matrix effects as a similarly large polarity range of endogenous background elutes with the analytes. Due to the small volume of blank matrix, conservative preparation was required for the calibration standards and a cassette analysis approach that depended on a multiplex assay to analyse respective organs from different experiments in the same batch was necessary. The multiplex method for these samples also remained a very convenient approach and is still recommended for future experiments to save on blank matrix and decrease run time.

Another concern in quantification was determining the range of calibration curves. The liver had concentrations as high as 4000 ng/ml before correcting, while the other tissues showed much lower concentrations ranging between 10 – 1000 ng/ml. Therefore, choosing an ideal range for calibration standards when the concentrations of final samples are unknown is difficult and method development should aim to keep the range as wide as possible without losing the integrity of the accuracy and precision in quantification.

Future suggestions for bioanalytical methods aimed at organ distribution studies include persisting with a multiplex assay to evaluate similar compounds in the same organ batch with care taken to assess and limit possible matrix effects. This includes starting method development with an optimised liquid-liquid or solid-phase extraction that will also preserve the LC/MS/MS instrument from contamination of the high background. Cross-validating organ tissues with a single surrogate organ tissue or whole blood was considered, but was not possible for these analytes as evident by the great diversity in respective organ calibration curves. Method development exclusively in liver homogenate with final methods transferred to other organs produced adequate results and should be similarly applied in future experiments. When selecting a final calibration curve range, it is important to keep

in mind that an improved extraction method will give similar sensitivity as whole blood extractions. It is also important to acknowledge the greater objective of preclinical screening, which includes identifying promising compounds that are expected to have high exposures. Emphasis on the lower range of quantification therefore becomes less important and a low concentration limit related to final *in vivo* concentration rather than instrument capability should be defined.

5.5.3 Animal procedure

Rinsing the organs with saline during organ harvest was performed to remove excess whole blood as the whole blood concentration could greatly influence results. This procedure poses its own limitations though, as the equilibrium between the vascular system and tissues can shift quickly to allow analytes to leach out into the saline. The animal procedures to harvest organs were therefore performed as efficiently as possible to minimise the time from initial cardiac puncture to flash freezing the samples, with an average of 12 minutes. It is important to note, however, that the respective analytes could be lost during this procedure resulting in lower observed concentration values in the tissues.

5.5.4 Non-linear mixed effect modelling attempt and non-compartmental analysis compromise

An initial five-compartment model starting with the metabolite data input as separate compartments did not work in the Monolix® software. Possible reasons for this included the complexity of the metabolic model where metabolism between fusidic acid, 3-ketofusidic acid and 3-epifusidic acid appeared to be reversible. The precision of the organ concentration data was not ideal considering the complexity of the organ harvesting and bioanalytical methods. Overall, the sparse data did not support the complexity of the model. Moreover, looking at the pharmacokinetic profiles, it seems the tissues equilibrated reasonably quickly with the central compartment, and therefore speculatively, there would not be much benefit in modelling the whole kinetics as opposed to calculating their relative exposures. Nonlinear mixed effects modelling (and the Monolix® software) are generally applied to population pharmacokinetic models, which are not as complex as tissue distribution models and require many more compartments and parameters. Concomitant estimation of all parameters from the current data was not feasible, and fixing some of the parameters appeared somewhat arbitrary without strong supporting evidence. Other software packages tailored for systems modelling include features and libraries aimed at assisting the researcher to fix parameters to reasonable values, and such

solutions may have proved more suitable for the interpretations of these results. However, these software packages are costly, require ad hoc training and were deemed outside of the scope of this project, especially when weighed against the objectives of fusidic acid repositioning where the mouse model was already found inappropriate for future evaluation.

It was therefore chosen to evaluate and compare organ distribution of the analytes exclusively by NCA techniques and calculate the ratio between the observed concentrations in the different organs. The area under the terminal log-linear phase of the curve to infinity (AUC_{∞}) was chosen for comparison. As discussed in previous chapters, there are many limitations to NCA and accuracy of the approximated AUC_{∞} to true area under the curve depends on the number of concentration-time points, the selected time points and whether log-linear decline is appropriate. Nevertheless, in this comparative situation, NCA was deemed the best option to obtain AUC_{∞}, which is used to compare organ distribution in similar studies.[219]

The sampling schedule for this experiment was aimed at evaluating the elimination phase and therefore excluded initial absorption. The initial plan was to use a modelling approach to supplement the lack of information on absorption in this experiment using data from the original whole blood pharmacokinetics. Since that approach proved unfeasible, as explained above, the lack of absorption phase was problematic for the NCA-based estimation of total AUC. In Figure 5-8 is shown the original whole blood pharmacokinetic profile of **GKFA16** (oral 25 mg/kg) with the organ distribution whole blood pharmacokinetic profile of **GKFA16** (oral 10 mg/kg) and respective semi-log plot to illustrate the loss of the absorption phase AUC and subsequent restriction in analysis.

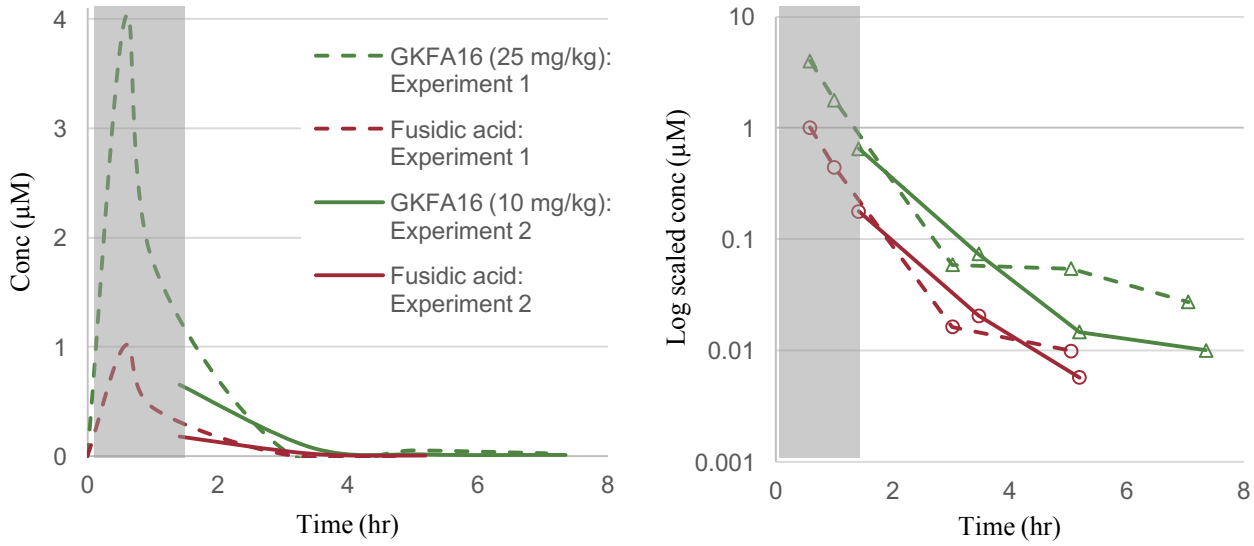

Figure 5-8: NCA limitations of organ distribution time points
The concentration-time profile for Experiment 1 and 2 that evaluated blood pharmacokinetics and organ distribution respectively and the log-linear graph show the lost information in absorption phase represented by the grey rectangle.

To overcome this limitation, the results are therefore not considered for the initial concentration time point and the values reported are not total AUC. In this analysis, only the terminal component of the AUC was considered, with the assumption that this is when the distribution to the tissues has reached an equilibrium with the whole blood. This assumption is supported by visual inspection of the pharmacokinetic profiles, which in a log-plot appear parallel in this terminal phase, and by the fact that the concentration ratios remain reasonably constant over time in this phase, as shown in Figure 5-8.

While this simplified approach prevented proper characterising of the absorption phase, it provided insight into the equilibrium between the concentrations after the transitory absorption phase, and one could argue that these values are closer to the steady-state equilibrium, which is therapeutically more relevant.

5.5.5 Organ distribution profiles

Figure 5-9 presents the linear pharmacokinetic plots of the fusidic acid, **GKFA16** and **GKFA17** experiments for each respective organ with observations represented by crosses and the mean concentration by organ and analyte shown by a solid line of appropriate colour. Figure 5-10 contains the semi-log pharmacokinetic plots with similar format, omitting brain concentrations. Figure 5-11 shows the respective AUC_{∞} values to compare exposures in relevant organs.

In Figure 5-12 is shown the natural logarithmic function of respective organ AUC_{∞} to whole blood AUC_{∞} to visualise the magnitude of the partitioning exposure, i.e. AUC_{∞} above 0 represents partitioning into relevant organ and below 0 shows partitioning into whole blood.

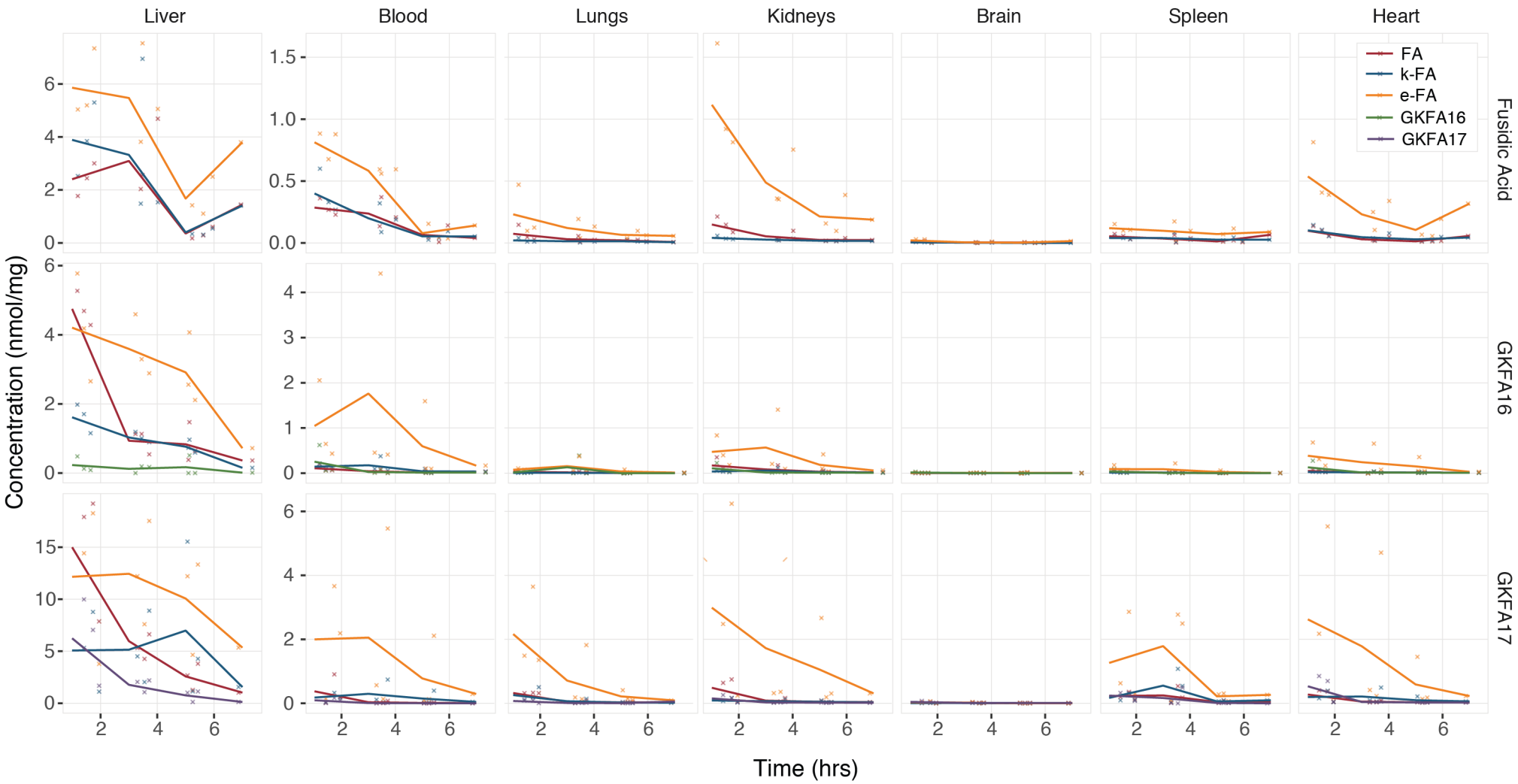

Figure 5-9: Linear organ distribution profiles

Linear concentration time plots for the fusidic acid, **GKFA16** and **GKFA17** experiments stratified by experiment and organ. Individual observations are represented by crosses. Each metabolite is represented by a different colour, namely **GKFA16**; green, **GKFA17**; purple, fusidic acid (FA); red, 3-ketofusidic acid (k-FA); blue, and 3-epifusidic acid; e-FA (yellow).

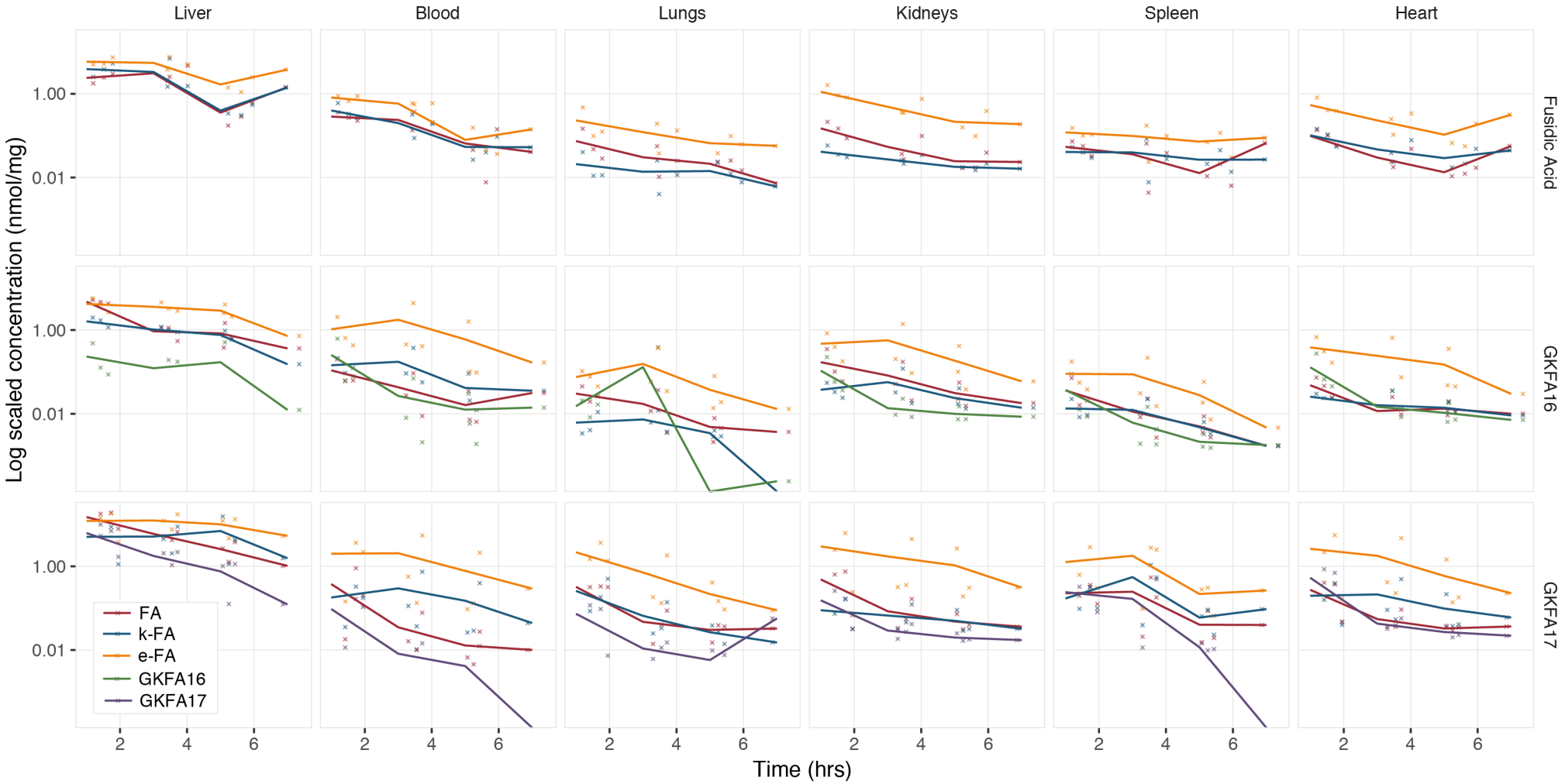

Figure 5-10: Log-linear organ distribution profiles

Log scaled organ distribution plots to better compare their pharmacokinetic profiles on a more convenient scale for the fusidic acid, **GKFA16** and **GKFA17** experiments stratified by experiment and organ. Individual observations are represented by crosses. Each metabolite is represented by a different colour, namely **GKFA16**; green, **GKFA17**; purple, fusidic acid (FA); red, 3-ketofusidic acid (k-FA); blue, and 3-epifusidic acid; e-FA (yellow).

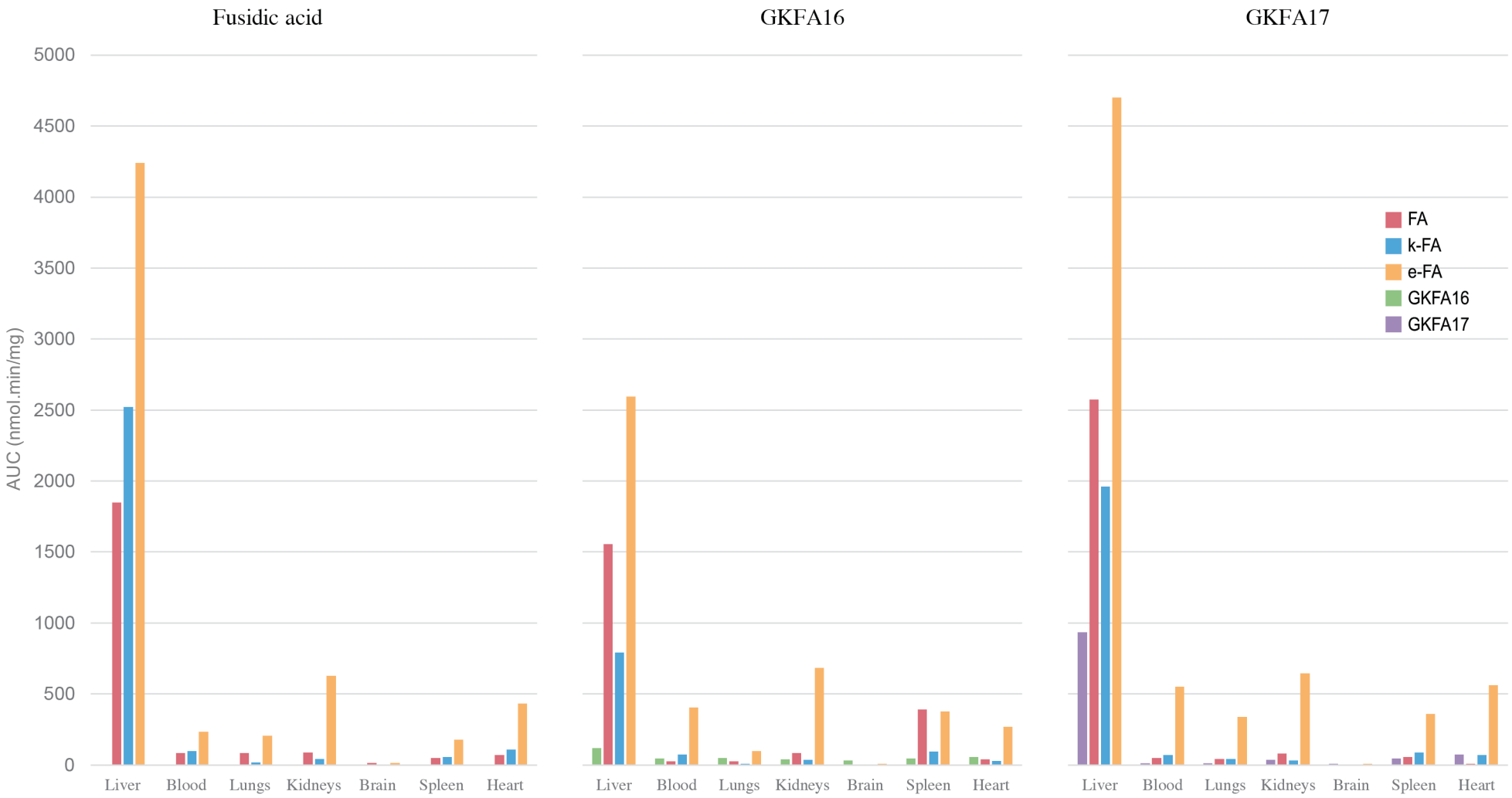

Figure 5-11: Comparison of C-3 ester prodrugs and metabolite exposure

Figure 5-12: Log ratio of organ to blood exposures

The organ distribution results showed a high first pass effect for fusidic acid, **GKFA16** and **GKFA17**. This rapid metabolism increased the exposure of 3-epifusidic acid resulting in the highest exposure of the rodent-specific metabolite in all organs. The high concentrations observed in the liver suggest that the compounds were well absorbed with **GKFA17** administration showing the highest observed concentrations of fusidic acid and the respective C-3 prodrug. However, little of this exposure made it into systemic circulation as hepatic elimination reduced the percentage of observed active compound concentrations in whole blood to a concentration less than 2 nmol/mg, compared to the liver concentrations that were well above 2 nmol/mg.

It is known that fusidic acid crosses the blood brain barrier by approximately 7%[220] and the C-3 ester prodrugs investigated were found to be similarly poorly blood brain barrier permeable. The negligible concentrations observed could likely be from unavoidable whole blood contamination during brain harvesting and future experiments should examine cerebrospinal fluid instead. Further discussions exclude brain distribution of the compounds.

Heart, spleen and lung concentrations were similar for the respective compounds suggesting their peripheral distribution to be non-discriminatory between these sites. The kidneys had the second highest concentrations of 3- epifusidic acid, which fits renal extraction of the compound. This was true for all analytes, except 3-ketofusidic acid and **GKFA16**, which had higher exposure ratios in the blood compared to the kidneys. This does not mean that **GKFA16** and 3-ketofusidic acid are not renally cleared as the partitioning values only represent the compound's affinity for kidney or whole blood tissue, not their final interaction.

Caution should be applied in interpreting the results, as increased distribution or partitioning into tissues does not necessarily translate into efficacy. Organ distribution is the first barrier in reaching mycobacteria sites, but the increase in distribution could be due to binding of the compound to unwanted membranes etc. not allowing the compound to elicit an effect.

Generally, the prodrugs preferentially partitioned into tissues more than blood, except for the kidney partitioning of **GKFA16**. This is a positive result that the prodrugs were effective in increasing distribution when compared to fusidic acid administration, where fusidic acid preferentially partitions into blood for all organs except the liver and kidney. The prodrugs also altered the trend of fusidic acid partitioning and a higher ratio of fusidic acid was observed for the spleen and heart tissues compared to blood. This is likely due to bioactivation of the better-distributed prodrugs in the organs releasing fusidic acid. This finding was unfortunately not observed for the lung tissue that carries the highest mycobacterium burden. Total lung exposure of the C-3 ester prodrugs compared to fusidic

acid did not show an improvement. The concentration time curves reveal that there was an initial high concentration of **GKFA16** and **GKFA17**, but their rapid elimination did not sustain exposure in the lung.

Future experiments should look at bound and unbound fraction of compounds in the organ tissue, as it is the unbound fraction that can elicit an effect against the mycobacteria. Compounds progressed to animal efficacy should attempt to repeat the organ distribution studies to compare infected vs. uninfected tissues which could show different exposures.

5.6 Conclusion

In Table 5-4 is shown the summarised pharmacokinetic profiles of the active analytes, fusidic acid, 3-ketofusidic acid, **GKFA16** and **GKFA17** of the three organ distribution experiments.

Table 5-4: Summarised lung profiles of active analytes

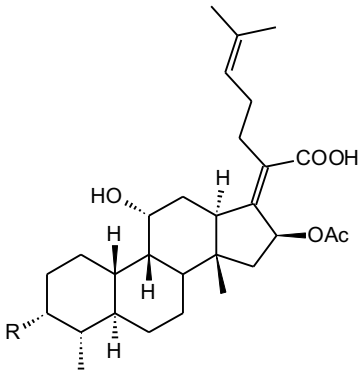

Fusidic Acid	**GKFA16**	**GKFA17**
	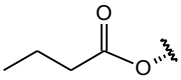	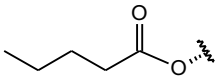

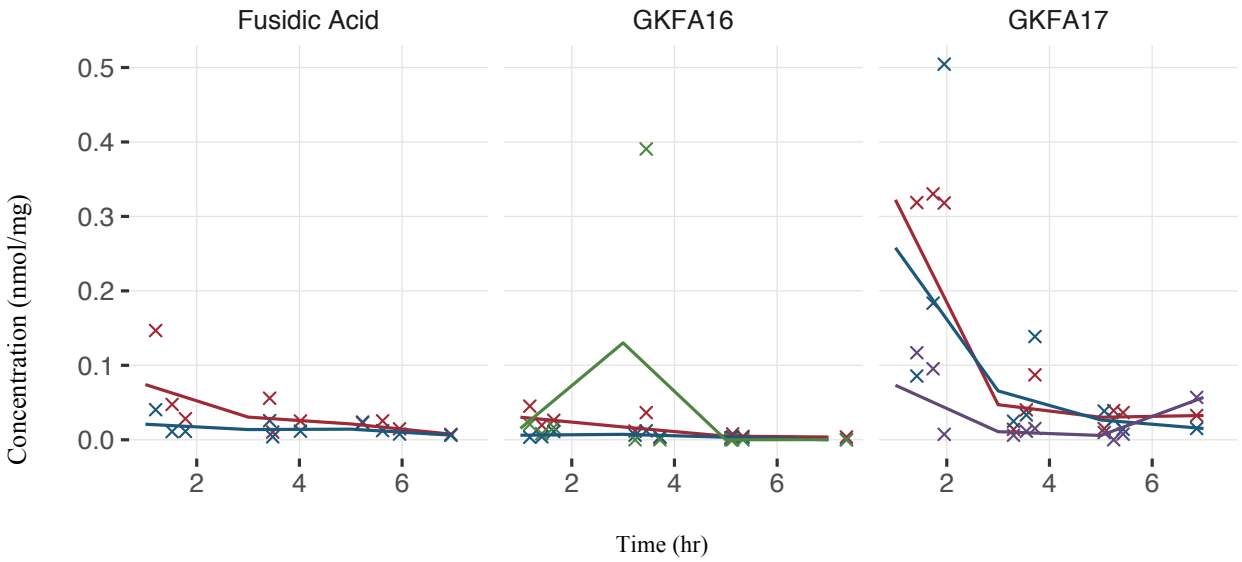

The aim of the prodrugs to improve the pharmacokinetic properties of fusidic acid including distribution was successful. The C-3 ester prodrugs showed improved partitioning into peripheral tissues compared to fusidic acid and showed a favourable fusidic acid ratio in the peripheral tissues compared to blood after prodrug administration. The C-3 ester fusidic acid prodrugs are therefore still

promising to pursue towards the repositioning of fusidic acid, despite the drawback of the high rodent specific metabolite exposures that limited analytical interpretation. The organ distribution study showed that the 3-epifusidic acid metabolite was present at highest concentrations in all organs and again highlighted the inappropriateness of the mouse model for further fusidic acid evaluation.

The bioanalytical method development was challenging and could be improved significantly, but the found method was not found to be suitable to show the trends in partitioning and exposure that was required from this project. Future experiments could improve on the bioanalytical outcomes and find the optimised balance between accuracy and efficiency at a preclinical stage.

Implementation of a mechanistic model for these compounds proved unfeasible due to the complexity of the metabolism and the limited information contained in the collected data, affected by quantification uncertainty due to the complicated experimental procedures and limited data points. It is therefore not possible to comment on the benefit of adding a modelling step, but it is advised that the difficulty in the implementation of a mechanistic model while characterising the pharmacokinetics may outweigh the advantages at this early preclinical stage. Further, the ability to extrapolate these animal results to humans are poor due to the rodent specific metabolism. A full-fledged mechanistic approach, supported by dedicated software may prove more feasible and yield results that are more accurate. However, future assessment in the use of these models should weigh the effort of implementation in a drug discovery screening cascade and aim to simplify solutions that can easily be applied to diverse compounds.

The distribution results are a positive step in the objective of improving compound pharmacokinetics for tuberculosis as the results show rational drug design with renewed pharmacokinetic objectives can potentially rescue compounds with poor distribution properties. Increased screening of future drug leads while simultaneously expanding techniques to get closer to the site of mycobacterial infection, will aid in increasing existing knowledge of what is the ideal pharmacokinetics of a tuberculosis drug lead and how existing compounds can be optimised to improve their pharmacokinetics.

6 CONCLUSION

6.1 General objectives

Overall, the results from this project added a positive level of interpretation of the potential drug-like properties of the analysed compounds, through means of their preclinical pharmacokinetic evaluation. Insights were gained into the murine pharmacokinetics of four antimalarial compounds, including a bioequivalence study, and two antituberculosis prodrugs and their metabolites. The individual studies were used as a foundation to compare NLME modelling techniques with traditional NCA, and expand the methods of this preclinical lab to include capsule dosing and organ distribution evaluation.

Reflecting on the original objectives, adequate development of bioanalytical methods using LC/MS/MS quantification to evaluate pharmacokinetics of antimalarial and antituberculosis drug leads in mice preceded modelling evaluation, with suggestions on future improvement. Expansion of pharmacokinetic methods as better screening tools for the evaluation of in-house compounds was successful, including capsule dosing, organ distribution studies for mechanistic pharmacokinetics, and simulating model results to evaluate PK/PD relationships and mouse to human translation.

It was found that the implementation of simple general pharmacokinetic models with NLME aimed at preclinical evaluation was often straightforward. Considering the compounds analysed followed non-linear elimination, NLME would be more correct in interpreting clearance and volume. This improved half-life estimations and bioavailability due to improved calculations compared to NCA estimations on half-life and outdated bioavailability methods that utilise the trapezoidal rule. This is vital in compound screening and progression. Refining techniques to include organ distribution and

capsule dosing also had a positive impact and proved useful at compound screening with constructive feedback to improve compound optimisation that is paramount to drug discovery.

6.2 Summary of compounds evaluated

Pharmacokinetic evaluation of three benzoxazole amodiaquine analogues in mice revealed excellent pharmacokinetics with the best performing compound, **DS23B**, showing a bioavailability of 54% and half-life of 51 hrs. Simulated retrospective PK/PD relationships assisted by NLME modelling was simple and beneficial to project outcomes, guiding future compound optimisation of this series to improve pharmacokinetic properties for a time above IC_{50} drive in efficacy. Future studies should include pharmacokinetic sampling during efficacy assessment with the aim of including PK/PD analysis in one model.

Evaluation of a cyclodextrin formulation study suggests a pH-dependent increase in solubility led to improved pharmacokinetic properties. NLME showed increased bioavailability and a less variable rate of absorption of the cyclodextrin complex that was beneficial to improving consistent compound exposures in mice. Still, the results displayed for both the formulation and active pharmaceutical ingredient mouse groups had high variability, making conclusions speculative. Suggested future studies should consider higher mouse numbers (n = 5) and increased sampling time points around the expected absorption phase. It is also recommended that capsule dosing be implemented for efficacy studies in the *Plasmodium berghei* infected mouse model, with simultaneous pharmacokinetic evaluation. Notwithstanding criticisms around this method, the undemanding implementation of the capsule dosage form will allow for advantageous PK/PD evaluation and improved accuracy and comparison of the results.

Pharmacokinetic analysis of fusidic acid, its 3-ketofusidic acid metabolite and novel fusidic acid C-3 ester prodrugs uncovered that the species-specific metabolite 3-epifusidic acid had a detrimental effect on compound exposure in mice. This rodent specific metabolite was retrospectively quantified, avoiding a repeat animal experiment. Organ distribution of the C-3 ester prodrugs showed improved absorption and tissue distribution of the C-3 ester prodrugs. These results support the original objective of the fusidic acid C-3 ester prodrugs to improve drug concentrations at the site of mycobacterial infection with the aim of repositioning fusidic acid for tuberculosis.

6.3 Non-linear mixed effects modelling compared to non-compartmental analysis

It was found that implementing NLME modelling at an earlier stage in preclinical screening required little effort, once a standard set of pharmacokinetic models was developed. These models can be easily applied to future studies. Three basic models based on fundamental one-, two- and three-compartment models were implemented, and this model library was easily applicable to most data with only minor modifications necessary to some compounds. In terms of efficiency, straightforward compounds were faster to analyse by NLME compared to NCA, due to NLME automatically compiling individual profiles and analysing the data as a single set. This also had the advantage of increasing robustness of the data in the case where some mouse profiles were insufficient in statistical strength, such as the formulation study in Chapter 3, or data lacking essential elimination phase concentration-time points, e.g. the amodiaquine analogues presented in Chapter 2. The limitations of NCA became apparent when comparing bioavailability data, and 3 out of the 8 compounds studied showed a difference of up to 20% in bioavailability.

This is an important consideration as preclinical screening is a process of elimination where the best compounds are progressed further in a resource limited screening cascade. A bioavailability estimate out by 20% is detrimental and could lose a potential clinical candidate to an inadequate lead.

NLME modelling therefore added confidence in the pharmacokinetic interpretation and a level of decisiveness that will aid future screening.

6.4 Limitations

A concern of the results presented was the robustness of the bioanalytical methods used. In the scope of evaluating compounds at a preclinical level, the balance between accuracy of quantification and time spent on method development is shifted to be able to analyse more compounds in a short amount of time. The motivation behind this was that at a preclinical stage, objectives are limited to first assess trends and compare compounds to guide future decision-making. In hindsight, more effort could have been spent on the quantification methods to improve data precision. In terms of the quality of data, more accurate data are easier to input into NLME models with less strain on the analysis. The balance between time and effort of quantification methods should be reassessed in future studies.

Modelling approaches were difficult to assess for the cyclodextrin formulation study presented in Chapter 3. This was a result of a minimal preliminary study design that did not provide adequate data

to draw concrete conclusions. Here the fundamental issue was the preclinical limitations set out in the original ethics protocol, with specified sampling times and animal numbers. These results will assist in future ethics applications to improve the animal experiment protocol.

The tissue distribution studies were laborious and careful consideration is needed for which compounds to progress to tissue distribution evaluation. Since a mechanistic pharmacokinetic model for the fusidic acid compounds could not be implemented, the benefit of adding a modelling step at this stage in preclinical evaluation cannot be assessed. It was also found that the development of more sophisticated mechanistic models to analyse experiments can quickly become too complex and the additional effort could end up outweighing the advantages, especially considering potential poor extrapolation as in the case of the fusidic acid analogues. Future assessment should weigh the effort of implementation in a drug discovery screening cascade to the knowledge gained. A fully-fledged mechanistic model with dedicated software may prove more suitable and is likely to provide results that are more accurate, but it was deemed outside the scope of the current work. Future attempts should simplify the models with the goal that they can be easily applied to a diverse range of leads.

6.5 Acknowledgment of the multidisciplinary approach

It is fundamental to recognise that this project depended on a multidisciplinary approach that added strength to the results. For the benzoxazole amodiaquine study, efficacy data from the Swiss Tropical and Public Health Institute (Basel, Switzerland) was used retrospectively to evaluate PK/PD drivers and *in vitro* ADME results from the Drug Discovery and Development Centre (H3D), Cape Town (South Africa) added to the interpretation. The efforts of the Centre for Supramolecular Chemistry Research Centre, University of Cape Town (South Africa) aided in further formulation techniques to ensure uniform particle size for the cyclodextrin complex study and kinetic solubility from the ADME team clarified the pharmacokinetic results. The fusidic acid study had the advantage of metabolite identification from the Department of Chemistry, University of Cape Town (South Africa) before progressing to pharmacokinetic evaluation and is highly recommended. It meant knowledge was gained on which metabolites to expect and how to could plan accordingly with synthetic chemist to obtain the metabolite when compound pharmacokinetics showed it was vital to the understanding of the *in vivo* properties of fusidic acid.

Future improvements should include an optimised screening cascade of these methods. It is suggested that *in vitro* ADME analysis precede *in vivo* evaluation with emphasis on adequate and consistent solubility as Chapter 2 and 3 showed. *In vitro* metabolite identification with recommendations on

transitions to include in the bioanalytical method is greatly supported by the findings in Chapter 4 and will be a useful strategy for future evaluation. it is recommended that pharmacokinetics and pharmacodynamics of antimalarial drug leads should be evaluated simultaneously in one model with the aid of NLME modelling techniques. This will improve PK/PD interpretation and reduce animal experiments. This cascade is not advisable for antituberculosis leads due to the length of time required for the tuberculosis mouse model. In this case, it is recommended that pharmacokinetic evaluation proceed first and compounds with the most promising pharmacokinetic properties progressed to *in vivo* efficacy with additional pharmacokinetic sampling to confirm exposures. Chapter 5 suggests tissue distribution evaluation can be used as a problem-solving technique and the recommendation here is that it be reserved for compounds that have an inexplicable mismatch in pharmacokinetic and pharmacodynamic results. An intermediate assessment that focuses on quantifying lung and whole blood exposure, before evaluating other collected organs could be useful in increasing efficiency if bioanalytical methods are difficult to implement.

In conclusion, the pharmacokinetic evaluation of these compounds was thoughtfully used and proved fundamental in asking and raising future questions about the current methods. They also proved beneficial in suggesting improved actions to elevate the drug discovery outcomes of the research unit.

7 EXPERIMENTAL RECORDS

7.1 Reagents and solvents

Acetonitrile and methanol (Burdick and Jackson, LC-MS) were purchased from Honeywell International Inc. (Muskegon, MI, USA) and formic acid from Merck (Johannesburg, South Africa). Ammonium hydroxide solution, dimethyl sulfoxide (DMSO), polyethylene glycol (PEG), ethanol (EtOH), polypropylene glycol (PPG), hydroxypropyl methylcellulose (HPMC) were purchased from Sigma-Aldrich (Johannesburg, South Africa). All water used was purified by a Milli-Q reverse osmosis system from EMD Millipore (Microsep, Tygervalley, South Africa).

7.2 Antimalarial benzoxazole amodiaquine analogues

The experimental records for the "Chapter 2: Antimalarial benzoxazole analogues of amodiaquine" project (page 26) are presented in the following sections.

7.2.1 LC/MS/MS Quantification

A brief overview of the final LC/MS/MS method was presented in Chapter 2, section 2.4.2, on page 34. Expanded sample preparation, instrumentation settings and quantification statistics are presented here.

7.2.1.1 Sample preparation

A protein precipitation method was used to extract samples at room temperature. An extraction volume of 20 µl of the thawed whole blood sample was precipitated with 240 µl acetonitrile solution containing 100 ng/ml structurally similar internal standard. The double blank samples were extracted with pure acetonitrile. Samples were vortexed for 1 minute and then centrifuged for 5 minutes at 10

000 rcf. A 200 µl volume of the resulting supernatant was transferred to a 96 well plate and dried under nitrogen and 100 µl of 20% acetonitrile (v/v) in 0.1% formic acid in water (v/v) added to each well. A 10 µl injection volume was used for LC-MS/MS quantification.

7.2.1.2 Instrumentation

Original LC/MS/MS analysis for **DS23B**, **DS48B** and **DS50B** was performed on an Agilent 1100 series binary pump (Agilent, CA, USA) interfaced to an AB Sciex API 3200® mass spectrometer (AB Sciex, Ontario, Canada) with an electrospray ion (ESI) source. Subsequent 16 day repeat experiments of **DS23B** and **DS50B** was performed on an Agilent 1200 series binary pump (Agilent, CA, USA) interfaced to an AB Sciex API 4000Q® mass spectrometer (AB Sciex, Ontario, Canada) with an ESI source in positive mode.

7.2.1.3 Mass spectrometer conditions

Figure 7-1 shows the initial product ion scans (MS/MS) spectrum of the analytes and their most intense fragmentation illustrated.

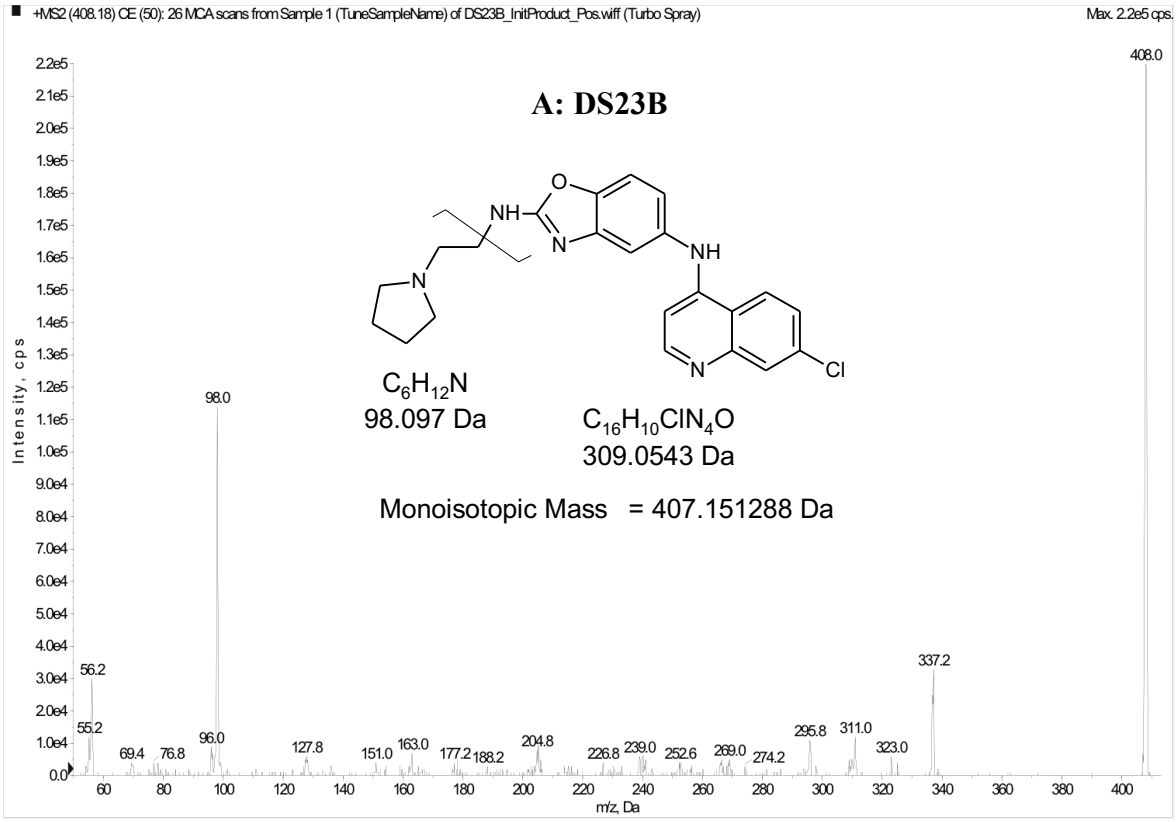

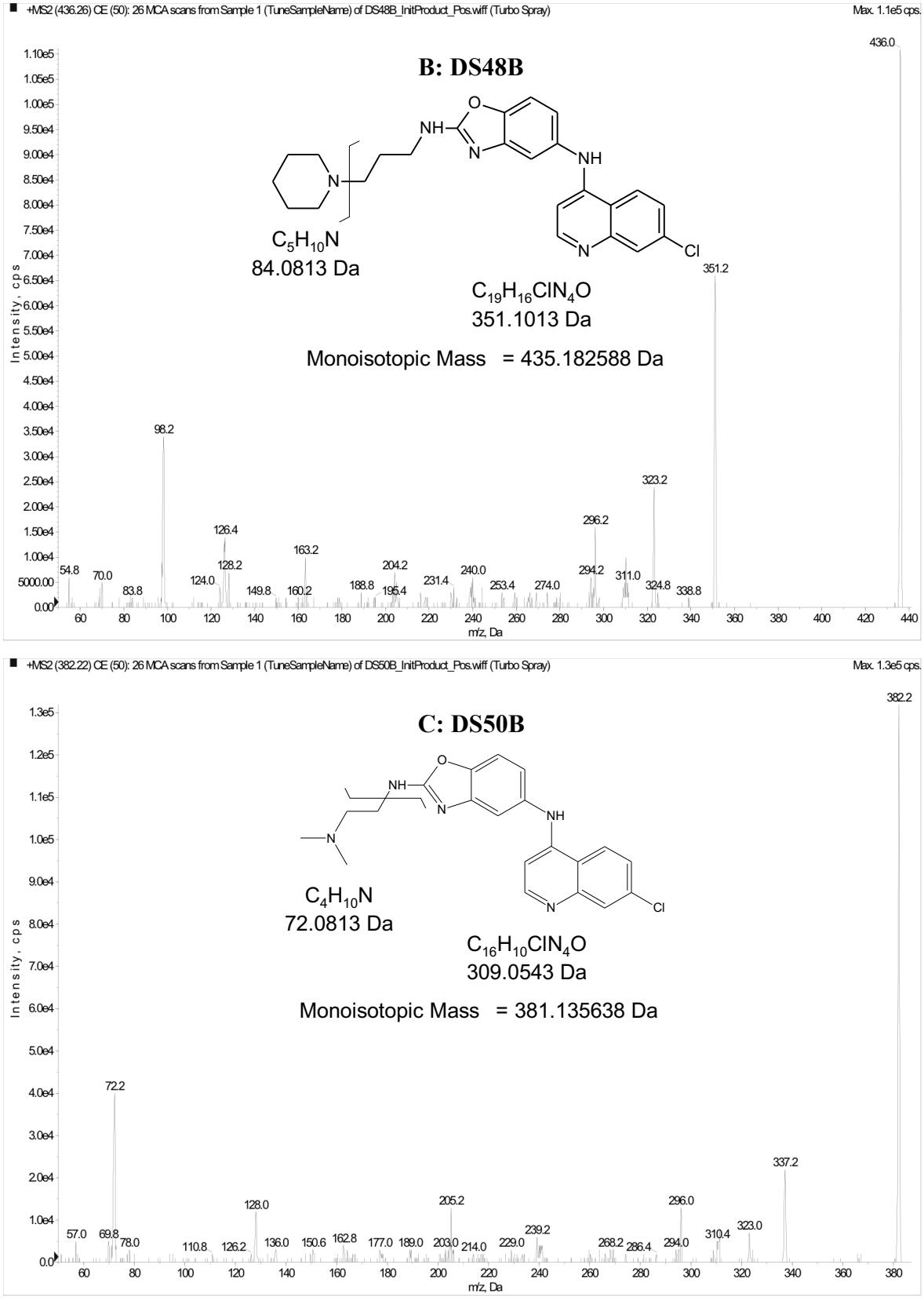

Figure 7-1: Initial product ion scans of benzoxazole amodiaquine analogues

The MS/MS scans of A; **DS23B**, B; **DS48B** and C; **DS50B**. The figure contains the compound structure and fragmentation that relates to the most intense MS/MS peak.

The final settings of the instrument for each of the benzoxazole analogues of amodiaquine are summarised in Table 7-1.

Table 7-1: Mass spectrometer settings of benzoxazole amodiaquine analogues

Source settings

CUR	IS (kV)	TEM (°C)	GS1	GS2
20	5500	500	60	40

Compound settings		Q1	Q3	Dwell	DP	EP	CEP	CE	CXP
		(Da)	(Da)	(msec)	(V)	(V)	(V)	(V)	(V)
DS23B	Quant	408.182	98.0	150	45	9	25	50	1
	Qual	408.182	337.1	150	70	12	10	50	7
DS48B	Quant	436.260	351.2	150	55	10	30	40	6
	Qual	436.260	98.1	150	55	7	30	50	1
DS50B	Quant	382.219	72.0	150	45	11	10	45	1
	Qual	382.219	337.0	150	65	8	10	30	7

Note: CUR; curtain gas flow, IS; IonSpray voltage, TEM; Temperature, GS1; nebuliser gas, GS2; turbo-gas, Q1; first quadrupole, Q3; third quadrupole, Dwell; dwell time (time instrument records ion intensity of fragment), DP; declustering potential, EP entrance potential, CEP; collision cell exit potential, CE; collision energy, Quant; quantifier ion, Qual; qualifier ion.

7.2.1.4 HPLC conditions

Gradient chromatography shown in Table 7-2 and Table 7-3 was performed on a Waters Xterra™ MS C_{18} (2.1 x 30 mm, 3.5 µm) reverse phase column with mobile phases A; 0.03% ammonium hydroxide:water (v/v) and B; 0.03% ammonium hydroxide:acetonitrile (v/v). Carry over was minimized by injecting blank methanol solvent between samples.

Table 7-2: Gradient chromatography steps of DS23B and DS50B analogues

Step	Total Time (min)	Flow Rate (µl/min)	A (%)	B (%)
0	0	600	80	20
1	1.5	600	80	20
2	3	600	0	100
3	4.9	600	0	100
4	5	600	80	20
5	10	600	80	20

Mobile Phases A; 0.03% ammonium hydroxide:water (v/v) and B; 0.03% ammonium hydroxide:acetonitrile (v/v).

Table 7-3: Gradient chromatography steps of DS48B

Step	Total Time (min)	Flow Rate (µl/min)	A (%)	B (%)
0	0	400	95	5
1	0.3	400	95	5
2	0.7	400	0	100
3	4.0	400	0	100
4	4.1	400	95	5
5	7	400	95	5

Mobile Phases A; 0.03% ammonium hydroxide:water (v/v) and B; 0.03% ammonium hydroxide:acetonitrile (v/v).

7.2.1.5 Quantification

Table 7-4 contains quantification statistics from the final batches analysed.

Table 7-4: Quantification statistics of benzoxazole amodiaquine analogues

Sample	Expected conc (ng/ml)	Number	Mean conc (ng/ml)	S.D.	Precision (%CV)	Accuracy (%Norm)
DS23B						
S6	9.77	2 of 2	10.1	0.189	1.87	104
S5	39.1	2 of 2	34.3	1.73	5.06	87.6
S4	156	2 of 2	166	2.64	1.59	107
S3	625	2 of 2	645	21.5	3.33	103
S2	2500	2 of 2	2460	206	8.38	98.4
S1	5000	2 of 2	5010	65.8	1.31	100
QC L	20	2 of 2	20	6.63	33.2	100
QC M	2000	1 of 1	2040	N/A	N/A	102
QC H	4000	2 of 2	3910	1320	33.6	97.8
DS48B						
S6	2	2 of 2	2.34	0.58	24.8	117
S5	10	2 of 2	8.98	0.924	10.3	89.8
S4	50	2 of 2	44.6	0.316	0.71	89.2
S3	250	2 of 2	261	4.88	1.87	104
S2	2500	2 of 2	2490	201	8.06	99.6
S1	5000	2 of 2	5000	361	7.21	100
QC L	10	2 of 2	11	3.07	28.0	110
QC M	2000	2 of 2	2020	29.0	1.44	101
QC H	4000	2 of 2	3800	304	7.99	95.1
DS50B						
S6	9.766	1 of 1	11.2	N/A	N/A	115
S5	39.063	2 of 2	39.9	3.53	8.84	102
S4	156.25	2 of 2	158	5.39	3.41	101
S3	625	2 of 2	532	0.409	0.0769	85.1
S2	2500	2 of 2	2630	231	8.79	105
S1	5000	1 of 1	4910	N/A	N/A	98.2
QC L	19.5	1 of 1	19.8	N/A	N/A	101
QC M	2000	2 of 2	2250	67.2	2.99	113
QC H	4000	2 of 2	3960	475	12.0	99.0

Note: Standards S1-S6) were used for the calibration curves. Quality controls (QC) low (L), medium (M) and high (H). S.D.: Standard deviation

In Figure 7-2 is shown the respective calibration curves of the final analysed batches for the benzoxazole analogues of amodiaquine with their respective regression values. Quantification used quadratic regression of the analyte area/internal standard area vs concentration with 1/x weighting. All calibration curves showed regression above 0.990.

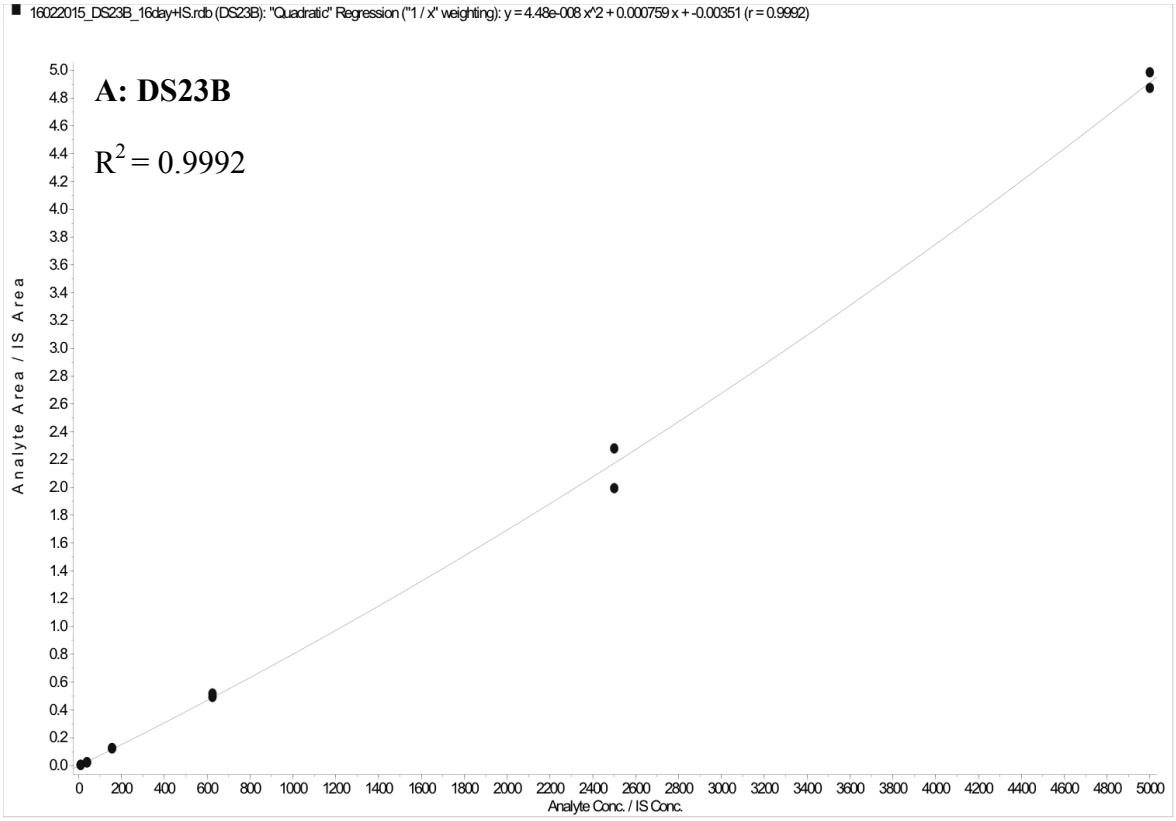

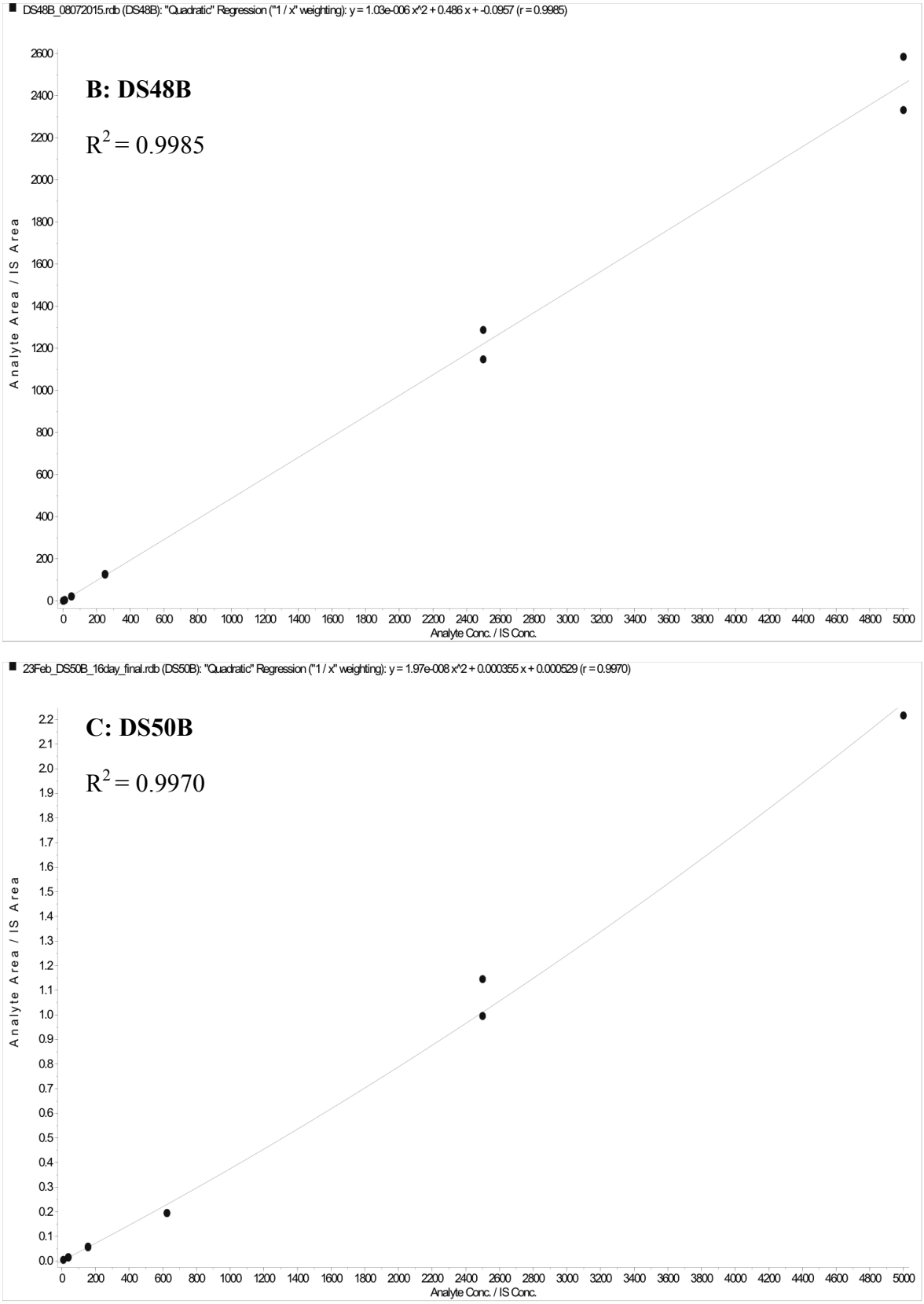

Figure 7-2: Calibration curves of benzoxazole amodiaquine analogues

The calibration curve of A: **DS23B**, B: **DS48B** and C: **DS50B** constructed from calibration standards made in whole blood.

The low quality control samples of each analyte with respective internal standard is shown in Figure 7-3.

In Figure 7-4 is shown the blank samples injected after the highest concentration standard from the final batches analysed with their respective carry-over displayed. All samples showed carry-over less than the accepted 20% allowed.

A: DS23B 19.3 ng/ml

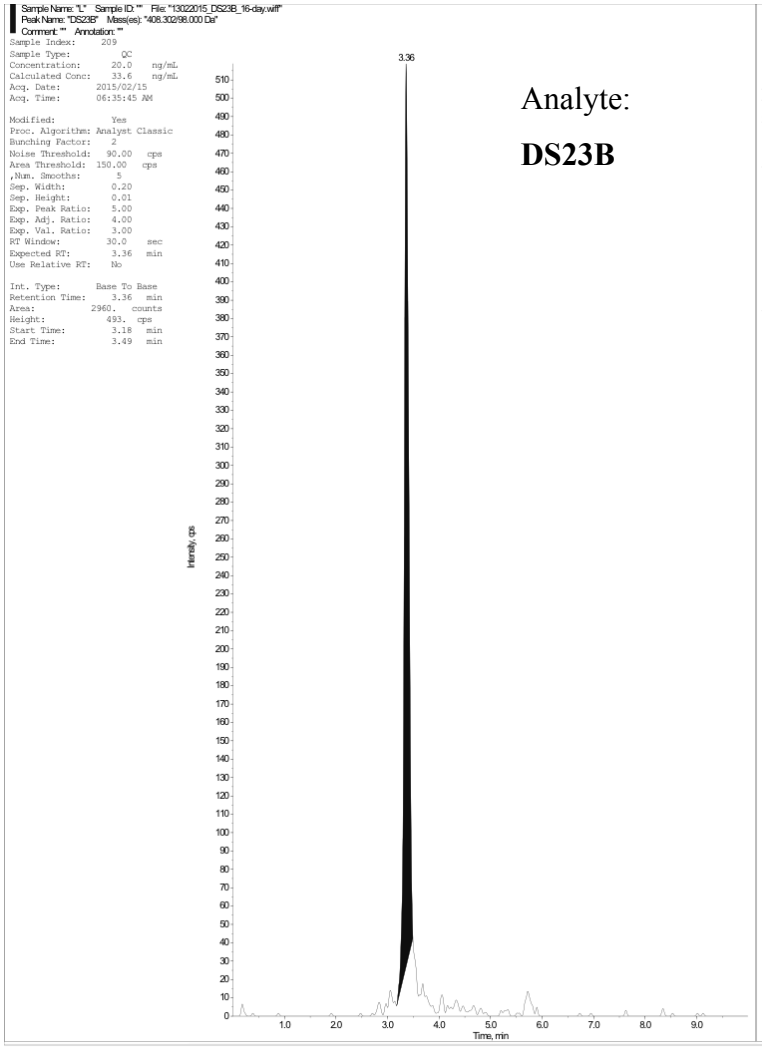

Analyte:

DS23B

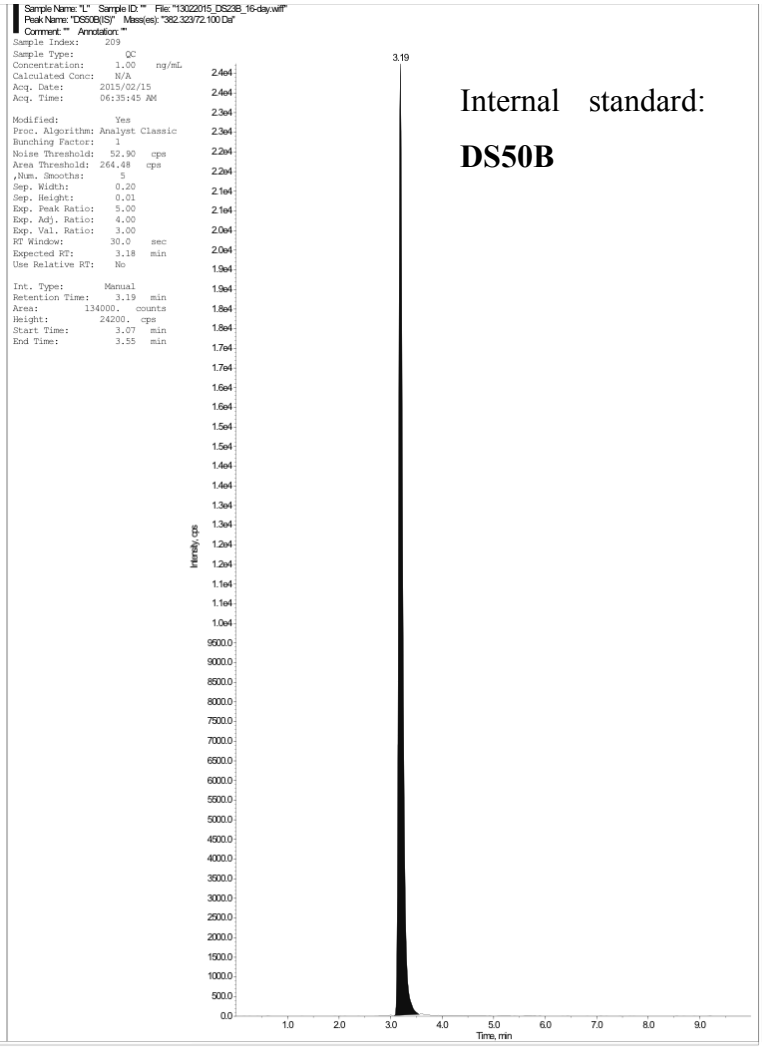

Internal standard:

DS50B

B: DS48B 10 ng/ml

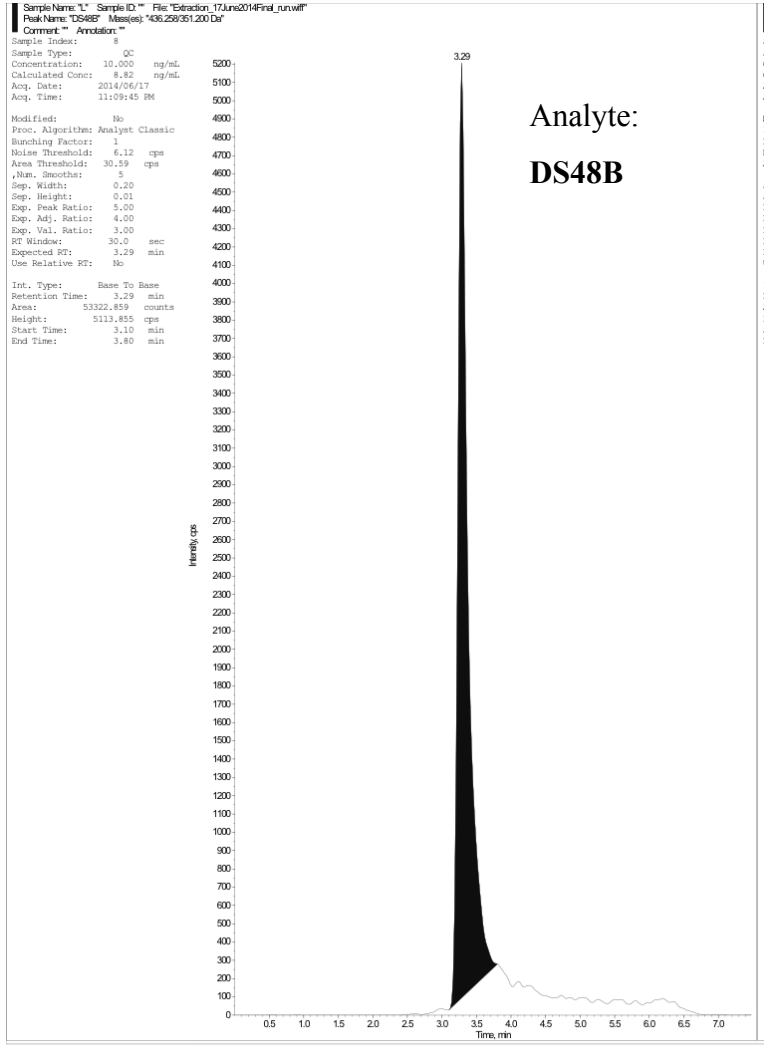

Analyte:

DS48B

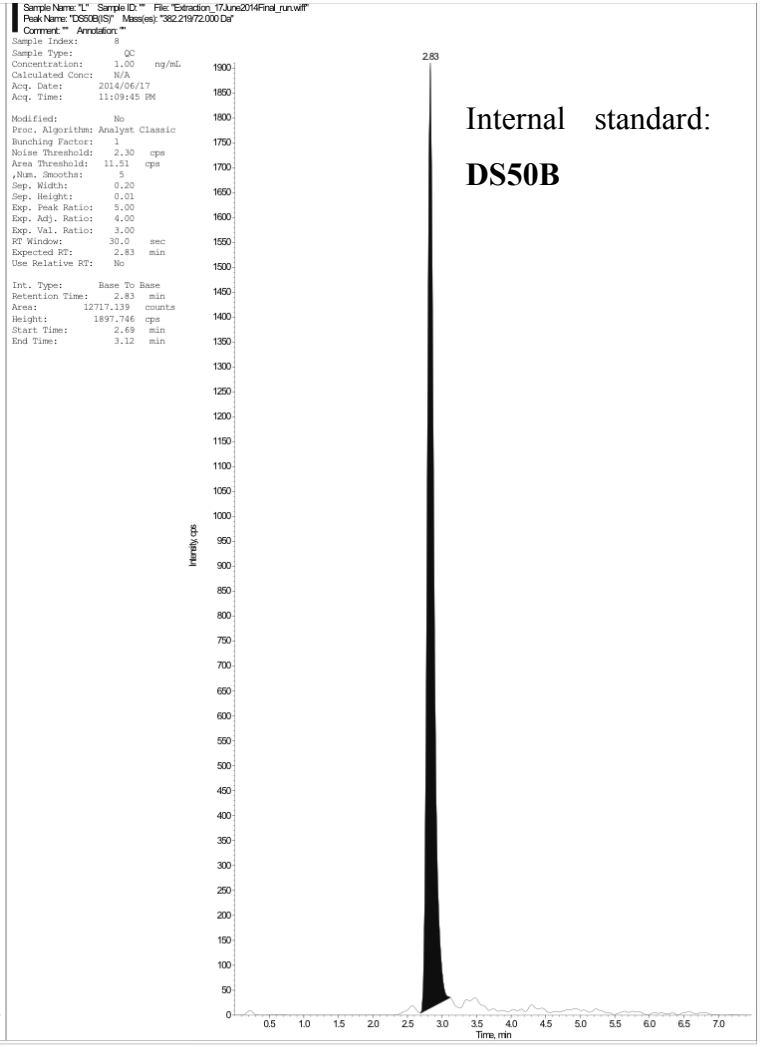

Internal standard:

DS50B

C: DS50B 19.3 ng/ml

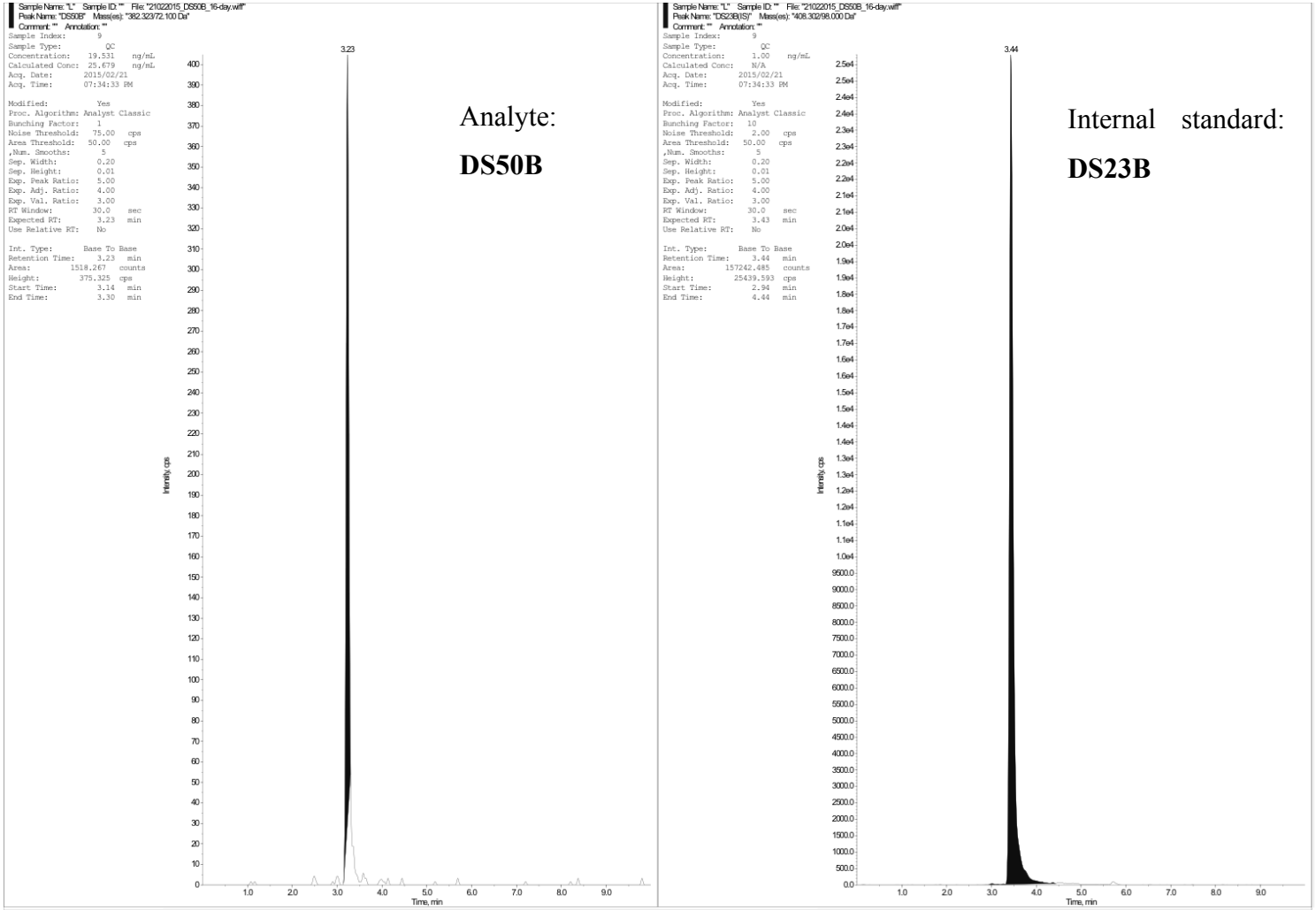

Figure 7-3: Low quality controls of benzoxazole analogues. Low quality controls of A: **DS23B**, B: **DS48B** and C: **DS50B** with respective internal standard.

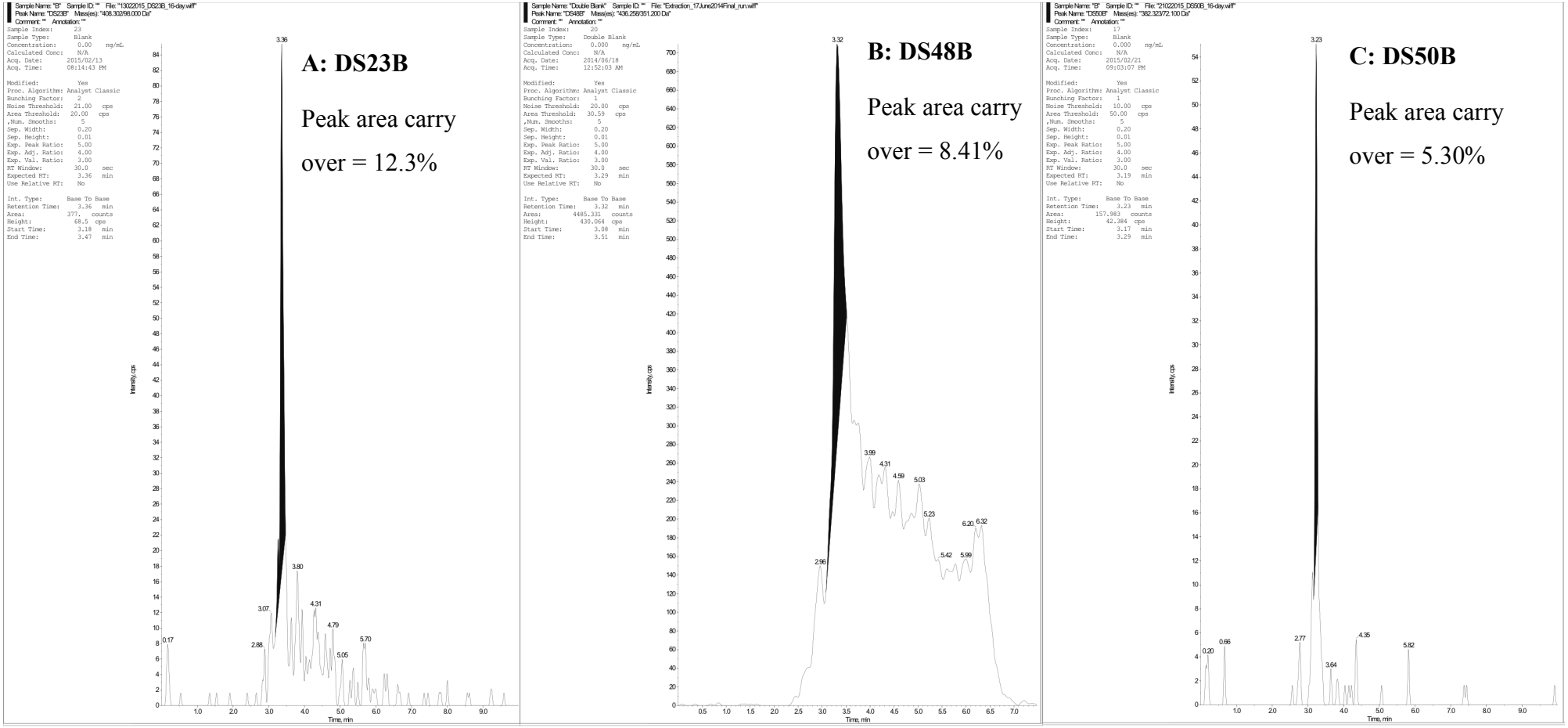

Figure 7-4: Blank samples of benzoxazole amodiaquine analogues

Integrated blank samples of A: **DS23B**. B: **DS48B** and C: **DS50B**. Respective carry over is shown and all fell below the accepted 20%.

7.2.2 Animal records

The animal experiments performed for the benzoxazole analogous of amodiaquine were described in Chapter 2, section 2.4.3, page 36.

In Table 7-5 to Table 7-7 is shown the experimental record sheets of the animal experiments. They contain exact sampling times, summary of dosage formulations and animal weight and sex.

Table 7-5: DS48B 24 hr animal experiment

Oral/IV dose - compound **DS48B** (24 hrs)

Date:	24 April 2014		IV solution			Oral suspension		
Ethics no:	013/028							
Dose: Oral	20	mg/kg	Weighed:	2.48	mg	Weighed:	2.52	mg
Dose: IV	5	mg/kg	in	100	µL DMSO	in	1000	µL 0.5% HPMC
Collect 20 µL blood samples in heparin tubes, vortex, on ice				100	µL EtOH			
Freeze samples at -80°C				300	µL PEG 400			
				500	µL PPG			

Collection times

Mouse	M1♂ IV	M2♂ IV	M3♂ IV	M4♂ ORAL	M5♂ ORAL	M6♂ ORAL
Mass (g)	25.4	29.3	26.1	27.9	27.1	27.9
Volume (µL)	60	60	60	250	250	250
Dose time	08:31:00	08:33:00	08:35:00	08:44:00	08:45:00	08:46:00
5 min	08:38:00	08:40:00	08:38:00	-	-	-
0.5	09:02:00	09:03:00	09:03:00	09:13:00	09:14:00	09:15:00
1	09:32:00	09:33:00	09:34:00	09:41:00	09:43:00	09:46:00
3	11:32:00	11:34:00	11:35:00	11:37:00	11:38:00	11:39:00
5	13:31:00	13:34:00	13:36:00	13:39:00	13:41:00	13:42:00
7	15:31:00	15:34:00	15:37:00	15:39:00	15:41:00	15:42:00
24	08:16:00	08:17:00	08:18:00	08:19:00	08:20:00	08:21:00

Table 7-6: DS23B 15 day animal experiment

Oral/IV dose - compound **DS23B** (15 days)

Date:			18 November 2014				
Ethics no:			013/028				
Dose: Oral			10	mg/kg			
Dose: IV			2.5	mg/kg			
Collect 20 µL blood samples in heparin tubes, vortex, on ice							
Freeze samples at -80°C							
IV solution				Oral suspension			
Weighed:	1.27	mg		Weighed:	0.82	mg	
in	100	µL DMSO		in	1000	µL 0.5% HPMC	
	100	µL EtOH					
	300	µL PEG 400					
	500	µL PPG					

Collection times

	M1♂ IV	M2♂ IV	M3♂ IV	M4♀ ORAL	M5♀ ORAL	M6♀ ORAL
Mass (g)	30.1	30.0	29.5	20.2	20.8	20.1
Volume (µL)	60	60	60	150	150	150
Dose	08:01:00	08:02:00	08:03:00	07:56:00	07:56:00	07:56:00
5 min	08:06:00	08:07:00	08:08:00	-	-	-
hr: 1	09:01:00	09:02:00	09:03:00	09:04:00	09:05:00	09:06:00
3	11:01:00	11:02:00	11:04:00	11:05:00	11:06:00	11:07:00
5	13:00:00	13:02:00	13:04:00	13:06:00	13:07:00	13:08:00
8	16:01:00	16:01:00	16:04:00	16:06:00	16:07:00	16:09:00
24	09:00:00	09:02:00	09:04:00	09:06:00	09:07:00	09:08:00
27	12:02:00	12:03:00	12:05:00	-	-	-
32	16:00:00	16:03:00	16:03:00	-	-	-
48	09:00:00	09:01:00	09:02:00	09:06:00	09:10:00	09:11:00
72	-	-	-	09:15:00	09:16:00	09:17:00
96	-	-	-	08:13:00	08:14:00	08:15:00
120	-	-	-	08:30:00	08:31:00	08:32:00
144	-	-	-	09:27:00	09:28:00	09:29:00
168	-	-	-	09:08:00	09:09:00	09:10:00
192	-	-	-	07:32:00	07:33:00	07:34:00
216	-	-	-	07:01:00	07:02:00	07:03:00
240	-	-	-	10:01:00	10:02:00	10:03:00
264	-	-	-	10:05:00	10:06:00	10:07:00
288	-	-	-	07:03:00	07:04:00	07:05:00
312	-	-	-	06:55:00	06:56:00	06:57:00
336	-	-	-	07:47:00	07:48:00	07:49:00
360	-	-	-	07:09:00	07:10:00	07:11:00

Table 7-7: DS50B 15 day animal experiment

Oral/IV dose - compound **DS50B** (15 days)

Date:	19 November 2014					
Ethics no:	013/028					
Dose: Oral	10 mg/kg					
Dose: IV	2.5 mg/kg					
Collect 20 µL blood samples in heparin tubes, vortex, on ice						
Freeze samples at -80°C						

IV solution			Oral suspension		
Weighed:	1.27	mg	Weighed:	1.51	mg
in	100	µL DMSO	in	1000	µL 0.5% HPMC
	100	µL EtOH			
	300	µL PEG 400			
	500	PPG			

Collection times

	M1♂ IV	M2♂ IV	M3♂ IV	M4♀ ORAL	M5♀ ORAL	M6♀ ORAL
Mass (g)	28.8	28.1	26.4	18.7	21.1	21.1
Volume (µL)	60	60	60	150	150	150
Dose	08:09:00	08:10:00	08:11:00	07:57:00	07:58:00	07:58:00
5 min	08:14:00	08:15:00	08:16:00	-	-	-
hr: 1	09:08:00	09:09:00	09:10:00	09:11:00	09:12:00	09:13:00
3	11:09:00	11:11:00	11:12:00	11:13:00	11:14:00	11:15:00
5	13:11:00	13:13:00	13:14:00	13:14:00	13:16:00	13:17:00
8	16:13:00	16:14:00	16:15:00	16:17:00	16:18:00	16:19:00
24	09:11:00	09:13:00	09:15:00	09:17:00	09:18:00	09:19:00
27	12:07:00	12:08:00	12:09:00	-	-	-
32	16:05:00	16:05:00	16:06:00	-	-	-
48	09:04:00	09:05:00	09:06:00	09:12:00	09:13:00	09:14:00
72	-	-	-	09:20:00	09:21:00	09:22:00
96	-	-	-	08:20:00	08:21:00	08:22:00
120	-	-	-	08:35:00	08:36:00	08:37:00
144	-	-	-	09:34:00	09:35:00	09:36:00
168	-	-	-	09:12:00	09:13:00	09:14:00
192	-	-	-	07:40:00	07:41:00	07:42:00
216	-	-	-	07:05:00	07:06:00	07:07:00
240	-	-	-	10:05:00	10:06:00	10:07:00
264	-	-	-	10:10:00	10:11:00	10:12:00
288	-	-	-	07:10:00	07:11:00	07:12:00
312	-	-	-	07:00:00	07:01:00	07:02:00
336	-	-	-	07:50:00	07:51:00	07:52:00
360	-	-	-	07:13:00	07:14:00	07:15:00

7.2.3 Individual concentration profiles & data analysis

7.2.3.1 Non-compartmental analysis

The summarised pharmacokinetic results of the formulation study were presented in Table 2-6 to Table 2-9, starting in section 2.5.3.1, page 73. The expanded individual results with individual raw concentration vs time data is presented below for in Table 7-8 and respective non-compartmental analysis results for each individual subject in Table 7-9 for **DS23B**, and similarly Table 7-10 and Table 7-11 for **DS48B**, and Table 7-12 and Table 7-13 for **DS50B**.

Table 7-8: Individual concentrations (µM) of DS23B

IV:	M1		M2		M3	Mean	
Time	Conc (µM)	Time	Conc (µM)	Time	Conc (µM)	Time (hr)	Conc (µM)
0.0833	8.43	0.0833	11.4	0.0833	9.83	0.0833	9.88
1	3.9	1	4.09	1	3.63	1	3.87
3	2.13	3	2.36	3.02	3.31	3.01	2.6
4.98	0.454	5	0.588	5.02	0.569	5	0.537
8	0.861	7.98	0.927	8.02	1.18	8	0.989
25	0.61	25	0.726	25	1.12	25	0.82
28	0.895	28	0.534	28	1.11	28	0.847
32	0.517	32	0.522	32	0.64	32	0.56
49	0.809	49	0.686	49	0.91	49	0.802
P.O.:	M4		M5		M6	Mean	
Time	Conc (µM)	Time	Conc (µM)	Time	Conc (µM)	Time (hr)	Conc (µM)
1.13	1.52	1.15	4.12	1.17	1.67	1.15	2.44
3.15	4.95	3.17	8.14	3.18	4.07	3.17	5.72
5.17	4.56	5.18	7.7	5.2	3.29	5.18	5.18
8.17	1.83	8.18	3.58	8.22	3.73	8.19	3.05
25.2	1.9	25.2	2.77	25.2	1.82	25.2	2.16
49.2	0.699	49.2	2.07	49.3	1.49	49.2	1.42
73.3	1.39	73.3	0.682	73.4	0.895	73.3	0.988
96.3	0.785	96.3	1.5	96.3	0.488	96.3	0.923
121	0.287	121	0.74	121	0.319	121	0.449
146	0.169	146	0.466	146	0.175	146	0.27
169	0.155	169	0.192	169	0.153	169	0.167
192	0.13	192	0.174	192	0.0907	192	0.132
215	0.0581	215	0.166	215	0.119	215	0.114
242	0.0657	242	0.0976	242	0.0878	242	0.0837
266	0.0346	266	0.0951	266	0.0405	266	0.0567
287	0.0238	287	0.0412	287	0.0419	287	0.0356
311	0.0289	311	0.0387	311	0.0275	311	0.0317
336	0.0179	336	0.0255	336	0.0244	336	0.0226
359	0.0203	359	0.0225	359	0.0235	359	0.0221

Note: M1 represents individual mouse 1, M2 individual mouse 2 etc. M1 – M3 received intravenous (IV) doses and M4 – M6 received oral (P.O.; per os) doses.

Table 7-9: Non-compartmental analysis of DS23B

IV	M1	M2	M3	Mean	S.E.
Apparent half-life (h)	83.7	83.2	81.4	82.8	0.686
Blood Clearance (ml/min/kg)	6.96	0.00233	6.57	4.51	2.26
Vc (L/kg)	1.12	5.82×10^{-5}	0.799	0.639	0.322
Vss (L/kg)	16.6	6.67	20.3	14.5	4.08
$AUC_{0\text{-}inf}$ (μM.min)	24400	7820	10000	14100	5190
P.O.	M4	M5	M6	Mean	S.E.
Apparent half-life (h)	48.1	47.2	51.3	48.9	1.27
$AUC_{0\text{-}inf}$ (μM.min)	10400	17200	11400	13000	2120

Note: IV; intravenous, P.O.; per os/oral, Vc; central volume, Vss; volume at steady state, $AUC_{0\text{-}\infty}$; area under the curve from time zero to infinity. Individual values corresponding to the same labelled raw concentration vs time data is represented with the calculated mean and standard error of the mean (S.E.).

Table 7-10: Individual concentrations (μM) of DS48B

IV:	M1		M2		M3	Mean	
Time	Conc (μM)	Time	Conc (μM)	Time	Conc (μM)	Time (hr)	Conc (μM)
0.117	1.68	0.117	1.72	0.05	2.29	0.0944	1.9
0.517	0.853	0.5	0.564	0.467	0.874	0.494	0.764
1.02	0.273	1	0.463	0.983	0.672	1	0.47
3.02	0.404	3.02	0.346	3	0.459	3.01	0.403
5	0.317	5.02	0.284	5.02	0.314	5.01	0.305
7	0.236	7.02	-	7.03	0.136	7.02	0.186
23.8	0.0849	23.7	0.0771	23.7	0.0798	23.7	0.0806
P.O.:	M4		M5		M6	Mean	
Time	Conc (μM)	Time	Conc (μM)	Time	Conc (μM)	Time (hr)	Conc (μM)
0.483	0.415	0.483	0.296	0.483	0.326	0.483	0.346
0.95	1.16	0.967	0.273	1	1.08	0.972	0.837
2.88	1.1	2.88	0.603	2.88	1.19	2.88	0.964
4.92	0.801	4.93	0.601	4.93	0.847	4.93	0.749
6.92	0.764	6.93	0.541	6.93	0.75	6.93	0.685
23.6	0.239	23.6	0.184	23.6	0.259	23.6	0.227

Note: M1 represents individual mouse 1, M2 individual mouse 2 etc. M1 – M3 received intravenous (IV) doses and M4 – M6 received oral (P.O.; per os) doses.

Table 7-11: Non-compartmental analysis of DS48B

IV	M1	M2	M3	Mean	S.E.
Apparent half-life (h)	9.72	9.21	9.59	9.51	0.153
Blood Clearance (ml/min/kg)	32.6	28.2	32.5	31.1	1.45
Vc (L/kg)	6.88	3.27	6.89	5.68	1.21
Vss (L/kg)	24.3	23.9	24.2	24.2	0.122
$AUC_{0\text{-}inf}$ (μM.min)	420	416	470	435	17.2
P.O.	M4	M5	M6	Mean	S.E.
Apparent half-life (h)	9.86	11.5	10.1	10.5	0.498
$AUC_{0\text{-}inf}$ (μM.min)	1080	741	1120	983	122

Note: IV; intravenous, P.O.; per os/oral, Vc; central volume, Vss; volume at steady state, $AUC_{0\text{-}\infty}$; area under the curve from time zero to infinity. Individual values corresponding to the same labelled raw concentration vs time data is represented with the calculated mean and standard error of the mean (S.E.).

Table 7-12: Individual concentrations (μM) of DS50B

IV:	M1		M2		M3	Mean	
Time	Conc (μM)	Time	Conc (μM)	Time	Conc (μM)	Time (hr)	Conc (μM)
0.0833	7.07	0.0833	10.2	0.0833	13.1	0.0833	10.1
0.983	2.62	0.983	4.98	0.983	3.58	0.983	3.73
3	2.17	3.02	3.64	3.02	2.53	3.01	2.78
5.03	0.998	5.05	1.14	5.05	0.892	5.04	1.01
8.07	0.903	8.07	1.03	8.07	1.05	8.07	0.996
25	1.48	25	0.656	25.1	0.508	25	0.88
28	0.449	28	0.416	28	0.497	28	0.454
31.9	0.469	31.9	0.33	31.9	0.325	31.9	0.374
48.9	0.484	48.9	0.312	48.9	0.467	48.9	0.421
P.O.:	M4		M5		M6	Mean	
Time	Conc (μM)	Time	Conc (μM)	Time	Conc (μM)	Time (hr)	Conc (μM)
1.23	2.3	1.23	5.34	1.25	4.27	1.24	3.97
3.27	3.4	3.27	4.95	3.28	6.72	3.27	5.02
5.28	3.88	5.3	4.92	5.32	5.22	5.3	4.67
8.33	2.61	8.33	3.12	8.35	3.8	8.34	3.18
25.3	0.67	25.3	1.46	25.4	1.79	25.3	1.3
49.2	0.593	49.3	0.983	49.3	0.913	49.3	0.83
73.4	0.406	73.4	0.615	73.4	1.16	73.4	0.727
96.4	0.213	96.4	0.523	96.4	0.336	96.4	0.357
121	0.19	121	0.242	121	0.23	121	0.221
146	0.0798	146	0.201	146	0.228	146	0.17
169	0.0921	169	0.145	169	0.0936	169	0.11
192	0.0785	192	0.0458	192	0.114	192	0.0793
215	0.0714	215	0.0853	215	0.052	215	0.0695
242		242	0.0331	242	0.0172	242	0.0252
266		266	0.033	266		266	0.033

Note: M1 represents individual mouse 1, M2 individual mouse 2 etc. M1 – M3 received intravenous (IV) doses and M4 – M6 received oral (P.O.; per os) doses.

Table 7-13: Non-compartmental analysis of DS50B

IV	M1	M2	M3	Mean	S.E.
Apparent half-life (h)	36	22.2	32.1	30.1	4.12
Blood Clearance (ml/min/kg)	1.43	1.57	0.734	1.24	0.259
Vc (L/kg)	0.0394	0.0160	0.00296	0.0195	0.0107
Vss (L/kg)	0.698	0.0914	0.0138	0.268	0.216
$AUC_{0\text{-}inf}$ (µM.min)	4860	4530	10300	6570	1880
P.O.	M4	M5	M6	Mean	S.E.
Apparent half-life (h)	43.7	39.8	34.1	39.2	2.78
$AUC_{0\text{-}inf}$ (µM.min)	6300	9790	11000	9050	1420

Note: IV; intravenous, P.O.; per os/oral, Vc; central volume, Vss; volume at steady state, $AUC_{0\text{-}\infty}$; area under the curve from time zero to infinity. Individual values corresponding to the same labelled raw concentration vs time data is represented with the calculated mean and standard error of the mean (S.E.).

7.2.3.2 Non-linear mixed effects modelling

As described in Chapter 2, section 2.4.5, page 39 the benzoxazole analogues of amodiaquine and amodiaquine best fit a two-compartment model. The median values for the cohort are presented with their respective standard error and relative standard error determined by linearization of their Fischer information matrix. The fixed effects, covariate model, omega and sigma model values are shown in Table 7-14.

Table 7-14: Parameter estimations of benzoxazole amodiaquine analogues

	DS23B			DS48B			DS50B			Amodiaquine		
	Parameter	s.e. (lin)	r.s.e.(%)	Parameter	s.e. (lin)	r.s.e.(%)	Parameter	s.e. (lin)	r.s.e.(%)	Parameter	s.e. (lin)	r.s.e.(%)
Fixed effects:												
Foral	0.544	0.083	15	0.613	0.076	12	0.46	0.074	16	0.486	0.062	13
ka (hr^{-1})	0.244	0.064	26	0.434	0.11	25	0.24	0.06	25	0.735	0.14	18
V (L)	0.0179	0.003	17	0.178	0.04	22	0.0186	0.0028	15	0.11	0.015	13
Cl (L/h)	0.00177	0.00013	7	0.0571	0.005	9	0.00251	0.00016	6	0.0838	0.0085	10
Q (L/h)	0.00958	0.0015	16	0.317	0.079	25	0.0072	0.0017	23	0.142	0.024	17
Vp (L)	0.0969	0.0071	7	0.533	0.073	14	0.102	0.007	7	0.239	0.032	13
Covariate model:												
Beta Cl (tWEIGHT)	0.75	-	-	0.75	-	-	0.75	-	-	-	-	-
Beta V (tWEIGHT)	1	-	-	1	-	-	1	-	-	-	-	-
Beta Vp (tWEIGHT)	1	-	-	1	-	-	1	-	-			
Parameter variability:												
Omega Foral	0.197	0.093	47	0	-	-	0.253	-	-	0	-	-
Omega ka	0	-	-	0	-	-	0.0603	0.65	1.09E+03	0	-	-
Omega V	0	-	-	0	-	-	0	-	-	0	-	-
Omega Cl	0	-	-	0	-	-	0	-	-	0.336	0.044	13
Omega Q	0	-	-	0	-	-	0.461	-	-	0	-	-
Omega Vp	0	-	-	0	-	-	0	-	-	0	-	-
Sigma model:												
Proportional	0.335	0.026	8	0.322	0.036	11	0.308	0.0094	3	0.382	0.026	7
Constant	0	-	-	0	-	-	0	-	-	0	-	-

Note: Foral; bioavailability, ka; rate of absorption, V; central volume, Cl; clearance, Q; inter-compartmental clearance, Vp; peripheral volume. Standard error (s.e.) and relative standard error (r.s.e) expressed as a percentage of the population estimate were estimated by linearization of the Fisher information matrix. The covariate tWEIGHT is defined as the transformed log individual mass of each mouse, centred around the median of the cohort mass. Parameter values equal to zero are parameters that were excluded from the model based on their statistical insignificance as determined by -2LL.

In Figure 7-5, shown below, is the individual plots and parameter information of each subject.

A: DS23B

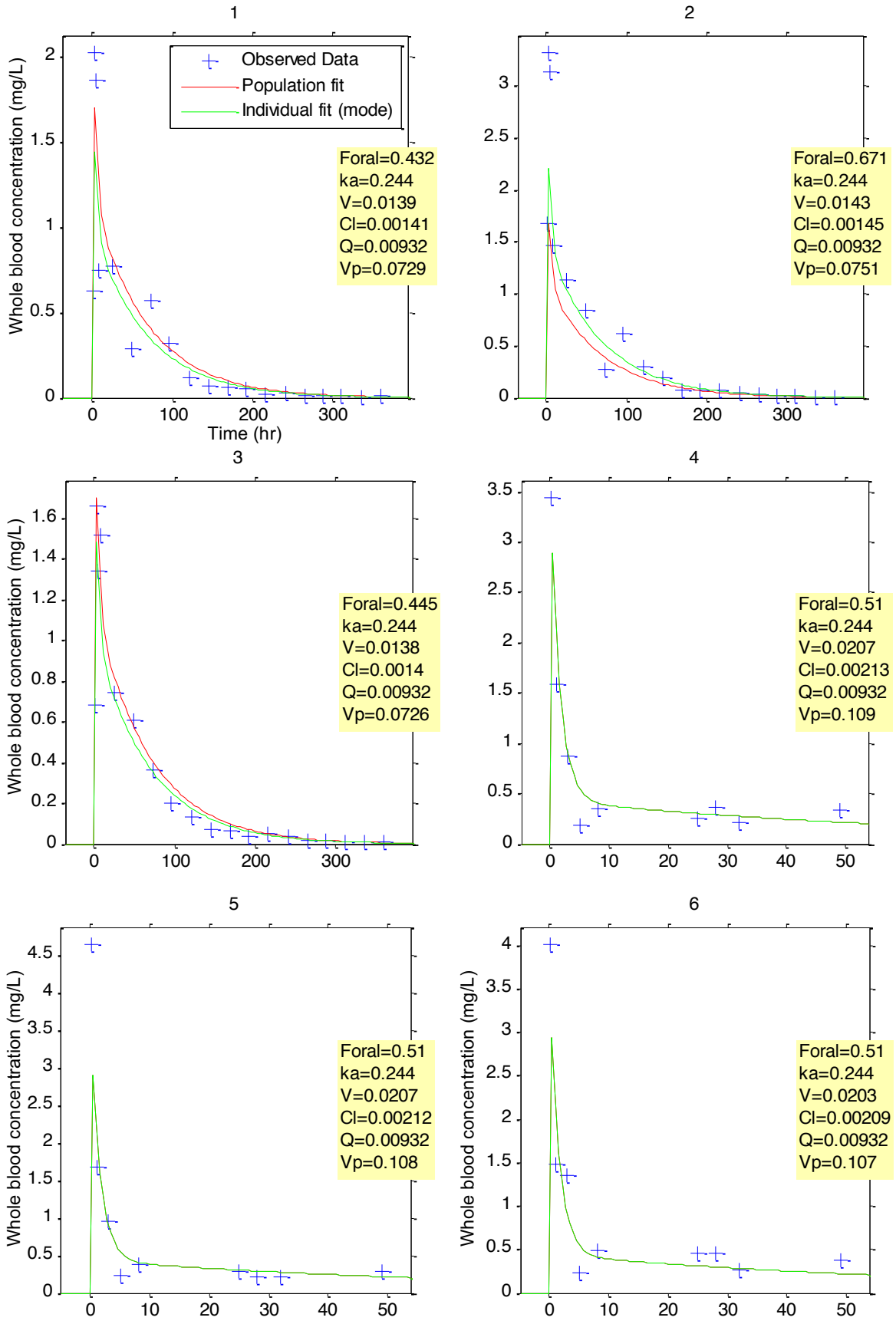

B: DS48B

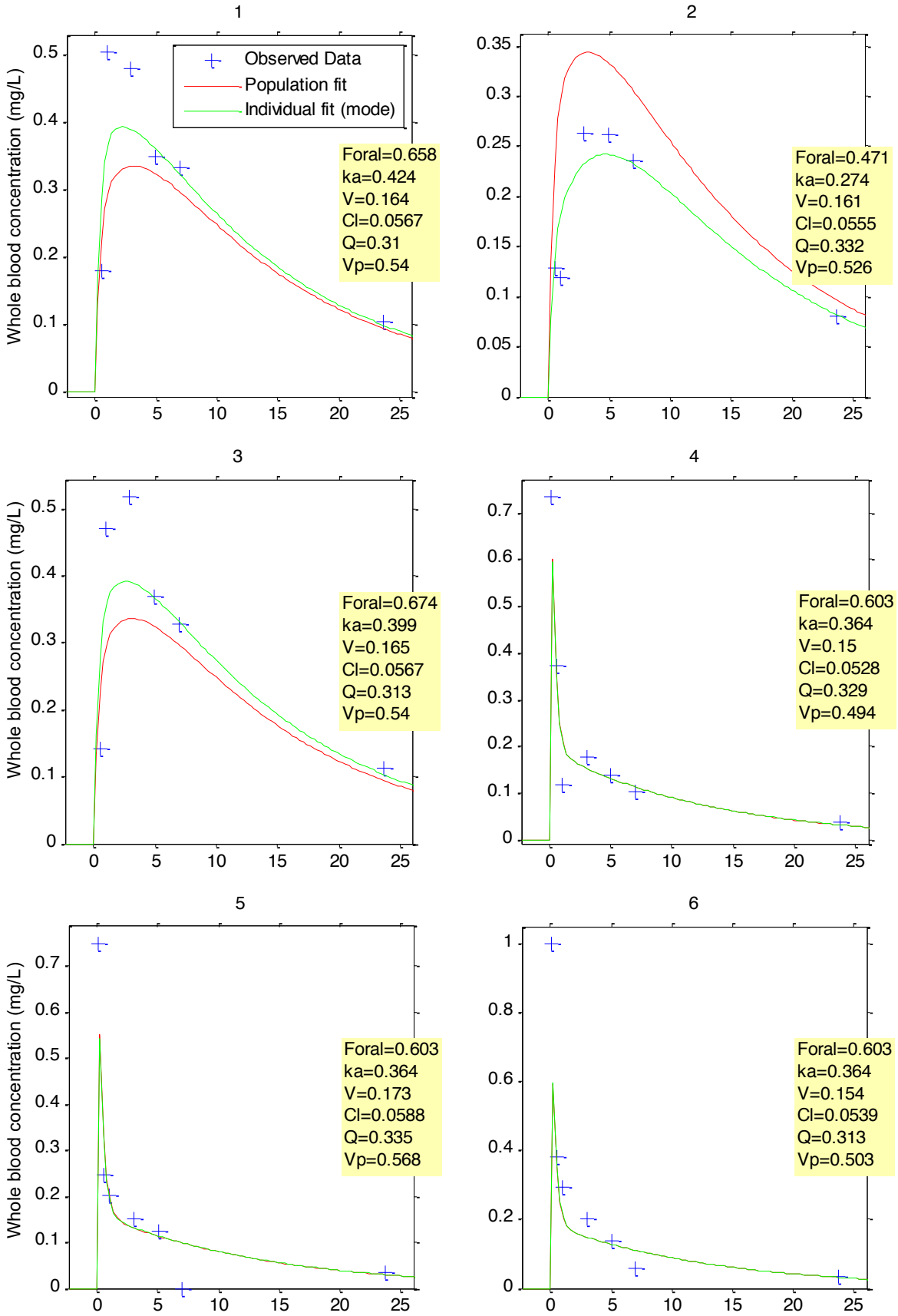
1
Observed Data
Population fit
Individual fit (mode)
Foral=0.658
ka=0.424
V=0.164
Cl=0.0567
Q=0.31
Vp=0.54
2
Foral=0.471
ka=0.274
V=0.161
Cl=0.0555
Q=0.332
Vp=0.526
3
Foral=0.674
ka=0.399
V=0.165
Cl=0.0567
Q=0.313
Vp=0.54
4
Foral=0.603
ka=0.364
V=0.15
Cl=0.0528
Q=0.329
Vp=0.494
5
Foral=0.603
ka=0.364
V=0.173
Cl=0.0588
Q=0.335
Vp=0.568
6
Foral=0.603
ka=0.364
V=0.154
Cl=0.0539
Q=0.313
Vp=0.503
Whole blood concentration (mg/L)

C: DS50B

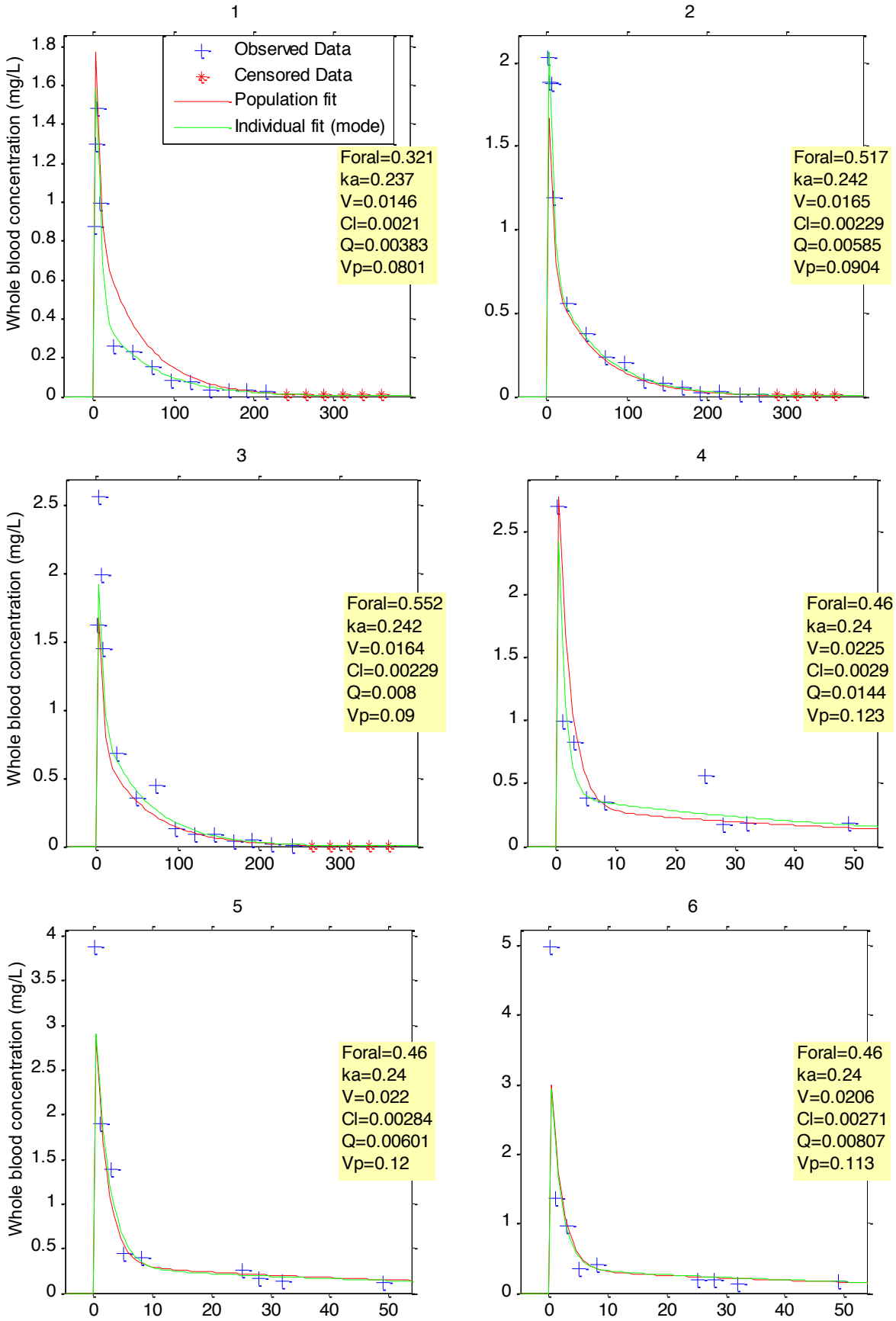
1
Observed Data
Censored Data
Population fit
Individual fit (mode)
Foral=0.321
ka=0.237
V=0.0146
Cl=0.0021
Q=0.00383
Vp=0.0801
2
Foral=0.517
ka=0.242
V=0.0165
Cl=0.00229
Q=0.00585
Vp=0.0904
3
Foral=0.552
ka=0.242
V=0.0164
Cl=0.00229
Q=0.008
Vp=0.09
4
Foral=0.46
ka=0.24
V=0.0225
Cl=0.0029
Q=0.0144
Vp=0.123
5
Foral=0.46
ka=0.24
V=0.022
Cl=0.00284
Q=0.00601
Vp=0.12
6
Foral=0.46
ka=0.24
V=0.0206
Cl=0.00271
Q=0.00807
Vp=0.113
Whole blood concentration (mg/L)

D: Amodiaquine

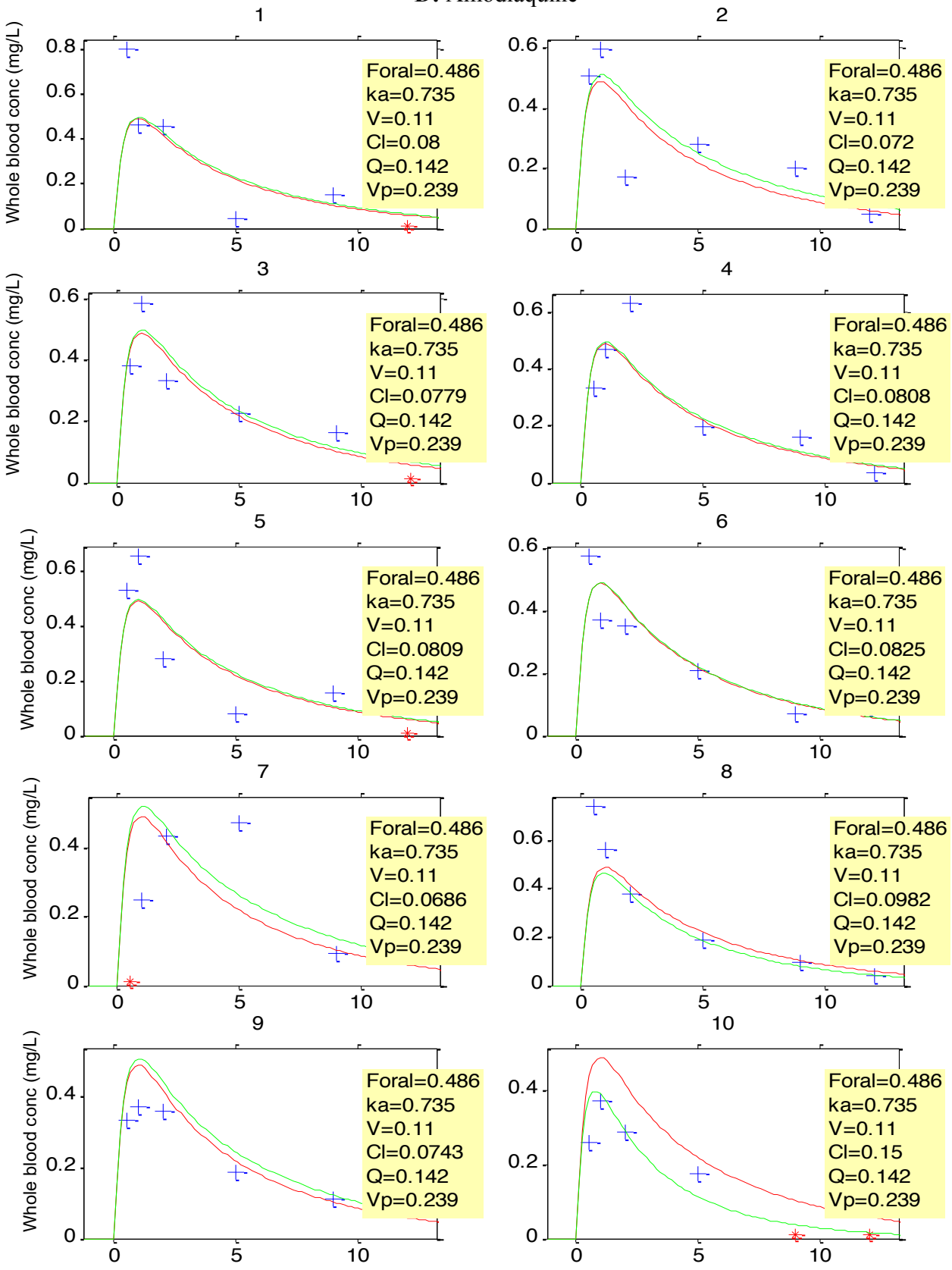

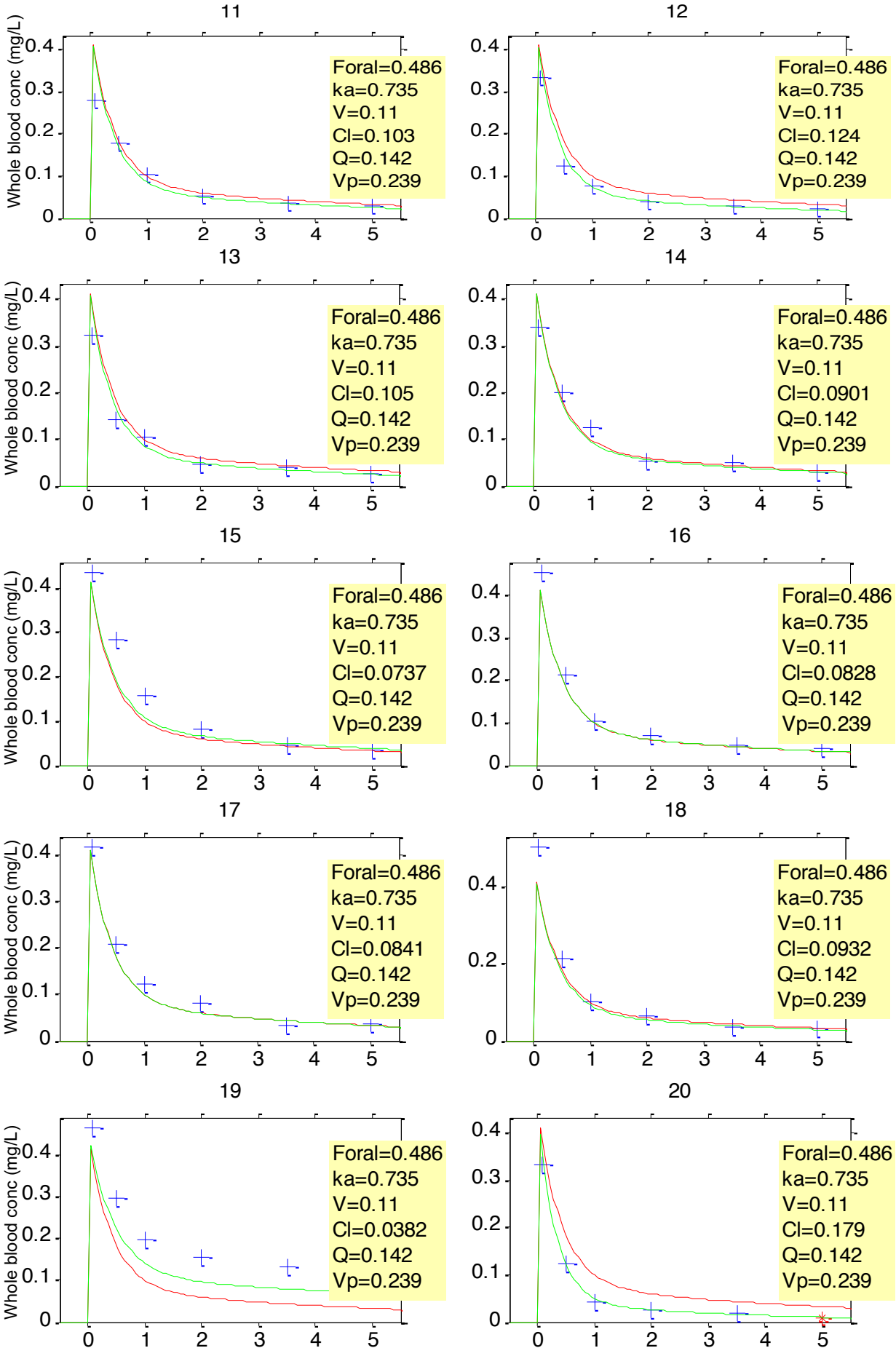
11
Whole blood conc (mg/L)
Foral=0.486
ka=0.735
V=0.11
Cl=0.103
Q=0.142
Vp=0.239
12
Foral=0.486
ka=0.735
V=0.11
Cl=0.124
Q=0.142
Vp=0.239
13
Foral=0.486
ka=0.735
V=0.11
Cl=0.105
Q=0.142
Vp=0.239
14
Foral=0.486
ka=0.735
V=0.11
Cl=0.0901
Q=0.142
Vp=0.239
15
Foral=0.486
ka=0.735
V=0.11
Cl=0.0737
Q=0.142
Vp=0.239
16
Foral=0.486
ka=0.735
V=0.11
Cl=0.0828
Q=0.142
Vp=0.239
17
Foral=0.486
ka=0.735
V=0.11
Cl=0.0841
Q=0.142
Vp=0.239
18
Foral=0.486
ka=0.735
V=0.11
Cl=0.0932
Q=0.142
Vp=0.239
19
Foral=0.486
ka=0.735
V=0.11
Cl=0.0382
Q=0.142
Vp=0.239
20
Foral=0.486
ka=0.735
V=0.11
Cl=0.179
Q=0.142
Vp=0.239

Figure 7-5: Individual plots of the benzoxazole amodiaquine analogues

The graphical diagnostic individual fit output of all individual mice for A: **DS23B**, B: **DS48B**, C: **DS50B**, D: Amodiaquine. The blue crosses represent the observed concentration data points from the experiment, the red stars represent the "censored" or below limit of quantification (BLQ) data and the green line represents the individual fit after parameter variability for respective individual mice are included. The population fit represented by the red line, is the median of the cohort of both the oral and intravenous groups. The individual parameters of each mice are shown in the yellow legend.

7.3 Antimalarial aminopyridine in the form of its cyclodextrin inclusion complex

The experimental records for the "Chapter 3: Aminopyridine in the form of its cyclodextrin inclusion complex" project (page 102) are presented in the following sections.

7.3.1 LC/MS/MS

A brief overview of the final LC/MS/MS method was presented in Chapter 3, section 3.4.2, page 110. Expanded sample preparation, instrumentation settings and quantification statistics are presented below.

7.3.1.1 Sample preparation

A protein precipitation method was used to extract samples at room temperature. An extraction volume of 20 µl of the thawed whole blood sample was precipitated with 240 µl of a 100 ng/ml structurally similar internal standard solution in methanol, except for the double blank sample extracted with pure methanol. Samples were vortexed for 1 minute and then centrifuged for 5 minutes at 10 000 rcf. A 200 µl volume of the resulting supernatant was transferred to a 96 well plate and dried under nitrogen and 100 µl of 5% acetonitrile (v/v) in 0.1% formic acid in water (v/v) added to each well. A 5 µl injection volume was used for LC-MS/MS quantification.

7.3.1.2 Instrumentation

LC-MS/MS analysis was performed on an Agilent 1200 series binary pump (Agilent, CA, USA) interfaced to an AB Sciex API 4000Q® mass spectrometer (AB Sciex, Ontario, Canada) with an electrospray ion (ESI) source in positive mode.

7.3.1.3 Mass spectrometer conditions

Figure 7-6 shows the initial product ion scans (MS/MS) spectrum of the analyte and the most intense fragmentation illustrated. The settings of the apparatus are summarised in Table 7-14.

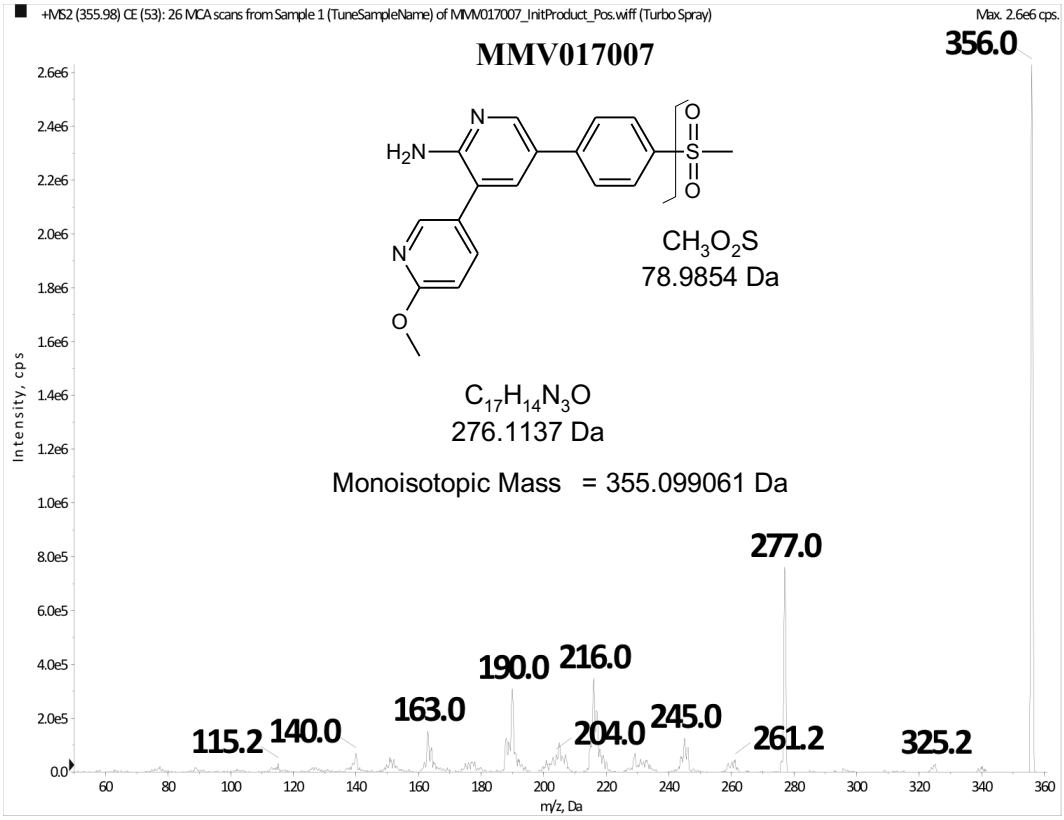

Figure 7-6: Initial product ion scan of MMV017007

The MS/MS scans of **MMV017007**. The figure contains the compound structure and fragmentation that relates to the most intense MS/MS peak.

Table 7-15: Mass spectrometer settings of MMV017007

Source settings

CUR	IS (KV)	TEM (°C)	GS1	GS2
20	5500	400	60	40

Compound settings		Q1	Q3	Dwell	DP	EP	CE	CXP
		(Da)	(Da)	(msec)	(V)	(V)	(V)	(V)
007	Quant	355.983	277.0	150	116	10	49	18
	Qual	355.983	190.0	150	116	10	87	10

Note: CUR; curtain gas flow, IS; IonSpray voltage, TEM; Temperature, GS1; nebuliser gas, GS2; turbo-gas, Q1; first quadrupole, Q3; third quadrupole, Dwell; dwell time (time instrument records ion intensity of fragment), DP; declustering potential, EP entrance potential, CEP; collision cell exit potential, CE; collision energy, Quant; quantifier ion, Qual; qualifier ion.

7.3.1.4 HPLC conditions

Gradient chromatography steps shown in Table 7-16 was performed on a Phenomenex® Kinetex PFP (2.1 x 50 mm, 2.6 µm) reverse phase column with mobile phases A; 0.1% formic acid:water (v/v) and B; 0.1% formic acid:acetonitrile (v/v) at a flow rate of 200 µl/min, Table 7-16.

Table 7-16: Gradient chromatography steps of MMV017007

Step	Total Time (min)	Flow Rate (µl/min)	A (%)	B (%)
0	0	200	95	5
1	0.5	200	95	5
2	2	200	0	100
3	3.5	200	0	100
4	3.6	200	95	5
5	6.5	200	95	5

The gradient steps used mobile phases A; 0.1% formic acid:water (v/v) and B; 0.1% formic acid:acetonitrile on a Phenomenex® Kinetex PFP (2.1 x 50 mm, 2.6 µm) reverse phase column.

7.3.1.5 Quantification

In Table 7-17 is shown the quantification statistics from the final batches measured for MMV017007.

Table 7-17: Quantification statistics of MMV017007

MMV017007						
Sample	Expected conc (ng/ml)	Number	Mean conc (ng/ml)	S.D.	Precision (%CV)	Accuracy (%Norm)
S7	4.12	2 of 2	4.08	0.413	10.1	99.1
S6	12.3	2 of 2	11.5	0.185	1.61	93.4
S5	37.0	2 of 2	42.1	0.888	2.11	114
S4	111	2 of 2	105	7.39	7.02	94.9
S3	333	2 of 2	325	11.4	3.50	97.7
S2	1000	2 of 2	1010	86.4	8.54	101
S1	3000	2 of 2	3000	117	3.90	99.9
QC L	10	2 of 2	9.80	0.358	3.66	98.0
QC M	2000	2 of 2	1160	56.8	4.89	96.8
QC H	4000	2 of 2	2340	58.9	2.52	97.3

Note: Standards (S1-S7) were used for the calibration curves. Quality controls (QC) low (L), medium (M) and high (H).

The calibration curves of the final analysed batches for MMV017007 is shown in Figure 7-7. Quantification used quadratic regression of the analyte area/internal standard area vs concentration with 1/x weighting. A regression value of 0.9991 was achieved.

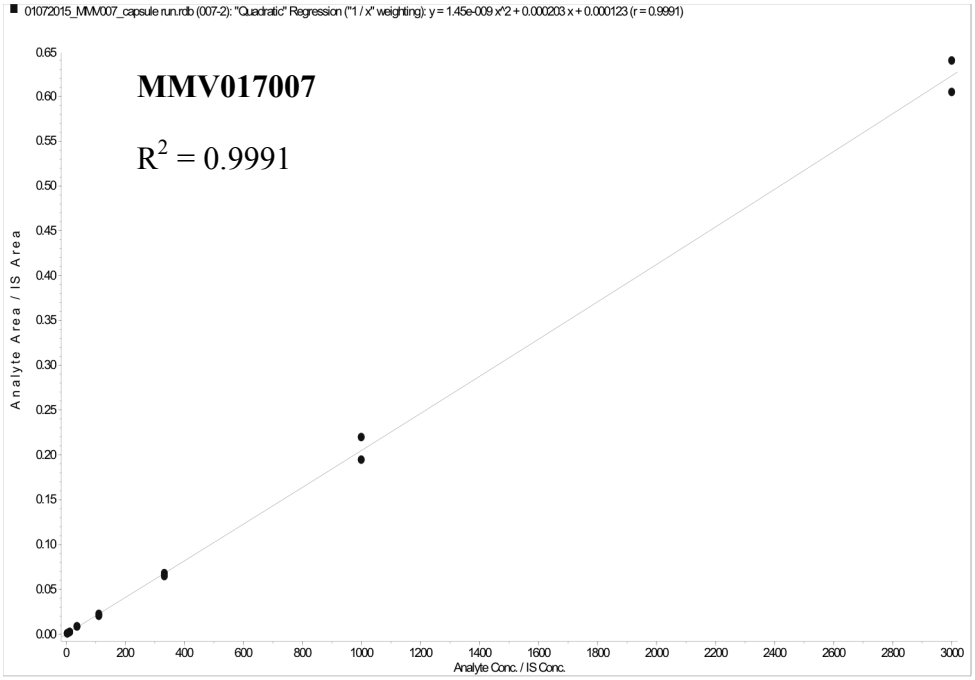

Figure 7-7: Calibration curve of MMV017007

The blank sample injected after the highest concentration standard from the final batch analysed to display any signs of carry-over is shown in Figure 7-8. No carry-over was observed for the analyte. In Figure 7-9 is shown the integrated lowest quality control of MMV017 alongside its internal standard to display suitable peak to noise ratio for quantification.

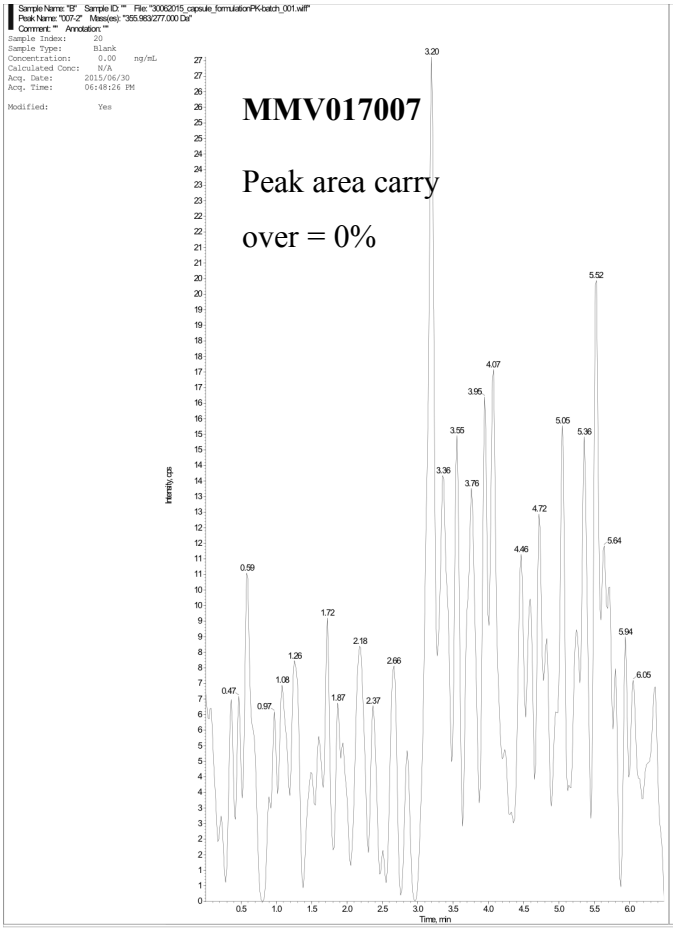

Figure 7-8: Blank sample of MMV017007

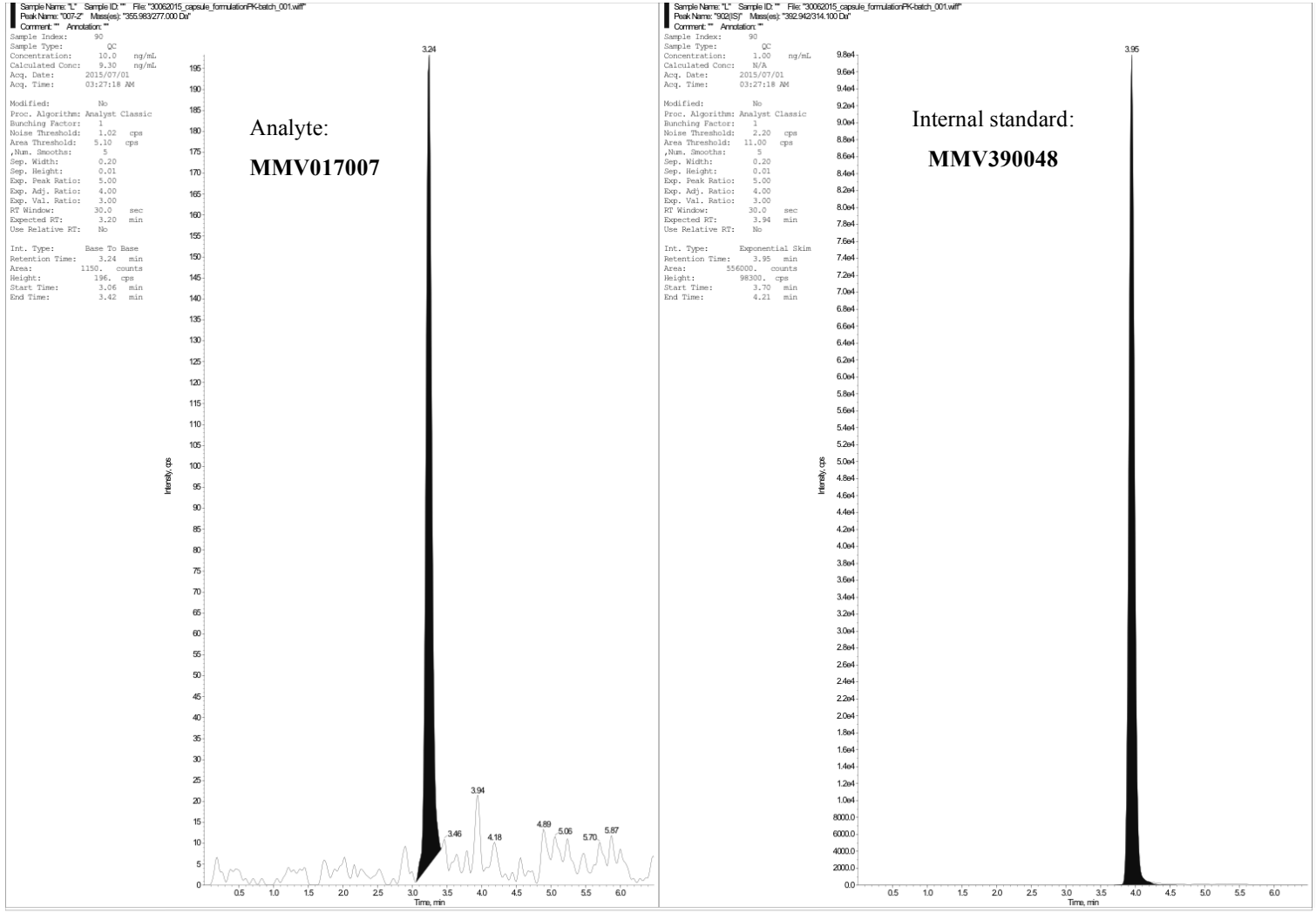

Figure 7-9: Low quality control of MMV017007

7.3.2 Animal experiment

The animal experiments performed for the antimalarial aminopyridine project were described in Chapter 3, section 3.4.3.1, page 111.

The experimental record sheet of the animal experiments is shown below in Table 7-18. It contains exact sampling times, summary of dosage formulations and animal weight and sex.

Table 7-18: MMV017007 formulation animal experiment

Oral/IV dose - compound **MMV017007** formulation

Date:	29-Jul-15		IV solution			Oral capsules		
Ethics no:	013/028					Total mass of formulation		
Dose: Oral	5	mg/kg	Weighed:	1.24	mg	CapA001	543	µg
Dose: IV	2.5	mg/kg	in	100	µL DMSO	CapA002	498	µg
				100	µL EtOH	CapA003	481	µg
				300	µL PEG 400	CapB001	120	µg
				500	µL PPG	CapB002	112	µg
						CapB003	83.0	µg

Mouse	Mass (g)	Dose (µg)	Dose time	5 min	30 min	1 hr	3 hr	5 hr	8 hr	24 hr
M1 IV♂	31.3	74.4	08:07:00	08:13:00	08:37:00	09:07:00	11:06:00	13:06:00	16:05:00	07:30:00
M2 IV♂	31.0	74.4	08:10:00	08:14:00	08:38:00	09:09:00	11:07:00	13:08:00	16:06:00	07:32:00
M3 IV♂	29.0	74.4	08:11:00	08:14:00	08:39:00	09:10:00	11:09:00	13:09:00	16:07:00	07:33:00
M4♀ Cap A	23.4	114	08:29:00	-	08:57:00	09:29:00	11:29:00	13:28:00	16:29:00	07:45:00
M5♀ Cap A	23.0	105	08:32:00	-	08:58:00	09:31:00	11:31:00	13:29:00	16:31:00	07:46:00
M6♀ Cap A	23.4	101	08:34:00	-	08:59:00	09:32:00	11:32:00	13:31:00	16:37:00	07:47:00
M7♀ Cap B	23.9	120	08:48:00	-	09:18:00	09:46:00	11:48:00	13:47:00	16:34:00	07:49:00
M8♀ Cap B	23.6	112	08:45:00	-	09:17:00	09:44:00	11:47:00	13:48:00	16:36:00	07:51:00
M9♀ Cap B	24.5	83.0	08:47:00	-	09:18:00	09:46:00	11:49:00	13:49:00	16:36:00	07:52:00

7.3.3 Individual concentration profiles & data analysis

7.3.3.1 Non-compartmental analysis

The summarised pharmacokinetic results of the formulation study were presented in Table 3-3, starting in section 3.4.4, page 112. The expanded individual results with individual raw concentration vs time data is presented below in Table 7-19 and respective non-compartmental analysis results for each individual subject in Table 7-20 for both **MMV017007** and its cyclodextrin inclusion complex, **DMB·007**.

Table 7-19: Individual concentrations (µM) of 007 formulation experiment

IV

M1		M2		M3		Mean	
Time	Conc (µM)	Time	Conc (µM)	Time	Conc (µM)	Time (hr)	Conc (µM)
0.1	8.78	0.0667	7.34	0.05	9.82	0.0722	8.65
0.5	7.03	0.467	6.42	0.467	7.43	0.478	6.96
1	5.82	0.983	5.85	0.983	6.58	0.989	6.09
2.98	5.77	2.95	4.98	2.97	5.26	2.97	5.34
4.98	4.9	4.97	2.84	4.97	3.71	4.97	3.82
7.97	2.93	7.93	1.84	7.93	2.62	7.94	2.46
23.4	0.512	23.4	0.0554	23.4	0.195	23.4	0.254

DMB·007

M4		M5		M6		Mean	
Time	Conc (µM)	Time	Conc (µM)	Time	Conc (µM)	Time (hr)	Conc (µM)
0.467	0.0279	0.433	0.00872	0.417	0	0.439	0.0122
1	0.0642	0.983	0.00816	0.967	0.00338	0.983	0.0252
3	0.793	2.98	0.0146	2.97	0.298	2.98	0.369
4.98	1.72	4.95	2.61	4.95	4.61	4.96	2.98
8	1.34	7.98	2.61	8.05	2.95	8.01	2.3
23.3	0.422	23.2	0.357	23.2	0.107	23.2	0.295

007

M7		M8		M9		Mean	
Time	Conc (µM)	Time	Conc (µM)	Time	Conc (µM)	Time (hr)	Conc (µM)
0.817	0.00394	0.75	0.0019	0.733	0.0112	0.767	0.00568
1.28	0.0076	1.2	0.0022	1.2	0.00254	1.23	0.00411
3.32	0.116	3.25	3.66	3.25	3.04	3.27	2.27
5.3	0.712	5.27	3.1	5.25	2.58	5.27	2.13
8.08	0.304	8.07	3.12	8.03	1.34	8.06	1.59
23.3	0.0255	23.3	0.132	23.3	0.0257	23.3	0.061

Note: M1 represents individual mouse 1, M2 individual mouse 2 etc. M1 – M3 received intravenous (IV) doses, M4 to M6 received a single oral dose of DMB·007 in capsule formulation and similarly M7 to M8 received a single dose of MMV017007 in capsule formulation.

Table 7-20: Non-compartmental analysis of 007 formulation study

IV	M1	M2	M3	Mean	S.E.
Apparent half-life (h)	4.48	3.26	5.98	4.58	0.787
Blood Clearance (ml/min/kg)	1.53	2.35	1.94	1.94	0.236
Vd (L/kg)	0.844	0.644	0.717	0.735	0.0584
$AUC_{0\text{-}inf}$ (µM.min)	4400	2870	3720	3670	443
DMB·007	M4	M5	M6	Mean	S.E.
Apparent half-life (h)	9.45	5.58	3.34	6.12	1.79
$AUC_{0\text{-}inf}$ (µM.min)	1670	2220	2490	2130	241
007	M7	M8	M9	Mean	S.E.
Apparent half-life (h)	4.48	4.18	2.8	3.82	0.516
$AUC_{0\text{-}inf}$ (µM.min)	317	2790	1530	1550	715

Note: IV; intravenous, P.O.; per os/oral, Vc; central volume, Vss; volume at steady state, $AUC_{0\text{-}\infty}$; area under the curve from time zero to infinity. Individual values corresponding to the same labelled raw concentration vs time data is represented with the calculated mean and standard error of the mean (S.E.).

7.3.3.2 Non-linear mixed effects modelling

Table 7-21 and Table 7-22 presents the non-linear mixed effects model parameter estimates, typical values and variability of the random effects (on approximate %CV scale), together with their precision reported as standard error for separate and joint analysis of **DMB·007** and **007** respectively.

As described in Chapter 3, section 3.4.5, page 113 several attempts to find an ideal non-linear mixed effects model that could describe the data were performed. The non-linear mixed model parameter estimates for the different approaches are presented in Table 7-21 to Table 7-22. The median values for the cohort are presented with their respective standard error and relative standard error determined by linearization of their Fischer information matrix. The fixed effects, covariate model, omega and sigma model values are shown in each table.

The individual plots alongside population mean and parameter information of each subject is shown below respective parameter estimates in Figure 7-10 and Figure 7-11.

Table 7-21: Parameter estimation of the separate data set model

	DMB·007			007		
	Parameter	s.e. (lin)	r.s.e.(%)	Parameter	s.e. (lin)	r.s.e.(%)
Fixed effects:						
Foral	0.224	0.13	57	0.224	0.13	57
ka (hr^{-1})	1.83	1.4	75	1.83	1.4	75
V (L)	0.0266	-	-	0.0266	-	-
Cl (L/h)	0.00402	-	-	0.00402	-	-
Tlag (hr)	2.74	0.38	14	2.74	0.38	14
Covariate Model:						
Beta Cl (tWeight)	0.75	-	-	0.75	-	-
Beta V (tWeight)	1	-	-	1	-	-
Parameter variability						
Foral	0.971	0.41	42	0.971	0.41	42
ka	0.152	2	1.32E+03	0.152	2	1.32E+03
V	0	-	-	0	-	-
Cl	0.203	-	-	0.203	-	-
Tlag	0.133	0.091	68	0.133	0.091	68
Residual error (random error):						
Proportional	0.00211	0.01	481	0.00211	0.01	481
Constant	0.201	0.031	16	0.201	0.031	16

Note: Foral; bioavailability, ka; rate of absorption, V; central volume, Cl; clearance, Tlag; absorption delay time. Standard error (s.e.) and relative standard error (r.s.e) expressed as a percentage of the population estimate were estimated by linearization of the Fisher information matrix. The covariate tWeight is defined as the transformed log individual mass of each mouse centred around the median of the cohort mass. Parameter values equal to zero are parameters that were excluded from the model based on their statistical insignificance as determined by -2LL.

Table 7-22: Parameter estimation of the joint data set model

	Parameter	s.e. (lin)	r.s.e.(%)	p-value
Fixed effects:				
Foral	0.249	0.11	46	
ka (hr^{-1})	0.815	0.23	28	
V (L)	0.0205	0.0007	3	
Cl (L/hr)	0.00351	0.00045	13	
Tlag (hr)	2.83	0.21	8	
Covariate Model:				
Beta Cl (tWeight)	0.75	-	-	-
Beta V (tWeight)	1	-	-	-
Beta Foral (formulation)	-0.148	0.65	437	0.82
Beta ka (formulation)	0.768	0.68	89	0.26
Beta Tlag (formulation)	-0.0249	0.15	589	0.87
Parameter variability:				
Omega Foral	0.78	0.23	29	
Omega ka	0.0925	0.9	973	
Omega V	0	-	-	
Omega Cl	0.35	0.089	25	
Omega Tlag	0.126	0.042	33	
Residual error:				
Proportional	0.00723	0.0046	64	
Constant	0.121	0.019	16	
Final experimental group parameters:				
Foral (**DMB·007**)	0.249	0.11	46	
Foral (**007**)	0.215	0.099	46	
ka (**DMB·007**)	0.815	0.23	28	
ka (**007**)	1.76	1.1	63	
Tlag (**DMB·007**)	2.83	0.21	8	
Tlag (**007**)	2.76	0.35	13	

Note: Foral; bioavailability, ka; rate of absorption, V; central volume, Cl; clearance, Tlag; absorption delay time. Standard error (s.e.) and relative standard error (r.s.e) expressed as a percentage of the population estimate were

estimated by linearization of the Fisher information matrix. The covariate tWeight is defined as the transformed log individual mass of each mouse centred around the median of the cohort mass. The parameters of the formulation and parent when modelled as categorical variables are represented in the final section of the table. Parameter values equal to zero are parameters that were excluded from the model based on their statistical insignificance as determined by -2LL.

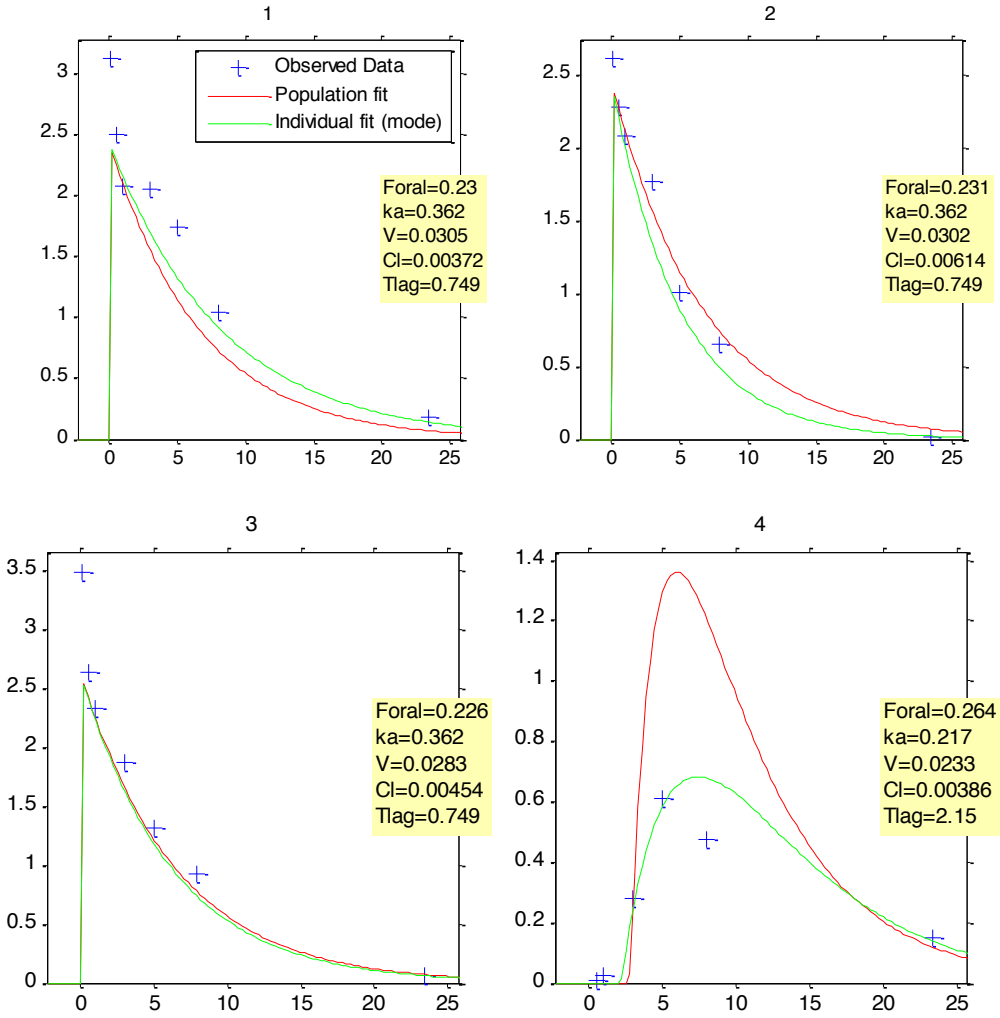

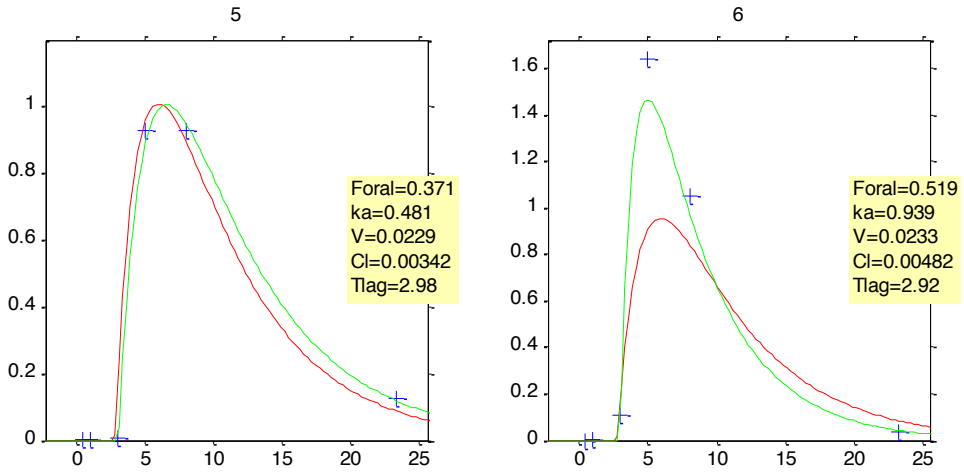

Figure 7-10: Individual plots of the separate data model

The graphical diagnostic individual fit output of all individual mice for the A: IV, B: DMB·007 and C: MMV017007 API formulation. The blue crosses represent the observed concentration data points from the experiment and the green line represents the individual fit after parameter variability for respective individual mice are included. The population fit represented by the red line, is the median of the cohort of both the oral and intravenous groups. The individual parameters of each mice are shown in the yellow legend.

A: IV formulation

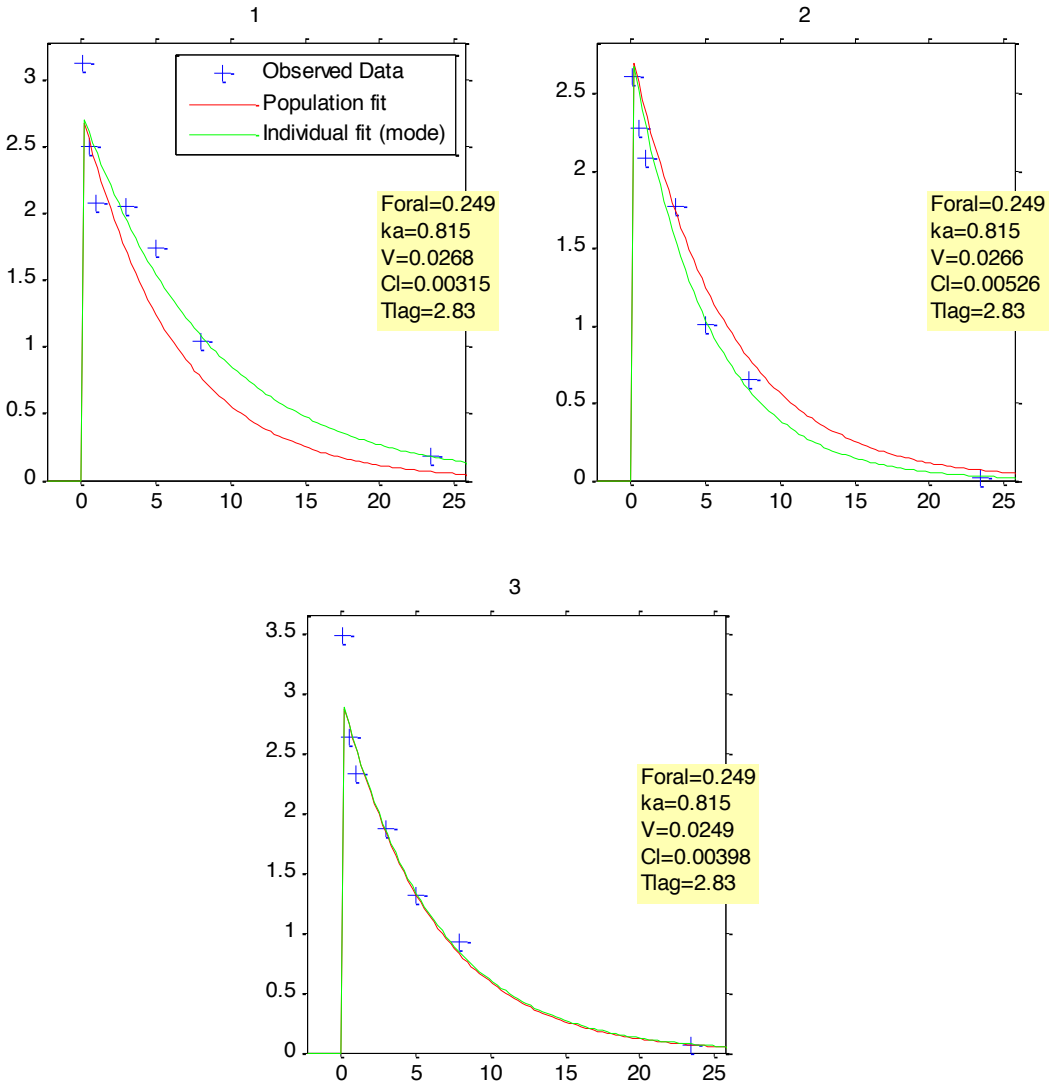

B: DMB·007 formulation

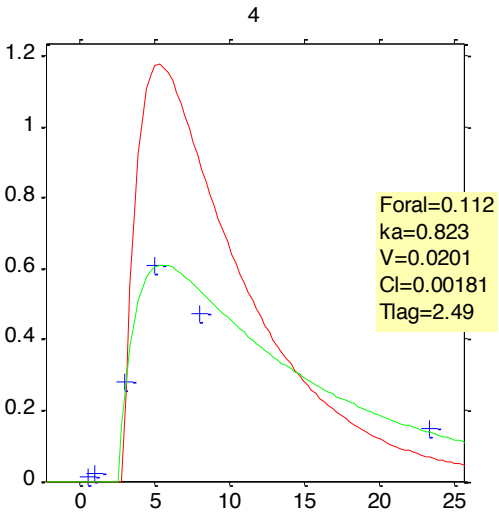

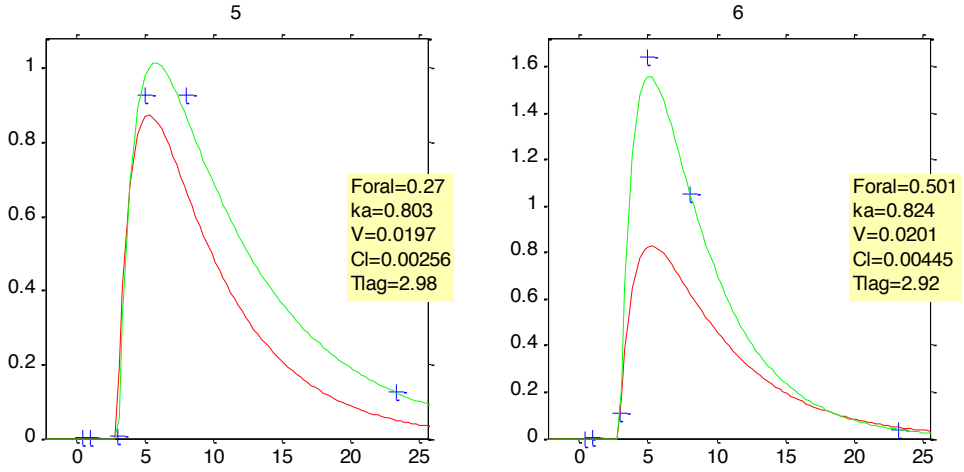

C: MMV017007 formulation

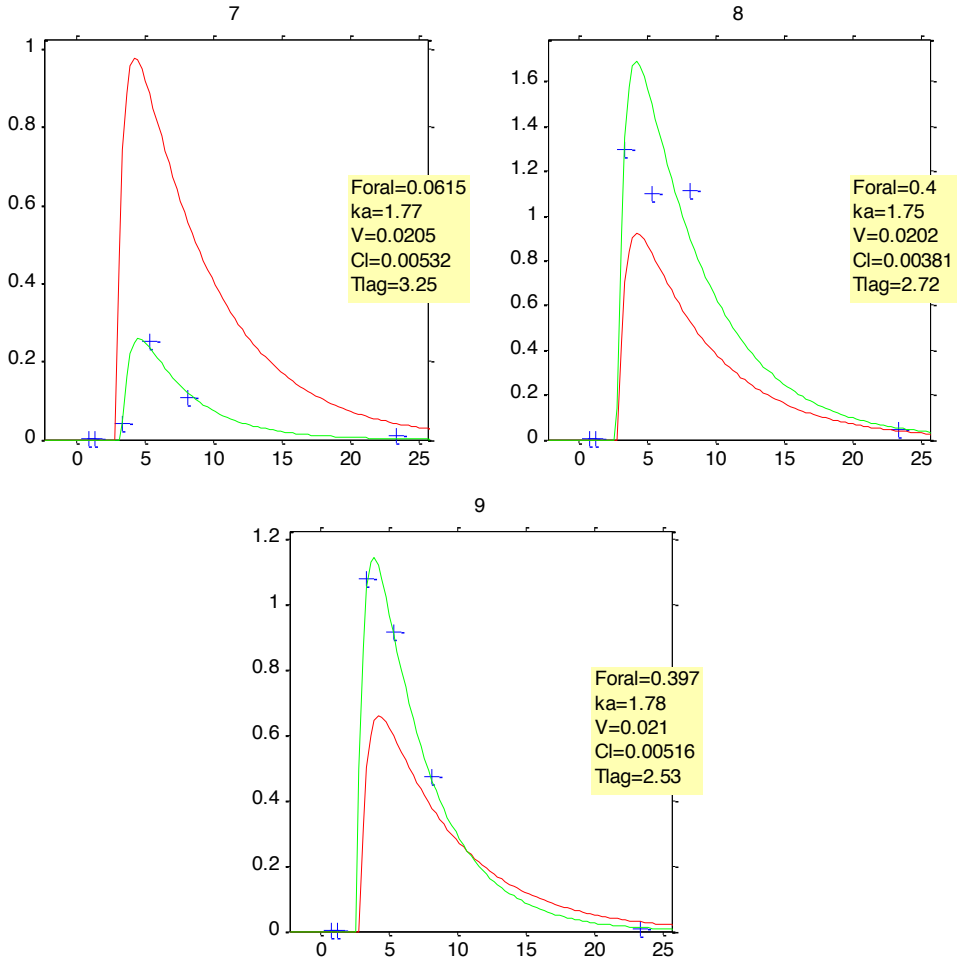

Figure 7-11: Individual plots of joint data set model

The graphical diagnostic individual fit output of all individual mice for the A: IV, B: DMB·007 and C: MMV017007 API formulation. The blue crosses represent the observed concentration data points from the experiment and the green line represents the individual fit after parameter variability for respective individual mice are included. The population fit represented by the red line, is the median of the cohort of both the oral and intravenous groups. The individual parameters of each mice are shown in the yellow legend.

7.4 Fusidic acid prodrugs for potential repositioning in tuberculosis

The experimental records for the "Chapter 4: Fusidic acid prodrugs for potential repositioning in tuberculosis" project (page 125) are presented in the following sections.

7.4.1 LC/MS/MS

A brief overview of the final LC/MS/MS method was presented in Chapter 4, section 4.4.2, on page 133. Expanded sample preparation, instrumentation settings and quantification statistics are presented in the sections below.

7.4.1.1 Sample preparation

A protein precipitation method was used to extract samples at room temperature. An extraction volume of 20 µl of the thawed whole blood sample was precipitated with 240 µl of a 100 ng/ml structurally similar internal standard solution in methanol, except for the double blank sample extracted with pure methanol. Samples were vortexed for 1 minute and then centrifuged for 5 minutes at 10 000 rcf. A 200 µl volume of the resulting supernatant was transferred to a 96 well plate and dried under nitrogen, and 100 µl of 20% methanol (v/v) in 0.03% ammonium hydroxide in water (v/v) added to each well. A 5 µl injection volume was used for LC-MS/MS quantification.

7.4.1.2 Instrumentation

LC-MS/MS analysis was performed on an Agilent 1200 series binary pump (Agilent, CA, USA) interfaced to an AB Sciex API 4500® mass spectrometer (AB Sciex, Ontario, Canada) with an electrospray ion (ESI) source in positive mode.

7.4.1.3 Mass spectrometer conditions

Figure 7-12 shows the initial product ion scans (MS/MS) spectrum of the analytes and their most intense fragmentation illustrated. The settings of the apparatus are summarised in Table 7-23.

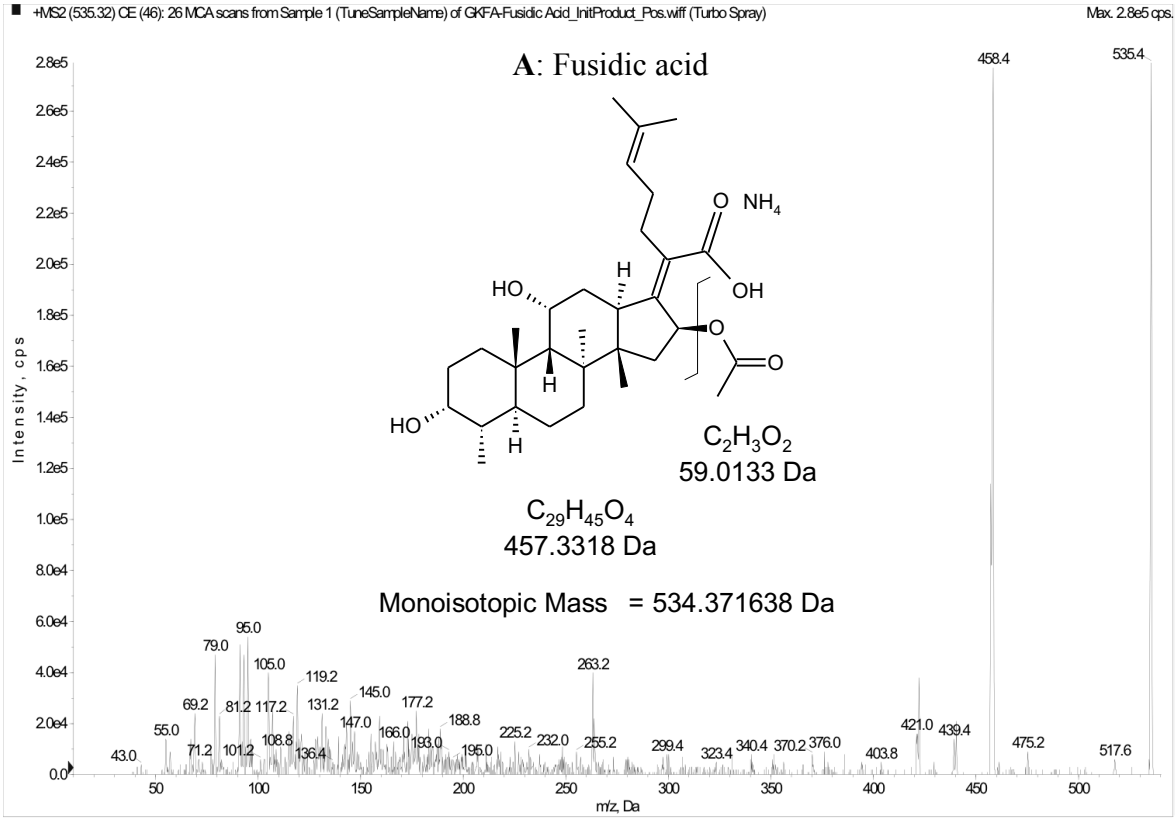
+MS2 (535.32) CE (46): 26 MCA scans from Sample 1 (TuneSampleName) of GKFA-Fusidic Acid_InitProduct_Pos.wiff (Turbo Spray)
Max. 2.8e5 cps.
A: Fusidic acid
Intensity, cps
m/z, Da
458.4
535.4
C2H3O2
59.0133 Da
C29H45O4
457.3318 Da
Monoisotopic Mass = 534.371638 Da

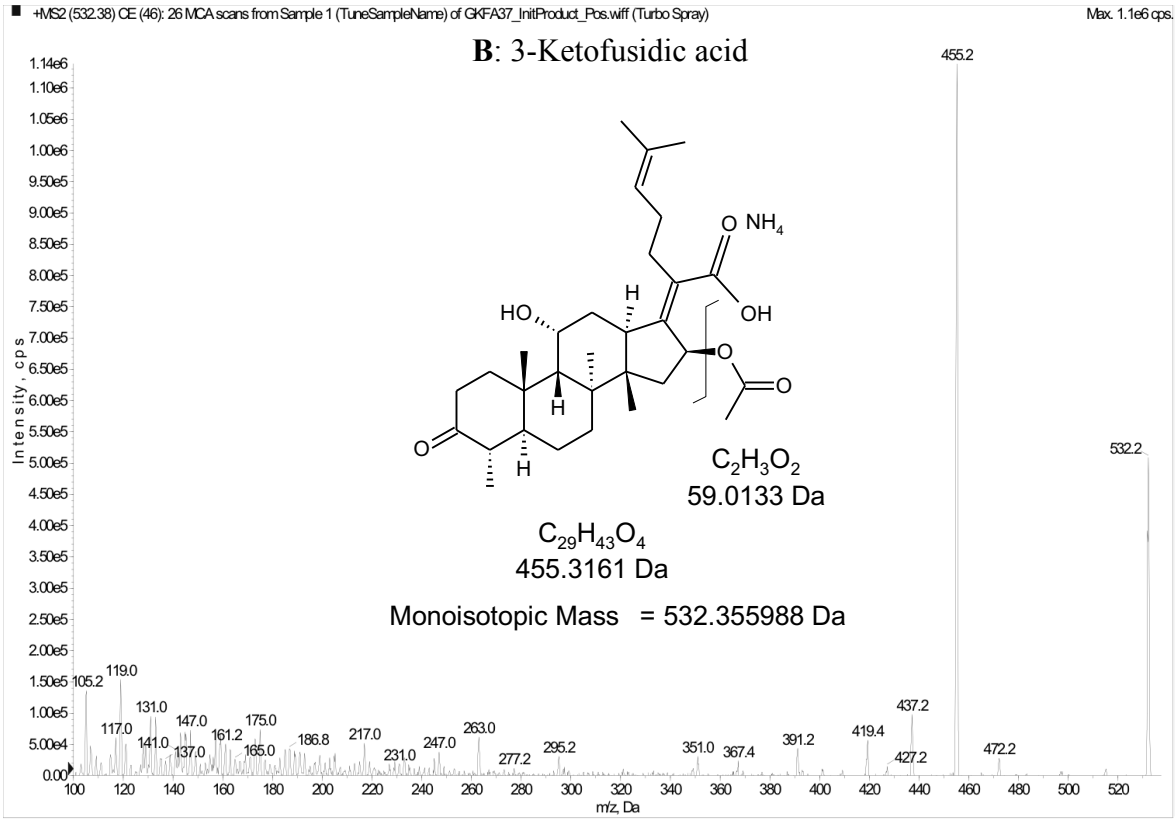
+MS2 (532.38) CE (46): 26 MCA scans from Sample 1 (TuneSampleName) of GKFA37_InitProduct_Pos.wiff (Turbo Spray)
Max. 1.1e6 cps.
B: 3-Ketofusidic acid
Intensity, cps
m/z, Da
455.2
532.2
C2H3O2
59.0133 Da
C29H43O4
455.3161 Da
Monoisotopic Mass = 532.355988 Da

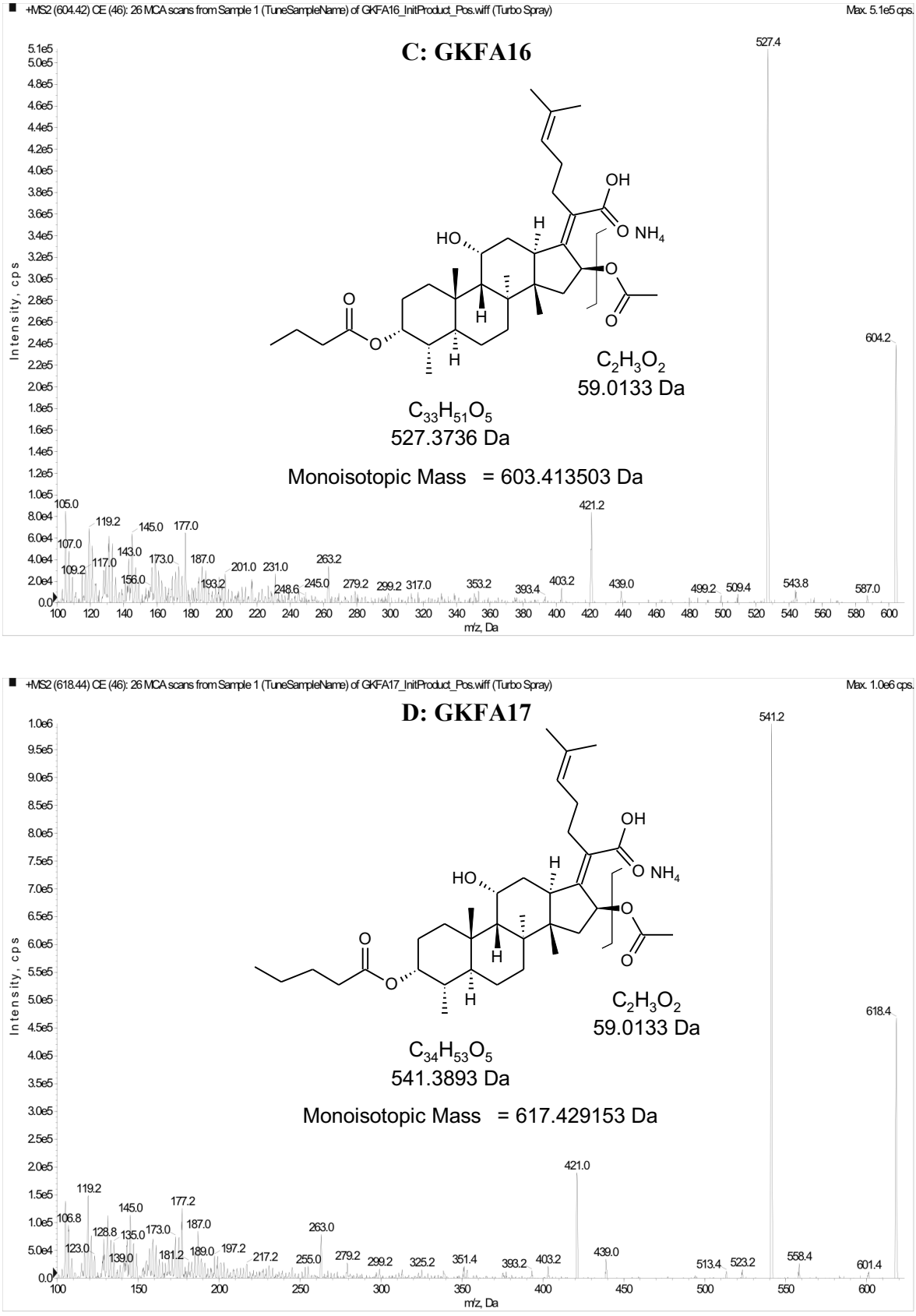

Figure 7-12: Initial product ion scans of fusidic acid compounds

The MS/MS scans of A: fusidic acid, B: 3-ketofusidic acid, C: **GKFA16** and D: **GKFA17**. The figure contains the compound structure and fragmentation that relates to the most intense MS/MS peak.

Table 7-23: Mass spectrometer settings of fusidic acid compounds

Source settings

CUR	IS (KV)	TEM (°C)	GS1	GS2
30	5500	350	30	50

Compound settings		Q1	Q3	Dwell	DP	EP	CEP	CE
		(Da)	(Da)	(msec)	(V)	(V)	(V)	(V)
Fusidic acid	Quant	534.379	457.2	60	51	10	27	10
	Qual	534.379	263.0	60	51	10	17	14
3-ketofusidic acid	Quant	532.323	455.2	60	86	10	17	14
	Qual	532.323	437.2	60	86	10	27	14
GKFA16	Quant	604.424	527.2	60	61	10	17	16
	Qual	604.424	421.1	60	61	10	31	14
GKFA17	Quant	618.440	541.2	60	60	10	17	16
	Qual	618.440	421.1	60	60	10	29	14

Note: CUR; curtain gas flow, IS; IonSpray voltage, TEM; Temperature, GS1; nebuliser gas, GS2; turbo-gas, Q1; first quadrupole, Q3; third quadrupole, Dwell; dwell time (time instrument records ion intensity of fragment), DP; declustering potential, EP entrance potential, CEP; collision cell exit potential, CE; collision energy, Quant; quantifier ion, Qual; qualifier ion.

7.4.1.4 HPLC conditions

Gradient chromatography shown in Table 7-24 was performed on a Phenomenex® Kinetex C_{18} (2.1 x 50 mm, 2.6 µm) reverse phase column with mobile phases A; 0.03% ammonium hydroxide:water (v/v) and B; 0.03% ammonium hydroxide:acetonitrile (v/v) at a flow rate of 300 µl/min.

Table 7-24: Gradient chromatography steps of fusidic acid compounds

Step	Total Time (min)	Flow Rate (µl/min)	A (%)	B (%)
0	0	300	92	8
1	1	300	92	8
2	1.1	300	0	100
3	4.5	300	0	100
4	4.6	300	92	8
5	11	300	92	8

The gradient steps used mobile phases A; 0.03% ammonium hydroxide:water (v/v) and B; 0.03% ammonium hydroxide:acetonitrile (v/v) on a Phenomenex® Kinetex C_{18} (2.1 x 50 mm, 2.6 µm) reverse phase column.

7.4.1.5 Quantification

Table 7-25 to 7-32 presents the quantification statistics of the fusidic acid compounds.

Table 7-25: Quantification statistics of GKFA16 experiment

GKFA16 experiment

Fusidic acid						
Sample	Expected conc (ng/ml)	Number	Mean conc (ng/ml)	S.D.	Precision (%CV)	Accuracy (%Norm)
S7	2	2 of 2	2.01	0.132	6.59	100
S6	10	2 of 2	9.86	0.961	9.75	98.6
S5	50	2 of 2	47	2.11	4.48	94
S4	100	2 of 2	101	3.25	3.22	101
S3	500	2 of 2	518	50.5	9.75	104
S2	2500	1 of 1	2720	N/A	N/A	N/A
S1	5000	2 of 2	4890	55.1	1.13	97.9
QC L	6	1 of 1	7.35	N/A	N/A	123
QC M	2000	1 of 1	2200	N/A	N/A	110
QC H	4000	2 of 2	3740	86.6	2.32	93.5
3-ketofusidic acid						
S7	2	2 of 2	2	0.429	21.4	100
S6	10	1 of 1	10.1	N/A	N/A	101
S5	50	2 of 2	46.1	4.03	8.74	92.2
S4	100	2 of 2	102	7.92	7.77	102
S3	500	2 of 2	511	76	14.9	102
S2	2500	1 of 1	2750	N/A	N/A	110
S1	5000	2 of 2	4880	232	4.75	97.7
QC L	6	1 of 1	6.35	N/A	N/A	106
QC M	2000	1 of 1	2350	N/A	N/A	118
QC H	4000	2 of 2	3780	356	9.42	94.5
GKFA16						
S7	2	2 of 2	2.03	0.417	20.5	102
S6	10	1 of 1	8.49	N/A	N/A	84.9
S5	50	2 of 2	47.9	1.89	3.94	95.8
S4	100	2 of 2	97.6	1.06	1.09	97.6
S3	500	2 of 2	538	119	22.1	108
S2	2500	1 of 1	2820	N/A	N/A	113
S1	5000	2 of 2	4860	137	2.83	97.1
QC L	6	1 of 1	5.78	N/A	N/A	96.3
QC M	2000	1 of 1	2470	N/A	N/A	123
QC H	4000	2 of 2	4100	182	4.43	103

Note: Standards (S1-S7) were used for the calibration curves. Quality controls (QC) low (L), medium (M) and high (H).

Table 7-26: Quantification statistics of GKFA17 experiment

GKFA17 experiment

Fusidic acid						
Sample	Expected conc (ng/ml)	Number	Mean conc (ng/ml)	S.D.	Precision (%CV)	Accuracy (%Norm)
S7	2	2 of 2	2.01	0.404	20.1	100
S6	10	1 of 1	9.66	N/A	N/A	96.6
S5	50	2 of 2	50.1	8.18	16.3	100
S4	100	2 of 2	91.5	12	13.1	91.5
S3	500	2 of 2	533	61.6	11.6	107
S2	2500	2 of 2	2640	202	7.65	106
S1	5000	2 of 2	4840	1180	24.4	96.8
QC L	6	2 of 2	6.01	0.524	8.72	100
QC M	2000	2 of 2	2240	401	17.9	112
QC H	4000	2 of 2	4090	909	22.2	102
3-Ketofusidic acid						
S7	2	1 of 1	1.74	N/A	N/A	86.8
S6	10	2 of 2	11.1	0.997	8.98	111
S5	50	2 of 2	49	8.6	17.6	97.9
S4	100	2 of 2	88.6	14	15.8	88.6
S3	500	2 of 2	555	30.7	5.53	111
S2	2500	2 of 2	2440	17.4	0.715	97.4
S1	5000	1 of 1	5050	N/A	N/A	101
QC L	6	1 of 1	5.8	N/A	N/A	96.7
QC M	2000	1 of 1	1910	N/A	N/A	95.6
QC H	4000	2 of 2	3510	40.2	1.15	87.7
GKFA17						
S7	2	2 of 2	2.11	0.0825	3.92	105
S6	10	1 of 1	10.1	N/A	N/A	101
S5	50	2 of 2	48.8	3.67	7.52	97.6
S4	100	2 of 2	96.7	9.24	9.55	96.7
S3	500	2 of 2	499	0.0638	0.0128	99.8
S2	2500	2 of 2	2510	66.2	2.64	100
S1	5000	2 of 2	4990	339	6.79	99.9
QC L	6	2 of 2	6.08	0.101	1.66	101
QC M	2000	2 of 2	2220	34.4	1.55	111
QC H	4000	2 of 2	4190	30.9	0.738	105

Note: Standards (S1-S7) were used for the calibration curves. Quality controls (QC) low (L), medium (M) and high (H).

Table 7-27: Quantification statistics of fusidic acid experiment

Fusidic acid experiment

Fusidic acid						
Sample	Expected conc (ng/ml)	Number	Mean conc (ng/ml)	S.D.	Precision (%CV)	Accuracy (%Norm)
S6	2	2 of 2	1.68	0.155	9.24	83.9
S5	50	2 of 2	54.9	7.42	13.5	110
S4	100	2 of 2	102	7.39	7.21	102
S3	500	2 of 2	530	21.3	4.01	106
S2	2500	2 of 2	2430	470	19.3	97.3
S1	5000	2 of 2	5020	1760	35.1	100
QC L	6	2 of 2	6.98	1.24	17.8	116
QC M	2000	2 of 2	1960	599	30.5	98.2
QC H	4000	2 of 2	3860	759	19.7	96.4
3-ketofusidic acid						
S6	2	2 of 2	1.81	0.811	44.9	90.3
S5	50	2 of 2	51.6	6.88	13.3	103
S4	100	2 of 2	100	6	5.98	100
S3	500	2 of 2	543	7.44	1.37	109
S2	2500	2 of 2	2420	450	18.6	96.9
S1	5000	2 of 2	5030	1500	29.8	101
QC L	6	2 of 2	6.25	0.982	15.7	104
QC M	2000	2 of 2	1970	639	32.5	98.5
QC H	4000	2 of 2	3910	908	23.3	97.7

Note: Standards (S1-S6) were used for the calibration curves. Quality controls (QC) low (L), medium (M) and high (H).

Table 7-28: Quantification statistics of 3-ketofusidic acid experiment

3-Ketofusidic acid experiment

3-Ketofusidic acid						
Sample	Expected conc (ng/ml)	Number	Mean conc (ng/ml)	S.D.	Precision (%CV)	Accuracy (%Norm)
S7	2	2 of 2	2.01	0.123	6.09	101
S6	10	2 of 2	9.86	2.94	29.8	98.6
S5	50	2 of 2	44.3	9.07	20.5	88.5
S4	100	2 of 2	98.5	2.74	2.78	98.5
S3	500	2 of 2	552	50.2	9.1	110
S2	2500	2 of 2	2710	392	14.5	108
S1	5000	1 of 1	4500	N/A	N/A	90
QC L	6	2 of 2	6.19	1.1	17.8	103
QC M	2000	2 of 2	2000	132	6.6	99.8
QC H	4000	2 of 2	4240	524	12.4	106
Fusidic acid						
S7	2	2 of 2	2.07	0.414	20	103
S6	10	2 of 2	8.25	2.88	34.9	82.5
S5	50	2 of 2	54.3	3.31	6.1	109
S4	100	2 of 2	91.6	0.396	0.433	91.6
S3	500	2 of 2	557	43.1	7.73	111
S2	2500	2 of 2	2680	282	10.5	107
S1	5000	1 of 1	4560	N/A	N/A	91.2
QC L	6	2 of 2	5.68	0.863	15.2	94.6
QC M	2000	2 of 2	1990	138	6.93	99.4
QC H	4000	2 of 2	4200	510	12.1	105

Note: Standards (S1-S7) were used for the calibration curves. Quality controls (QC) low (L), medium (M) and high (H).

In Figure 7-13 is shown the respective calibration curves of the final analysed batches for the fusidic acid compounds with their respective regression values. Quantification used quadratic regression of the analyte area/internal standard area vs concentration with specified weighting. All calibration curves showed regression above 0.98.

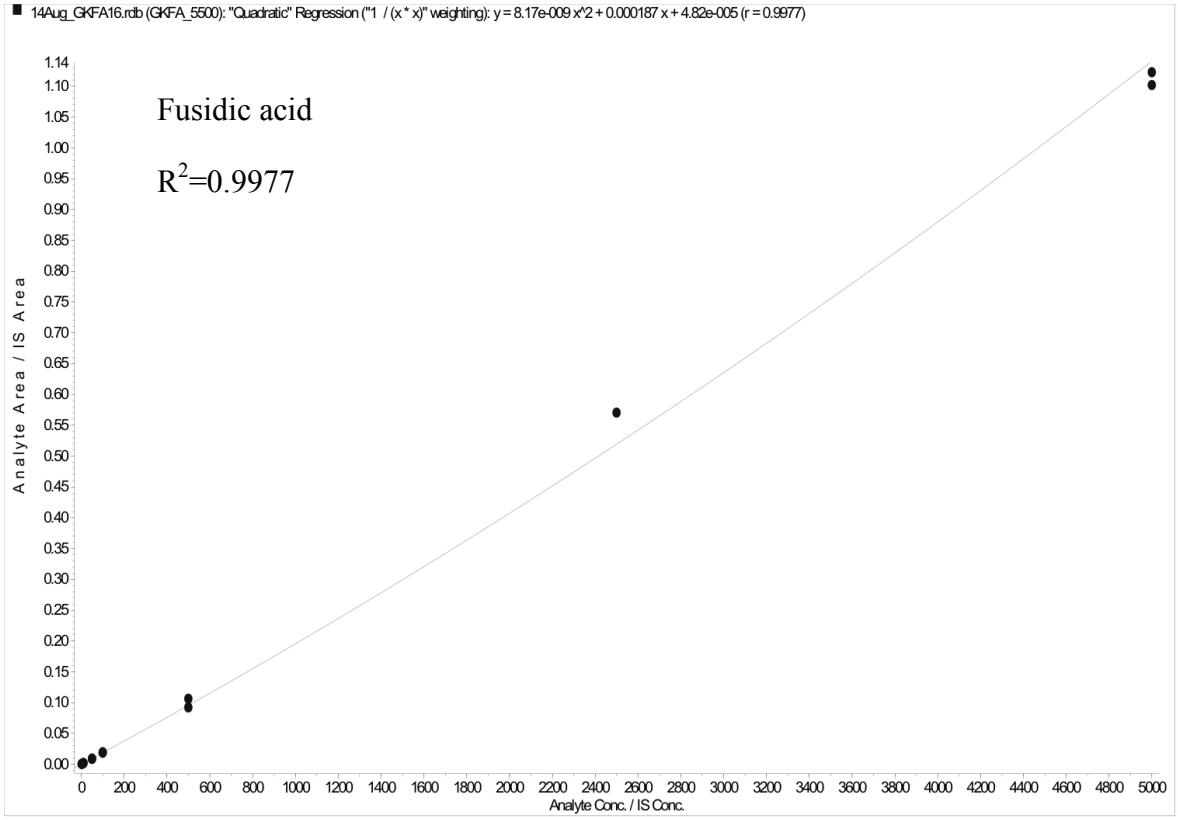
14Aug_GKFA16.rdb (GKFA_5500): "Quadratic" Regression ("1 / (x * x)" weighting): y = 8.17e-009 x^2 + 0.000187 x + 4.82e-005 (r = 0.9977)
Fusidic acid
R2=0.9977
Analyte Area / IS Area
Analyte Conc. / IS Conc.

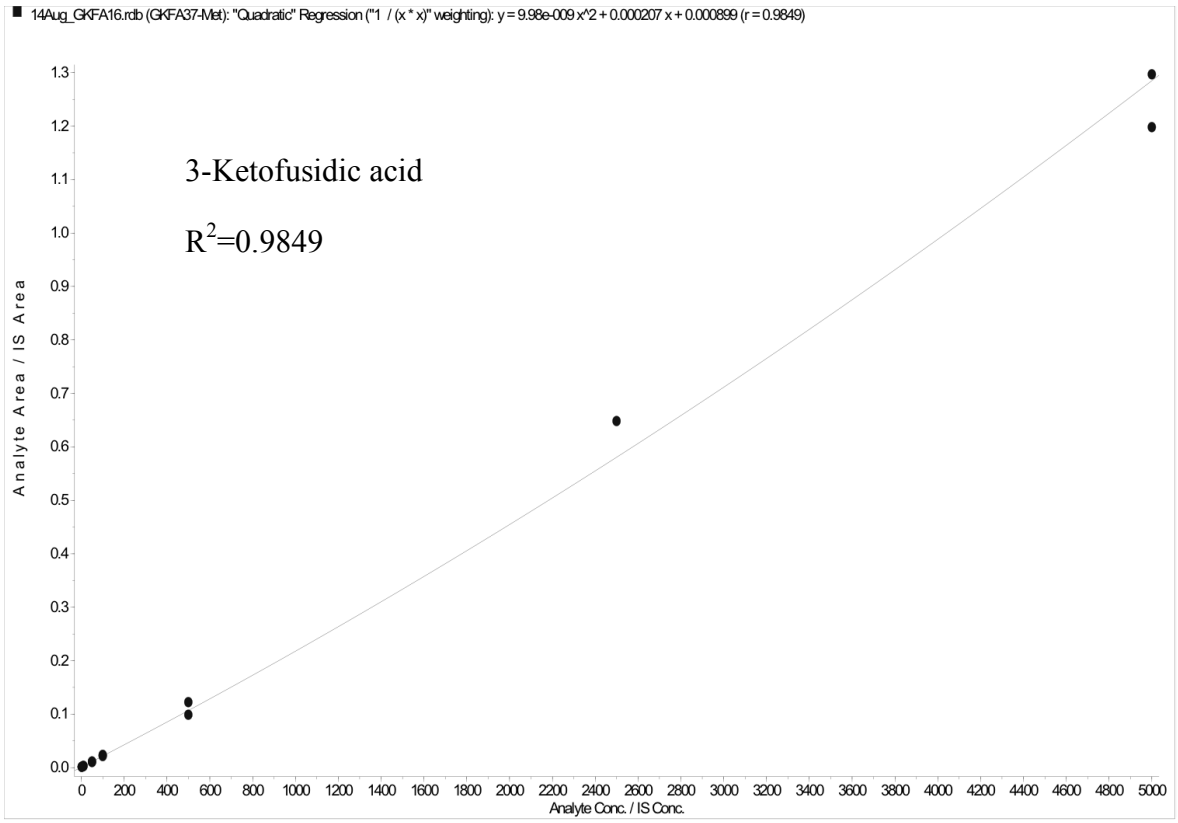
14Aug_GKFA16.rdb (GKFA37-Met): "Quadratic" Regression ("1 / (x * x)" weighting): y = 9.98e-009 x^2 + 0.000207 x + 0.000899 (r = 0.9849)
3-Ketofusidic acid
R2=0.9849
Analyte Area / IS Area
Analyte Conc. / IS Conc.

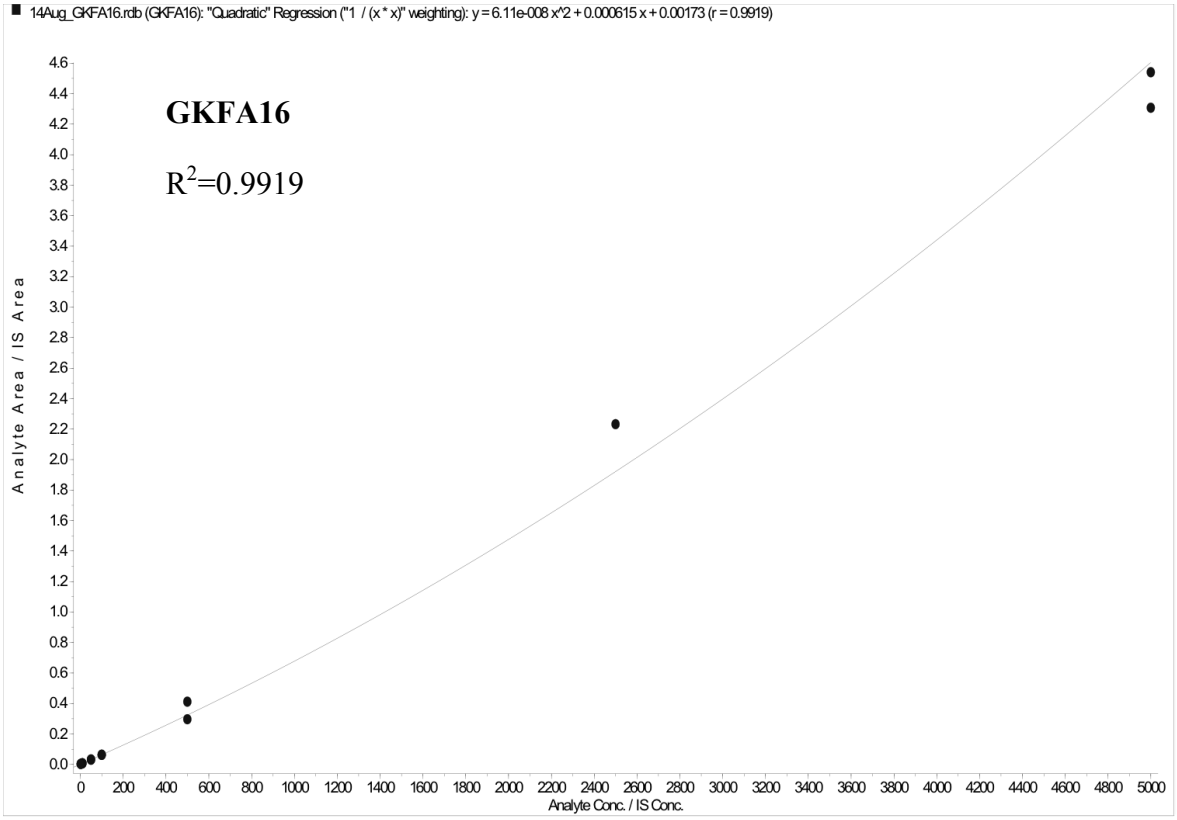

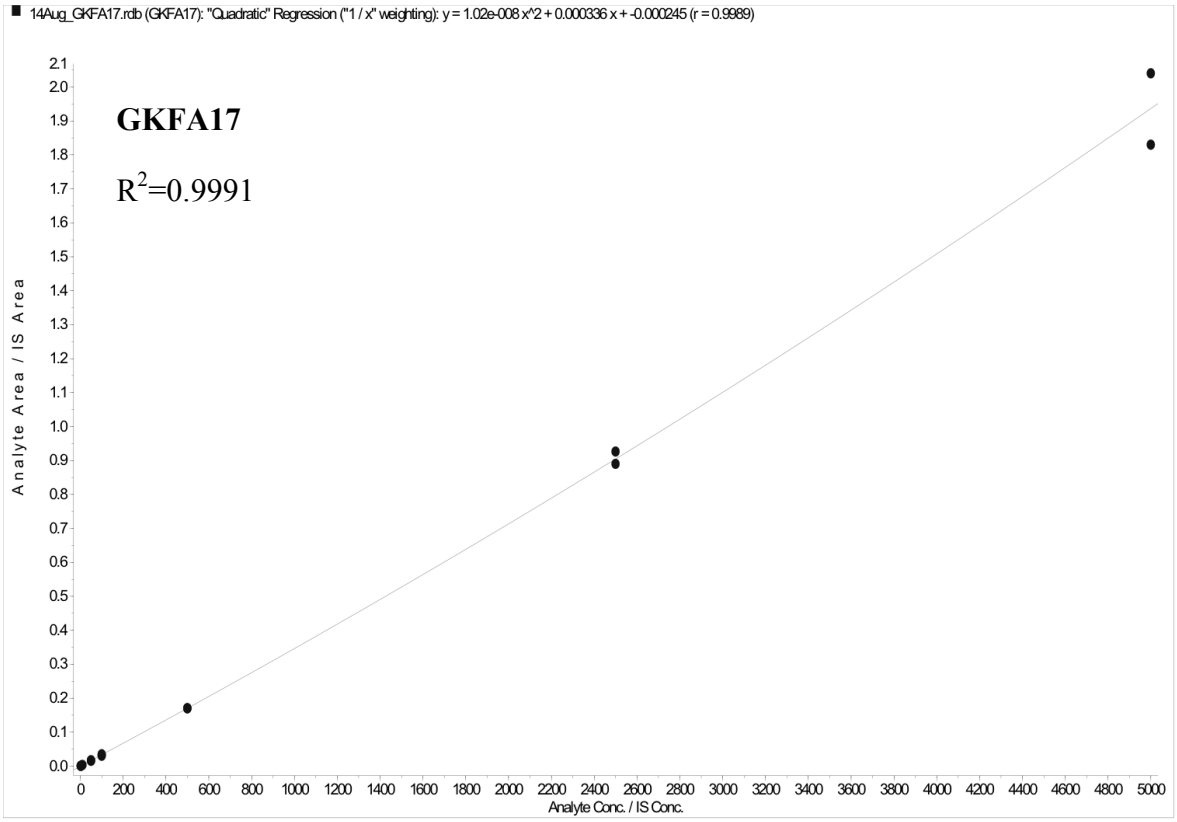

Figure 7-13: Calibration curves of fusidic acid analogues

The calibration curve of A: Fusidic acid, B: 3-Keto-fusidic acid, C: **GKFA16** and D: **GKFA17** constructed from calibration standards made in whole blood.

The low quality control samples of each analyte with respective internal standard is shown in Figure 7-14.

In Figure 7-15 is shown the blank samples injected after the highest concentration standard from the final batches analysed with their respective carry-over displayed. All samples showed carry-over below the accepted 20% allowed.

A: Fusidic acid (6 ng/ml)

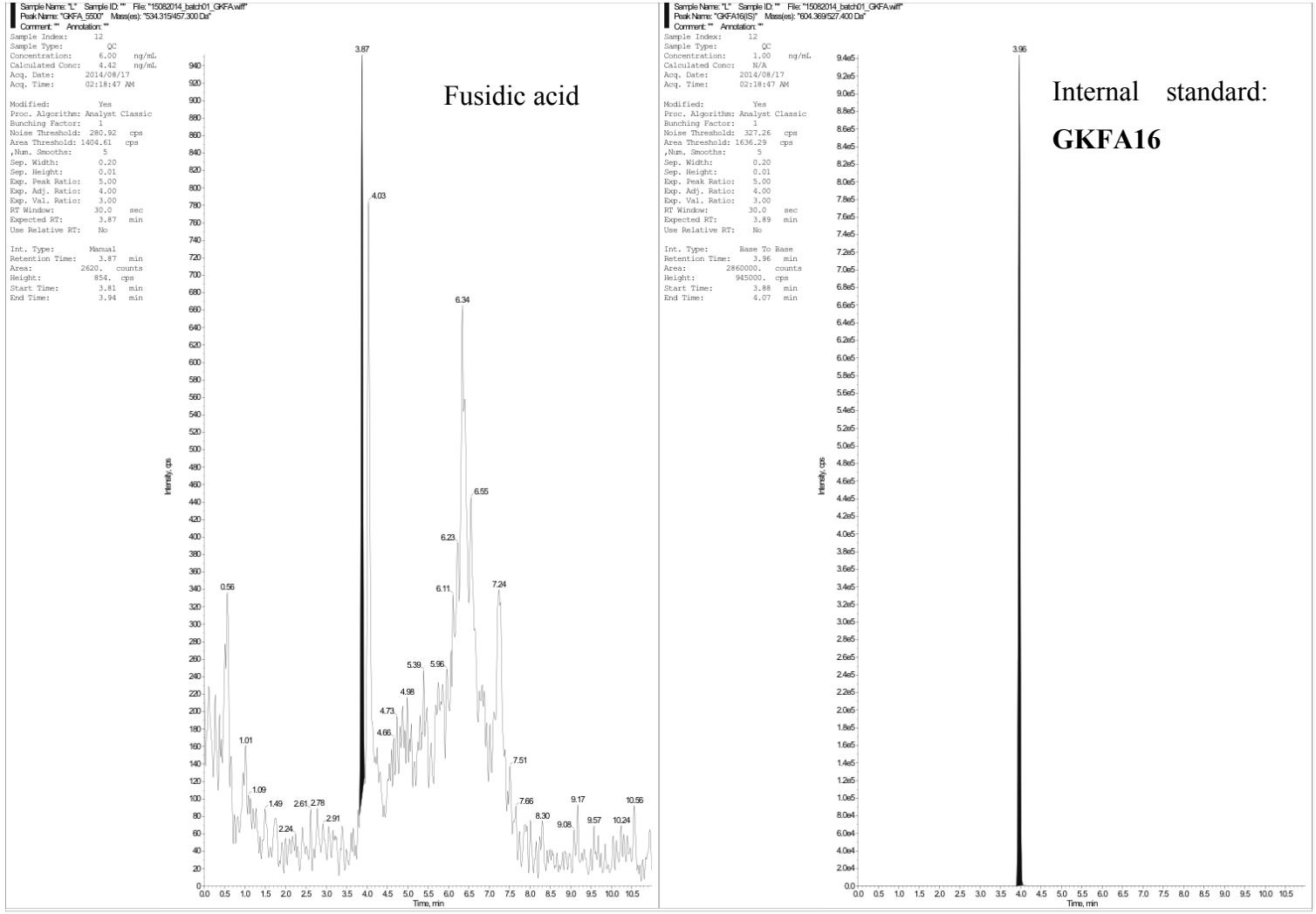

B: 3-Ketofusidic acid (6 ng/ml)

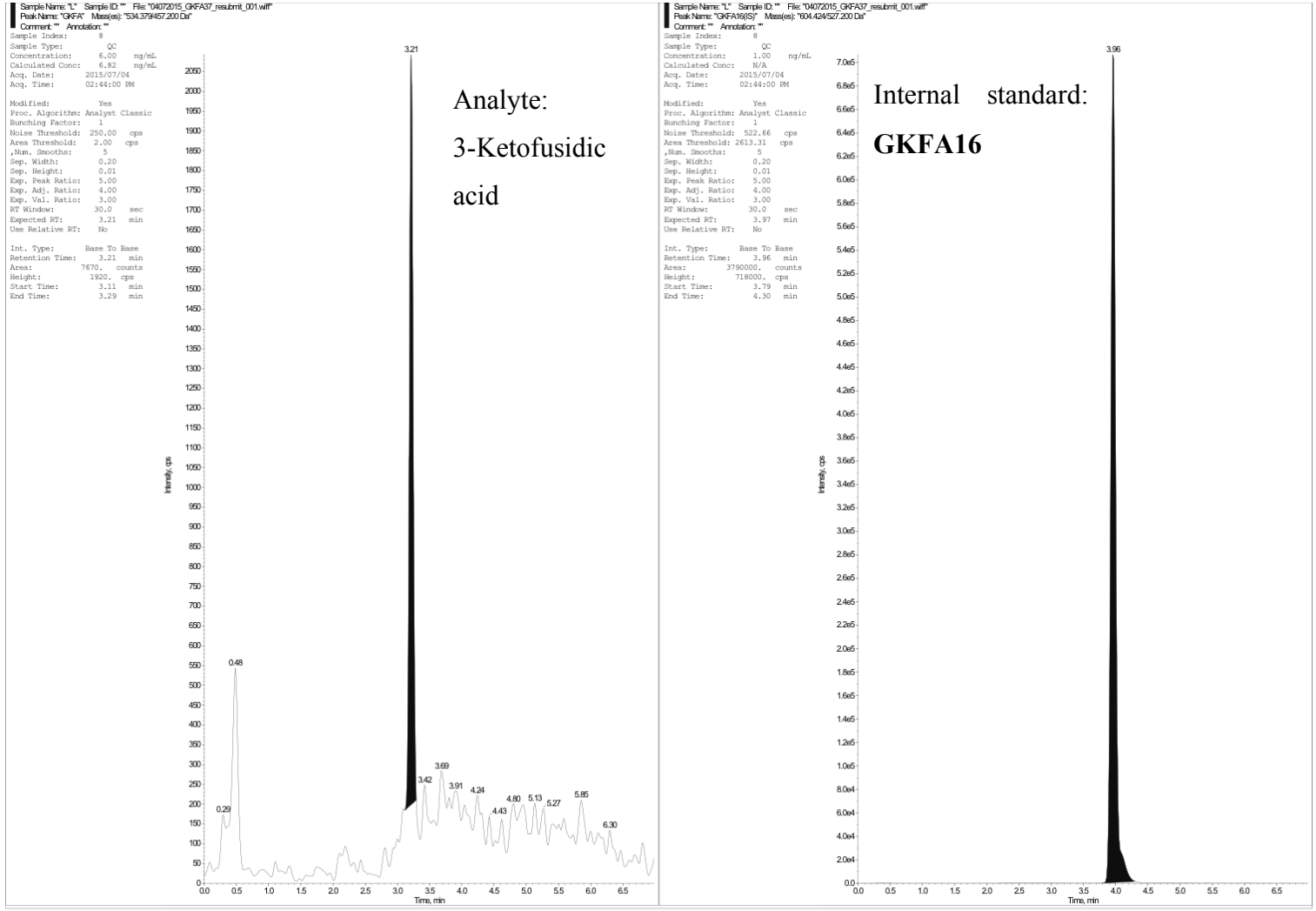

C: **GKFA16** (6 ng/ml)

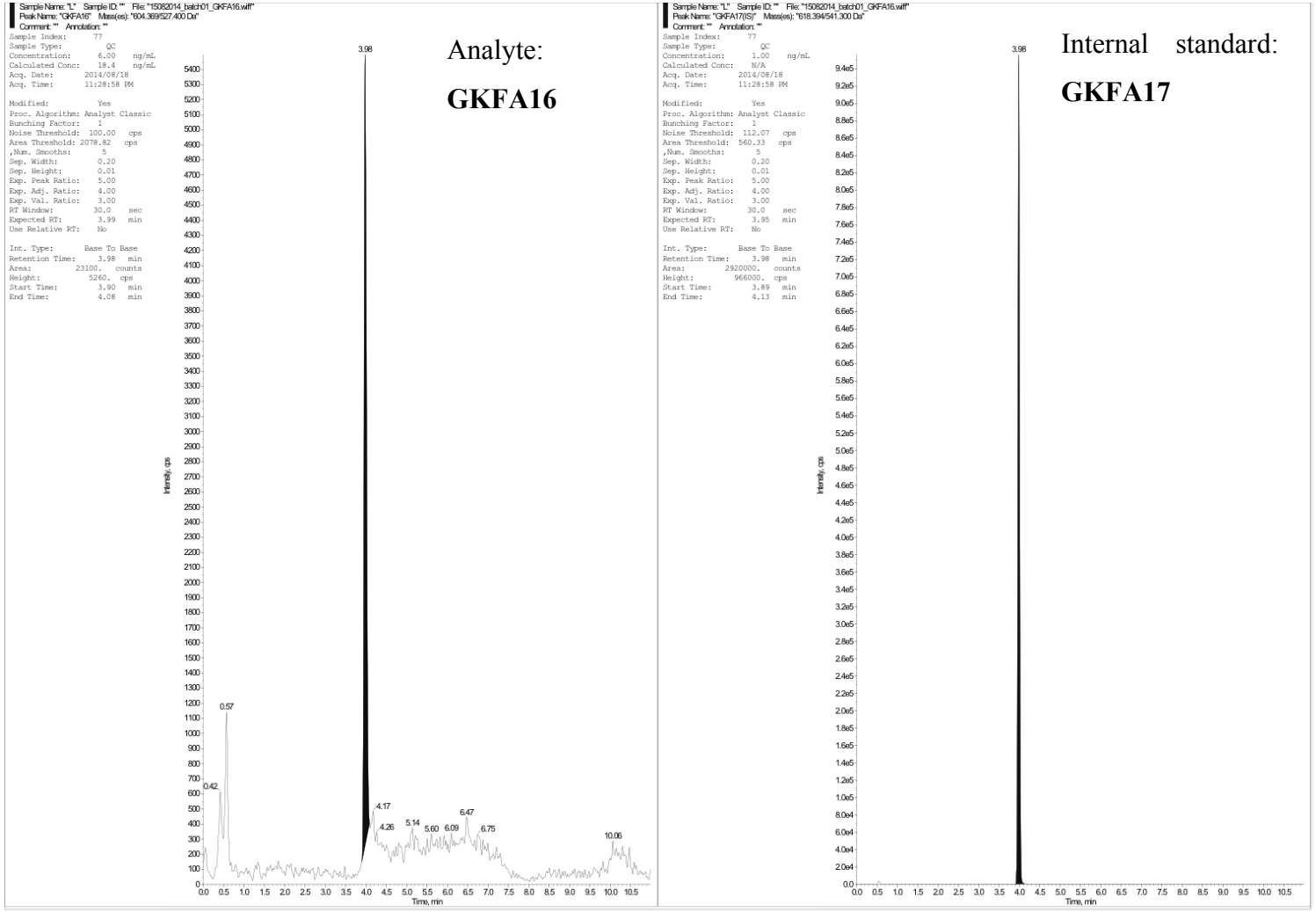

D: **GKFA17 (6 ng/ml)**

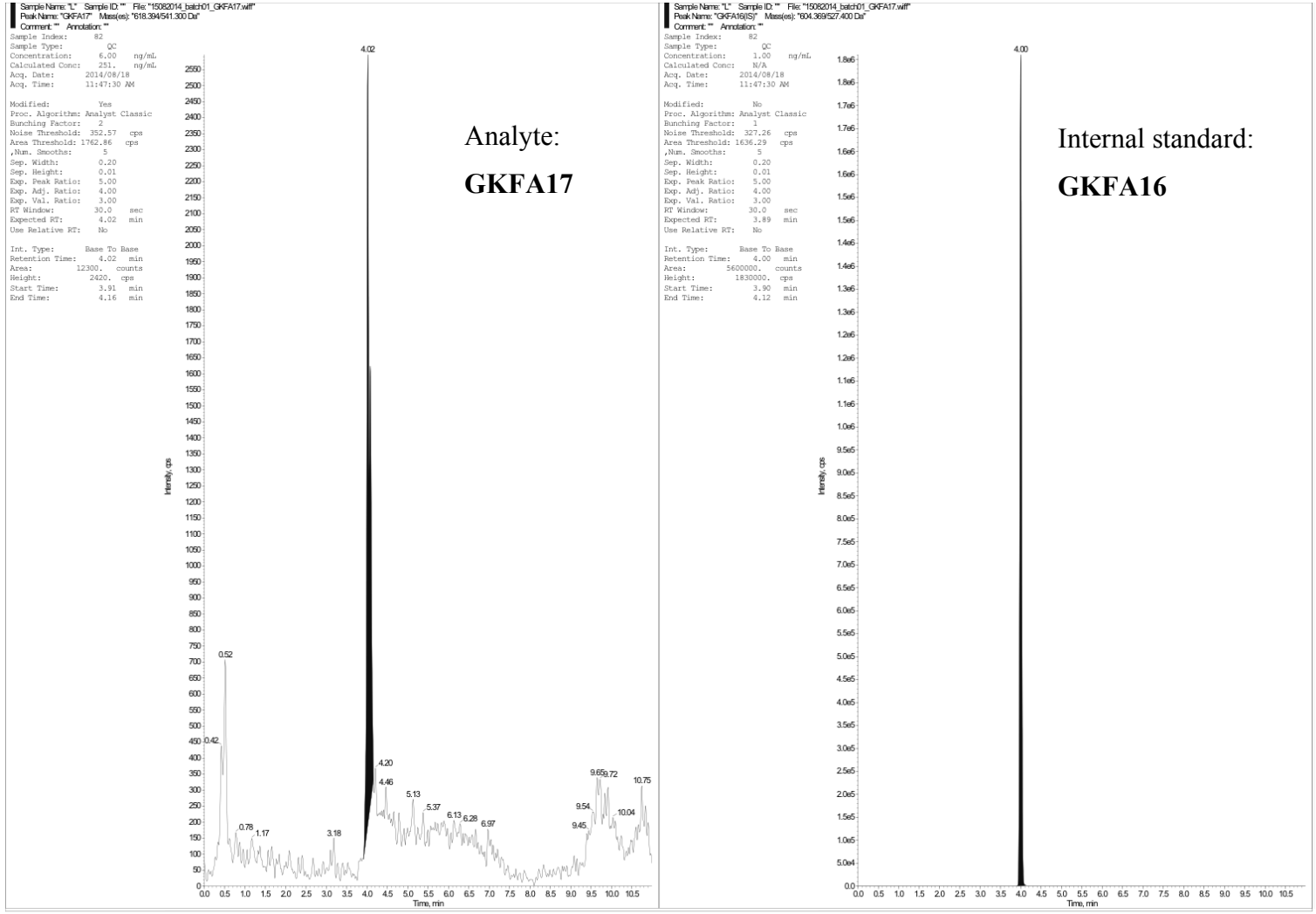

Figure 7-14: Low quality controls (6 ng/ml) of fusidic acid analytes Low quality controls of A: **DS23B**, B: **DS48B** and C: **DS50B** with respective internal standard.

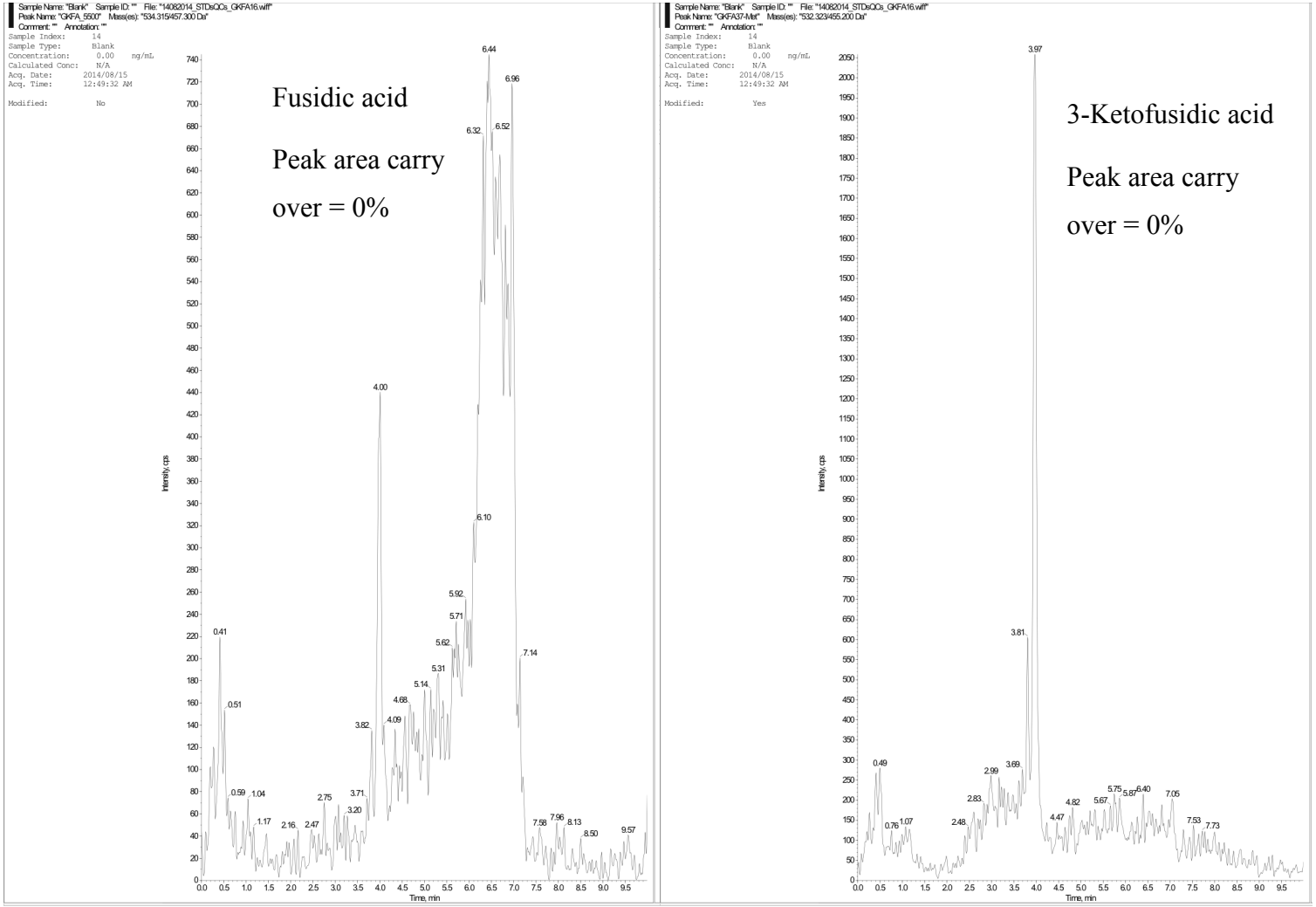
Sample Name: "Blank" Sample ID: "" File: "14082014_STDsQCs_GKFA16.wiff"
Peak Name: "GKFA_5500" Mass(es): "534.315/457.300 Da"
Comment: "" Annotation: ""
Sample Index: 14
Sample Type: Blank
Concentration: 0.00 ng/mL
Calculated Conc: N/A
Acq. Date: 2014/08/15
Acq. Time: 12:49:32 AM
Modified: No
Fusidic acid
Peak area carry
over = 0%
Intensity, cps
Time, min
Sample Name: "Blank" Sample ID: "" File: "14082014_STDsQCs_GKFA16.wiff"
Peak Name: "GKFA37-Met" Mass(es): "532.323/455.200 Da"
Comment: "" Annotation: ""
Sample Index: 14
Sample Type: Blank
Concentration: 0.00 ng/mL
Calculated Conc: N/A
Acq. Date: 2014/08/15
Acq. Time: 12:49:32 AM
Modified: Yes
3-Ketofusidic acid
Peak area carry
over = 0%
Intensity, cps
Time, min

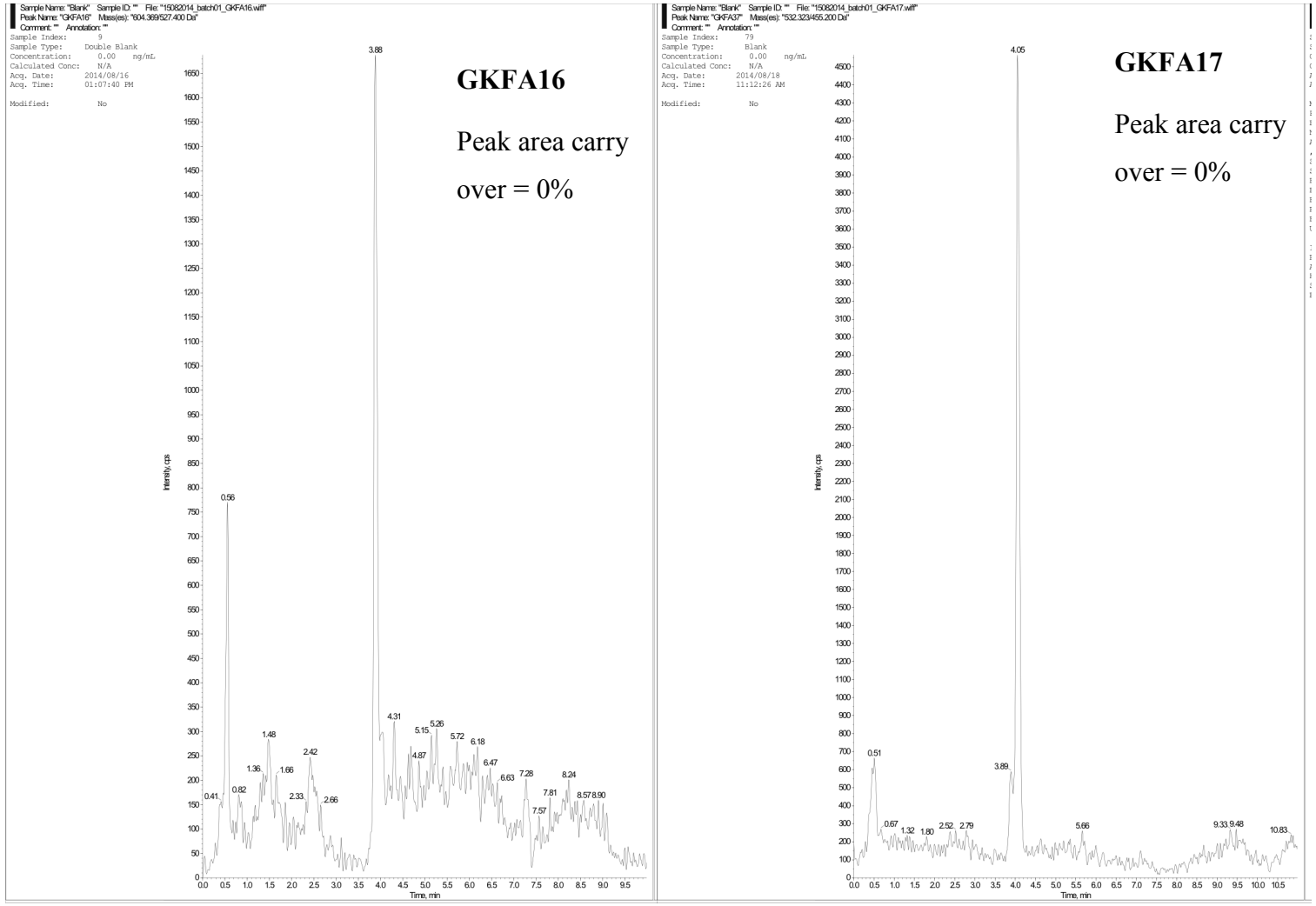

Figure 7-15: Blank samples of fusidic acid compound evaluation.

7.4.2 Animal experiment

The animal experiments performed for the fusidic acid analogues were described in Chapter 4, section 4.4.3.1, page 135.

In Table 7-29 to Table 7-32 are shown the experimental record sheets of the animal experiments. They contain exact sampling times, summary of dosage formulations and animal weight and sex.

Table 7-29: Fusidic acid animal experiment

Oral/IV dose - compound fusidic acid

Date:	3 June 2014		IV solution			Oral suspension		
Ethics no:	013/032							
Dose: Oral	25	mg/kg	Weighed:	1.25	mg	Weighed:	2.35	mg
Dose: IV	2.5	mg/kg		100	µL DMSO		1000	µL 0.5% HPMC
				100	µL EtOH			
				300	µL PEG 400			
				500	µL PPG			
			Dose:	60 µL		Dose:	250 µL	

Mouse	Weight (g)	Dose time	5 min	30 min	1	3	5	7
M1♂ IV	28.3	08:04:00	08:09:00	08:34:00	09:04:00	11:04:00	13:02:00	15:04:00
M2♂ IV	29.2	08:05:00	08:10:00	08:36:00	09:05:00	11:08:00	13:05:00	15:10:00
M3♂ IV	31.6	08:06:00	08:10:00	08:36:00	09:06:00	11:11:00	13:06:00	15:11:00
M4♂ ORAL	26.4	08:17:00	-	08:47:00	09:17:00	11:14:00	13:17:00	15:17:00
M5♂ ORAL	27.2	08:18:00	-	08:48:00	09:18:00	11:15:00	13:18:00	15:18:00
M6♂ ORAL	25.4	08:19:00	-	08:49:00	09:19:00	11:16:00	13:19:00	15:19:00

Table 7-30: 3-Ketofusidic acid animal experiment

Oral/IV dose – compound 3-ketofusidic acid

Date:	30 Oct 2014		IV solution			Oral suspension			
Ethics no:	013/032								
Dose: Oral	20	mg/kg	Weighed:	2.48	mg	Weighed:	2.45	mg	
Dose: IV	5	mg/kg		100	µL DMSO		1000	µL 0.5% HPMC	
				100	µL EtOH				
				300	µL PEG 400				
				500	µL PPG				
			Dose:	60 µL			Dose:	180 µL	
Mouse	Weight (g)	Dose time	5 min	30 min	1	3	5	7	24
M1♂ IV	28.1	08:04:00	07:13:00	07:18:00	07:44:00	08:14:00	10:14:00	12:14:00	15:11:00
M2♂ IV	30.6	08:05:00	07:15:00	07:19:00	07:45:00	08:16:00	10:16:00	12:15:00	15:12:00
M3♂ IV	29.1	08:06:00	07:16:00	07:20:00	07:46:00	08:18:00	10:18:00	12:16:00	15:14:00
M4♀ ORAL	22.2	08:17:00	07:10:00	-	07:40:00	08:11:00	10:06:00	12:10:00	15:06:00
M5♀ ORAL	21.8	08:18:00	07:10:00	-	07:41:00	08:12:00	10:08:00	12:11:00	15:08:00
M6♀ ORAL	21.1	08:19:00	07:10:00	-	07:42:00	08:13:00	10:10:00	12:12:00	15:10:00

Table 7-31: GKFA16 animal experiment

Oral/IV dose - compound **GKFA16**

Date:	18 June 2014		IV solution			Oral suspension		
Ethics no:	013/032							
Dose: Oral	25	mg/kg	Weighed:	1.25	mg	Weighed:	2.47	mg
Dose: IV	3	mg/kg		100	µL DMSO		1000	µL 0.5% HPMC
				100	µL EtOH			
				300	µL PEG 400			
				500	µL PPG			
			Dose:	60 µL		Dose:	250 µL	

Mouse	Weight (g)	Dose time	5 min	30 min	1	3	5	7
M1♂ IV	28.1	07:50:00	07:55:00	08:20:00	08:55:00	10:52:00	12:54:00	14:55:00
M2♂ IV	26.4	07:51:00	07:56:00	08:21:00	09:27:00	10:53:00	12:55:00	14:58:00
M3♂ IV	26.4	07:52:00	07:57:00	08:22:00	08:58:00	10:54:00	12:56:00	15:00:00
M4♂ ORAL	24.3	07:44:00	-	08:14:00	08:44:00	10:48:00	12:48:00	14:51:00
M5♂ ORAL	25.7	07:45:00	-	08:15:00	08:44:00	10:49:00	12:50:00	14:53:00
M6♂ ORAL	26.4	07:45:00	-	08:16:00	08:46:00	10:50:00	12:52:00	14:54:00

Table 7-32: GKFA17 animal experiment

Oral/IV dose - compound **GKFA17**

Date:	18 June 2014		IV solution			Oral suspension		
Ethics no:	013/032							
Dose: Oral	25	mg/kg	Weighed:	1.47	mg	Weighed:	2.38	mg
Dose: IV	3	mg/kg		100	µL DMSO		1000	µL 0.5% HPMC
				100	µL EtOH			
				300	µL PEG 400			
				500	µL PPG			
			Dose:	60 µL		Dose:	250 µL	

Mouse	Weight (g)	Dose time	5 min	30 min	1	3	5	7
M1♂ IV	27.8	08:47:00	08:52:00	09:18:00	09:47:00	11:44:00	13:48:00	15:46:00
M2♂ IV	28.2	08:48:00	08:53:00	09:19:00	09:48:00	11:46:00	13:50:00	15:47:00
M3♂ IV	25.6	08:49:00	08:54:00	09:20:00	09:48:00	11:47:00	13:52:00	15:48:00
M4♂ ORAL	24.2	08:39:00	-	09:14:00	09:39:00	11:39:00	13:41:00	15:42:00
M5♂ ORAL	21.6	08:40:00	-	09:15:00	09:40:00	11:41:00	13:43:00	15:43:00
M6♂ ORAL	26.1	08:40:00	-	09:17:00	09:40:00	11:42:00	13:45:00	15:44:00

7.4.3 Individual concentration profiles & data analysis

7.4.3.1 Non-compartmental analysis

The summarised pharmacokinetic results of the formulation study were presented in Table 4-4 to Table 4-7, starting in section 4.5.3.1, page 144. The expanded individual results with individual raw concentration vs time data is presented below in

Table 7-33 to Table 7-40 for fusidic acid, 3-ketofusidic acid, **GKFA16** and **GKFA17** respectively. Similarly non-compartmental analysis results by compound are presented in Table 7-37 to Table 7-40.

Table 7-33: Individual concentrations (µM) of fusidic acid experiment

IV							
M1	Time (hr)	0.0833	0.5	1	3	4.97	7
Conc	FA (µM)	3.51	0.804	0.372	-	-	-
Conc	k-FA (µM)	0.0146	0.0241	0.0309	-	-	-
Conc	e-FA (µM)	3.55	0.0605	0.0574	-	-	-
M2	Time (hr)	0.0833	0.517	1	3.05	5	7.08
Conc	FA (µM)	1.66	0.539	0.304	0.161	0.0129	0.00448
Conc	k-FA(µM)	0.0103	0.01	0.00907	0.0458	0.0192	-
Conc	e-FA(µM)	1.68	0.0205	0.055	0.045	-	0.00322
M3	Time (hr)	0.0667	0.5	1	3.08	5	7.08
Conc	FA(µM)	1.11	0.709	0.552	0.256	0.0351	0.0198
Conc	k-FA(µM)	0.00746	0.0245	0.0262	0.00174	0.0311	0.00614
Conc	e-FA(µM)	1.13	0.0874	0.0891	0.063	0.0432	-
Mean	Time (hr)	0.0778	0.506	1	3.04	4.99	7.06
Conc	FA(µM)	2.09	0.684	0.41	0.209	0.024	0.0121
Conc	k-FA(µM)	0.0108	0.0195	0.0221	0.0238	0.0251	0.00307
Conc	e-FA(µM)	2.12	0.0561	0.0672	0.054	0.0432	0.00161
P.O							
M4	Time (hr)		0.5	1	2.95	5	7
Conc	FA(µM)		1.3	0.725	0.189	0.0758	0.0581
Conc	k-FA(µM)		0.229	0.189	0.0452	0.0532	0.0416
Conc	e-FA(µM)		5.1	0.924	0.0938	0.0886	0.0349
M5	Time (hr)		0.5	1	2.95	5	7
Conc	FA(µM)		0.711	0.467	0.0328	0.0183	0.0191
Conc	k-FA(µM)		0.237	0.239	0.0252	0.0425	0.0249
Conc	e-FA(µM)		1.01	0.711	0.0256	0.0572	0.179
M6	Time (hr)		0.5	1	2.95	5	7
Conc	FA(µM)		1.62	1.12	0.0537	0.0328	0.031
Conc	k-FA(µM)		0.272	0.305	0.0276	0.0829	0.0639
Conc	e-FA(µM)		1.7	1.52	0.045	0.0601	0.112
Mean	Time (hr)		0.5	1	2.95	5	7
Conc	FA(µM)		1.21	0.769	0.0917	0.0423	0.0361
Conc	k-FA(µM)		0.246	0.244	0.0327	0.0595	0.0434
Conc	e-FA(µM)		2.6	1.05	0.0548	0.0686	0.109

Note: M1 represents individual mouse 1, M2 individual mouse 2 etc. M1 – M3 received intravenous (IV) doses and M4 – M6 received oral (P.O.; per os) doses.

Table 7-34: Individual concentration (µM) of 3-ketofusidic acid experiment

IV								
M1	Time (hr)	0.0833	0.517	1.02	3.02	5.02	7.97	24
Conc	k-FA(µM)	2.42	0.543	0.161	0.0132	0.00605	0.0103	0.00018
Conc	FA(µM)	0.0375	0.0097	0.00815	0.00517	0.00017	0.00325	-
Conc	e-FA(µM)	14.6	8.01	2.82	0.0957	0.0211	0.122	-
M2	Time(hr)	0.0667	0.5	1.02	3.02	5	7.95	24
Conc	k-FA(µM)	1.9	0.471	0.121	0.0146	0.0299	0.0146	0.00035
Conc	FA(µM)	0.0163	0.00726	0.00879	0.00406	-	0.00071	-
Conc	e-FA(µM)	11.9	4.85	1.65	0.0726	0.138	0.154	-
M3	Time (hr)	0.0667	0.5	1.03	3.03	5	7.97	24
Conc	k-FA(µM)	3.03	0.776	0.233	0.0256	0.0115	0.0359	0.00055
Conc	FA(µM)	0.042	0.0103	0.00623	0.00284	0.00023	0.0213	-
Conc	e-FA(µM)	16.4	8.99	2.31	0.174	0.027	0.128	0.0307
Mean	Time (hr)	0.0722	0.506	1.02	3.02	5.01	7.96	24
Conc	k-FA(µM)	2.45	0.597	0.172	0.0178	0.0158	0.0202	0.00036
Conc	FA(µM)	0.032	0.00909	0.00772	0.00403	0.00013	0.00842	-
Conc	e-FA(µM)	14.3	7.29	2.26	0.114	0.0619	0.135	0.0102
P.O.								
M4	Time (hr)		0.5	1.02	2.93	5	7.93	24
Conc	k-FA(µM)		1.43	0.572	0.347	0.271	0.743	0.00152
Conc	FA(µM)		0.0221	0.00552	0.00515	0.00439	0.00915	-
Conc	e-FA(µM)		0.948	0.28	0.268	0.199	0.637	-
M5	Time (hr)		0.517	1.03	2.97	5.02	7.97	24
Conc	k-FA(µM)		3.99	2.93	1.29	0.593	0.287	0.00206
Conc	FA(µM)		0.0656	0.0439	0.0107	0.00704	0.00447	-
Conc	e-FA(µM)		5.56	3	1.65	0.654	0.623	-
M6	Time (hr)		0.533	1.05	3	5.03	8	24
Conc	k-FA(µM)		5	1.81	1.17	0.723	0.655	0.00764
Conc	FA(µM)		0.0884	0.0308	0.00952	0.009	0.0116	0.00025
Conc	e-FA(µM)		3.06	0.895	0.708	0.454	0.481	0.00058
Mean	Time (hr)		0.517	1.03	2.97	5.02	7.97	24
Conc	k-FA(µM)		3.47	1.77	0.935	0.529	0.562	0.00374
Conc	FA(µM)		0.0587	0.0267	0.00845	0.00681	0.0084	8.4E-05
Conc	e-FA		5.31	1.79	0.292	0.204	0.252	0.00019

Note: M1 represents individual mouse 1, M2 individual mouse 2 etc. M1 – M3 received intravenous (IV) doses and M4 – M6 received oral (P.O.; per os) doses.

Table 7-35: Individual concentrations (µM) of GKFA16 experiment

IV							
M1	Time (hr)	0.0833	0.517	1	2.95	5.02	6.98
Conc(µM)	**GKFA16**	2.45	1.05	0.813	0.153	0	0
Conc(µM)	FA	0.628	0.349	0.496	0.109	0.00698	0.00897
Conc(µM)	k-FA	0.00973	0.0109	0.0181	0.0214	0.00439	0.013
Conc(µM)	e-FA	0	0	0	0	0	0
M2	Time (hr)	0.0833	0.517	1	2.97	5.03	6.98
Conc(µM)	**GKFA16**	3.08	0.998	0.608	0.107	-	-
Conc(µM)	FA	0.721	0.378	0.372	0.229	0.00795	0.0215
Conc(µM)	k-FA	0.0204	0.0129	0.0225	0.0249	0.00472	0.00998
Conc(µM)	e-FA	-	-	-	0.0168	-	-
M3	Time (hr)	0.0833	0.517	0.983	2.97	5.05	6.98
Conc(µM)	**GKFA16**	3.64	0.816	0.389	0.0662	-	-
Conc(µM)	FA	0.44	0.19	0.136	0.194	0.0112	-
Conc(µM)	k-FA	0.00868	0.00806	0.0111	0.0245	0.00581	0.00305
Conc(µM)	e-FA	-	-	-	0.0231	-	-
Mean	Time	0.0833	0.517	0.994	2.96	5.03	6.98
Conc(µM)	**GKFA16**	3.06	0.953	0.603	0.108	-	-
Conc(µM)	FA	0.596	0.306	0.335	0.177	0.00872	0.0102
Conc(µM)	k-FA	0.0129	0.0106	0.0172	0.0236	0.00497	0.00867
Conc(µM)	e-FA	-	-	-	0.0133	-	-
P.O.							
M4	Time (hr)		0.583	1	3	5.03	7.05
Conc(µM)	**GKFA16**		3.7	1.13	0.0543	0.112	-
Conc(µM)	FA		1.26	0.316	0.0246	0.0386	0.0127
Conc(µM)	k-FA		0.19	0.105	0.0256	0.0835	0.0414
Conc(µM)	e-FA		1.13	0.3	0.00591	0.0236	0.00876
M5	Time (hr)		0.583	1	3.02	5.05	7.05
Conc(µM)	**GKFA16**		4.01	1.79	0.059	0.0545	0.0273
Conc(µM)	FA		1.01	0.444	0.0164	0.00998	-
Conc(µM)	k-FA		0.118	0.125	0.0101	0.0268	0.0254
Conc(µM)	e-FA		0.488	0.444	-	-	0.00517
M6	Time (hr)		0.617	1	3.03	5.08	7.07
Conc(µM)	**GKFA16**		8.83	7.51	0.161	0.102	0.0487
Conc(µM)	FA		2.93	2.33	0.0359	0.0266	0.0172
Conc(µM)	k-FA		0.264	0.499	0.0208	0.0278	0.0342
Conc(µM)	e-FA		2.07	3.8	0.0122	0.00953	0.0103
Mean	Time (hr)		0.594	1	3.02	5.06	7.06
Conc(µM)	**GKFA16**		5.51	3.48	0.0915	0.0897	0.0253
Conc(µM)	FA		1.73	1.03	0.0256	0.025	0.00996
Conc(µM)	k-FA		0.191	0.243	0.0188	0.046	0.0337
Conc(µM)	e-FA		1.23	1.51	0.00602	0.0111	0.00809

Table 7-36: Individual concentrations (µM) of GKFA17

IV							
M1	Time(hr)	0.0833	0.517	1	2.95	5.02	6.98
Conc(µM)	**GKFA17**	0.906	0.263	0.193	0.0526	0.00585	-
Conc(µM)	FA	0.572	0.215	0.185	0.134	0.00886	-
Conc(µM)	k-FA	0.00332	0.00365	0.00089	0.0162	-	0.00109
Conc(µM)	e-FA	0	0	0	0	0	0
M2	Time(hr)	0.0833	0.517	1	2.97	5.03	6.98
Conc(µM)	**GKFA17**	0.821	0.207	0.232	0.0422	0.0113	-
Conc(µM)	FA	0.537	0.17	0.146	0.0808	0.0152	0.00812
Conc(µM)	k-FA	0.00109	-	-	0.0109	0.0052	0.00114
Conc(µM)	e-FA	-	-	-	0.0324	-	-
M3	Time(hr)	0.0833	0.517	0.983	2.97	5.05	6.98
Conc(µM)	**GKFA17**	1.04	0.197	0.215	0.0371	0.00812	-
Conc(µM)	FA	0.709	0.177	0.18	0.0868	0.0173	0.00959
Conc(µM)	k-FA	0.00402	0.00039	0.00305	0.0157	0.00437	0.00014
Conc(µM)	e-FA	-	-	-	0.0446	0.0105	-
Mean	Time(hr)	0.0833	0.517	0.994	2.96	5.03	6.98
Conc(µM)	**GKFA17**	0.923	0.222	0.214	0.044	0.00842	-
Conc(µM)	FA	0.606	0.187	0.17	0.101	0.0138	0.0059
Conc(µM)	k-FA	0.00281	0.00135	0.00131	0.0143	0.00319	0.00079
Conc(µM)	e-FA	-	-	-	0.0444	0.00351	-
P.O.							
M4	Time(hr)		0.583	1	3	5.03	7.05
Conc(µM)	**GKFA17**		1.5	1.26	0.045	0.0116	-
Conc(µM)	FA		3.06	1.56	0.0422	0.0242	0.0112
Conc(µM)	k-FA		0.841	0.672	0.0359	0.0736	0.026
Conc(µM)	e-FA		10.5	5.66	0.0914	0.228	0.0464
M5	Time(hr)		0.583	1	3.02	5.05	7.05
Conc(µM)	**GKFA17**		3.52	0.508	0.021	-	-
Conc(µM)	FA		4.88	0.771	0.0271	0.0182	0.0225
Conc(µM)	k-FA		2.82	0.722	0.032	0.0487	0.0757
Conc(µM)	e-FA		19.3	3.78	0.0553	0.0727	0.165
M6	Time(hr)		0.617	1	3.03	5.08	7.07
Conc(µM)	**GKFA17**		1.73	0.561	0.0726	-	0.0124
Conc(µM)	FA		2.34	0.473	0.1	0.0168	0.0145
Conc(µM)	k-FA		0.777	0.243	0.0652	0.0827	0.0522
Conc(µM)	e-FA		8.91	1.68	0.269	0.259	0.148
Mean	Time(hr)		0.594	1	3.02	5.06	7.06
Conc(µM)	**GKFA17**		2.25	0.776	0.0462	0.00387	0.00414
Conc(µM)	FA		3.43	0.935	0.0566	0.0197	0.016
Conc(µM)	k-FA		1.48	0.546	0.0444	0.0683	0.0513
Conc(µM)	e-FA		12.9	3.71	0.138	0.187	0.12

Note: M1 represents individual mouse 1, M2 individual mouse 2 etc. M1 – M3 received intravenous (IV) doses and M4 – M6 received oral (P.O.; per os) doses.

Table 7-37: Non-compartmental analysis of fusidic acid parent

IV	M1	M2	M3	Mean	S.E.
Apparent half-life (h)	1.1	0.286	1.07	0.819	0.267
Blood Clearance (ml/min/kg)		53.1	42.8	47.9	4.22
Vc (L/kg)		2.17	3.81	2.99	0.817
Vss (L/kg)		7.22	5.54	6.38	0.686
AUC0-inf (µM.min)		91.9	109	101	7.02
P.O.	M4	M5	M6	Mean	S.E.
Apparent half-life (h)	1.46	1.23	1.1	1.27	0.106
$AUC_{0\text{-}inf}$ (µM.min)	135	66	146	116	25.1

Note: IV; intravenous, P.O.; per os/oral, Vc; central volume, Vss; volume at steady state, $AUC_{0\text{-}inf}$; area under the curve from time zero to infinity. Individual values corresponding to the same labelled raw concentration vs time data is represented with the calculated mean and standard error of the mean (S.E.).

Table 7-38: Non-compartmental analysis of 3-ketofusidic acid parent

IV	M1	M2	M3	Mean	S.E.
Apparent half-life (h)	3.35	3.44	3.57	3.45	0.0636
Blood Clearance (ml/min/kg)	125	138	83.4	116	16.6
Vc (L/kg)	3.17	3.84	3.52	3.51	0.192
Vss (L/kg)	45.3	36.7	32.4	38.1	3.79
AUC0-inf (µM.min)	82	68.2	119	89.7	15.1
P.O.	M4	M5	M6	Mean	S.E.
Apparent half-life (h)	2.49	2.29	2.74	2.51	0.129
$AUC_{0\text{-}inf}$ (µM.min)	591	747	918	752	94.3

Note: IV; intravenous, P.O.; per os/oral, Vc; central volume, Vss; volume at steady state, $AUC_{0\text{-}inf}$; area under the curve from time zero to infinity. Individual values corresponding to the same labelled raw concentration vs time data is represented with the calculated mean and standard error of the mean (S.E.).

Table 7-39: Non-compartmental analysis of GKFA16 parent

IV	M1	M2	M3	Mean	S.E.
Apparent half-life (h)	0.627	0.681	0.925	0.744	0.0916
Blood Clearance (ml/min/kg)	24	29.6	3.93	19.2	7.78
Vc (L/kg)	0.257	0.689	0.886	0.611	0.186
Vss (L/kg)	0.273	1.43	2.14	1.28	0.545
AUC0-inf (μM.min)	196	169	133	166	18.2
P.O.	M4	M5	M6	Mean	S.E.
Apparent half-life (h)	0.415	1.12	0.907	0.814	0.209
$AUC_{0\text{-}inf}$ (μM.min)	218	280	893	464	215

Note: IV; intravenous, P.O.; per os/oral, Vc; central volume, Vss; volume at steady state, $AUC_{0\text{-}inf}$; area under the curve from time zero to infinity. Individual values corresponding to the same labelled raw concentration vs time data is represented with the calculated mean and standard error of the mean (S.E.).

Table 7-40: Non-compartmental analysis of GKFA17 parent

IV	M1	M2	M3	Mean	S.E.
Apparent half-life (h)	0.62	0.882	0.494	0.665	0.114
Blood Clearance (ml/min/kg)	75.5	99.7	39.5	71.6	17.5
Vc (L/kg)	0.55	2.01	0.14	0.903	0.566
Vss (L/kg)	0.569	5.57	0.145	2.1	1.74
AUC0-inf (μM.min)	64.5	48.2	136	82.9	26.9
P.O.	M4	M5	M6	Mean	S.E.
Apparent half-life (h)	0.935	1.52	1.58	1.34	0.206
$AUC_{0\text{-}inf}$ (μM.min)	144	147	109	133	12.2

Note: IV; intravenous, P.O.; per os/oral, Vc; central volume, Vss; volume at steady state, $AUC_{0\text{-}inf}$; area under the curve from time zero to infinity. Individual values corresponding to the same labelled raw concentration vs time data is represented with the calculated mean and standard error of the mean (S.E.).

7.4.3.2 Non-linear mixed effects modelling

Expanded from the summarised results shown in Chapter 4, section 4.5.3, page 144, Table 7-41 presents the non-linear mixed effects model parameter estimates.

The median values for the cohort are presented with their respective standard error and relative standard error determined by linearization of their Fischer information matrix. The fixed effects, covariate model, omega and sigma model values are shown.

.

Table 7-41: Parameter estimation of fusidic acid compounds

	Fusidic acid			3-Ketofusidic acid			**GKFA16**			**GKFA17**		
	Parameter	s.e. (lin)	r.s.e.(%)	Parameter	s.e. (lin)	r.s.e.(%)	Parameter	s.e. (lin)	r.s.e.(%)	Parameter	s.e. (lin)	r.s.e.(%)
Fixed Effects:												
Foral	0.124	0.032	26	3.03	0.68	22	0.435	0.15	35	0.445	0.064	14
ka (hr^{-1})	2.58	1.4	54	0.408	0.079	19	18	25	138	3	-	-
V (L)	0.0529	0.014	26	0.0898	0.027	30	0.0334	0.0063	19	0.0969	0.016	16
Cl (L/h)	0.0871	0.0098	11	0.232	0.039	17	0.0604	0.0066	11	0.201	0.017	9
Q (L/h)	0.0505	0.017	34	0.0898	0.033	37	0.0216	0.015	71	0.0676	0.052	77
Vp (L)	0.0748	0.017	22	0.248	0.073	29	0.0242	0.007	29	0.112	0.023	21
Covariate model:												
Beta V(t_WT)	1	-	-	1	-	-	1	-	-	1	-	-
Beta Cl (tWT)	0.75	-	-	0.75	-	-	0.75	-	-	0.75	-	-
Beta Vp(t_WT)	1	-	-	1	-	-	1	-	-	1	-	-
Parameter variability:												
Omega Foral	0.351	0.19	53	0	-	-	0.547	0.27	50	0.0411	0.39	961
Omega ka	0.0996	2.6	2.6E+03	0.165	0.19	116	1.06	1.2	110	0.19	0.31	164
Omega V	0	-	-	0	-	-	0.0898	0.44	494	0	-	-
Omega Cl	0	-	-	0.131	0.071	54	0.0877	0.13	144	0	-	-
Omega Q	0	-	-	0	-	-	1.48	0.58	39	1.71	0.66	39
Omega Vp	0	-	-	0	-	-	0.156	1.5	979	0	-	-
Sigma model:												
Proportional	0.00345	0.0033	96	0	-	-	0.00979	0.0076	78	0	-	-
Constant	0.405	0.069	17	0.498	0.063	13	0.322	0.11	35	0.303	0.034	11

Note: Foral; bioavailability, ka; rate of absorption, V; central volume, Cl; clearance, Q; inter-compartmental clearance, Vp; peripheral volume. Standard error (s.e.) and relative standard error (r.s.e) expressed as a percentage of the population estimate were estimated by linearization of the Fisher information matrix. The covariate tWT is defined as the transformed log individual mass of each mouse, centred around the median of the cohort mass. Parameter values equal to zero are parameters that were excluded from the model based on their statistical insignificance as determined by -2LL.

In Figure 7-16, shown below, is the individual plots and parameter information of each subject.

A: Fusidic acid

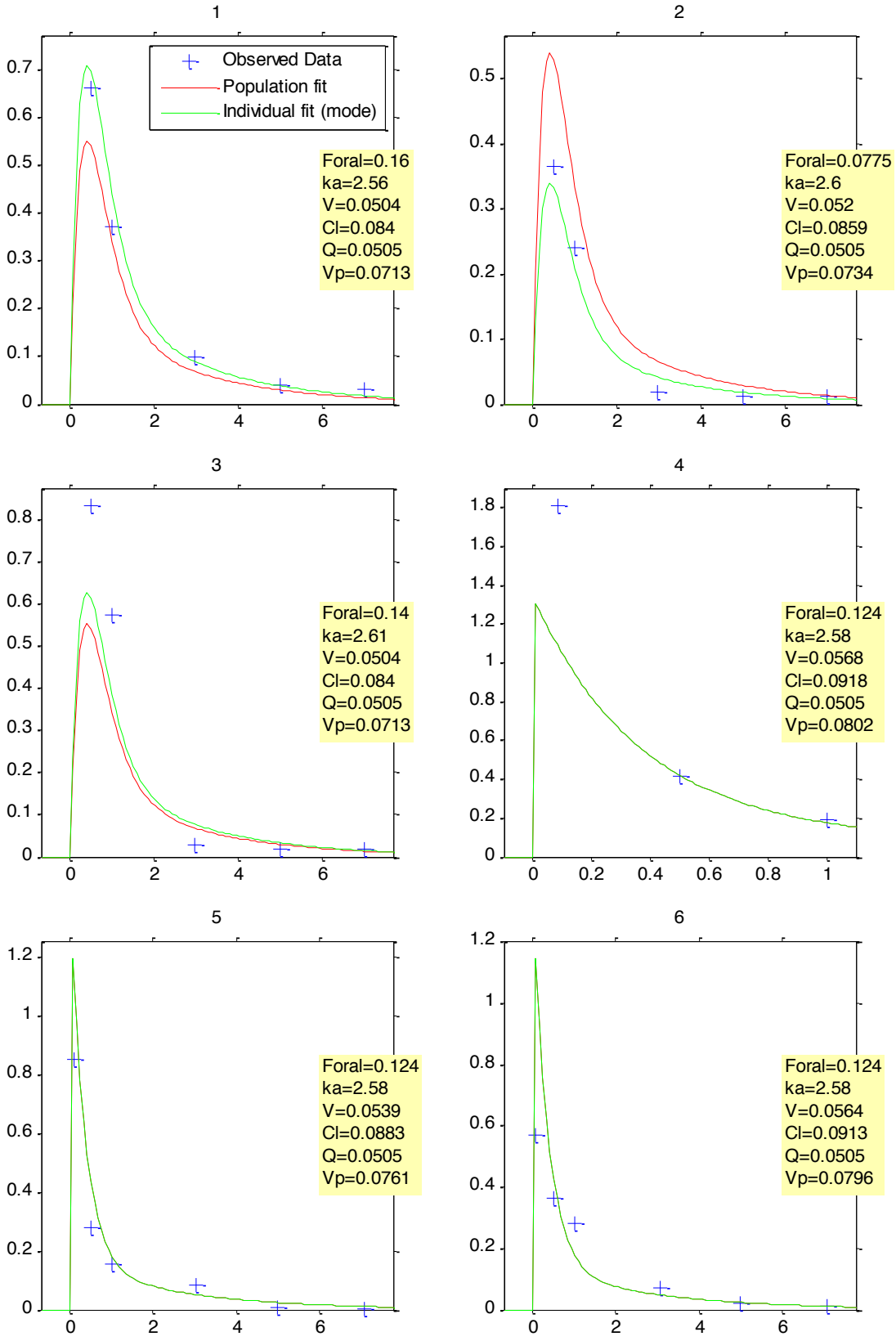

B: 3-Ketofusidic acid

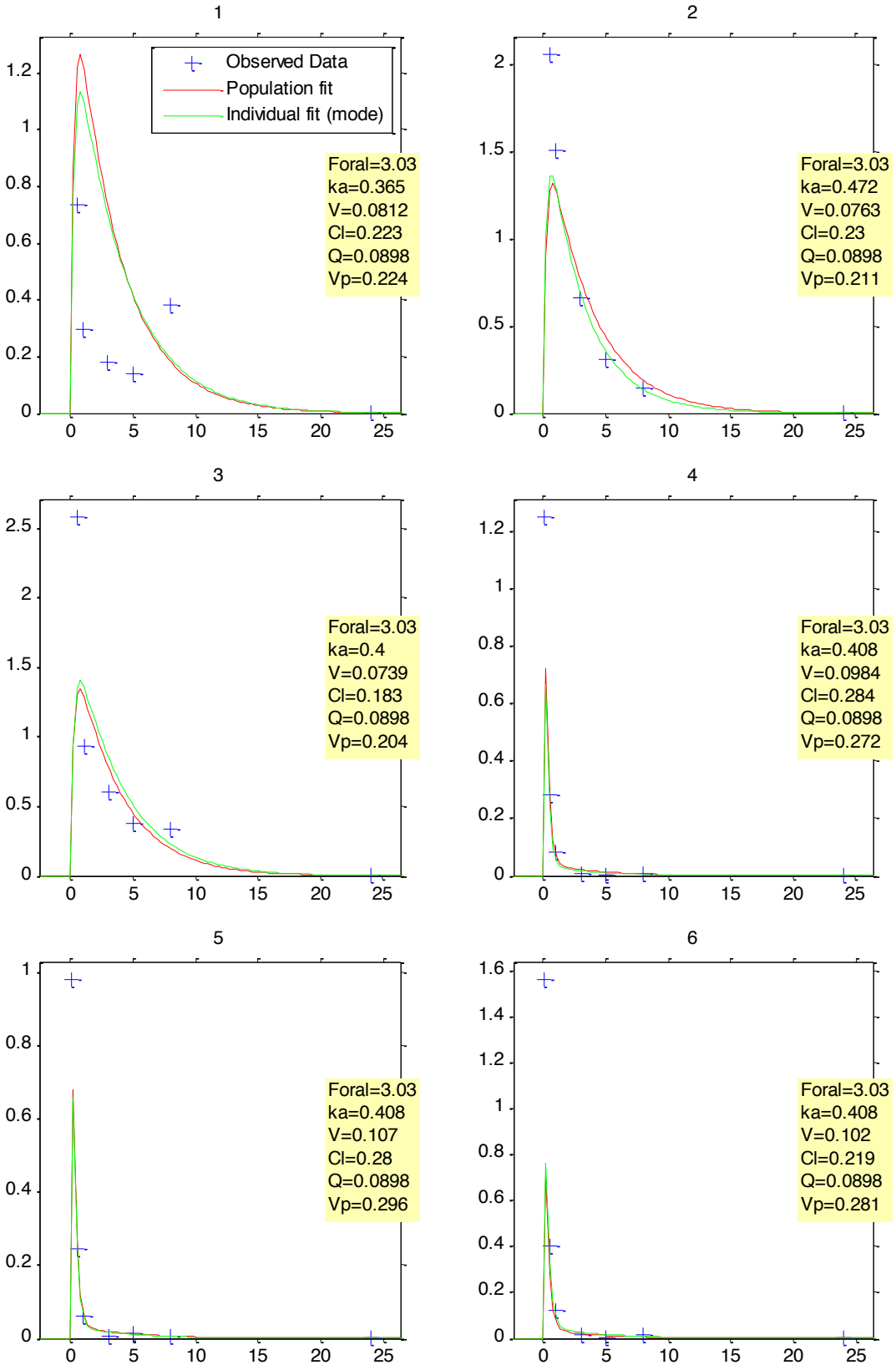

C: GKFA16

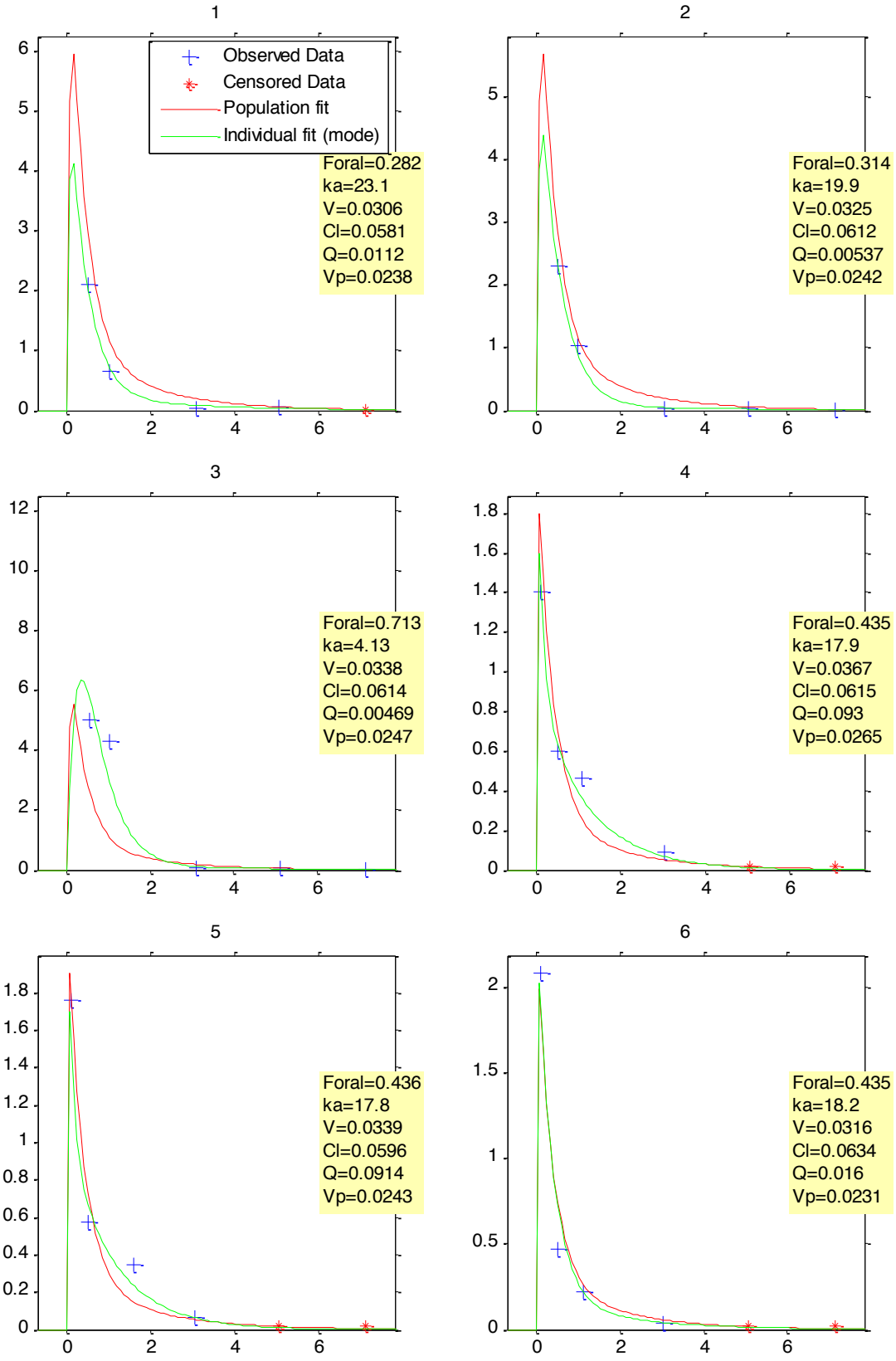
1
Observed Data
Censored Data
Population fit
Individual fit (mode)
Foral=0.282
ka=23.1
V=0.0306
Cl=0.0581
Q=0.0112
Vp=0.0238
2
Foral=0.314
ka=19.9
V=0.0325
Cl=0.0612
Q=0.00537
Vp=0.0242
3
Foral=0.713
ka=4.13
V=0.0338
Cl=0.0614
Q=0.00469
Vp=0.0247
4
Foral=0.435
ka=17.9
V=0.0367
Cl=0.0615
Q=0.093
Vp=0.0265
5
Foral=0.436
ka=17.8
V=0.0339
Cl=0.0596
Q=0.0914
Vp=0.0243
6
Foral=0.435
ka=18.2
V=0.0316
Cl=0.0634
Q=0.016
Vp=0.0231

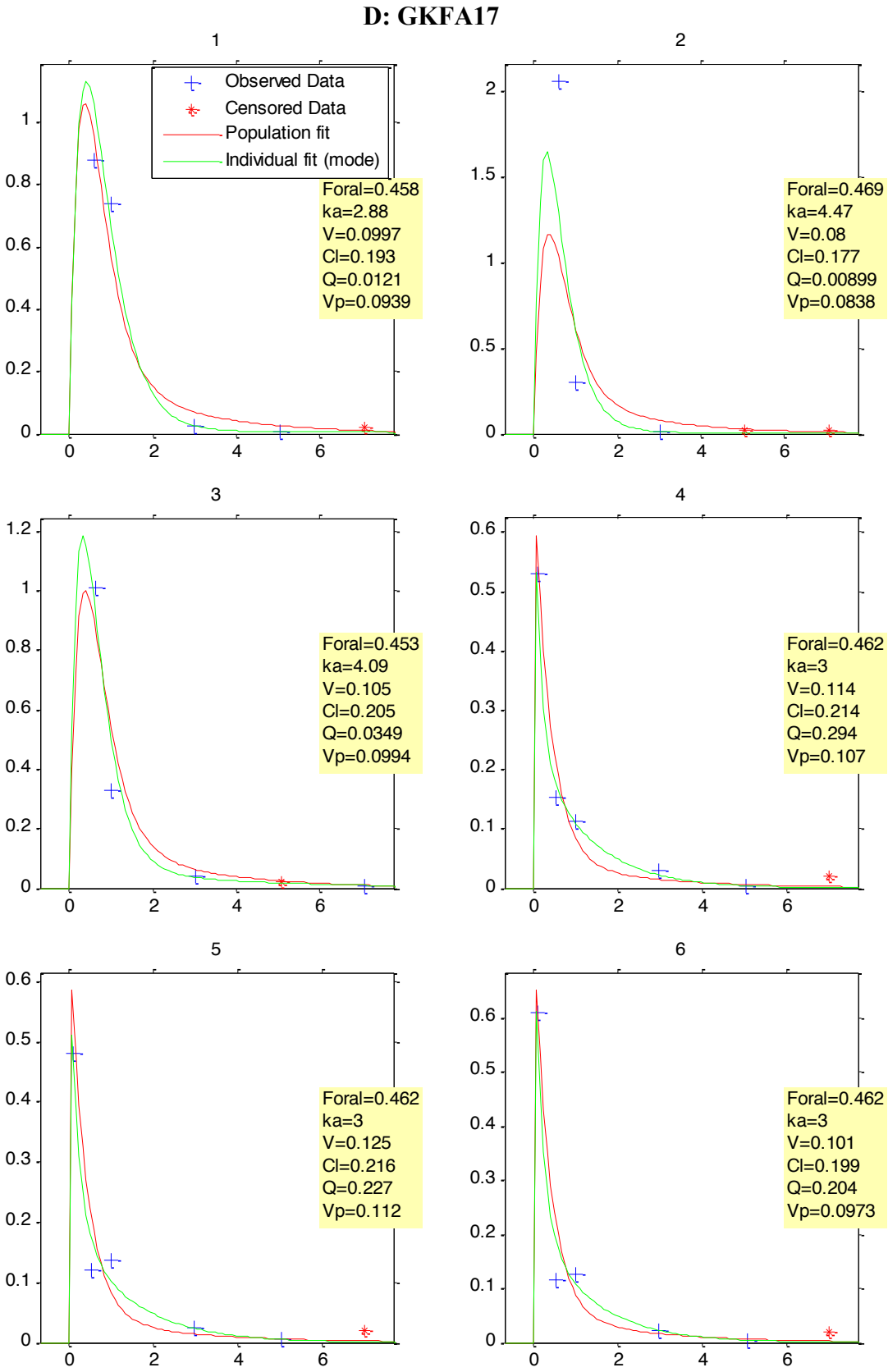

Figure 7-16: Individual plots of fusidic acid compounds

The graphical diagnostic individual fit output of all individual mice for A: fusidic acid, B: 3-keto-fusidic acid, C: **GKFA16**, D: **GKFA17**. The blue crosses represent the observed concentration data points from the experiment, the red stars represent the "censored" or below limit of quantification (BLQ) data and the green line represents the individual fit

after parameter variability for respective individual mice are included. The population fit represented by the red line, is the median of the cohort of both the oral and intravenous groups. The individual parameters of each mice are shown in the yellow legend.

7.5 Organ distribution of fusidic acid prodrugs

7.5.1 LC/MS/MS

7.5.1.1 Sample preparation

A liquid-liquid method was used to extract homogenized organ and whole blood samples on ice. A 20 µl volume of 250 ng/ml structurally similar internal standard solution in pH 3 universal buffer was added to the thawed sample except for the double blank sample that did not contain any internal standard in the buffer added, and briefly vortexed. An extraction volume of 250 µl ethyl acetate was added and samples were vortexed for 1 minute to allow analytes to move into the organic phase and then centrifuged for 5 minutes at 10 000 rcf. A 200 µl volume of the resulting ethyl acetate organic layer was transferred to a 96 well plate and dried under nitrogen and 100 µl of 20% methanol (v/v) in 0.03% ammonium hydroxide in water (v/v) added to each well. A 5 µl injection volume was used for LC-MS/MS quantification.

7.5.1.2 Mass spectrometer conditions and instrumentation

Same as previously described in Section 7.4.1.1.

7.5.1.3 HPLC conditions

Gradient chromatography shown in Table 7-42 was performed on a Phenomenex® Kinetex C_{18} (2.1 x 50 mm, 2.6 µm) reverse phase column with mobile phases A; 0.03% ammonium hydroxide:water (v/v) and B; 0.03% ammonium hydroxide:acetonitrile (v/v) at a flow rate of 400 µl/min. The resulting chromatogram in Figure 7-17 shows a representative chromatogram of a medium quality control spleen sample of the fusidic acid compounds.

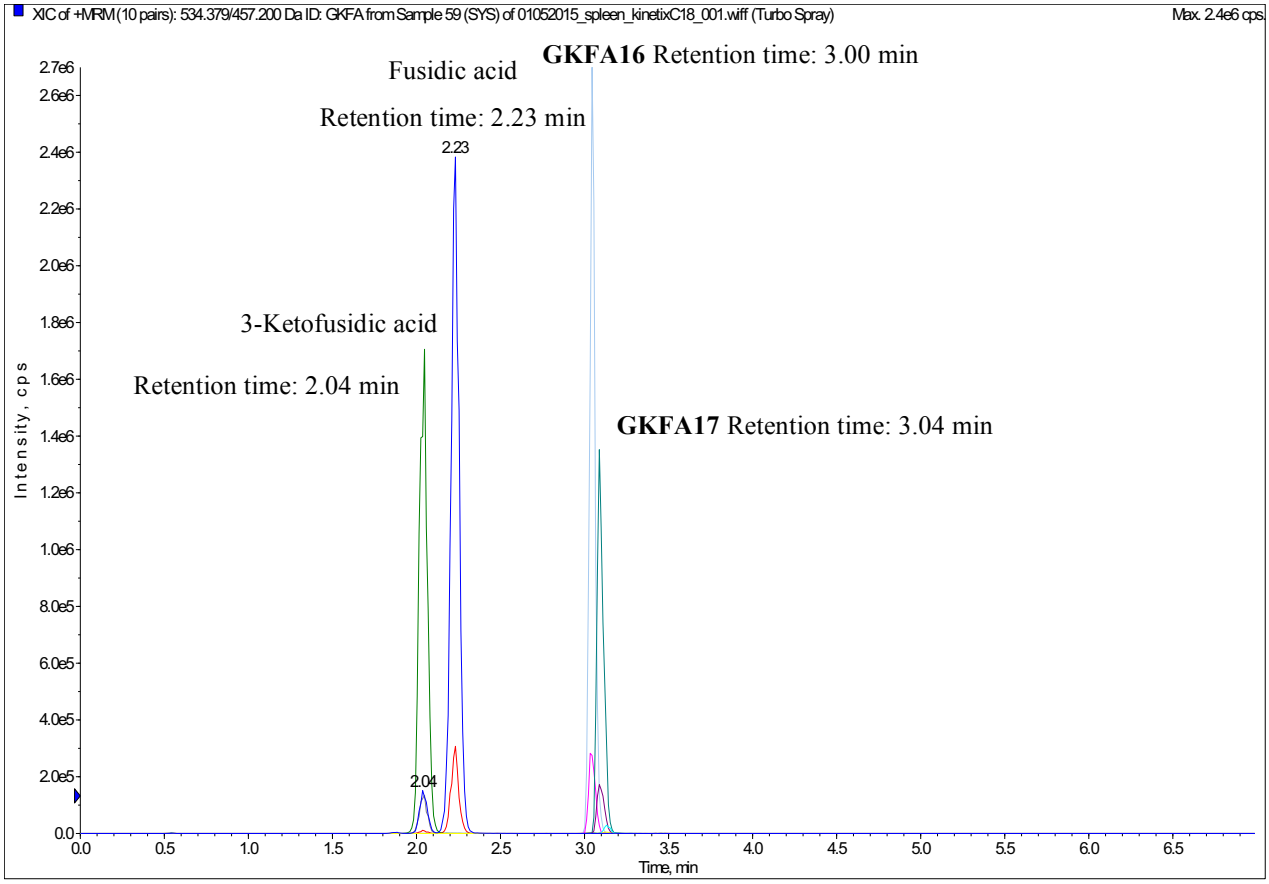

Figure 7-17: Representative chromatogram of an organ sample

Table 7-42: Gradient chromatography steps used for organ samples

Step	Total Time (min)	Flow Rate (µl/min)	A (%)	B (%)
1	0.0	400	80	20
2	0.70	400	80	20
3	1.00	400	0	100
4	3.50	400	0	100
5	3.60	400	95	5
6	7.00	400	95	5

A: Whole blood 10 ng/ml:

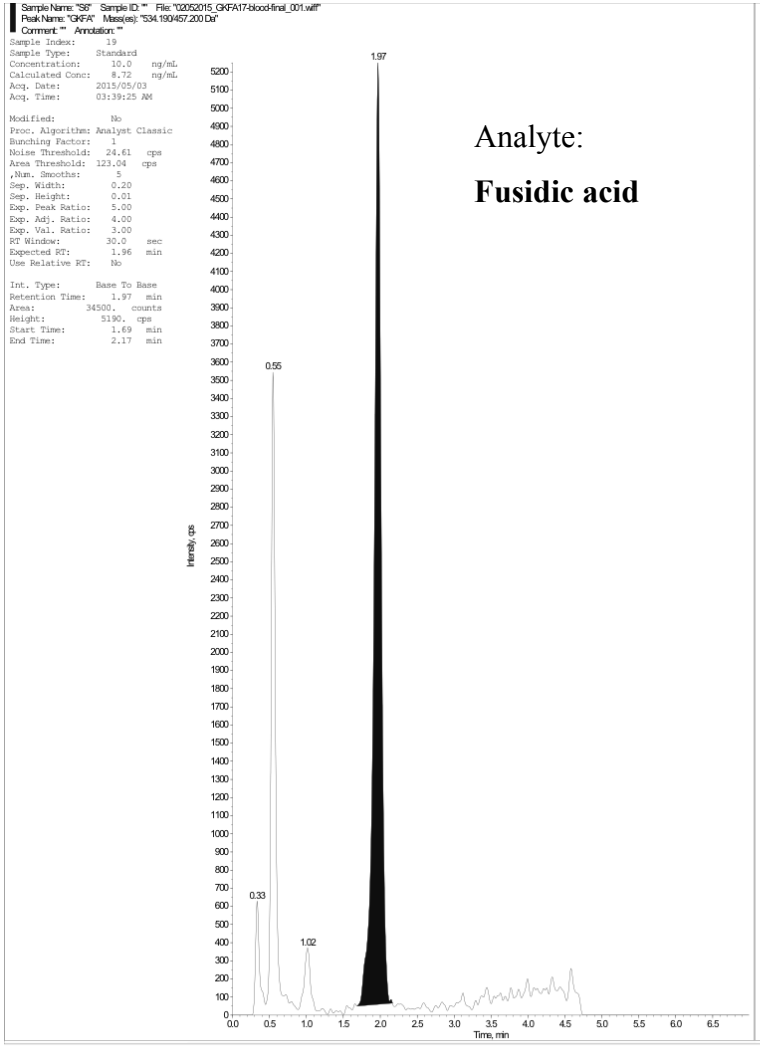

Analyte:

Fusidic acid

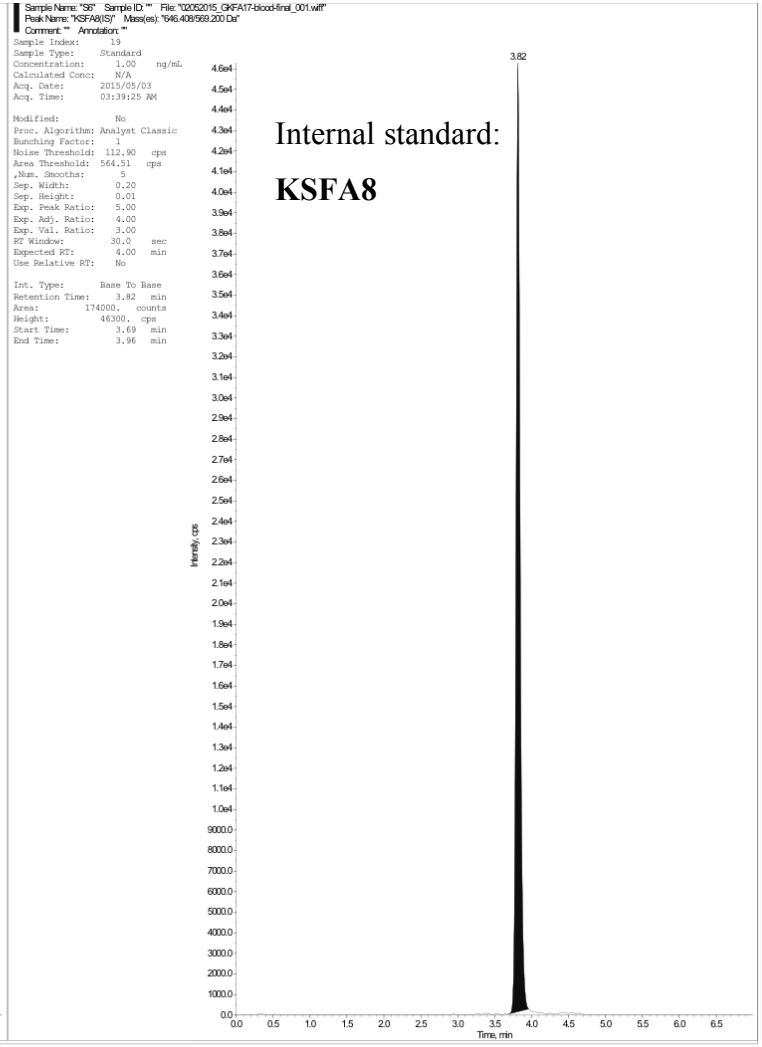

Internal standard:

KSFA8

B: Liver 50 ng/ml

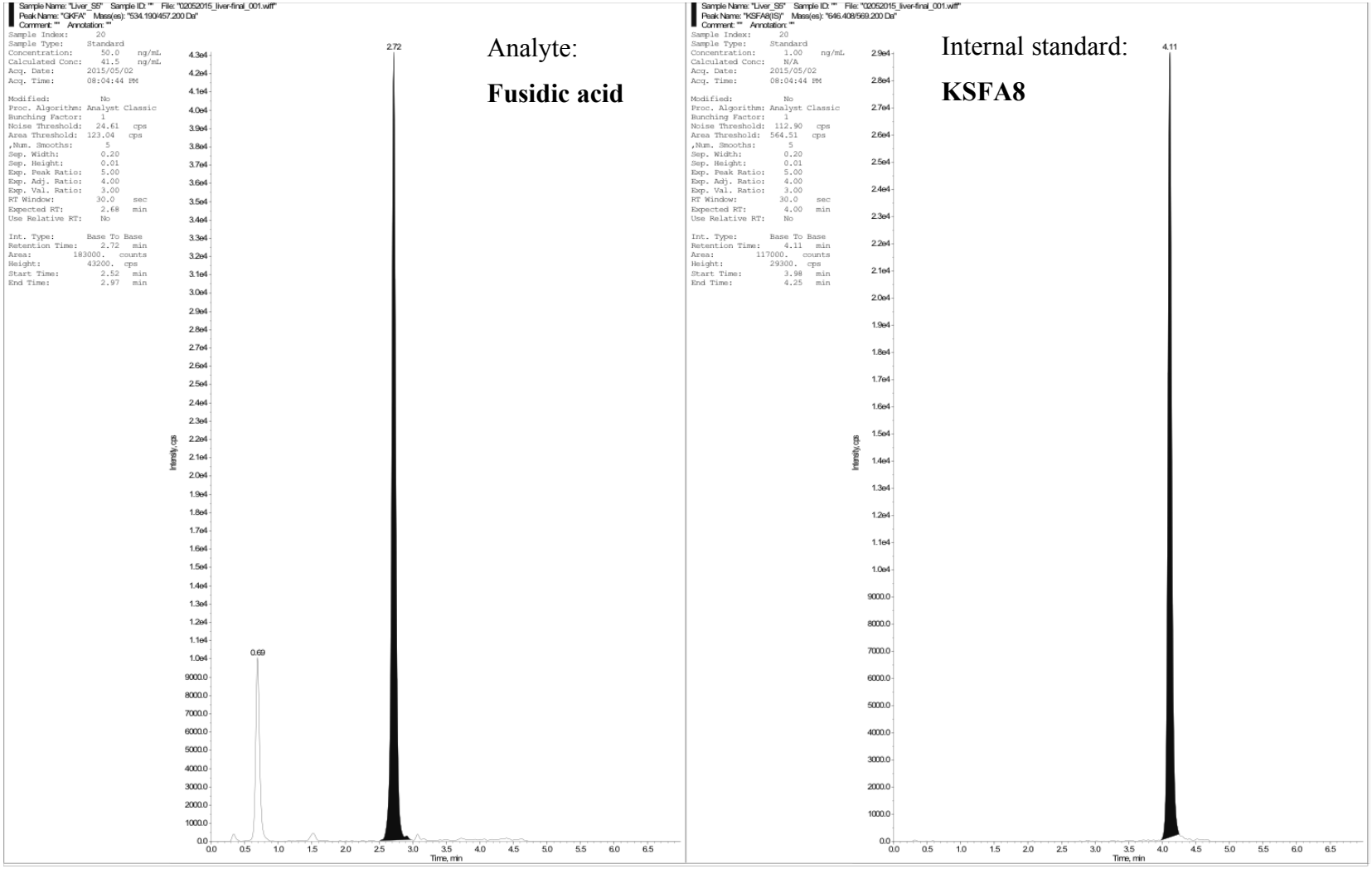

C: Lungs 10 ng/ml

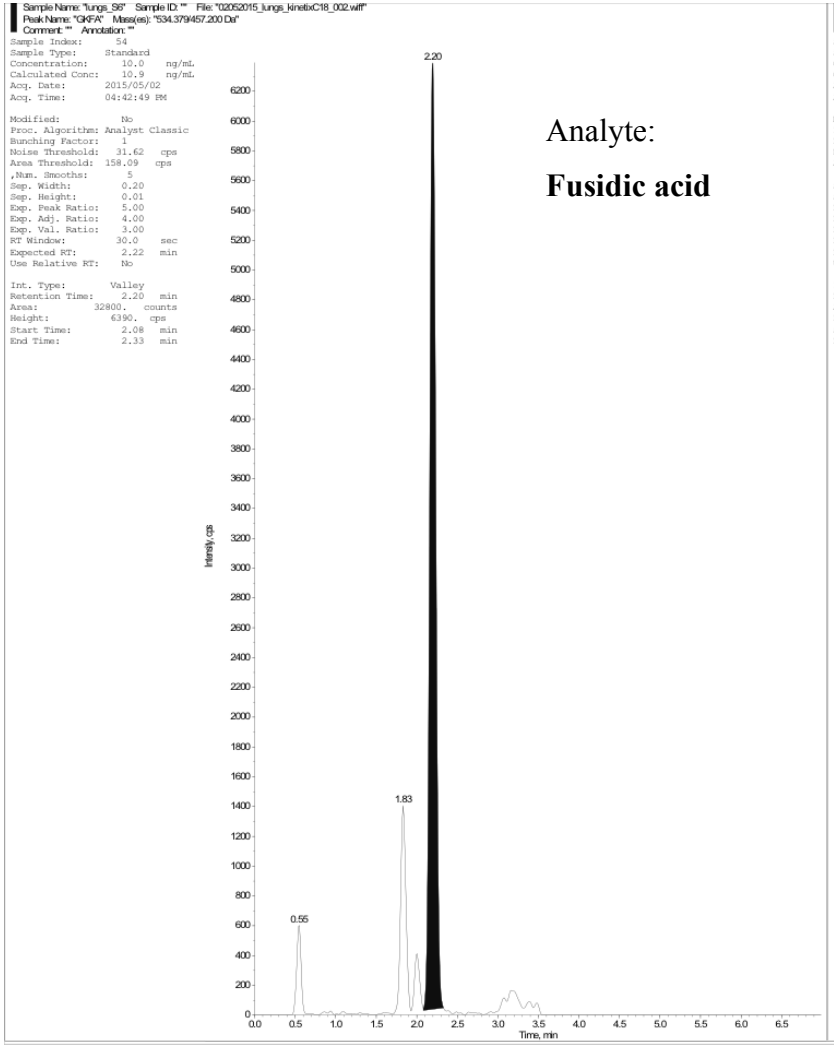

Analyte:

Fusidic acid

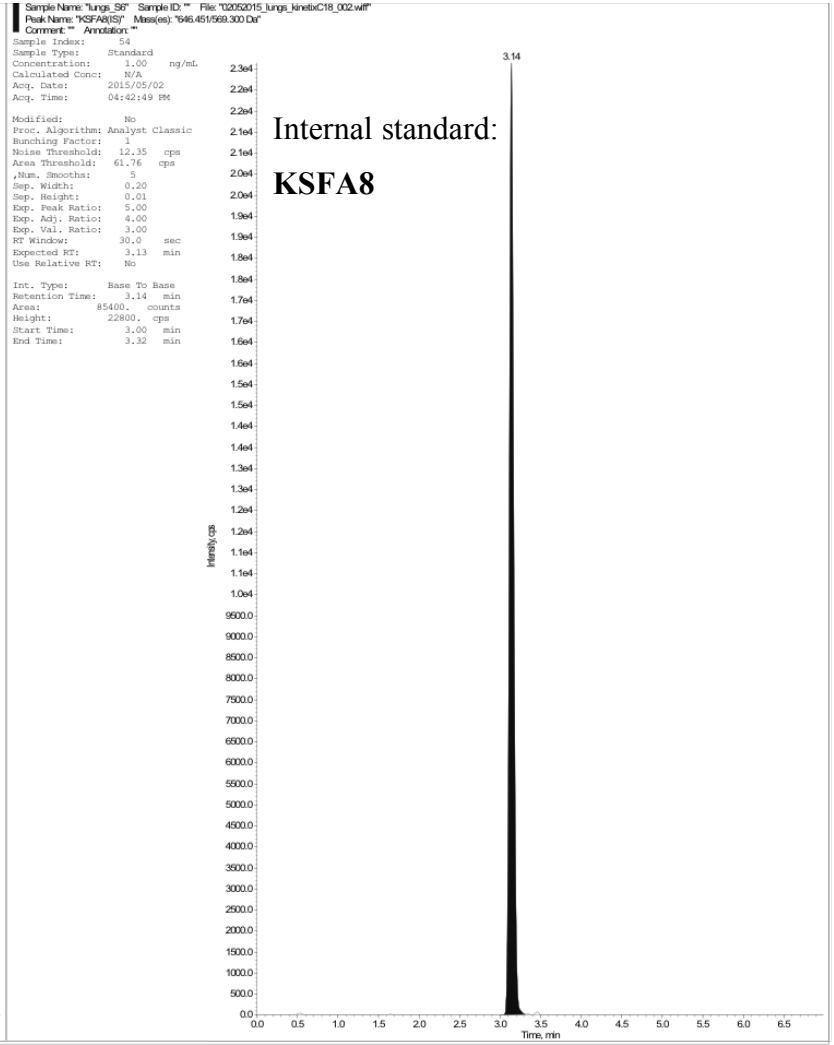

Internal standard:

KSFA8

D: Spleen 10 ng/ml

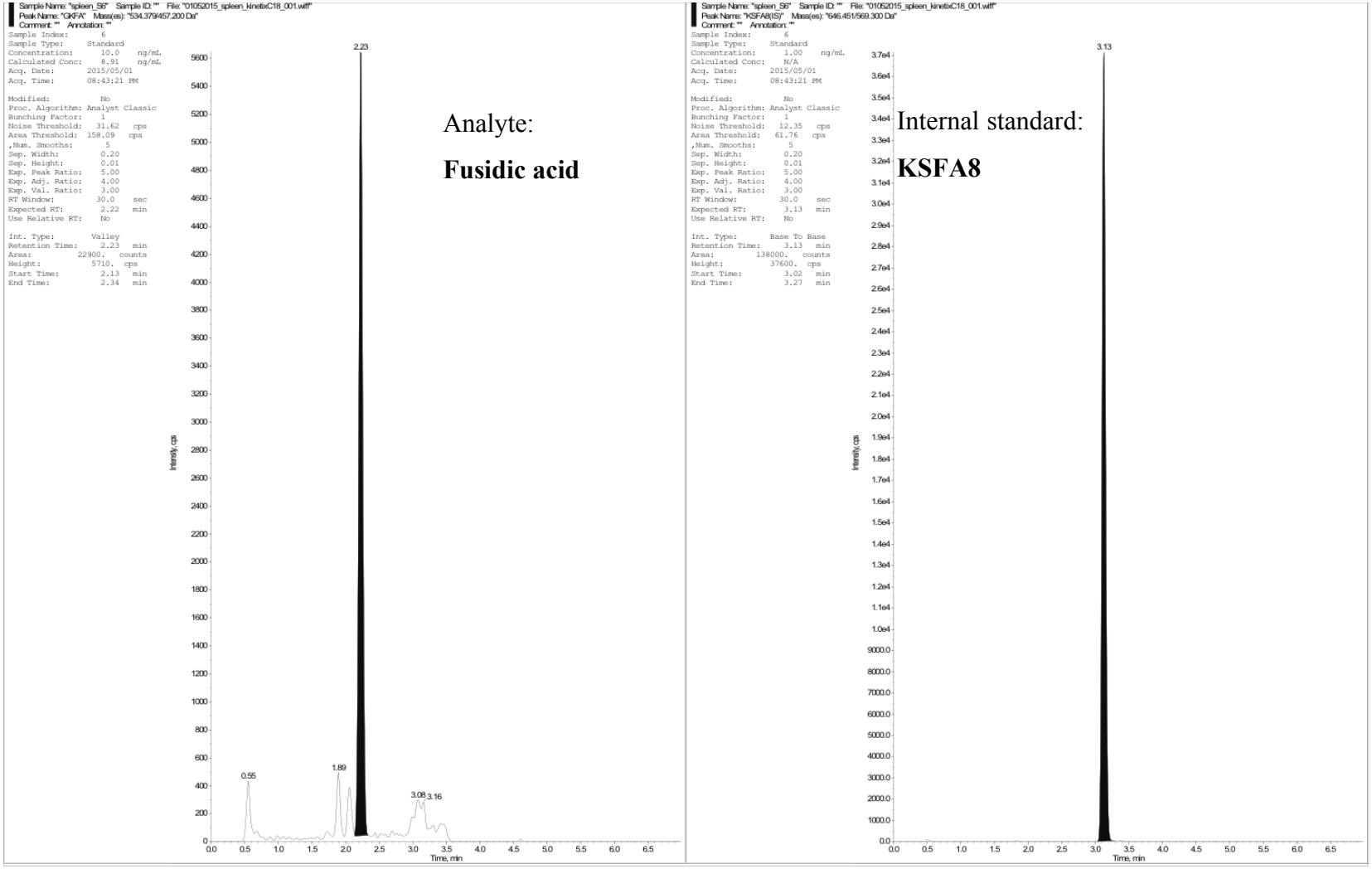

E: Kidneys 10 ng/ml

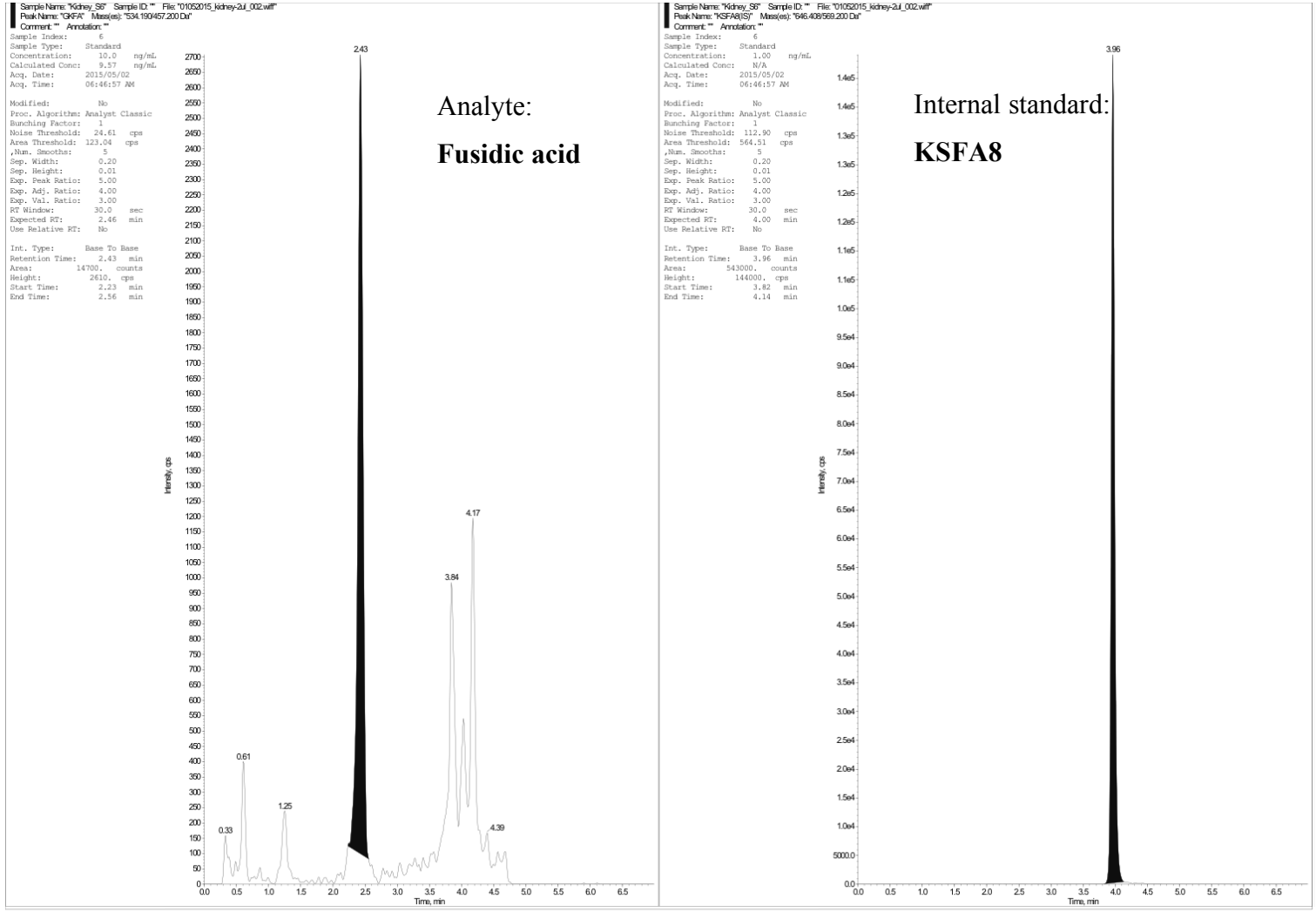

F: Heart 10 ng/ml

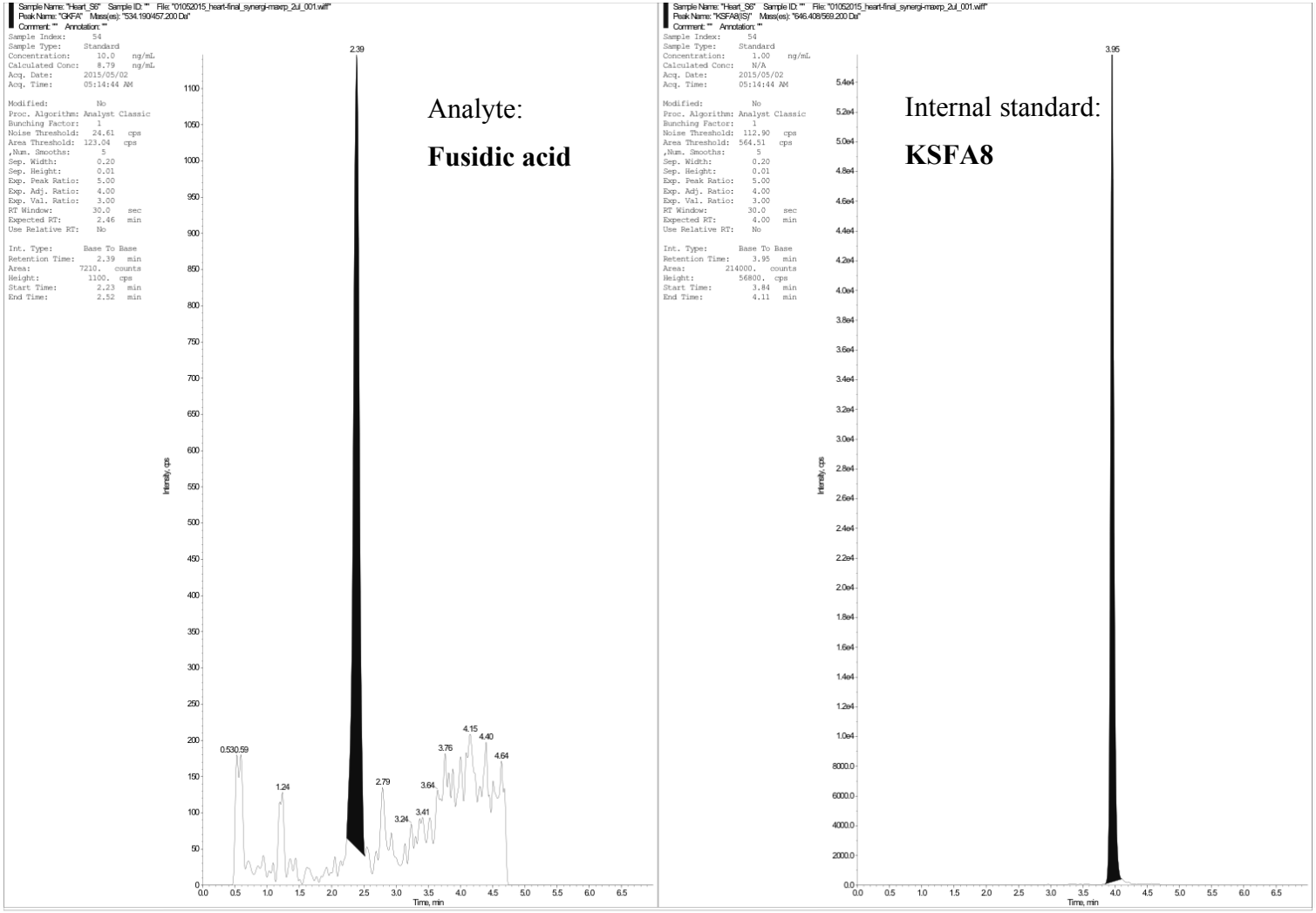

G: Brain 10 ng/ml

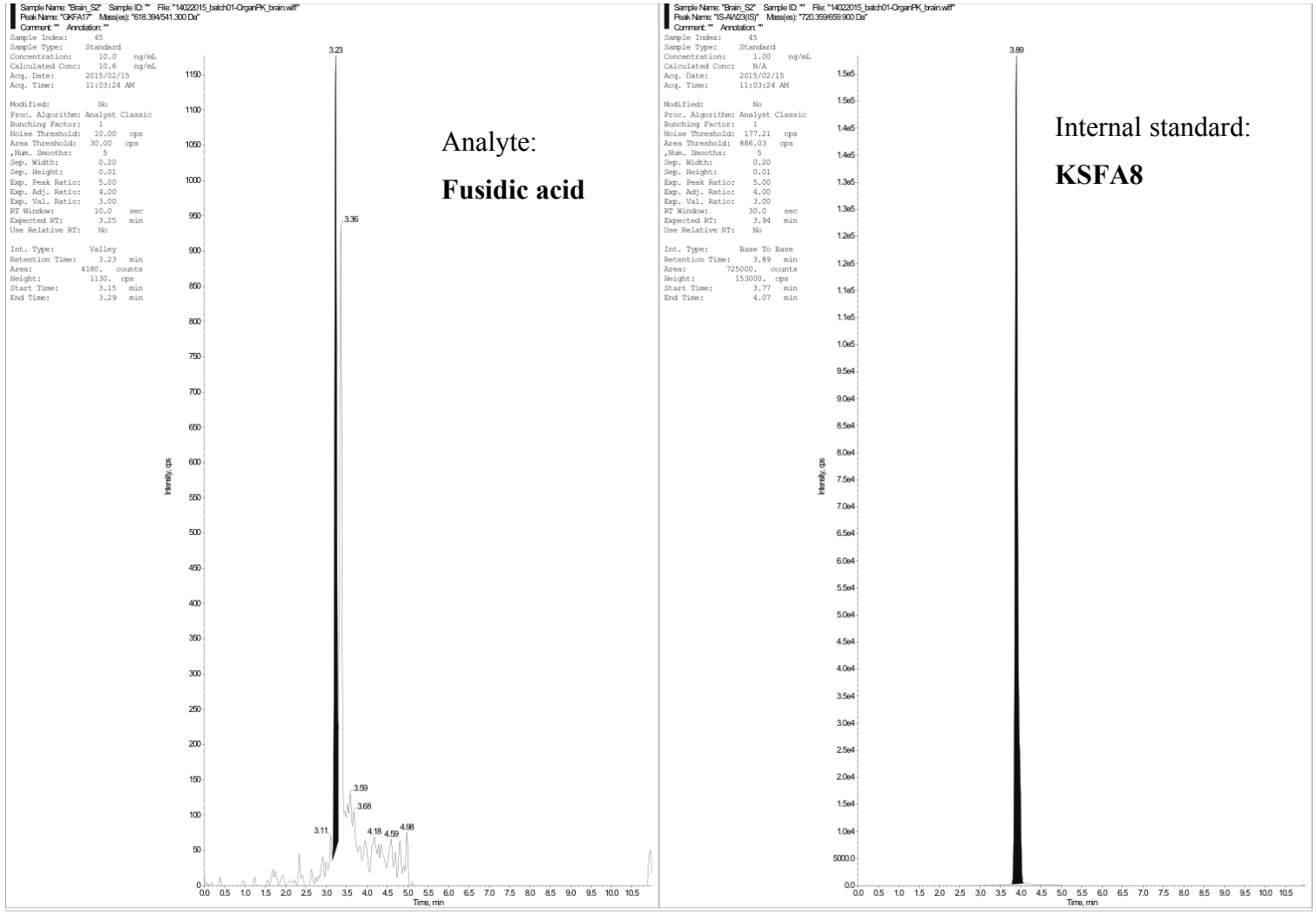

Figure 7-18: Lowest standards of organ samples

7.5.1.4 Quantification

Table 7-43 to Table 7-48 contains the quantification statistics of the organ assays, and shows representative calibration curves and blank samples from the final batches used for pharmacokinetic calculation. The low quality control samples of each analyte with respective internal standard is shown in Figure 7-14.

Table 7-43: Liver quantification statistics

Liver Sample	Exp conc (ng/ml)	Number	Mean conc (ng/ml)	S.D.	Precision (%CV)	Accuracy (%Norm)
FA						
S4	50	2 of 2	47.1	7.84	16.6	94.2
S3	100	2 of 2	107	6.75	6.33	107
S2	500	2 of 2	495	139	28.1	99
S1	2500	2 of 2	2500	407	16.3	99.8
k-FA						
S4	50	2 of 2	53.6	12.4	23.1	107
S3	100	2 of 2	91.8	18.3	19.9	91.8
S2	500	2 of 2	504	166	32.8	101
S1	2500	2 of 2	2500	363	14.5	99.8
GKFA16						
S4	50	2 of 2	57.3	3.32	5.78	115
S3	100	2 of 2	83.5	3.29	3.94	83.5
S2	500	2 of 2	508	126	24.8	102
S1	2500	2 of 2	2490	284	11.4	99.8
GKFA17						
S4	50	2 of 2	48.1	0.44	0.916	96.1
S3	100	2 of 2	104	7.15	6.86	104
S2	500	2 of 2	497	50.2	10.1	99.5
S1	2500	2 of 2	2490	353	14.2	99.7

Table 7-44: Lungs quantification statistics

Lungs Sample	Exp conc (ng/ml)	Number	Mean conc (ng/ml)	S.D.	Precision (%CV)	Accuracy (%Norm)
FA						
S5	10	2 of 2	9.16	2.42	26.4	91.6
S4	50	2 of 2	57.9	0.339	0.585	116
S3	100	2 of 2	92.4	6.45	6.98	92.4
S2	500	2 of 2	500	46.1	9.22	100
S1	2500	2 of 2	2500	250	10	99.8
k-FA						
S5	10	2 of 2	9.69	2.63	27.2	96.9
S4	50	2 of 2	58.3	0.648	1.11	117
S3	100	2 of 2	85.1	8.57	10.1	85.1
S2	500	2 of 2	506	71.6	14.2	101
S1	2500	2 of 2	2500	227	9.09	99.8
GKFA16						
S5	10	2 of 2	7.51	3.16	42	75.1
S4	50	2 of 2	60.5	7.53	12.4	121
S3	100	2 of 2	106	22.2	20.9	106
S2	500	2 of 2	486	79.7	16.4	97.2
S1	2500	2 of 2	2500	161	6.43	100
GKFA17						
S5	10	2 of 2	8.77	1.32	15.1	87.7
S4	50	2 of 2	60.3	5	8.29	121
S3	100	2 of 2	91.6	6.8	7.42	91.6
S2	500	2 of 2	499	66.8	13.4	99.7
S1	2500	2 of 2	2500	154	6.18	99.9

Table 7-45: Kidneys quantification statistics

Kidney Sample	Exp conc (ng/ml)	Number	Mean conc (ng/ml)	S.D.	Precision (%CV)	Accuracy (%Norm)
FA						
S5	10	2 of 2	11	1.86	16.9	110
S4	50	2 of 2	45.1	6.86	15.2	90.3
S3	100	2 of 2	68.6	9.76	14.2	91.4
S2	500	2 of 2	521	41.6	7.99	104
S1	2500	2 of 2	2480	147	5.93	99.3
k-FA						
S5	10	2 of 2	2.2	1.87	84.8	22
S4	50	2 of 2	38.7	8.94	23.1	77.4
S3	100	2 of 2	60.8	11.7	19.3	81.1
S2	500	2 of 2	523	31	5.93	105
S1	2500	2 of 2	2530	74.6	2.95	101
GKFA16						
S5	10	2 of 2	1.93	1.54	80.1	19.3
S4	50	2 of 2	39.9	8.37	21	79.9
S3	100	2 of 2	66.9	12	18	89.2
S2	500	2 of 2	571	20.8	3.64	114
S1	2500	2 of 2	2370	62.3	2.63	94.8
GKFA17						
S5	10	2 of 2	1.25	1.75	140	12.5
S4	50	2 of 2	38.3	7.11	18.6	76.6
S3	100	2 of 2	63.1	8.86	14	84.2
S2	500	2 of 2	559	15.1	2.7	112
S1	2500	2 of 2	2440	158	6.49	97.5

Table 7-46: Spleen quantification statistics

Spleen Sample	Exp conc (ng/ml)	Number	Mean conc (ng/ml)	S.D.	Precision (%CV)	Accuracy (%Norm)
FA						
S5	10	2 of 2	9.38	0.665	7.09	93.8
S4	50	2 of 2	53.7	16.1	29.9	107
S3	75	2 of 2	74.5	1.91	2.56	99.4
S2	500	2 of 2	497	99.9	20.1	99.3
S1	2500	2 of 2	2480	665	26.8	99.4
k-FA						
S5	10	2 of 2	9.62	0.16	1.66	96.2
S4	50	2 of 2	53.6	18.2	33.9	107
S3	75	2 of 2	72.6	0.446	0.614	96.8
S2	500	2 of 2	499	95.7	19.2	99.7
S1	2500	2 of 2	2490	726	29.2	99.4
GKFA16						
S5	10	2 of 2	9.41	0.547	5.81	94.1
S4	50	2 of 2	55.4	16.3	29.4	111
S3	75	2 of 2	71.4	5.09	7.12	95.3
S2	500	2 of 2	498	94.8	19	99.6
S1	2500	2 of 2	2500	450	18	99.8
GKFA17						
S5	10	2 of 2	9.51	2.03	21.3	95.1
S4	50	2 of 2	56.7	27.3	48.2	113
S3	75	2 of 2	68.4	2.33	3.4	91.3
S2	500	2 of 2	500	55.8	11.2	100
S1	2500	2 of 2	2490	501	20.1	99.7

Table 7-47: Brain quantification statistics

Brain Sample	Exp conc (ng/ml)	Number	Mean conc (ng/ml)	S.D.	Precision (%CV)	Accuracy (%Norm)
FA						
S5	10	2 of 2	10.2	1.55	15.2	102
S4	50	2 of 2	47	3.34	7.1	94
S3	100	2 of 2	92.5	4.2	4.54	92.5
S2	500	2 of 2	575	33	5.73	115
S1	2500	2 of 2	2440	830	34	97.7
k-FA						
S5	10	2 of 2	10.1	1.54	15.2	101
S4	50	2 of 2	47.5	3.91	8.22	95.1
S3	100	2 of 2	94.8	1.96	2.07	94.8
S2	500	2 of 2	555	6.35	1.14	111
S1	2500	2 of 2	2460	892	36.2	98.5
GKFA16						
S5	10	2 of 2	10.2	0.295	2.9	102
S4	50	2 of 2	46.2	1.58	3.41	92.4
S3	100	2 of 2	95.8	3.71	3.87	95.8
S2	500	2 of 2	563	39.1	6.94	113
S1	2500	2 of 2	2450	763	31.2	97.9
GKFA17						
S5	10	2 of 2	10.1	0.961	9.48	101
S4	50	2 of 2	46.9	2.52	5.38	93.9
S3	100	2 of 2	96.5	8.55	8.86	96.5
S2	500	2 of 2	553	22.6	4.09	111
S1	2500	2 of 2	2450	568	23.1	98.1

Table 7-48: Heart quantification statistics

Heart Sample	Exp conc (ng/ml)	Number	Mean conc (ng/ml)	S.D.	Precision (%CV)	Accuracy (%Norm)
FA						
S4	10	2 of 2	11.1	3.24	29.3	111
S3	50	2 of 2	44	9.57	21.7	88
S2	500	2 of 2	505	127	25.1	101
S1	2500	2 of 2	2490	504	20.2	99.7
k-FA						
S4	10	2 of 2	10.8	2.88	26.7	108
S3	50	2 of 2	45.7	7.44	16.3	91.4
S2	500	2 of 2	504	85.4	17	101
S1	2500	2 of 2	2490	443	17.8	99.8
GKFA16						
S4	10	2 of 2	11.5	4.88	42.3	115
S3	50	2 of 2	41.7	13.4	32.3	83.3
S2	500	2 of 2	506	211	41.8	101
S1	2500	2 of 2	2490	611	24.6	99.5
GKFA17						
S4	10	2 of 2	11.6	4.91	42.2	116
S3	50	2 of 2	41	13.8	33.6	82
S2	500	2 of 2	506	212	41.9	101
S1	2500	2 of 2	2480	740	29.8	99.3

In **Figure 7-19** is shown the respective calibration curves of the lung batch for the fusidic acid compounds with their respective regression values as example. Quantification used quadratic regression of the analyte area/internal standard area vs concentration with 1/x weighting. All calibration curves showed regression above 0.990.

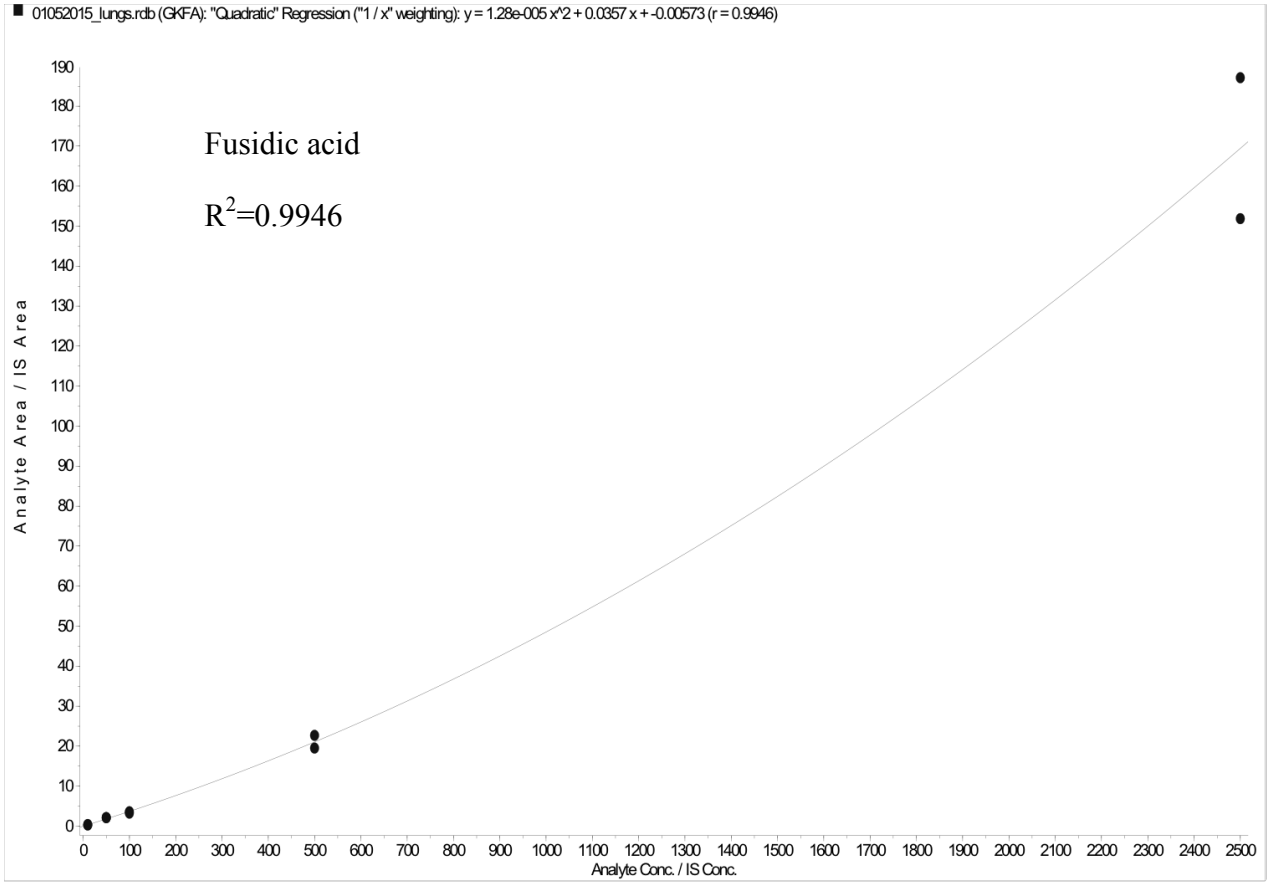
01052015_lungs.rdb (GKFA): "Quadratic" Regression ("1 / x" weighting): y = 1.28e-005 x^2 + 0.0357 x + -0.00573 (r = 0.9946)
Fusidic acid
R2=0.9946
Analyte Area / IS Area
Analyte Conc. / IS Conc.

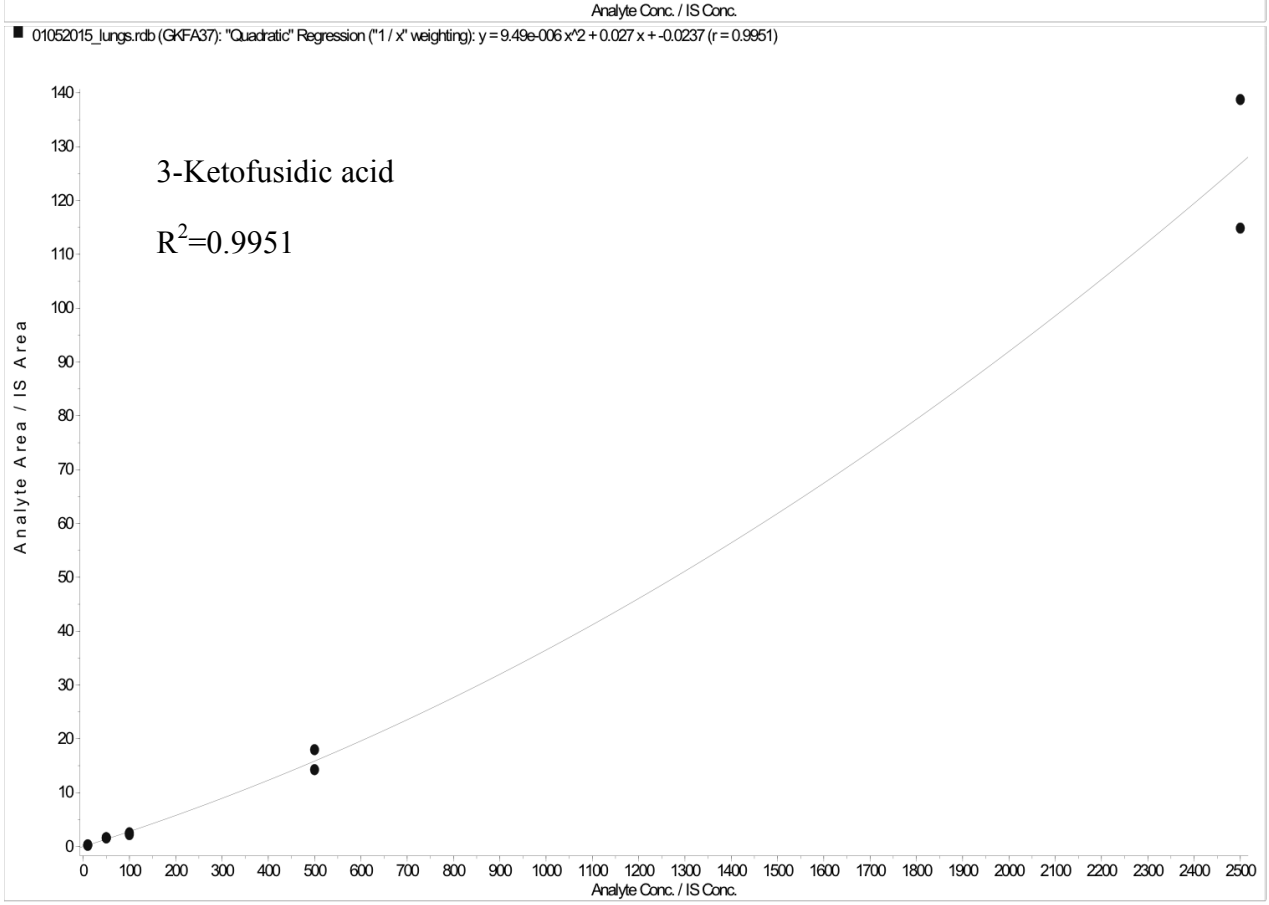
01052015_lungs.rdb (GKFA37): "Quadratic" Regression ("1 / x" weighting): y = 9.49e-006 x^2 + 0.027 x + -0.0237 (r = 0.9951)
3-Ketofusidic acid
R2=0.9951
Analyte Area / IS Area
Analyte Conc. / IS Conc.

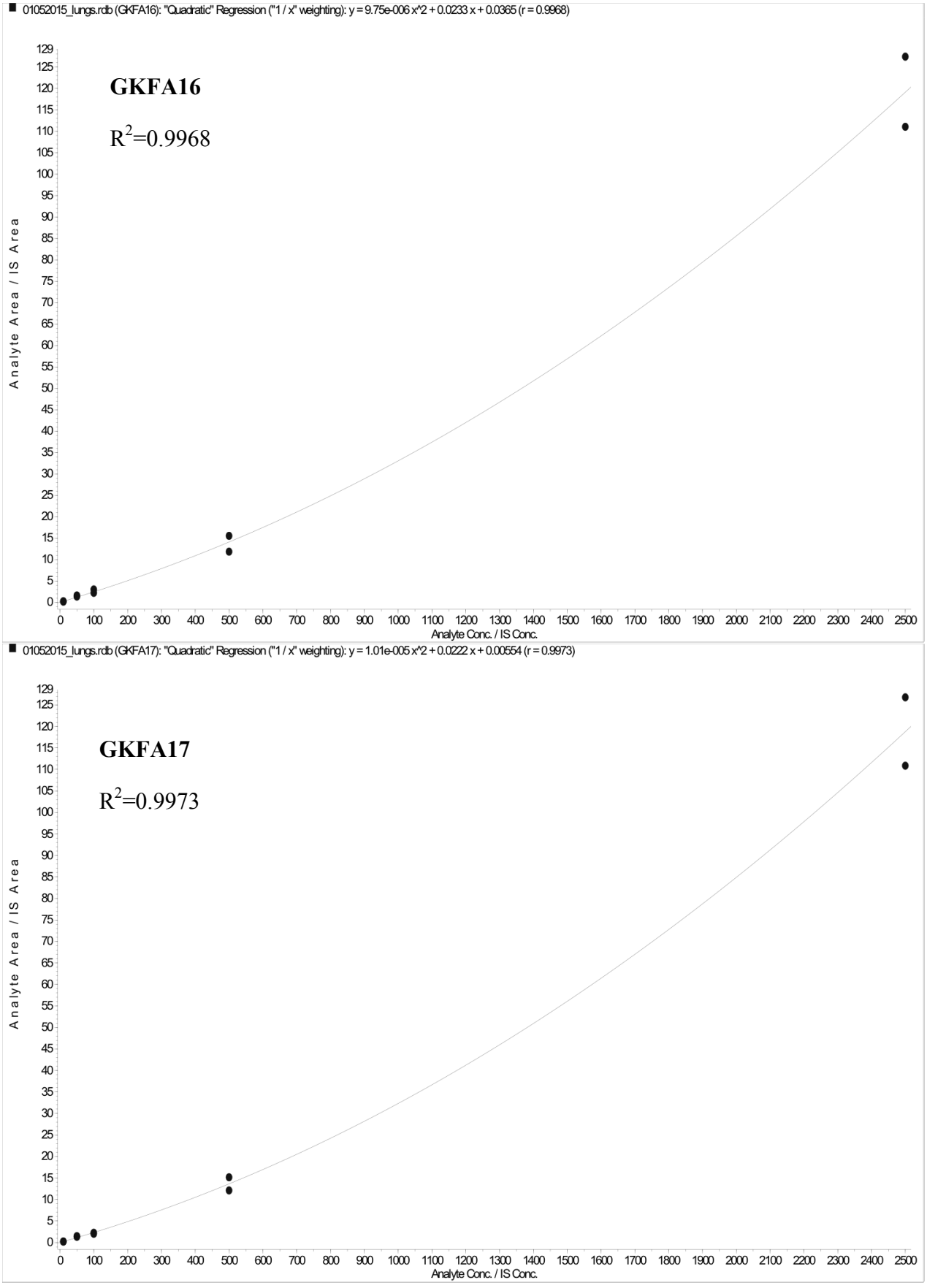

Figure 7-19: Representative calibration curves of lung samples

The low quality control samples of fusidic acid for each batch with respective internal standard is shown in Figure 7-20.

In Figure 7-21 is shown the blank samples injected after the highest concentration standard from the final batches analysed with their respective carry-over displayed. All samples showed carry-over below the accepted 20% allowed.

A: Whole blood 10 ng/ml:

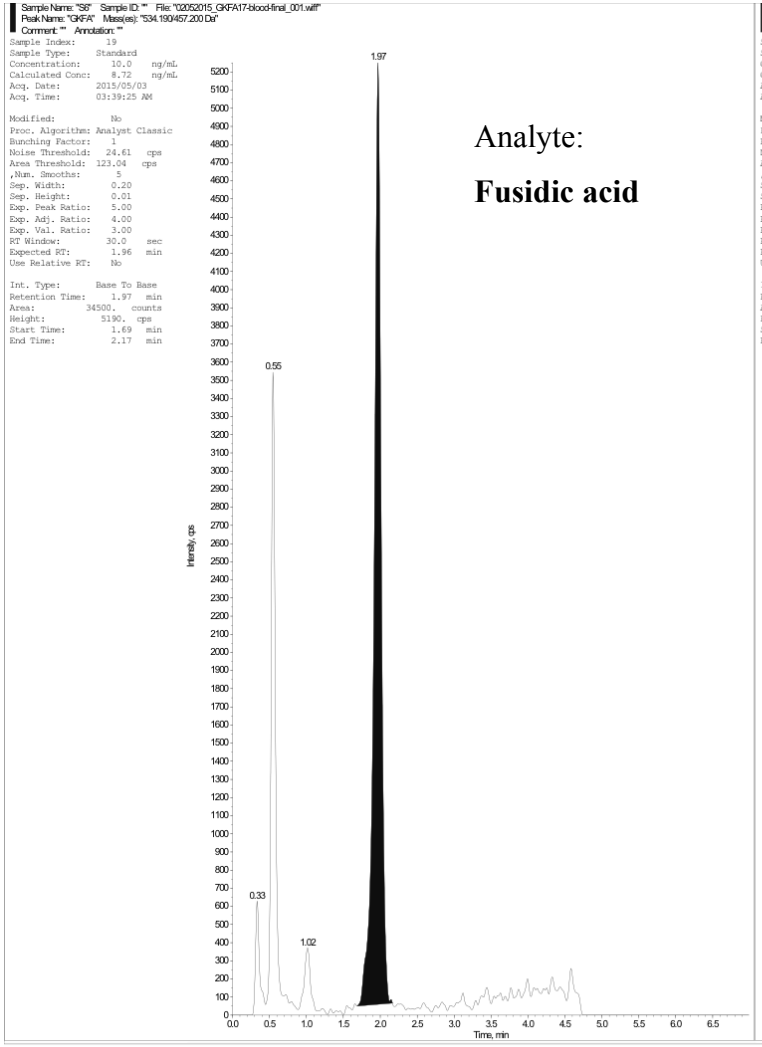

Analyte:

Fusidic acid

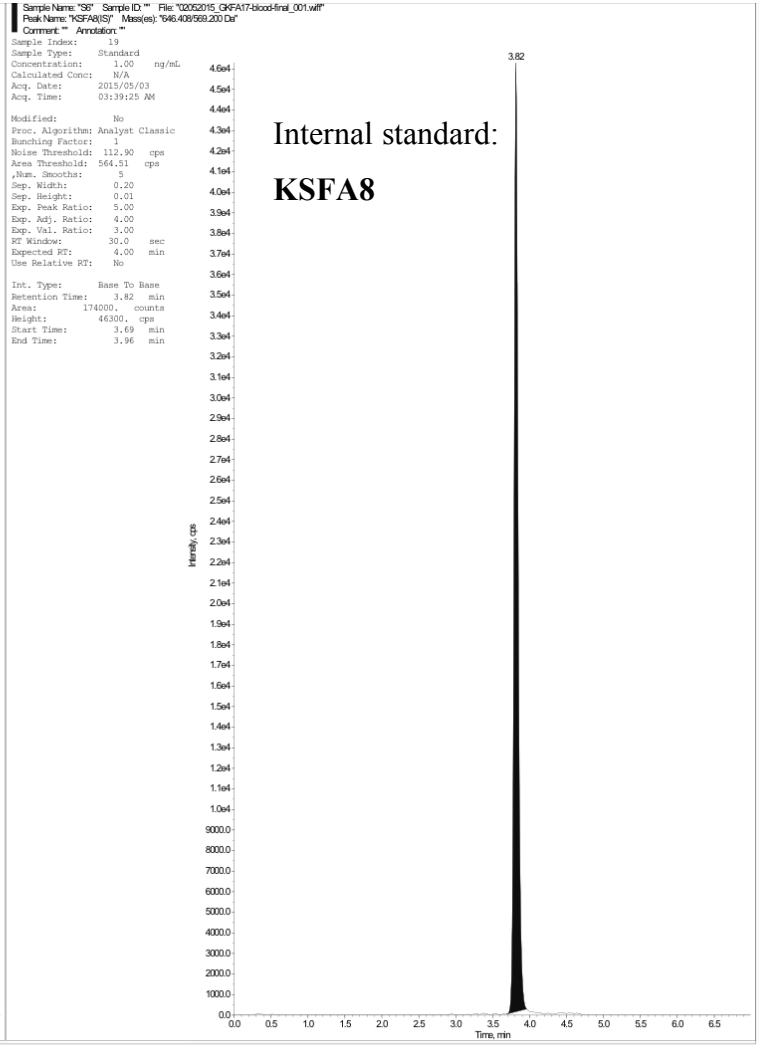

Internal standard:

KSFA8

B: Liver 50 ng/ml

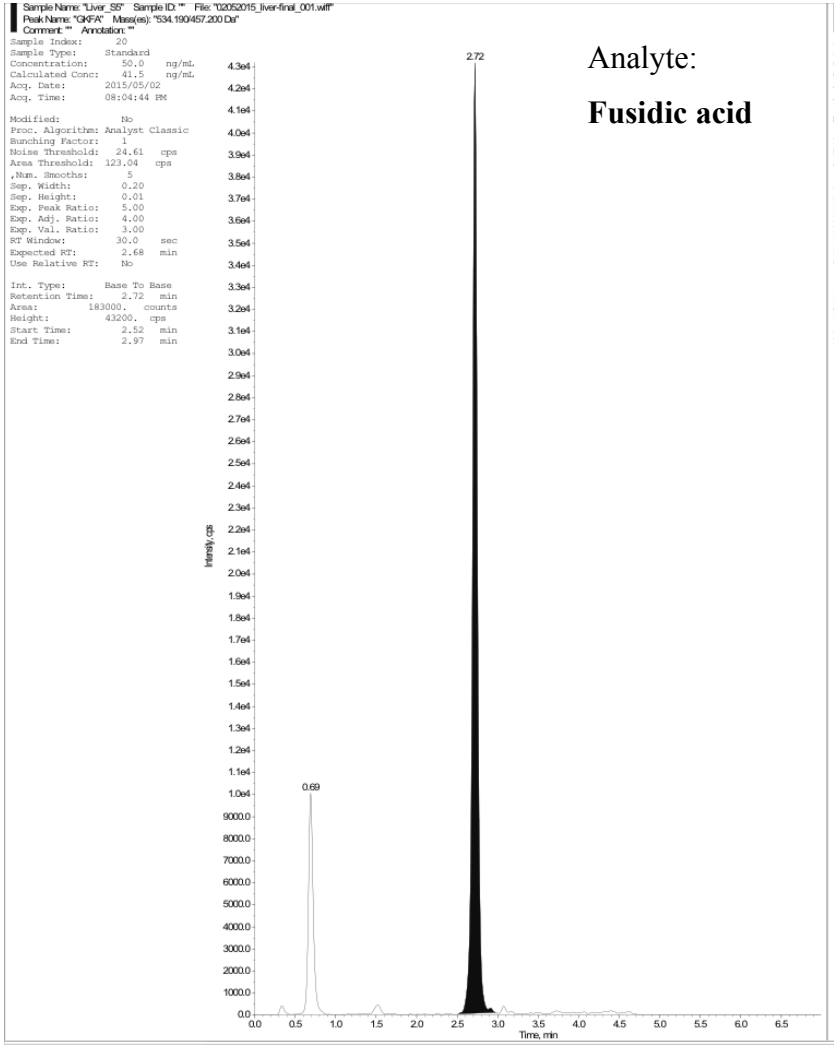

Analyte:

Fusidic acid

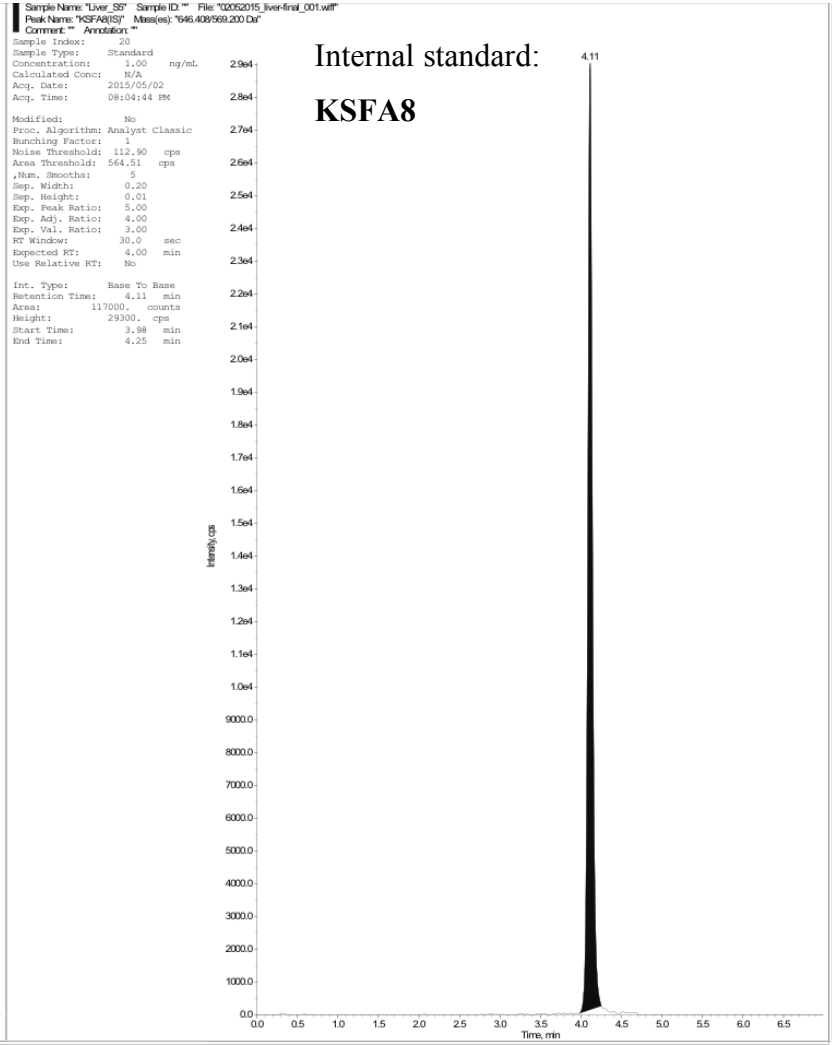

Internal standard:

KSFA8

C: Lungs 10 ng/ml

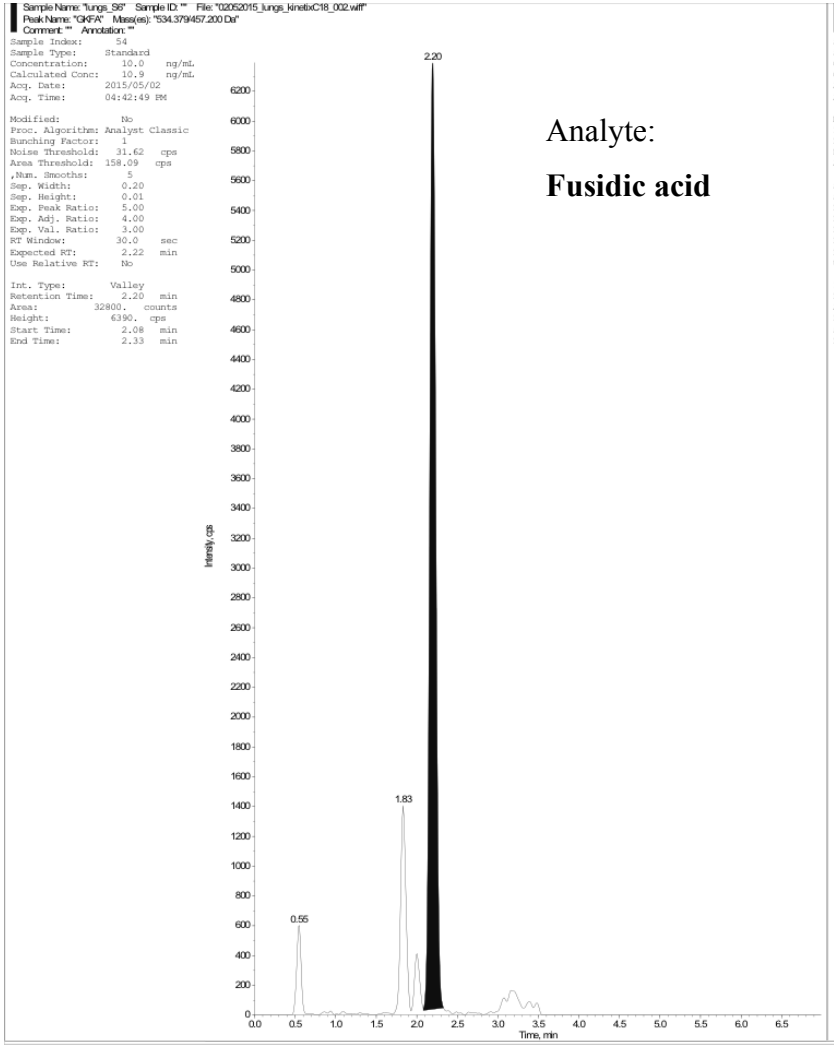

Analyte:

Fusidic acid

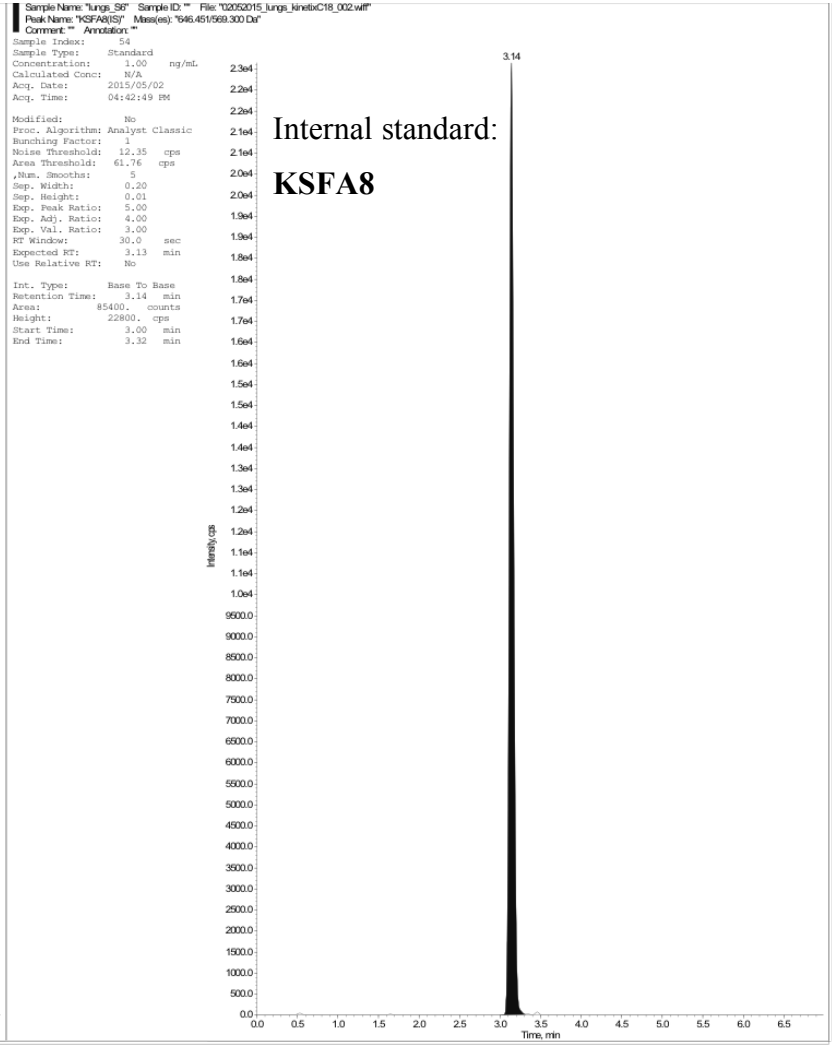

Internal standard:

KSFA8

D: Spleen 10 ng/ml

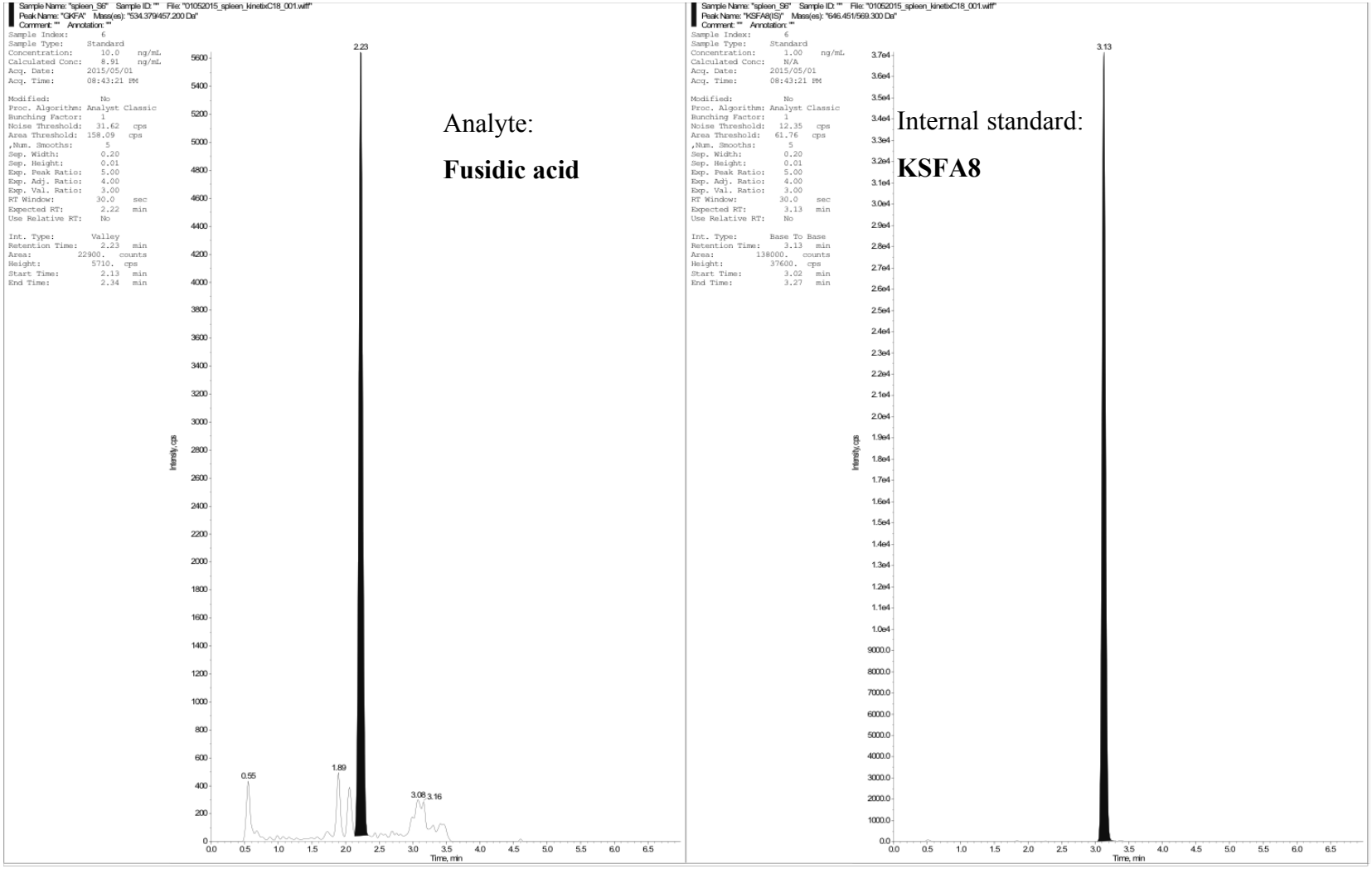

E: Kidneys 10 ng/ml

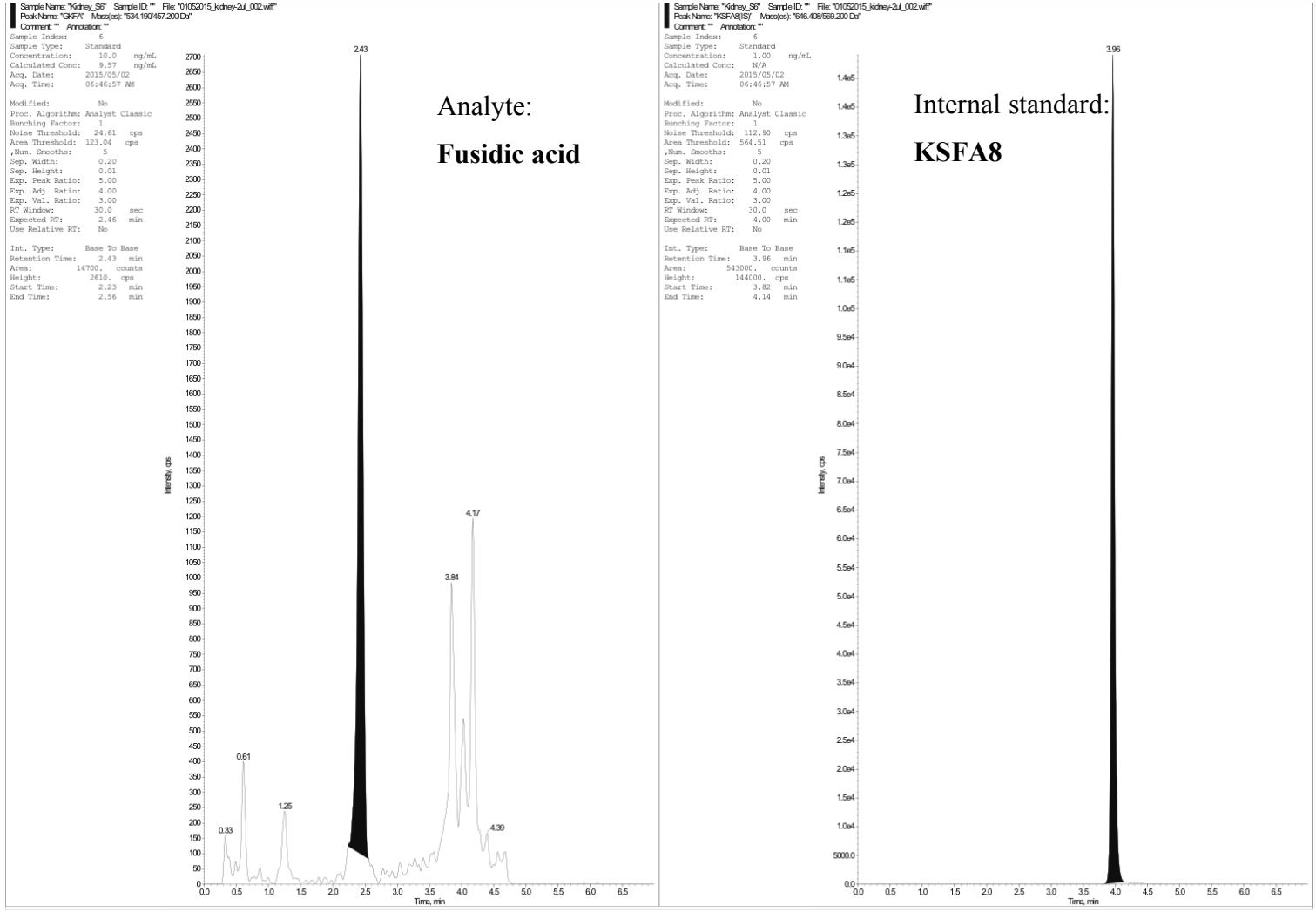

F: Heart 10 ng/ml

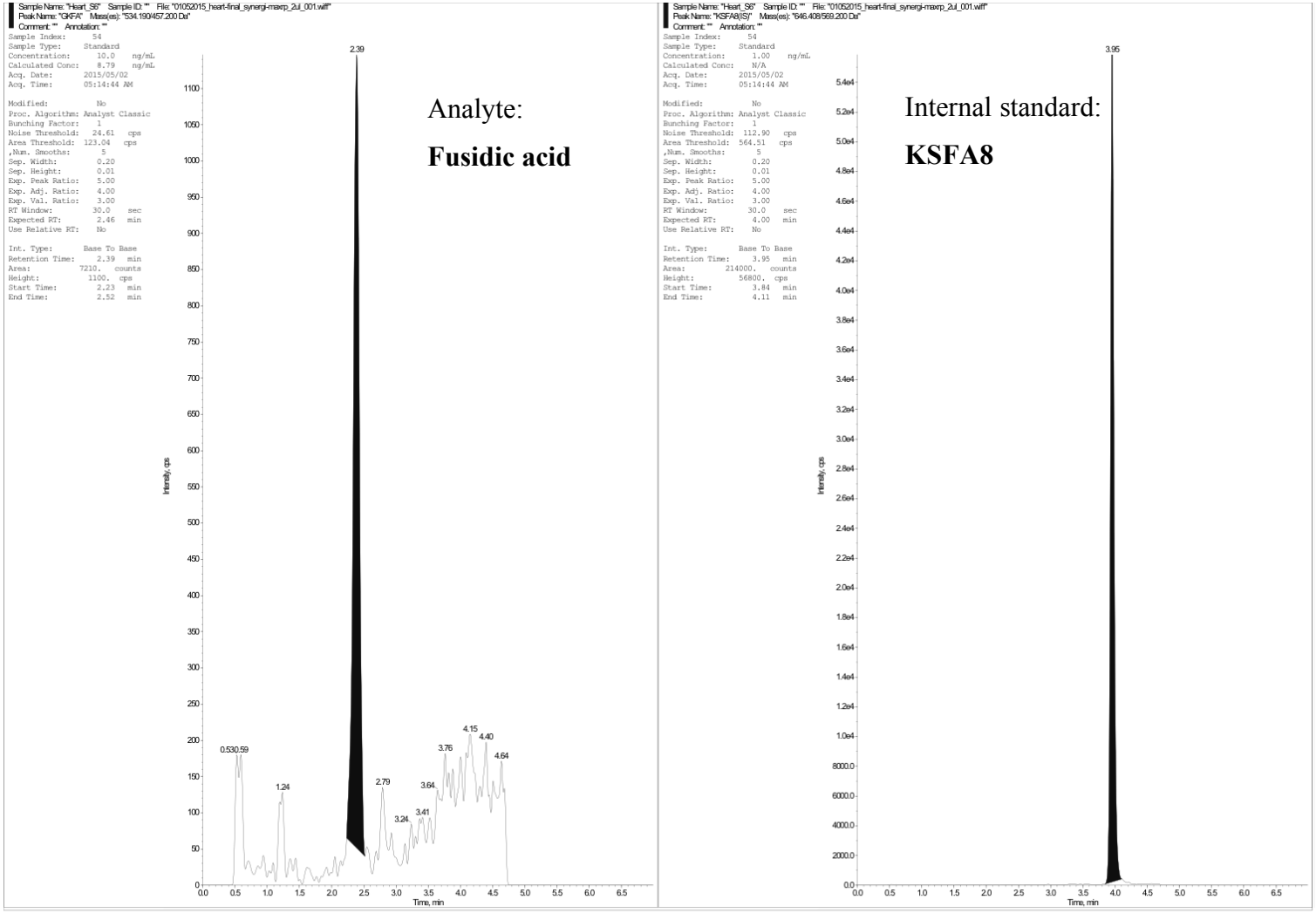

G: Brain 10 ng/ml

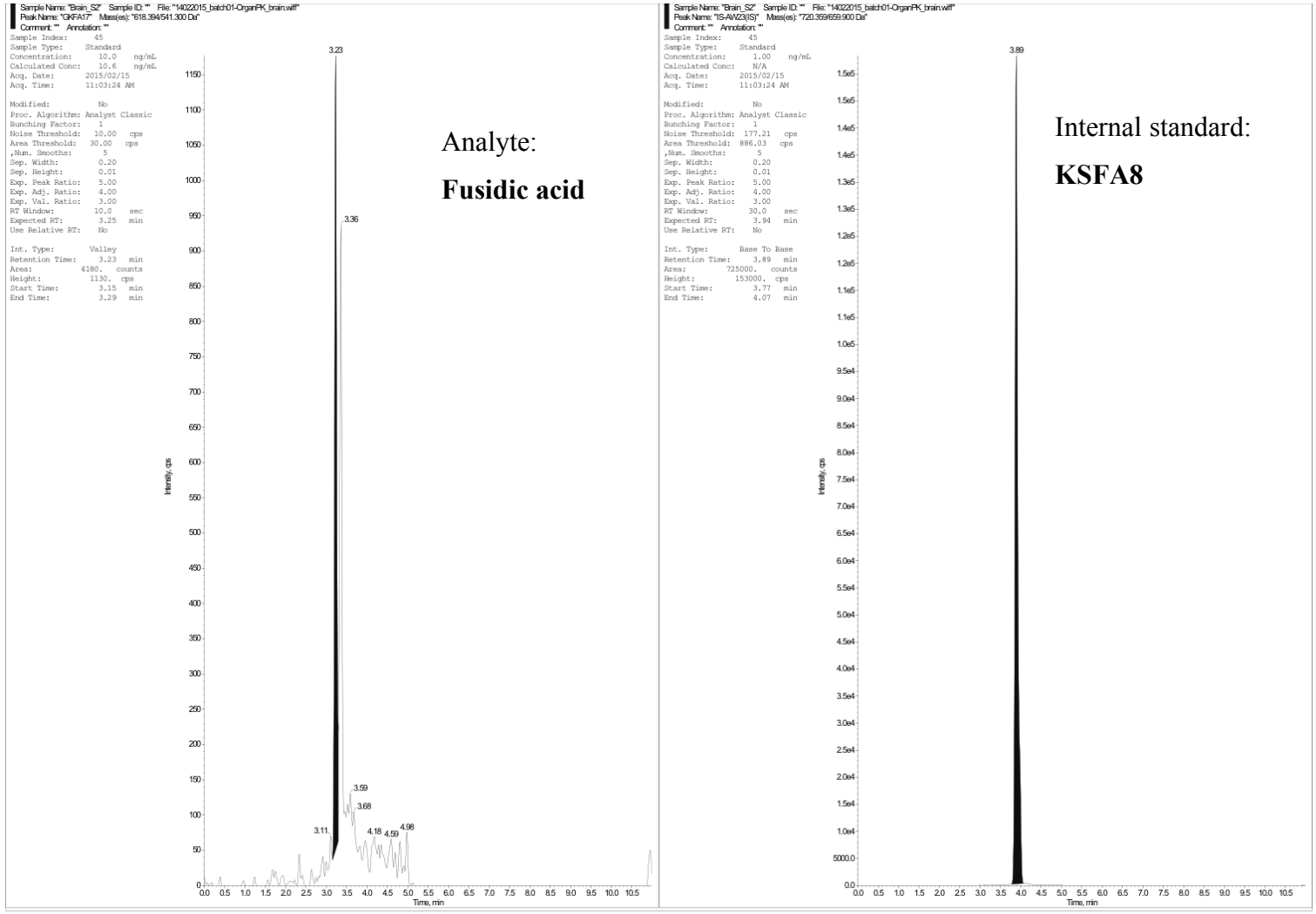

Figure 7-20: Lowest standards of organ samples

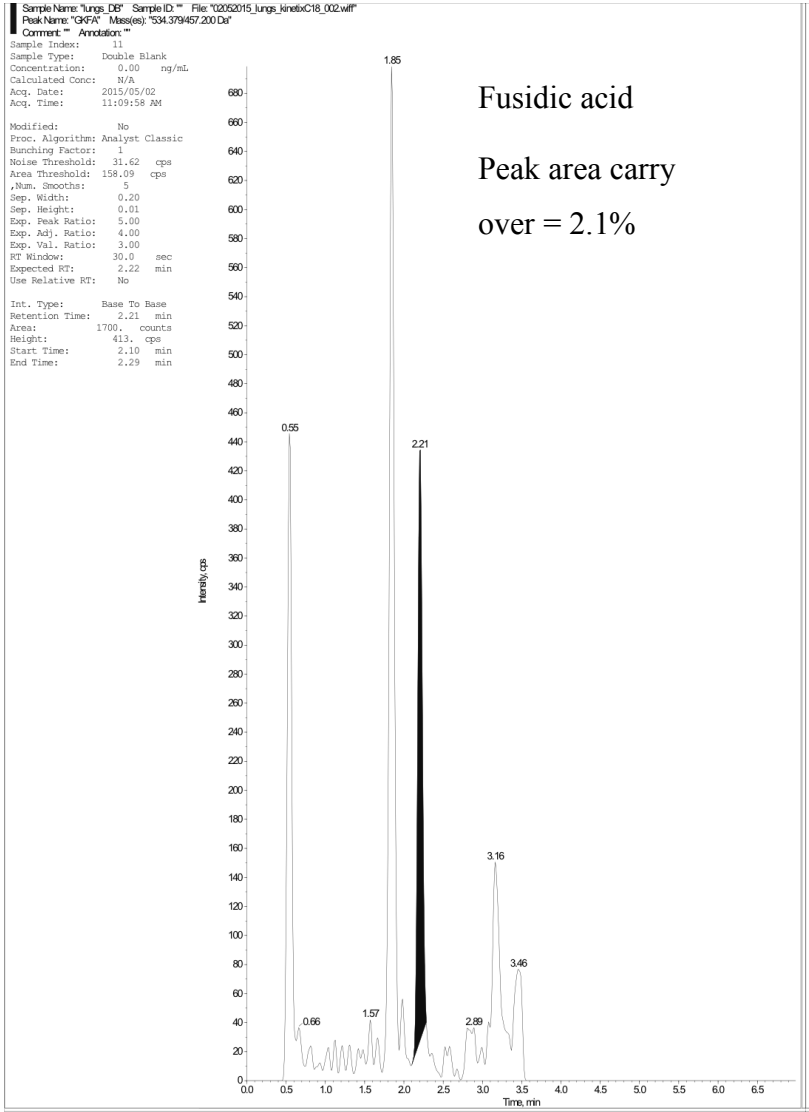

Fusidic acid

Peak area carry over = 2.1%

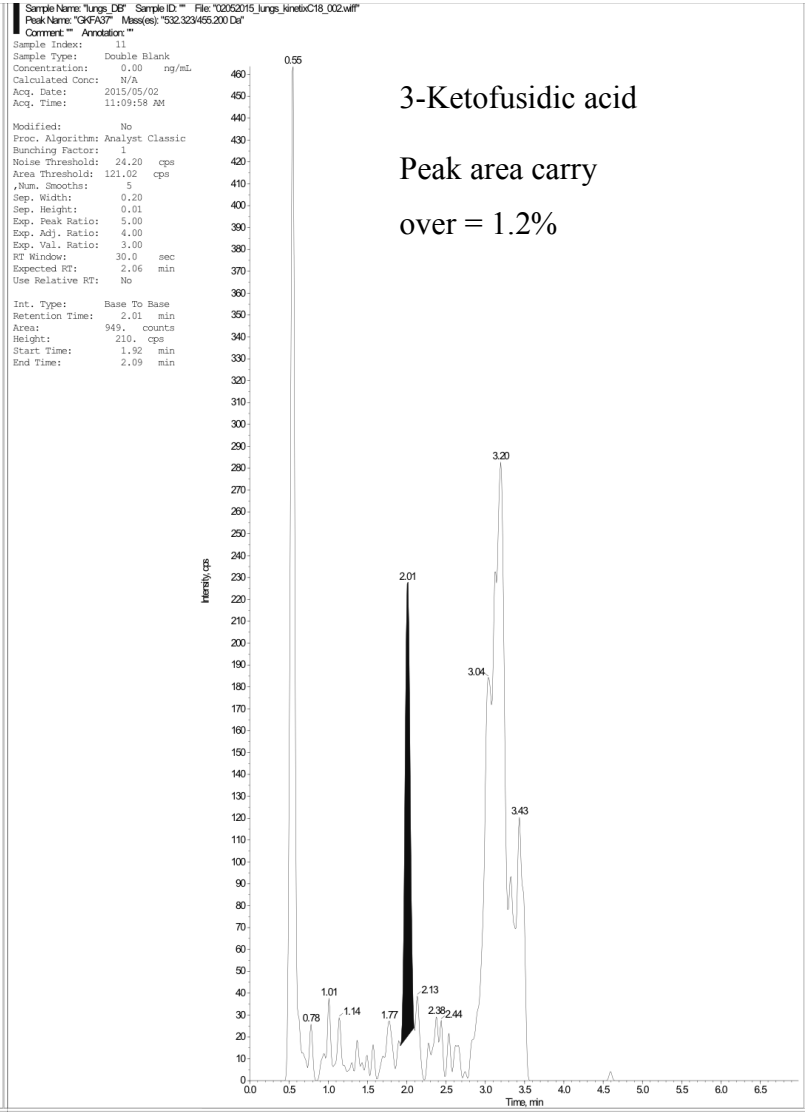

3-Ketofusidic acid

Peak area carry over = 1.2%

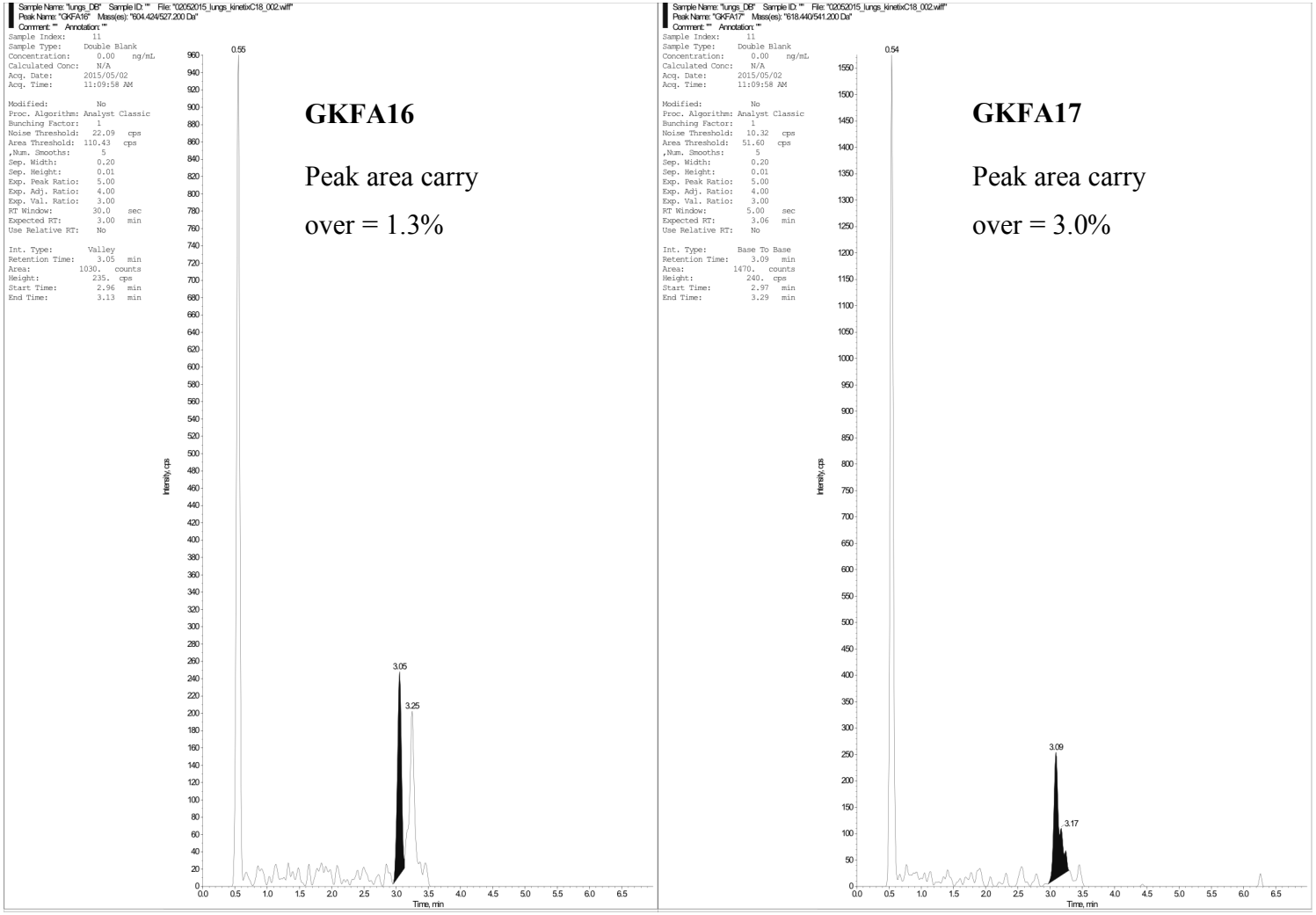

Figure 7-21: Representative blank samples of organ distribution.

7.5.1.5 Individual concentrations

Table 7-49: Mean concentration-time (nmol/mg) values of organ distribution experiments

FA experiment				**GKFA16** experiment					**GKFA17** experiment				
Blood				Blood					Blood				
Time	FA	k-FA	e-FA	Time	FA16	FA	k-FA	e-FA	Time	FA17	FA	k-FA	e-FA
1.5	0.286	0.399	0.813	1.42	0.253	0.109	0.144	1.04	6.87	-	0.0101	0.0441	0.293
3.64	0.238	0.199	0.583	3.47	0.0266	0.0429	0.175	1.76	5.25	0.00414	0.0128	0.15	0.779
5.6	0.0634	0.0625	0.0747	5.19	0.0126	0.0162	0.0414	0.597	3.52	0.00814	0.0349	0.297	2.05
6.95	0.0459	0.0266	0.155	7.35	0.014	0.0314	0.0355	0.167	1.7	0.0951	0.376	0.18	2
Liver				Liver					Liver				
Time	FA	k-FA	e-FA	Time	FA16	FA	k-FA	e-FA	Time	FA17	FA	k-FA	e-FA
1.5	4.81	7.78	11.7	1.42	0.465	9.5	3.23	8.41	6.87	0.123	1.02	1.56	5.35
3.64	6.19	6.65	10.9	3.47	0.245	1.87	2.06	7.18	5.25	0.758	2.58	6.98	10.1
5.6	1.56	1.51	4.94	5.19	0.341	1.67	1.53	5.83	3.52	1.77	5.4	5.15	12.4
6.95	0.348	0.68	2.84	7.35	0.0248	0.729	0.305	1.44	1.7	6.24	15	5.07	12.2
Lungs				Lungs					Lungs				
Time	FA	k-FA	e-FA	Time	FA16	FA	k-FA	e-FA	Time	FA17	FA	k-FA	e-FA
1.5	0.222	0.0626	0.694	1.42	0.0456	0.0909	0.0184	0.226	1.7	0.0897	0.322	0.258	2.16
3.64	0.0914	0.0412	0.363	3.47	0.391	0.0516	0.0219	0.466	3.52	0.0109	0.0471	0.0656	0.712
5.6	0.0473	0.0261	0.217	5.19	-	0.0145	0.00965	0.112	5.25	0.00578	0.0302	0.0266	0.217
6.95	0.0715	0.0682	0.114	7.35	0.00073	0.011	-	0.039	6.87	0.00733	0.0326	0.0151	0.089

Kidneys				Kidneys					Kidneys				
Time	FA	k-FA	e-FA	Time	FA16	FA	k-FA	e-FA	Time	FA17	FA	k-FA	e-FA
1.5	0.268	0.0742	2.01	1.42	-	0.307	0.0673	0.847	6.87	0.0155	0.0324	0.0289	0.28
3.64	0.0971	0.0487	0.879	3.47	-	0.148	0.102	1.02	5.25	0.0179	0.0431	0.045	0.95
5.6	0.0481	0.0316	0.404	5.19	0.00066	0.0562	0.0427	0.333	3.52	0.0263	0.076	0.0601	1.55
6.95	0.0303	0.0316	0.284	7.35	-	0.0323	0.0251	0.107	1.7	0.138	0.437	0.0803	2.69

Brain				Brain					Brain				
Time	FA	k-FA	e-FA	Time	FA16	FA	k-FA	e-FA	Time	FA17	FA	k-FA	e-FA
1.5	0.0283	0.0113	0.0572	1.42	0.0402	0.0248	-	0.00901	6.87	0.00932	0.00696	-	-
3.64	0.0103	0.0064	0.0147	3.47	0.0371	0.0101	-	0.0224	5.25	0.00989	0.00437	0.0016	0.00413
5.6	0.0126	-	0.0157	5.19	0.0143	0.0145	0.0011	0.0254	3.52	0.0122	0.0158	0.00807	0.0185
6.95	0.0172	-	0.0135	7.35	0.00509	0.0124	-	0.0028	1.7	0.0408	0.014	0.00473	0.028

Spleen				Spleen					Spleen				
Time	FA	k-FA	e-FA	Time	FA16	FA	k-FA	e-FA	Time	FA17	FA	k-FA	e-FA
1.5	0.162	0.122	0.359	1.42	0.0767	0.108	0.0402	0.27	6.87	-	0.0397	0.095	0.265
3.64	0.108	0.119	0.295	3.47	0.0481	0.0339	0.0371	0.263	5.25	0.0116	0.0403	0.0596	0.218
5.6	0.0941	0.0854	0.235	5.19	0.0418	0.015	0.0143	0.0834	3.52	0.167	0.247	0.553	1.79
6.95	0.0323	0.0635	0.21	7.35	0.0274	0.00512	0.00509	0.014	1.7	0.241	0.227	0.171	1.26

Heart				Heart					Heart				
Time	FA	k-FA	e-FA	Time	FA16	FA	k-FA	e-FA	Time	FA17	FA	k-FA	e-FA
1.5	0.295	0.305	1.61	1.42	0.386	0.144	0.0767	1.16	6.87	0.0219	0.0365	0.06	0.227
3.64	0.0899	0.14	0.694	3.47	0.044	0.0348	0.0481	0.728	5.25	0.027	0.0327	0.098	0.591
5.6	0.086	0.114	0.567	5.19	0.0317	0.0398	0.0418	0.449	3.52	0.0428	0.0549	0.213	1.78
6.95	0.0322	0.0523	0.201	7.35	0.0214	0.0301	0.0274	0.0895	1.7	0.532	0.275	0.198	2.62

Note: All concentration values expressed as nmol/mg and time in hrs

Table 7-50: AUC_{∞} values (min.nmol/mg) of organ distribution studies

	FA experiment				**GKFA16** experiment					**GKFA17** experiment			
	FA	k-FA	e-FA		FA16	FA	k-FA	e-FA		FA17	FA	k-FA	e-FA
Blood	85.1	96.8	234	Blood	46.6	24	72.1	405	Blood	11.4	49.1	71.4	551
Liver	1850	2520	4240	Liver	119	1550	791	2590	Liver	936	2570	1960	4700
Lungs	83.5	16.7	207	Lungs	49.3	22.9	5.52	96.6	Lungs	12.3	43.7	40.2	340
Kidneys	88	41.6	627	Kidneys	38.6	84.2	34.1	682	Kidneys	34.1	79	30.2	645
Brain	12.6	2.34	13	Brain	30.9	4.67	1.77	6.1	Brain	7.83	4.37	1.69	5.94
Spleen	48.8	55.8	177	Spleen	45.3	390	93.4	376	Spleen	44.3	56.3	87.5	359
Heart	69.2	107	433	Heart	57.3	39.4	28.5	268	Heart	74.8	7.41	68.2	560

8 REFERENCES

1 I. Kola and J. Landis, *Nat. Rev. Drug Discov.*, 2004, **3**, 711–5.

2 M. J. Waring, J. Arrowsmith, A. R. Leach, P. D. Leeson, S. Mandrell, R. M. Owen, G. Pairaudeau, W. D. Pennie, S. D. Pickett, J. Wang, O. Wallace and A. Weir, *Nat. Rev. Drug Discov.*, 2015, **14**, 475–486.

3 D. Cook, D. Brown, R. Alexander, R. March, P. Morgan, G. Satterthwaite and M. N. Pangalos, *Nat. Rev. Drug Discov.*, 2014, **13**, 419–31.

4 J. Hudson and H. F. Khazragui, *Drug Discov. Today*, 2013, **18**, 610–613.

5 E. M. Meslin, A. Blasimme and A. Cambon-Thomsen, *Clin. Transl. Med.*, 2013, **2**, 14.

6 PhRMA, Washington, DC, 2006.

7 S. Reagan-Shaw, M. Nihal and N. Ahmad, *FASEB J.*, 2008, **22**, 659–61.

8 C. C. Peck, in *Integration of Pharmacokinetics, Pharmacodynamics, and Toxicokinetics in Rational Drug Development*, Springer US, Boston, MA, 1993, pp. 1–5.

9 FDA, *Critical Path Opportunities List*, 2006.

10 M. H. Tarbit and J. Berman, *Curr. Opin. Chem. Biol.*, 1998, **2**, 411–6.

11 C. Li, B. Liu, J. Chang, T. Groessl, M. Zimmerman, Y. He, J. Isbell and T. Tuntland, *Drug Discov. Today*, 2013, **18**, 71–78.

12 D. Liu, H.-K. Lon, D. C. DuBois, R. R. Almon and W. J. Jusko, *J. Pharmacokinet. Pharmacodyn.*, 2011, **38**, 769–786.

13 S. H. Ingwersen, B. Kiehr, L. Iversen, M. P. Andersen, Y. Petersen and K. A. Rytved, *Eur. J. Drug Metab. Pharmacokinet.*, 2002, **27**, 203–212.

14 A. M. Dahlem, S. R. Allerheiligen and M. J. Vodicnik, *Toxicol. Pathol.*, 1995, **23**, 170–178.

15 J. van Bree, J. Nedelman, J.-L. Steimer, F. Tse, W. Robinson and W. Niederberger, *Drug Inf. J.*, 1994, **28**, 263–279.

16 J.-L. Steimer, S. Vozeh, A. Racine-Poon, N. Holford and R. O'Neill, Springer, Berlin, Heidelberg, 1994, pp. 405–451.

17 J. Gabrielsson, D. Weiner and J. Gabrielsson, *Pharmacokinetic & pharmacodynamic data analysis : concepts and applications*, Apotekarsocieteten, 2006.

18 J. B. Bulitta, N. H. G. Holford, J. B. Bulitta and N. H. G. Holford, in *Wiley StatsRef: Statistics Reference Online*, John Wiley & Sons, Ltd, Chichester, UK, 2014.

19 J. Gabrielsson and D. Weiner, in *Methods in molecular biology (Clifton, N.J.)*, 2012, vol. 929, pp. 377–389.

20 T. Jaki and M. J. Wolfsegger, *Stat. Med.*, 2012, **31**, 1059–1073.

21 M. Rowland, *Clinical pharmacokinetics : concepts and applications*, Williams & Wilkins, Baltimore, 1995.

22 W. R. Gillespie, *Clin. Pharmacokinet.*, 1991, **20**, 253–262.

23 T. T. Nguyen, C. Bazzoli and F. Mentré, *Stat. Med.*, 2012, **31**, 1043–1058.

24 J. H. Ware, *Am. Stat.*, 1985, **39**, 95.

25 W. R. Gillespie, *Clin. Pharmacokinet.*, 1991, **20**, 253–262.

26 E. M. P. Widmark and J. Tandberg, *Biochem Z*, 1924, **147**, 358–369.

27 T. Teorell, *Arch. Int. Pharmacodyn. Ther.*, 1937, **57**, 205–225.

28 J. G. Wagner, *Pharmacol. Ther.*, 1981, **12**, 537–62.

29 J. G. Wagner, *J. Pharmacokinet. Biopharm.*, 1975, **3**, 457–78.

30 J. Gabrielsson and D. Weiner, Humana Press, Totowa, NJ, 2012, pp. 377–389.

31 J. S. Owen and J. Fiedler-Kelly, *Introd. to Popul. Pharmacokinet. / Pharmacodyn. Anal. with Nonlinear Mix. Eff. Model.*, 2014, 1–8.

32 J. G. Wagner, *Fundamentals of clinical pharmacokinetics*, Drug Intelligence Publications, 1975.

33 J. G. Wagner, *Journal of pharmacokinetics and pharmacodynamics.*, [New York], 2001.

34 J. G. Wagner, *J. Pharmacokinet. Biopharm.*, 1975, **3**, 457–478.

35 J. G. Wagner, *J. Pharmacokinet. Biopharm.*, 1976, **4**, 395–425.

36 L. B. Sheiner and J.-L. Steimer, *Annu. Rev. Pharmacol. Toxicol.*, 2000, **40**, 67–95.

37 Y. Hashimoto and L. B. Sheiner, *J. Pharmacokinet. Biopharm.*, 1991, **19**, 333–53.

38 L. B. Sheiner, *Clin. Pharmacol. Ther.*, 1989, **46**, 605–615.

39 L. B. Sheiner, B. Rosenberg and K. L. Melmon, *Comput. Biomed. Res.*, 1972, **5**, 411–59.

40 S. Beal and L. Sheiner, *Am. Stat.*, 1980, **34**, 118.

41 L. B. Sheiner, B. Rosenberg and V. V Marathe, *J. Pharmacokinet. Biopharm.*, 1977, **5**, 445–79.

42 G. C. Pillai, F. Mentré and J.-L. Steimer, *J. Pharmacokinet. Pharmacodyn.*, 2005, **32**, 161–83.

43 L. B. Sheiner, *Ann. Intern. Med.*, 1975, **82**, 619.

44 L. B. Sheiner and T. M. Ludden, 1992, 185–209.

45 J. S. Barrett, M. J. Fossler, K. D. Cadieu and M. R. Gastonguay, *J. Clin. Pharmacol.*, 2008, **48**, 632–649.

46 J. V. S. Gobburu, *J. Clin. Pharmacol.*, 2010, **50**, 151S–157S.

47 J. V. S. Gobburu, *J. Clin. Pharmacol.*, 2010, **50**, 151S–157S.

48 L. Aarons, *Int. J. Clin. Pharmacol. Ther. Toxicol.*, 1992, **30**, 520–2.

49 L. Aarons, *Br. J. Clin. Pharmacol.*, 1991, **32**, 669–670.

50 L. Aarons, *Br. J. Clin. Pharmacol.*, 2005, **60**, 581–3.

51 D. R. Mould and R. N. Upton, *CPT pharmacometrics Syst. Pharmacol.*, 2012, **1**, e6.

52 G. E. P. Box, *J. Am. Stat. Assoc.*

53 M. Lavielle and F. Mentré, *J. Pharmacokinet. Pharmacodyn.*, 2007, **34**, 229–49.

54 P. L. S. Chan, P. Jacqmin, M. Lavielle, L. McFadyen and B. Weatherley, *J. Pharmacokinet. Pharmacodyn.*, 2011, **38**, 41–61.

55 M. Lavielle and F. Mentré, *J. Pharmacokinet. Pharmacodyn.*, 2007, **34**, 229–249.

56 P. Winstanley, G. Edwards, M. Orme and A. Breckenridge, *Br. J. Clin. Pharmacol.*, 1987,

23, 1–7.

57 R. Buller, M. L. Peterson, Ö. Almarsson and L. Leiserowitz, *Cryst. Growth Des.*, 2002, **2**, 553–562.

58 S. R. Hawley, P. G. Bray, P. M. O'Neill, D. J. Naisbitt, B. K. Park and S. A. Ward, *Antimicrob. Agents Chemother.*, 1996, **40**, 2345–9.

59 D. A. van Schalkwyk and T. J. Egan, *Drug Resist. Updat.*, 2006, **9**, 211–26.

60 X.-Q. Li, *J. Pharmacol. Exp. Ther.*, 2002, **300**, 399–407.

61 G. E. Childs, E. F. Boudreau, W. K. Milhous, T. Wimonwattratee, N. Pooyindee, L. Pang and D. E. Davidson, *Am. J. Trop. Med. Hyg.*, 1989, **40**, 7–11.

62 M. J. Rijken, R. McGready, V. Jullien, J. Tarning, N. Lindegardh, A. P. Phyo, A. K. Win, P. Hsi, M. Cammas, P. Singhasivanon, N. J. White and F. Nosten, *Antimicrob. Agents Chemother.*, 2011, **55**, 4338–42.

63 X.-Q. Li, A. Björkman, T. B. Andersson, M. Ridderström and C. M. Masimirembwa, *J. Pharmacol. Exp. Ther.*, 2002, **300**, 399–407.

64 N. White, S. Looareesuwan, G. Edwards, R. Phillips, J. Karbwang, D. Nicholl, C. Bunch and D. Warrell, *Br. J. Clin. Pharmacol.*, 1987, **23**, 127–135.

65 R. Kerb, R. Fux, K. Mörike, P. G. Kremsner, J. P. Gil, C. H. Gleiter and M. Schwab, *Lancet Infect. Dis.*, 2009, **9**, 760–774.

66 P. I. German and F. T. Aweeka, *Clin. Pharmacokinet.*, 2008, **47**, 91–102.

67 J. K. Baird, *N. Engl. J. Med.*, 2005, **352**, 1565–77.

68 B. M. Greenwood, K. Bojang, C. J. M. Whitty and G. A. T. Targett, *Lancet (London, England)*, 2005, **365**, 1487–98.

69 P. M. O'Neill, B. K. Park, A. E. Shone, J. L. Maggs, P. Roberts, P. A. Stocks, G. A. Biagini, P. G. Bray, P. Gibbons, N. Berry, P. A. Winstanley, A. Mukhtar, R. Bonar-Law, S. Hindley, R. B. Bambal, C. B. Davis, M. Bates, T. K. Hart, S. L. Gresham, R. M. Lawrence, R. A. Brigandi, F. M. Gomez-delas-Heras, D. V Gargallo and S. A. Ward, *J. Med. Chem.*, 2009, **52**, 1408–15.

70 J. N. Burrows, K. Chibale and T. N. Wells, *Curr Top Med Chem*, 2011, **11**, 1226–1254.

71 D. S. B. Ongarora, J. Gut, P. J. Rosenthal, C. M. Masimirembwa and K. Chibale, *Bioorg.*

Med. Chem. Lett., 2012, **22**, 5046–5050.

72 D. S. B. Ongarora, N. Strydom, K. Wicht, M. Njoroge, L. Wiesner, T. J. Egan, S. Wittlin, U. Jurva, C. M. Masimirembwa and K. Chibale, *Bioorg. Med. Chem.*, 2015, **23**, 5419–32.

73 Y. Younis, F. Douelle, D. González Cabrera, C. Le Manach, A. T. Nchinda, T. Paquet, L. J. Street, K. L. White, K. M. Zabiulla, J. T. Joseph, S. Bashyam, D. Waterson, M. J. Witty, S. Wittlin, S. A. Charman and K. Chibale, *J. Med. Chem.*, 2013, **56**, 8860–8871.

74 W. Peters, *Exp. Parasitol.*, 1965, **17**, 80–89.

75 D. A. Fidock, P. J. Rosenthal, S. L. Croft, R. Brun and S. Nwaka, *Nat. Rev. Drug Discov.*, 2004, **3**, 509–20.

76 J. F. Ryley and W. Peters, *Ann. Trop. Med. Parasitol.*, 1970, **64**, 209–22.

77 C. Le Manach, D. González Cabrera, F. Douelle, A. T. Nchinda, Y. Younis, D. Taylor, L. Wiesner, K. L. White, E. Ryan, C. March, S. Duffy, V. M. Avery, D. Waterson, M. J. Witty, S. Wittlin, S. A. Charman, L. J. Street and K. Chibale, *J. Med. Chem.*, 2014, **57**, 2789–2798.

78 P. Montaguti, E. Melloni and E. Cavalletti, *Arzneimittelforschung.*, 1994, **44**, 566–70.

79 B. J. Anderson and N. H. G. Holford, *Annu. Rev. Pharmacol. Toxicol.*, 2008, **48**, 303–32.

80 D. B. Klein, *SSRN Electron. J.*, , DOI:10.2139/ssrn.677447.

81 C. Yau, *R Tutorial with Bayesian Statistics Using OpenBUGS*, 2013.

82 E. I. Ette and P. J. Williams, *Pharmacometrics : the Science of Quantitative Pharmacology.*, Wiley, 2013.

83 S. B. Duffull, D. F. B. Wright and H. R. Winter, *Br. J. Clin. Pharmacol.*, 2011, **71**, 807–14.

84 M. E. Spilker and P. Vicini, *J. Biomed. Inform.*, 2001, **34**, 348–364.

85 D. W. A. (David W. A. . Bourne, *Mathematical modeling of pharmacokinetic data*, Technomic Pub. Co, 1995.

86 C. Chen, S. G. Wicha, G. J. de Knegt, F. Ortega, L. Alameda, V. Sousa, J. E. M. de Steenwinkel and U. S. H. Simonsson, *CPT Pharmacometrics Syst. Pharmacol.*, , DOI:10.1002/psp4.12226.

87 F. P. Combes, S. Retout, N. Frey and F. Mentré, *CPT Pharmacometrics Syst. Pharmacol.*, 2014, **3**, e109.

88 M. Diekstra, A. Fritsch, F. Kanefendt, J. Swen, D. Moes, F. Sörgel, M. Kinzig, C. Stelzer, D. Schindele, T. Gauler, S. Hauser, D. Houtsma, M. Roessler, B. Moritz, K. Mross, L. Bergmann, E. Oosterwijk, L. Kiemeney, H. Guchelaar and U. Jaehde, *CPT Pharmacometrics Syst. Pharmacol.*, 2017, **6**, 604–613.

89 R. J. Keizer, M. O. Karlsson and A. Hooker, *CPT Pharmacometrics Syst. Pharmacol.*, 2013, **2**, e50.

90 L. Kervezee, V. Gotta, J. Stevens, W. Birkhoff, I. Kamerling, M. Danhof, J. Meijer and J. Burggraaf, *CPT Pharmacometrics Syst. Pharmacol.*, 2016, **5**, 466–474.

91 J. Dumond, J. Chen, M. Cottrell, C. Trezza, H. Prince, C. Sykes, C. Torrice, N. White, S. Malone, R. Wang, K. Patterson, N. Sharpless and A. Forrest, *CPT Pharmacometrics Syst. Pharmacol.*, 2017, **6**, 128–135.

92 J. Gabrielsson, *Pharmacokinetic & pharmacodynamic data analysis : concepts and applications*, Apotekarsocieteten, [Stockholm], 2006.

93 T. M. Post, J. I. Freijer, B. A. Ploeger and M. Danhof, *J. Pharmacokinet. Pharmacodyn.*, 2008, **35**, 185–202.

94 L. B. Sheiner, S. L. Beal and A. Dunne, *J. Am. Stat. Assoc.*, 1997, **92**, 1235–1244.

95 N. Holford, in *Holford N*, 2005, p. Abstr 738.

96 M. O. Karlsson and N. Holford, in *PAGE 17*, 2008, p. Abstr 1434.

97 M. Bergstrand, A. C. Hooker, J. E. Wallin and M. O. Karlsson, *AAPS J.*, 2011, **13**, 143–51.

98 R. M. Savic, D. M. Jonker, T. Kerbusch and M. O. Karlsson, *J. Pharmacokinet. Pharmacodyn.*, 2007, **34**, 711–26.

99 S. L. Shafer, 1999.

100 A. Krause and P. J. Lowe, *CPT pharmacometrics Syst. Pharmacol.*, 2014, **3**, e116.

101 M. Kansy, F. Senner and K. Gubernator, *J. Med. Chem.*, 1998, **41**, 1007–10.

102 F. Wohnsland and B. Faller, *J. Med. Chem.*, 2001, **44**, 923–30.

103 A. P. Hill and R. J. Young, *Drug Discov. Today*, 2010, **15**, 648–55.

104 E. Kerns, 2008.

105 R. S. Obach, J. G. Baxter, T. E. Liston, B. M. Silber, B. C. Jones, F. Macintyre, D. J. Rance

and P. Wastall, *J. Pharmacol. Exp. Ther.*, 1997, **283**, 46–58.

106 J. Brian Houston, *Biochem. Pharmacol.*, 1994, **47**, 1469–1479.

107 W. Richmond, M. Wogan, J. Isbell and W. P. Gordon, *J. Pharm. Sci.*, 2010, **99**, 4463–8.

108 B. Davies and T. Morris, *Pharm. Res.*, 1993, **10**, 1093–1095.

109 Y. W. Alelyunas, L. Pelosi-Kilby, P. Turcotte, M.-B. Kary and R. C. Spreen, *J. Chromatogr. A*, 2010, **1217**, 1950–5.

110 S. Yu, S. Li, H. Yang, F. Lee, J.-T. Wu and M. G. Qian, *Rapid Commun. Mass Spectrom.*, 2005, **19**, 250–4.

111 G. Hochart, E. Paunescu, E. Boll and P. Melnyk, *Res. Rev. J. Med. Chem.*

112 X. Q. Li, A. Bjorkman, T. B. Andersson, L. L. Gustafsson and C. M. Masimirembwa, *Eur. J. Clin. Pharmacol.*, 2003, **59**, 429–442.

113 Y. Horiuchi, F. Hirayama and K. Uekama, *J. Pharm. Sci.*, 1990, **79**, 128–132.

114 K. Uekama, Y. Horiuchi, T. Irie and F. Hirayama, *Carbohydr. Res.*, 1989, **192**, 323–330.

115 T. Horikawa, F. Hirayama and K. Uekama, *J. Pharm. Pharmacol.*, 1995, **47**, 124–7.

116 I. J. Hidalgo, *Curr. Top. Med. Chem.*, 2001, **1**, 385–401.

117 R. B. van Breemen and Y. Li, *Expert Opin. Drug Metab. Toxicol.*, 2005, **1**, 175–185.

118 D. Gonzalez, S. Schmidt and H. Derendorf, *Clin. Microbiol. Rev.*, 2013, **26**, 274–88.

119 T. Bohnert and L.-S. Gan, *J. Pharm. Sci.*, 2013, **102**, 2953–94.

120 D. A. Smith, L. Di and E. H. Kerns, *Nat. Rev. Drug Discov.*, 2010, **9**, 929–939.

121 F. Keller, M. Maiga, H. H. Neumayer, H. Lode and A. Distler, *Eur. J. Drug Metab. Pharmacokinet.*, **9**, 275–82.

122 J. H. Lin, *Curr. Drug Metab.*, 2008, **9**, 46–59.

123 L. Shargel, S. Wu-Pong and A. B. C. Yu, *Applied biopharmaceutics & pharmacokinetics*, Appleton & Lange Reviews/McGraw-Hill, Medical Pub. Division, 2005.

124 M. Rowland, *Clin. Pharmacokinet.*, 1984, **9 Suppl 1**, 10–7.

125 S. Clarysse, J. Brouwers, J. Tack, P. Annaert and P. Augustijns, *Eur. J. Pharm. Sci.*, 2011, **43**, 260–269.

126 E. H. Kerns and L. Di, *Drug-like Properties: Concepts, Structure Design and Methods*, 2008.

127 S. Asha and M. Vidyavathi, *Appl. Biochem. Biotechnol.*, 2010, **160**, 1699–1722.

128 A. P. Li, *Drug Discov. Today Technol.*, 2005, **2**, 179–185.

129 D. J. Bickett, P. I. MacKenzie, M. E. Veronese and J. O. Miners, *Trends Pharmacol. Sci.*, 1993, **14**, 292–4.

130 M. Eichelbaum and O. Burk, *Nat. Med.*, 2001, **7**, 285–287.

131 M. B. Fisher, M. F. Paine, T. J. Strelevitz and S. A. Wrighton, *Drug Metab. Rev.*, 2001, **33**, 273–297.

132 E. H. Kerns and L. Di, *Drug-like Properties: Concepts, Structure Design and Methods*, Elsevier, 2008.

133 P. H. Hinderling, *Pharmacol. Rev.*, 1997, **49**, 279–95.

134 P. H. (Peter H. . Hinderling, E. F. Smith, A. M. Lefer and K. Schrör, *Drug distribution in the body : in vitro prediction and physiological interpretation*, Gustav Fischer Verlag, 1988.

135 Y. Younis, F. Douelle, D. González Cabrera, C. Le Manach, A. T. Nchinda, T. Paquet, L. J. Street, K. L. White, K. M. Zabiulla, J. T. Joseph, S. Bashyam, D. Waterson, M. J. Witty, S. Wittlin, S. A. Charman and K. Chibale, *J. Med. Chem.*, 2013, **56**, 8860–71.

136 S. Duffy and V. M. Avery, *Am. J. Trop. Med. Hyg.*, 2012, **86**, 84–92.

137 C. J. Harris, R. D. Hill, D. W. Sheppard, M. J. Slater and P. F. W. Stouten, *Comb. Chem. High Throughput Screen.*, 2011, **14**, 521–31.

138 Y. Younis, F. Douelle, T. S. Feng, D. G. Cabrera, C. Le Manach, A. T. Nchinda, S. Duffy, K. L. White, D. M. Shackleford, J. Morizzi, J. Mannila, K. Katneni, R. Bhamidipati, K. M. Zabiulla, J. T. Joseph, S. Bashyam, D. Waterson, M. J. Witty, D. Hardick, S. Wittlin, V. Avery, S. A. Charman and K. Chibale, *J. Med. Chem.*, 2012, **55**, 3479–3487.

139 T. Paquet, C. Le Manach, D. G. Cabrera, Y. Younis, P. P. Henrich, T. S. Abraham, M. C. S. Lee, R. Basak, S. Ghidelli-Disse, M. J. Lafuente-Monasterio, M. Bantscheff, A. Ruecker, A. M. Blagborough, S. E. Zakutansky, A.-M. Zeeman, K. L. White, D. M. Shackleford, J. Mannila, J. Morizzi, C. Scheurer, I. Angulo-Barturen, M. S. Martínez, S. Ferrer, L. M. Sanz, F. J. Gamo, J. Reader, M. Botha, K. J. Dechering, R. W. Sauerwein, A. Tungtaeng, P.

Vanachayangkul, C. S. Lim, J. Burrows, M. J. Witty, K. C. Marsh, C. Bodenreider, R. Rochford, S. M. Solapure, M. B. Jiménez-Díaz, S. Wittlin, S. A. Charman, C. Donini, B. Campo, L.-M. Birkholtz, K. K. Hanson, G. Drewes, C. H. M. Kocken, M. J. Delves, D. Leroy, D. A. Fidock, D. Waterson, L. J. Street and K. Chibale, *Sci. Transl. Med.*, 2017, **9**, eaad9735.

140 R. Lipp, *Am. Pharm. Rev.*

141 D. J. Abraham, *Burger's Medicinal Chemistry and Drug Discovery*, John Wiley & Sons, Inc., Hoboken, NJ, USA, 2003.

142 J. Szejtli, *Chem. Rev.*, 1998, **98**, 1743–1754.

143 J. Szejtli, 1988, pp. 79–185.

144 S. K. Das, R. Rajabalaya, S. David, N. Gani, J. Khanam and A. Nanda, *Res. J. Pharm. Biol. Chem. Sci.*, **4**, 975–8585.

145 T. Loftsson and D. Duchêne, *Int. J. Pharm.*, 2007, **329**, 1–11.

146 S. Shimpi, B. Chauhan and P. Shimpi, *Acta Pharm.*, 2005, **55**, 139–56.

147 T. Irie and K. Uekama, *J. Pharm. Sci.*, 1997, **86**, 147–162.

148 A. Gerlóczy, A. Fónagy, P. Keresztes, L. Perlaky and J. Szejtli, *Arzneimittelforschung.*, 1985, **35**, 1042–7.

149 L. M. Joseph, K. Chibale and M. R. Chaira, *J. Pharm. Sci.*, 2016, **105**, 3344–3350.

150 V. M. Rao and V. J. Stella, *J. Pharm. Sci.*, 2003, **92**, 927–32.

151 S. Stegemann, F. Leveiller, D. Franchi, H. de Jong and H. Lindén, *Eur. J. Pharm. Sci.*, 2007, **31**, 249–61.

152 N. Reix, P. Guhmann, W. Bietiger, M. Pinget, N. Jeandidier and S. Sigrist, *Int. J. Pharm.*, 2012, **422**, 338–340.

153 J. Li, Y. Bai, Y. Bai, R. Zhu, W. Liu, J. Cao, M. An, Z. Tan and Y. Chang, *Evidence-Based Complement. Altern. Med.*, 2017, **2017**, 1–12.

154 C. Liu, X. Gao, Y. Liu, M. Huang, D. Qu and Y. Chen, *Biomed. Pharmacother.*, 2017, **94**, 1048–1056.

155 Y. Zhang, Y. Cheng, Z. Liu, L. Ding, T. Qiu, L. Chai, F. Qiu, Z. Wang, W. Xiao, L. Zhao

and X. Chen, *J. Chromatogr. B*, 2017, **1061–1062**, 474–486.

156 J. Guan, X. Zhang, B. Feng, D. Zhao, T. Zhao, S. Chang, L. Wang and H. Zhu, *J. Sep. Sci.*, , DOI:10.1002/jssc.201700665.

157 W.-W. Dong, X.-Z. Han, J. Zhao, F.-L. Zhong, R. Ma, S. Wu, D. Li, L.-H. Quan and J. Jiang, *Biomed. Chromatogr.*, 2017, e4105.

158 B. Xu, Y. Wang and H. Zhu, *Pharmazie*, 2016, **71**, 76–83.

159 X. Chen, Z. Zhao, Y. Chen, X. Gou, Z. Zhou, G. Zhong, Y. Cai, M. Huang and J. Jin, *J. Ethnopharmacol.*, 2016, **192**, 362–369.

160 Z. Li, W. Zhang, Y. Gao, R. Xiang, Y. Liu, M. Hu, M. Zhou, X. Liu, Y. Wang, Z. He, Y. Sun and J. Sun, *Drug Deliv. Transl. Res.*, 2017, **7**, 100–110.

161 A. E. Hasbach, D. K. Langlois, E. J. Rosser and M. G. Papich, *J. Vet. Intern. Med.*, 2017, **31**, 1163–1169.

162 R. S. Witzig and S. G. Franzblau, *Antimicrob. Agents Chemother.*, 1993, **37**, 1997–9.

163 C. Cicek-Saydam, C. Cavusoglu, D. Burhanoglu, S. Hilmioglu, N. Ozkalay and A. Bilgic, *Clin. Microbiol. Infect.*, 2001, **7**, 700–702.

164 K. Fuursted, D. Askaard and V. Faber, *APMIS*, 1992, **100**, 663–667.

165 E. F. Scowen and L. P. Garrod, *Lancet*, 1962, **279**, 933–935.

166 G. Taylor and K. Bloor, *Lancet*, 1962, **279**, 935–937.

167 P. Collignon and J. Turnidge, *Int. J. Antimicrob. Agents*, 1999, **12**, S45–S58.

168 D. J. Biedenbach, P. R. Rhomberg, R. E. Mendes and R. N. Jones, *Diagn. Microbiol. Infect. Dis.*, 2010, **66**, 301–7.

169 J. Turnidge, *Int. J. Antimicrob. Agents*, 1999, **12**, S23–S34.

170 J. G. Still, K. Clark, T. P. Degenhardt, D. Scott, P. Fernandes and M. J. Gutierrez, *Clin. Infect. Dis.*, 2011, **52**, S504-12.

171 G. R. Willie, N. Richman, W. O. Godtfredsen and J. W. Bodley, *Biochemistry*, 1975, **14**, 1713–1718.

172 A. Okura, T. Kinoshita and N. Tanaka, *J. Antibiot. (Tokyo).*, 1971, **24**, 655–661.

173 D. N. Wilson, *Crit. Rev. Biochem. Mol. Biol.*, **44**, 393–433.

174 A. J. Payne, L. M. Neal and L. J. Knoll, *Parasitol. Res.*, 2013, **112**, 3859–63.

175 V. J. Stella, *Expert Opin. Ther. Pat.*, 2004, **14**, 277–280.

176 J. S. Valentino and W. N.-A. Kwame, *Adv. Drug Deliv. Rev.*, 2007, **59**, 677–694.

177 K. Beaumont, R. Webster, I. Gardner and K. Dack, *Curr. Drug Metab.*, 2003, **4**, 461–485.

178 P. Ettmayer, G. L. Amidon, B. Clement and B. Testa, *J. Med. Chem.*, 2004, 47, 2393–2404.

179 V. J. Stella, *Prodrugs : challenges and rewards*, Springer, 2007.

180 J. Rautio, H. Kumpulainen, T. Heimbach, R. Oliyai, D. Oh, T. Järvinen and J. Savolainen, *Nat. Rev. Drug Discov.*, 2008, **7**, 255–270.

181 K. M. Huttunen, H. Raunio and J. Rautio, *Pharmacol. Rev.*, 2011, **63**, 750–71.

182 K. N. White, V. L. Vale and D. B. Hope, *Biochem. Soc. Trans.*, 1994, **22**, 220S.

183 J. S. Munger, G. P. Shi, E. A. Mark, D. T. Chin, C. Gerard and H. A. Chapman, *J. Biol. Chem.*, 1991, **266**, 18832–8.

184 *Bioorg. Med. Chem. Lett.*, 2017, **27**, 658–661.

185 M. Njoroge, University of Cape Town, 2014.

186 E. Vicente, R. Villar, A. Burguete, B. Solano, S. Pérez-Silanes, I. Aldana, J. A. Maddry, A. J. Lenaerts, S. G. Franzblau, S.-H. Cho, A. Monge and R. C. Goldman, *Antimicrob. Agents Chemother.*, 2008, **52**, 3321–6.

187 A. J. M. Lenaerts, V. Gruppo, J. V. Brooks and I. M. Orme, *Antimicrob. Agents Chemother.*, 2003, **47**, 783–785.

188 A. J. Lenaerts, V. Gruppo, K. S. Marietta, C. M. Johnson, D. K. Driscoll, N. M. Tompkins, J. D. Rose, R. C. Reynolds and I. M. Orme, *Antimicrob. Agents Chemother.*, 2005, **49**, 2294–301.

189 A. J. Lenaerts, M. A. Degroote and I. M. Orme, *Trends Microbiol.*, 2008, **16**, 48–54.

190 M. A. De Groote, J. C. Gilliland, C. L. Wells, E. J. Brooks, L. K. Woolhiser, V. Gruppo, C. A. Peloquin, I. M. Orme and A. J. Lenaerts, *Antimicrob. Agents Chemother.*, 2011, **55**, 1237–47.

191 M. A. De Groote, V. Gruppo, L. K. Woolhiser, I. M. Orme, J. C. Gilliland and A. J. Lenaerts, *Antimicrob. Agents Chemother.*, 2012, **56**, 731–8.

192 T. P. Degenhardt, J. G. Still, K. Clark and P. Fernandes, ICAAC, San Francisco, 2009, p. 1.

193 B. M. Liederer and R. T. Borchardt, *J. Pharm. Sci.*, 2005, **94**, 2198–206.

194 J. B. Bulitta, O. O. Okusanya, A. Forrest, S. M. Bhavnani, K. Clark, J. G. Still, P. Fernandes and P. G. Ambroseb, *Antimicrob. Agents Chemother.*, 2013, **57**, 498–507.

195 B. Knippenberg, M. Page-Sharp, S. Salman, B. Clark, J. Dyer, K. T. Batty, T. M. E. Davis and L. Manning, *Antimicrob. Agents Chemother.*, 2016, **60**, 4940–55.

196 V. Dartois and C. E. Barry, *Bioorg. Med. Chem. Lett.*, 2013, **23**, 4741–50.

197 V. Dartois, *Nat. Rev. Microbiol.*, 2014, **12**, 159–67.

198 M. C. Kjellsson, L. E. Via, a. Goh, D. Weiner, K. M. Low, S. Kern, G. Pillai, C. E. Barry and V. Dartois, *Antimicrob. Agents Chemother.*, 2012, **56**, 446–457.

199 I. J. Kiss, E. Faragó, I. Juház, S. Bacsa and E. Fábián, *Int. J. Clin. Pharmacol. Biopharm.*, 1976, **13**, 42–7.

200 B. Prideaux, M. S. ElNaggar, M. Zimmerman, J. M. Wiseman, X. Li and V. Dartois, *Int. J. Mass Spectrom.*, 2015, **377**, 699–708.

201 B. M. Mayosi, L. J. Burgess and A. F. Doubell, *Circulation*, 2005, **112**, 3608–16.

202 J.-T. Wang, C.-C. Hung, W.-H. Sheng, J.-Y. Wang, S.-C. Chang and K.-T. Luh, *J. Microbiol. Immunol. Infect.*, 2002, **35**, 215–22.

203 H. LB, in *Antituberculosis drugs: pharmacokinetics*, ed. CRC Press, Boca Raton, FL, 1991, pp. 59–65.

204 J. P. DeVincenzo, S. E. Berning, C. A. Peloquin and R. N. Husson, *Ann. Pharmacother.*, 1999, **33**, 1184–8.

205 J. Shenje, F. Ifeoma Adimora-Nweke, I. L. Ross, M. Ntsekhe, L. Wiesner, A. Deffur, H. M. McIlleron, J. Pasipanodya, T. Gumbo and B. M. Mayosi, *EBioMedicine*, , DOI:10.1016/j.ebiom.2015.09.025.

206 G. An and M. E. Morris, *AAPS J.*, 2012, **14**, 352–64.

207 A. R. Maharaj, J. S. Barrett and A. N. Edginton, *AAPS J.*, 2013, **15**, 455–64.

208 R. S. DeWoskin and C. M. Thompson, *Regul. Toxicol. Pharmacol.*, 2008, **51**, 66–86.

209 J. Sager, M. Hsu, N. Isoherranen, L. Wienkers, J. Wahlstrom and R. Foti, *FASEB J*, 2014, **28**, 1064.9-.

210 N. Tsamandouras, A. Rostami-Hodjegan and L. Aarons, *Br. J. Clin. Pharmacol.*, 2015, **79**, 48–55.

211 N. Benowitz, R. P. Forsyth, K. L. Melmon and M. Rowland, *Clin. Pharmacol. Ther.*, 1974, **16**, 99–109.

212 N. Benowitz, R. P. Forsyth, K. L. Melmon and M. Rowland, *Clin. Pharmacol. Ther.*, 1974, **16**, 87–98.

213 K. Jorga, C. Chavanne, N. Frey, T. Lave, V. Lukacova, N. Parrott, R. Peck and B. Reigner, *Clin. Pharmacol. Ther.*, 2016, **100**, 761–769.

214 K. Allegaert, A. Smits and J. N. van den Anker, *J. Biomed. Biotechnol.*, 2012, **2012**, 1–3.

215 Z. Tylutki, S. Polak and B. Wiśniowska, *Curr. Pharmacol. Reports*, 2016, **2**, 171–177.

216 N. D. Pfeifer, S. L. Goss, B. Swift, G. Ghibellini, M. Ivanovic, W. D. Heizer, L. M. Gangarosa and K. L. R. Brouwer, *CPT pharmacometrics Syst. Pharmacol.*, 2013, **2**, e20.

217 B. Reisfeld, C. P. Metzler, M. a. Lyons, a. N. Mayeno, E. J. Brooks and M. a. DeGroote, *Antimicrob. Agents Chemother.*, 2012, **56**, 926–934.

218 M. a Lyons, B. Reisfeld, R. S. Yang and a J. Lenaerts, *Antimicrob Agents Chemother*, 2013, **57**, 1763–1771.

219 M. C. Kjellsson, L. E. Via, A. Goh, D. Weiner, K. M. Low, S. Kern, G. Pillai, C. E. Barry, V. Dartois and V. Dartois, *Antimicrob. Agents Chemother.*, 2012, **56**, 446–57.

220 T. Mindermann, W. Zimmerli, Z. Rajacic and O. Gratzl, *Acta Neurochir. (Wien).*, 1993, **121**, 12–4.